# SAND REPORT

SAND2005-3195
Unlimited Release
Printed June 2005

# Development of Bonded Composite Doublers for the Repair of Oil Recovery Equipment

Dennis Roach and Kirk Rackow

Prepared by
Sandia National Laboratories
Albuquerque, New Mexico 87185 and Livermore, California 94550

Sandia is a multiprogram laboratory operated by Sandia Corporation, a Lockheed Martin Company, for the United States Department of Energy under Contract DE-AC04-94AL85000.



Issued by Sandia National Laboratories, operated for the United States Department of Energy by Sandia Corporation.



Available to DOE and DOE contractors from
U.S. Department of Energy
Office of Scientific and Technical Information
P.O. Box 62
Oak Ridge, TN 37831

Telephone: (865)576-8401
Facsimile: (865)576-5728
E-Mail: reports@adonis.osti.gov
Online ordering: http://www.doe.gov/bridge

Available to the public from
U.S. Department of Commerce
National Technical Information Service
5285 Port Royal Rd
Springfield, VA 22161

Telephone: (800)553-6847
Facsimile: (703)605-6900
E-Mail: orders@ntis.fedworld.gov
Online order: http://www.ntis.gov/ordering.htm

SAND2005-3195
Unlimited Release
Printed June 2005

# Development of Bonded Composite Doublers for the Repair of Oil Recovery Equipment

Dennis Roach
Kirk Rackow
Airworthiness Assurance Department, 6252

Sandia National Laboratories
P. O. Box 5800
Albuquerque, NM 87185-0615

**Abstract**

An unavoidable by-product of a metallic structure's use is the appearance of crack and corrosion flaws. Economic barriers to the replacement of these structures have created an aging infrastructure and placed even greater demands on efficient and safe repair methods. In the past decade, an advanced composite repair technology has made great strides in commercial aviation use. Extensive testing and analysis, through joint programs between the Sandia Labs FAA Airworthiness Assurance Center and the aviation industry, have proven that composite materials can be used to repair damaged aluminum structure. Successful pilot programs have produced flight performance history to establish the durability of bonded composite patches as a permanent repair on commercial aircraft structures. With this foundation in place, this effort is adapting bonded composite repair technology to civil structures. The use of bonded composite doublers has the potential to correct the difficulties associated with current repair techniques and the ability to be applied where there are no rehabilitation options. It promises to be cost-effective with minimal disruption to the users of the structure. This report concludes a study into the application of composite patches on thick steel structures typically used in mining operations. Extreme fatigue, temperature, erosive, and corrosive environments induce an array of equipment damage. The current weld repair techniques for these structures provide a fatigue life that is inferior to that of the original plate. Subsequent cracking must be revisited on a regular basis. The use of composite doublers, which do not have brittle fracture problems such as those inherent in welds, can help extend the structure's fatigue life and reduce the equipment downtime. Two of the main issues for adapting aircraft composite repairs to civil applications are developing an installation technique for carbon steel and accommodating large repairs on extremely thick structures. This study developed and proved an optimum field installation process using specific mechanical and chemical surface preparation techniques coupled with unique, in-situ heating methods. In addition, a comprehensive performance assessment of composite doubler repairs was completed to establish the viability of this technology for large, steel structures. The factors influencing the durability of composite patches in severe field environments were evaluated along with related laminate design issues.

This work was performed for Syncrude Canada, Ltd. under Work-for-Others agreement 062010618. Sandia National Laboratories is a multiprogram laboratory operated by Sandia Corporation, a Lockheed Martin Company, for the United States Department of Energy's National Nuclear Security Administration under contract DE-AC04-94AL85000.

**Acknowledgements**

This work was sponsored by Syncrude Canada, Ltd. under Work-for-Others agreement 062010618. A program such as this would not succeed without the support of a number of research and on-site personnel at Syncrude. The authors would like to acknowledge the efforts put forth by the Syncrude research team (crack management project team) including Victor del Valle, Khaled Obaia, Gilbert Grondin, Silvia Gonzalez, Alaa Elwi, and Yue Yin. In addition, the authors would like to thank the following people for their project guidance and their assistance in the field tests: Mal Carroll, Jeremy Wong, Garret Hansen, Damien Reid, John Oxenford, Stefano Chiovelli and Stewart Johnson. At Sandia Labs, the NDI data acquisition was led by Tony Delong. Additional data acquisition and instrumentation was conducted by Phil Walkington and Mike Bode. The structural mechanics testing at Sandia Labs was supported by John Laing, Brenden Rogillio, John Hofer, and Tom Crenshaw. Finally, overall Sandia-Syncrude project oversight was provided by Victor del Valle and Khaled Obaia.

# Development of Bonded Composite Doublers for the Repair of Oil Recovery Equipment

## TABLE OF CONTENTS


| Section | Title | Page |
|---|---|---|
| EXECUTIVE SUMMARY | | 1 |
| 1.0 | PROJECT DESCRIPTION | 5 |
| 1.1 | Background | 5 |
| 1.2 | Goal of Effort | 6 |
| 1.3 | Bonded Composite Doubler Repair Method | 6 |
| 1.4 | Project Task Overview | 9 |
| 1.5 | Applications Identified | 11 |
| 1.6 | Downselection to First Repair Target | 11 |
| 2.0 | COMPOSITE DOUBLER INSTALLATION PROCESS ON CARBON STEEL STRUCTURES | 17 |
| 2.1 | Surface Preparation Options | 17 |
| 2.2 | Evaluation of Surface Preparation Options | 23 |
| 2.2.1 | Wedge Tests | 26 |
| 2.2.2 | Lap Shear Ultimate Failure Tests | 29 |
| 2.2.3 | Lap Shear Fatigue Durability Tests | 31 |
| 2.2.4 | Adhesive Modulus | 33 |
| 2.2.5 | Critical Crack Extension and Crack Arrest | 34 |
| 2.2.6 | Adhesive vs. Cohesive Fracture Surfaces | 37 |
| 2.3 | Final Determination of Optimum Process for Bonding Composites to Steel Structures | 38 |
| 2.4 | Heat Source-Sink Analysis | 41 |
| 3.0 | COMPOSITE DOUBLER DESIGN GUIDELINES AND VALIDATION FOR REPAIR OF STEEL STRUCTURES | 49 |
| 3.1 | Doubler Design Guidelines | 49 |
| 3.2 | Load Spectra Monitoring of Cable Shovel Boom | 52 |
| 3.2.1 | Modeling of Boom Structure on Cable Shovel | 55 |
| 3.2.2 | Fatigue Properties of Boom Structure | 58 |
| 3.3 | Damage Tolerance and Crack Mitigation of Composite Repair Method | 59 |
| 3.3.1 | Tension-Tension Fatigue Panels – Damage Tolerance and Crack Growth Testing | 59 |
| 3.3.2 | General Fatigue Specimen Description | 59 |

3.3.3 Composite Doubler Design for Tension Test Specimens 61
3.3.3.1 Calculation of Laminate-to-Steel Extensional Stiffness Ratio 62
3.3.3.2 Fatigue Test Specimen Design Features 63
3.3.3.3 Doubler Design Analysis -Performance Criteria and Trade-Off Study with Design Prototypes 65
3.3.4 Test Specimen Configurations 69
3.3.5 Load Spectrums and Instrumentation 74

4.0 PERFORMANCE OF COMPOSITE DOUBLER REPAIR METHOD ON STEEL STRUCTURES 79

4.1 Performance Results from Damage Tolerance Tension Tests 79
4.2 Through-Transmission Ultrasonic Inspection of Fatigue Coupons to Asssess Pre- and Post-Fatigue Damage 85
4.3 Strain Field Measurements 94
4.3.1 Strain Field Analysis 95
4.3.2 Stresses in Steel Plate and Composite Doubler 99
4.3.3 Load Transfer 103
4.3.4 Effects of Multiple Fatigue Lifetimes on Strain Fields 106
4.4 Residual Strength of Damaged Steel Structure with Composite Repairs 112
4.5 Response of Doublers in Extreme Shear & Bending Environments 119
4.5.1 Three Point Bending Test Description 119
4.5.2 Three Point Bending Test Results 122

5.0 NONDESTRUCTIVE INSPECTION OF COMPOSITE DOUBLER REPAIRS ON CARBON STEEL STUCTURES 127

5.1 Damage Tolerance Assessment and Inspection Intervals 127
5.2 Quality Assurance Coupons to Ensure Proper Surface Preparation 129
5.3 Inspection for Cracks in Parent Material Beneath Composite Doubler 129
5.3.1 Eddy Current Inspection 129
5.3.2 X-Ray Inspection 140
5.4 Nondestructive Inspection Methods for Patch and Bond Integrity 143
5.4.1 Pulse-Echo Ultrasonic Inspection 143
5.4.2 Thermographic Inspection 149

6.0 GENERAL ISSUES LEADING TO FIELD REPAIRS 155

6.1 Field Installation and Monitoring of a Composite Doubler Repair 155
6.2 Repair Considerations for Syncrude Applications 155
6.3 Large Scale Testing of Composite Doublers in the Laboratory 158
6.4 Living Infrastructure Concepts 159
6.4.1 Smart Structures - In-Situ Distributed Health Monitoring Sensors 159
6.4.2 Self-Healing Composite Structures 166

CONCLUSIONS 169

REFERENCES 171

APPENDICES

A — Photo Summary of Laminate Fabrication and Installation Process for Bonding Composite Doublers on Carbon Steel Structures 173
B — Installation Process for Repairing Carbon Steel Structures Using Bonded Composite Doublers 183
C — Design and Analysis Guidelines for Composite Doubler Repairs 213

**This Page Intentionally Left Blank**

# Development of Bonded Composite Doublers for the Repair of Oil Recovery Equipment

## EXECUTIVE SUMMARY

Syncrude is one of only a few companies in the world that extracts oil from "oil sand" (bitumen) mineral deposits. The technique involves a mining operation followed by a mechanical and chemical process to produce crude oil. Equipment damage, such as the frequent occurrence of cracking, is caused by high impact loads, high fatigue cycles, low operating temperatures and large component size. Shutdowns to repair equipment can cost in excess of $1M per day. As a result, any improvement in mining equipment operation and maintenance can lead to significant reductions in yearly operating budget. Current techniques for strengthening steel structures have several drawbacks including requiring heavy equipment for installation, poor fatigue performance, heat affected zones around welds, and the need for ongoing maintenance due to continued corrosion attack and crack growth.

In the past decade, an advanced composite repair technology has made great strides in commercial aviation use. Extensive testing and analysis, through joint programs between the Sandia Labs FAA Airworthiness Assurance Center and the aviation industry, have proven that composite materials can be used to repair damaged aluminum structure. Successful pilot programs have produced flight performance history to establish the viability and durability of bonded composite patches as a permanent repair on commercial aircraft structures. With this foundation in place, this effort is adapting bonded composite repair technology to civil, steel structures. The goal of this program is to establish the viability of using bonded composite doublers to repair equipment used in the oil recovery industry. This includes the development and validation of installation, design, analysis, inspection, and quality assurance processes and the comprehensive performance assessment of composite doublers in selected applications. The end product will provide more cost effective and reliable repairs than those currently employed.

Composite doublers offer enhanced safety through improved fatigue life and corrosion resistance. The engineering advantages include: 1) elimination of fastener holes or weld stress risers that produce new crack initiation sites, 2) superior flaw growth mitigation performance, 3) high strength-to-weight ratio, 4) high durability, 5) ability to tailor strength to meet anisotropy needs thus eliminating the undesirable stiffening of a structure in directions other than those required, 6) corrosion resistance, and 7) formability to complex contours. The economic advantages include rapid repair installations that reduce downtime and do not require future maintenance.

Two of the main issues for adapting aircraft composite repairs to civil applications are developing an installation technique for carbon steel and accommodating large repairs on extremely thick structures. This report presents a comprehensive assessment of different mechanical and chemical surface preparation techniques. The factors influencing the durability of composite patches in severe field environments were determined. This report also presents an extensive performance evaluation of composite doublers for the repair of carbon steel structures.

Damage tolerance, durability, crack mitigation, and ultimate strength tests were performed to quantify the capabilities of composite doubler repairs and to provide insights into the critical laminate design parameters. Finally, nondestructive inspection techniques were developed to adequately monitor the health of the patch and the parent structure. By encompassing all "cradle-to-grave" tasks - including design, analysis, installation, structural integrity and inspection - this study firmly established the capabilities of composite doubler repairs. Although an initial application was targeted, the tests were conducted such that the results are applicable to a very wide range of steel repair scenarios.

**Composite Doubler Installation Process** - In order to optimize surface preparation, the basic mechanisms of adhesion for structural adhesive bonding were considered: mechanical interlocking and chemically-enhanced bonding between the polymer and the adherend surface. Eight different processes were evaluated for bonding composite materials to steel structures. Wedge (crack growth), lap shear (fatigue and ultimate strength), and peel tests were completed on pristine and worst-case, environmentally-conditioned specimens to arrive at an optimum process for installing composite repairs. A field installation-friendly process was established that uses grit blasting, Silane chemical, and steel primer to produce a strong and durable bonded joint. In addition to being robust, the selected installation process is also inexpensive and uses readily available equipment and chemicals. Methods and equipment necessary for high-temperature and vacuum bag cures in the field were proven.

**Damage Tolerance** - One of the primary concerns surrounding composite doubler technology pertains to long-term survivability, especially in the presence of non-optimum installations. This test program demonstrated the damage tolerance capabilities of bonded composite doublers. The fatigue and strength tests quantified the structural response and crack abatement capabilities of Boron-Epoxy doublers in the presence of worst case flaw scenarios. The engineered flaws included cracks in the parent material and disbonds in the adhesive layer between the composite laminate and the steel structure. Environmental conditions representing temperature and humidity exposure were also included in the coupon tests. Stress, fatigue, and ultimate strength tests established the viability of composite doubler repairs to reinforce steel structures and minimize/eliminate the effects of cracks, corrosion or other flaws. As part of the performance testing, the repair designs were varied to quantify the relative importance of specific composite laminate features.

**Fatigue Performance** - If the optimum composite repair – protected sufficiently to minimize or eliminate the effects of environmental conditioning – is used as the final performance metric, the results presented above indicate that the fatigue life of steel structures can be extended by a factor of 2 to 10. Bonded composite doubler repairs can withstand 200,000 to 600,000 fatigue cycles while allowing little or no crack growth in the parent steel structure. These results were obtained for composite laminate designs that are 30% of the stiffness of the structure being repaired. These results were also obtained in the presence of extreme worst-case conditions including disbonds that removed 20% of the critical load transfer region in the doubler and also eliminated local reinforcement directly over the crack. Finally, the results are conservative since they were produced using stress spectrums that were up to three times as large as those measured in Syncrude equipment during normal operation.

**Stress/Strain Fields** - Strain field analyses for expected stress environments showed that the large disbonds, in excess of those which will be detected by NDI, and Boron-Epoxy water absorption did not affect the performance of the adhesive layer. The maximum doubler strains were found in the load transfer region around the perimeter (taper region) of the doubler. In all five doubler configurations, the strains monitored in this area were 50% - 80% of the total strain in the steel plate. For the normal stress spectrum, this value remained constant over four fatigue lifetimes indicating that there was no deterioration in the bond strength. During crack propagation, the stresses in the doubler increased to pick up the loads released by the plate. Data acquired during failure tests showed that the composite doubler was able to absorb stresses in the plastic regime and that extensive yielding of the steel was required to fail the installation. Also, stress risers, normally observed around flaws, were minimized by the doubler.

**Residual Strength** - Post-fatigue load-to-failure tests produced residual strength values for the composite-steel specimens. Even in the presence of severe worst case installations and extensive damage growth (fatigue cracks extending through 50% of the specimen width), it was seen that the doubler-reinforced plates were able to achieve residual tensile strengths (i.e. post-damage tensile strength) which exceeded the 65 ksi baseline value for this steel material. Thus, the Boron-Epoxy doubler was able to return the parent structure to its original strength and load carrying capability.

**Nondestructive Inspection** - Pulse-Echo ultrasonics can be easily implemented in the field using hand held inspection devices. Anomalies in A-Scan signals can be used to detect disbond and delamination flaws. The ultrasonic method developed in this study was shown to work well in mapping out flaw shapes and delineating the flaw edges. Even in the thick laminates needed for these repairs, pulse-echo UT is able to repetitively detect disbond flaws as small as 0.25" in diameter. Furthermore, the technique is able to map out a changing flaw profile - a cohesive failure in the adhesive caused by the crack propagating through the steel - during fatigue testing of the composite doubler. Crack detection in the parent steel material can be accomplished using conventional eddy current and X-ray techniques. Crack signals from the parent steel can be obtained through composite doublers in excess of 100 plies and greater than 0.6” thick.

The results presented in this report establish that composite doublers can be installed on steel structures to produce a superior repair with extended fatigue life. The use of composite doublers, which do not have brittle fracture problems such as those inherent in welds, can help extend the structure’s fatigue life and reduce the equipment downtime.

**This Page Intentionally Left Blank**

# Development of Bonded Composite Doublers for the Repair of Oil Recovery Equipment

## 1.0 PROJECT DESCRIPTION

### 1.1 Background

Advances in structural adhesives have permitted engineers to contemplate the use of bonded joints in areas that have long been dominated by mechanical fasteners and welds. Although strength, modulus, and toughness have been improved in modern adhesives, the typical concerns with using these polymers still exist. These include a strong sensitivity of mechanical properties to temperature change, concerns over durability in hot/wet environments, and an inability to quantify bond strength (i.e., identify weak bonds) in adhesive joints. As a result, deployment of bonded joints requires proper design as well as suitable surface preparation methods. This report describes a study into the use of bonded composite patches as a substitute for welding doubler plates to repair carbon steel structures.

Syncrude is one of only a few companies in the world that extracts oil from "oil sand" (bitumen) mineral deposits. The technique involves a mining operation followed by a mechanical and chemical process to produce crude oil. Syncrude is currently expanding it operations and opened up the first train of its first remote mining operation in July 2002. Current production targets of 260,000 barrels per day will expand to 465,000 by 2008 when the 2$^{nd}$ and 3$^{rd}$ trains come on line. Extreme fatigue, temperature, erosive, and corrosive environments induce an array of equipment damage. Shutdowns to repair equipment can cost in excess of $1M per day. As a result, any improvement in mining equipment operation and maintenance can lead to significant reductions in yearly operating budget. Almost all of mobile equipment has experienced different levels of cracking since operation started in 1978. This frequent occurrence of cracking is caused by high impact loads, high fatigue cycles, low operating temperature and large component size.

Figures 1 and 2 show several of the hydraulic and cable shovels along with the trucks used in the surface mining operation. The trucks hold from 240 to 380 tons of oil sand and can be filled in three to four passes of an excavation shovel. Fatigue cracks are commonly found in the body, arms, frames, and buckets of this equipment. The current weld repair techniques for these structures only provide a temporary fix that must be revisited on a regular basis. It is believed that the use of composite doublers, which do not have brittle fracture problems such as those inherent in welds, will help extend the fatigue life of Syncrude equipment and reduce the equipment downtime during mining operations. The bonded composite doubler repair technique was developed and validated for commercial aircraft in the Sandia Labs Airworthiness Assurance Center. The technique uses bonded composite laminates, or patches, in lieu of conventional, riveted or welded metallic doublers. Two of the main issues for adapting composite repairs to Syncrude applications were to develop an installation process for carbon steel structure and accommodating large repairs for structures up to 6" thick.

## 1.2 Goal of Effort

The goal of this program is to establish the viability of using bonded composite doublers to repair equipment used in the oil recovery industry. This includes the development and validation of installation, design, analysis, inspection, and quality assurance processes and the comprehensive performance assessment of composite doublers in the selected applications [1, 2]. The project will conclude with a complete technology transfer and integration of composite doubler repair technology into Syncrude's routine maintenance program. The end product will provide more cost effective and reliable repairs than those currently employed.


**Figure 1: Hydraulic Excavator**

**Figure 2: Cable Shovel**

## 1.3 Bonded Composite Doubler Repair Method

Figure 3 shows schematics of general composite doubler designs and basic design parameters such ply lay-up, ply orientation, patch shape and taper, and the bond layer. The number of plies and fiber orientation are determined by the nature of the reinforcement required (i.e. stress field and configuration of original structure). Sample composite doubler installations, showing two families of potential aircraft repair applications, are shown in Figure 4. The taper at the edge of the doubler is used to produce a gradually increasing stress gradient in the area of primary load transfer. A top ply of fiberglass is installed to supply mechanical and environmental protection for the installation. Flight demonstrations and operational testing have confirmed that under proper conditions, composite doublers can provide a long lasting and effective repair or structural reinforcement

It is believed that the use of composite doublers, which do not have brittle fracture problems such as those inherent in welds, will help extend the fatigue life of Syncrude equipment and reduce the equipment downtime during mining operations. The bonded composite doubler repair technique was evolved for U.S. commercial aircraft repairs at the Sandia Labs Airworthiness Assurance Center [3-8]. The technique uses bonded composite laminates, or patches, in lieu of conventional, riveted or welded metallic doublers to repair cracks, corrosion or other damage in metallic structures. Two of the main issues for adapting composite repairs to Syncrude applications are developing an installation process for carbon steel structure and accommodating

large repairs on structures up to 6" thick. Other impediments include the need to carry out the repairs in a field environment using a hot bonding process and dealing with complex and extreme three-dimensional stress fields in order to mitigate crack growth.

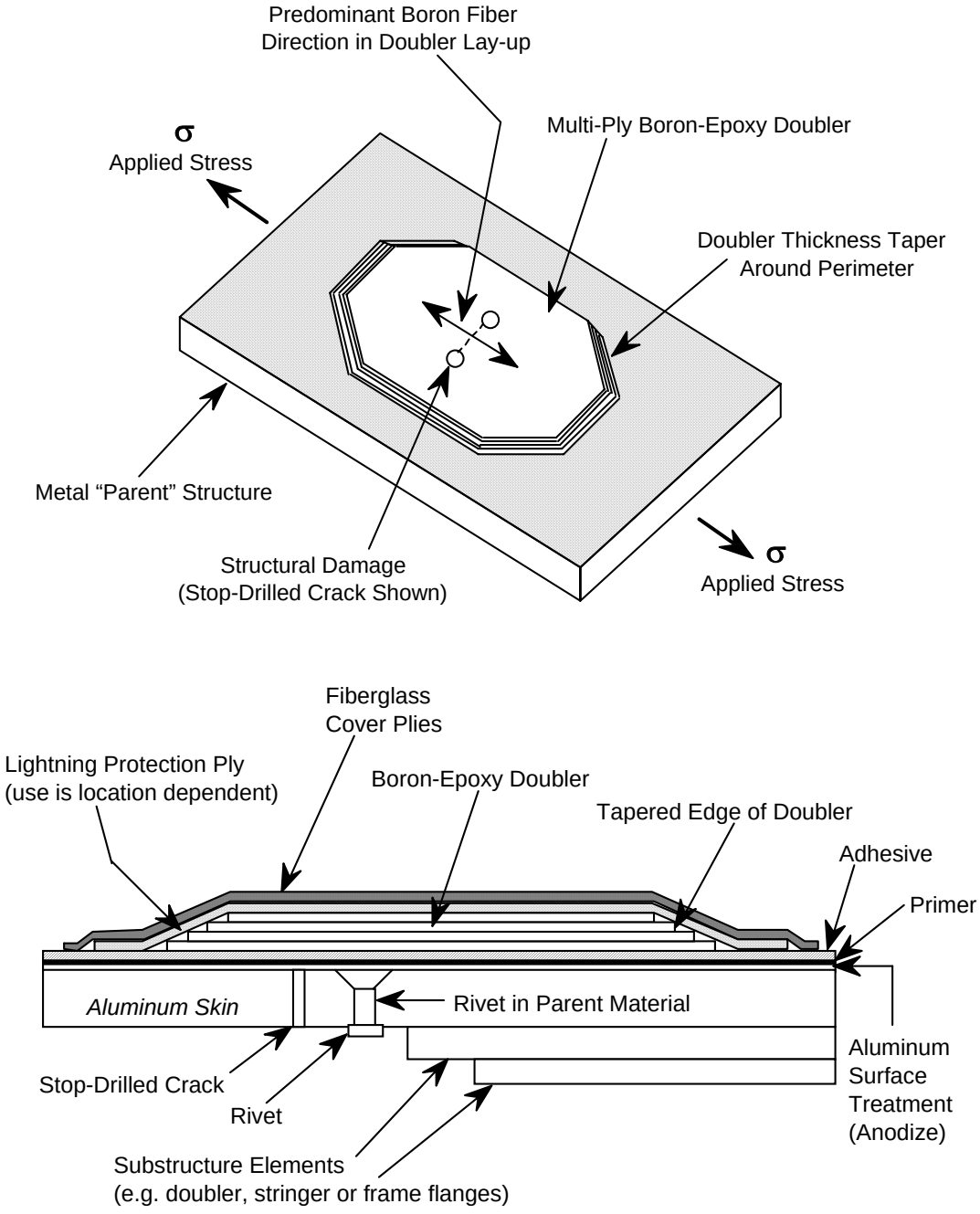


**Figure 3: Schematics Showing Bonded Composite Doubler Repair Method**

**Figure 4: Sample Composite Doubler Aircraft Repairs**

The repairs proposed in this study can best be described as a hybrid repair. First, the fatigue crack will be gouged out and the material will be replaced in a fill weld process. Next, instead of welding doubler plates over the damaged region or leaving the fill-weld as the only defense against crack re-initiation, a composite doubler will be installed using a hot bonding process [6-8]. It is believed that the fatigue performance of bonded composite doubler repairs will be superior to the equivalent welded connection in the high cycle, long life regime. This is due both to the lower stress concentrations and the minimization of the effects of inherent weld defects.

The advantages of the composite doubler repair approach include:

1. A bonded repair will help relieve the residual stresses brought on by traditional welding in thick structures. Adhesive bonding eliminates stress concentrations, and new potential crack initiation sites, caused by additional fastener holes or heat-affected weld regions.
2. Bonded repairs allow for rapid, coherent joining of materials. Load transfer occurs over the entire footprint of the doubler/adhesive (vs. discrete weld seams). The doubler can be tapered to gradually introduce the reinforcing effect. This greatly reduces stress concentrations associated with discretely fastened or welded repairs. The more uniform load distribution provided by bonded joints improves fatigue life.
3. Adhesive joints provide localized support around the damaged region thus providing better crack mitigation than traditional repairs. This phenomenon is shown in Figure 5 where the short spring of a bonded joint performs better than the long spring represented by fasteners or fillet welds that are spaced far apart.
4. Also, composite doublers can be tailored to meet specific anisotropy needs thus eliminating the undesirable stiffening of a structure in directions other than those required. The directional stiffness of composite doublers can be tailored to address the critical loads so that reinforcement is produced only in the necessary directions.
5. This repair resists corrosion which may eliminate the onset of stress corrosion cracking.
6. Composite laminates are easily formed to fit the contour of tight radius areas or complex shapes permitting the repair of irregular components.

7. Composite doubler repairs can be quickly installed so economic advantages stem primarily from time savings in repair installation and the secondary effect of reduced equipment downtime.

The high modulus of Boron-Epoxy composite material enables a doubler to effectively pick up load when bonded to a metal structure. Load transfer occurs by shear through the adhesive. Previous experience in aircraft applications has shown that the use of a single part toughened epoxy adhesive will produce optimum mechanical properties in the joint. All tests were conducted with AF163 adhesive which is cured with a hot bonding process. It is assumed that this film adhesive has sufficient gap filling properties to accommodate the small degree of surface irregularities expected in the Syncrude structures.

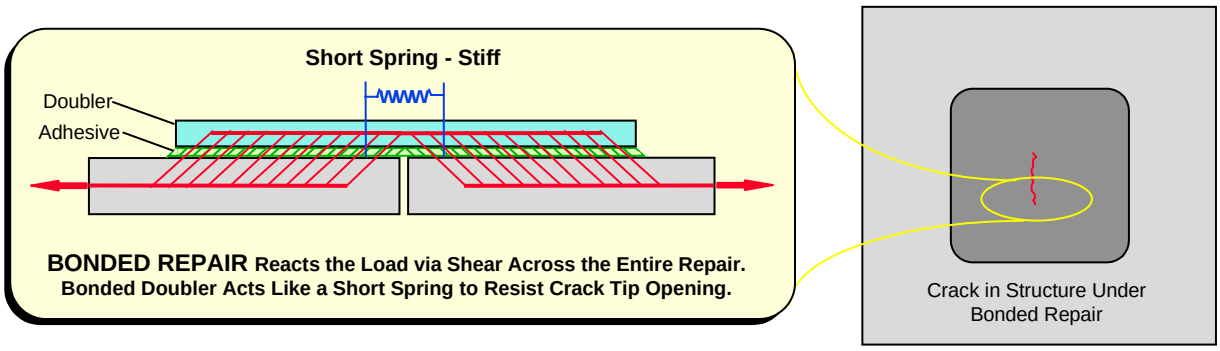


**A. Joint Continuity of Bonded Doubler Reduces Stress Levels in Damaged Region**

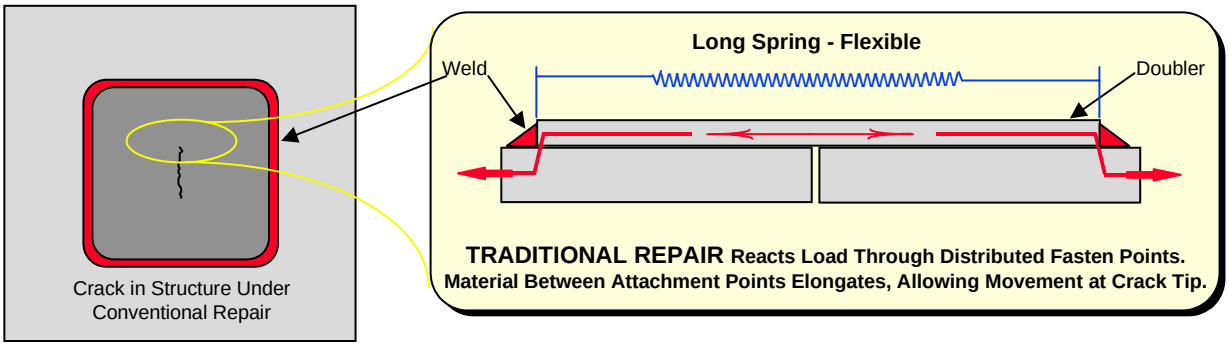


**B. Local Loading and Intermittent Connection Produced by Spaced Perimeter Welds**

**Figure 5: Short Spring Representing the Localized Crack Mitigation of Bonded Doublers Versus the Longer Spring That Allows Cracks to Open and Grow More Rapidly**

## 1.4 Project Task Overview

To demonstrate the capabilities of composite doubler technology, this project includes the following technical activities: 1) structural design of composite doublers, 2) development of doubler installation procedures, 3) structural evaluation of designs, 4) validation of inspection

procedures, 5) laboratory and full scale tests of composite doubler installations, and 6) real-time technology transfer through a Sandia Labs and Syncrude team. These activities will be carried out by Sandia Labs, Syncrude, and subcontractors as deemed appropriate in order to reliably integrate composite doublers into the oil recovery industry. The general issues which will be addressed are:

1. Patch Design and Analysis - critical patch parameters, stress and fatigue calculations that include damage tolerance analyses, and use of load spectra that represents Syncrude operating environment.
2. Patch Long Term Performance - strength, durability and reliability issues, flaw containment, optimum adhesive properties, and detrimental affects of operating environment.
3. Patch Installation and Surveillance - surface preparation, tooling, heat sinks, effect of underlying fasteners, field work, installer certification, quality assurance measures (nondestructive inspection (NDI) techniques to qualify and monitor repairs).

Engineering data, technical expertise, and project management experience gained from related efforts in the commercial aircraft industry will be used to guide and streamline this project. In order to demonstrate the promise of composite doublers before undertaking additional, focused tasks, this effort will be carried out in two distinct phases:

The joint proposal is set up in two phases:

1. Phase 1 is the "Technology Viability Assessment"

In this phase the suitability of this type of repair for Syncrude's mining equipment is evaluated. The first step of this stage is to identify a key damage location that would benefit and be suitable for this type of repair. In this phase the composite patch is designed and tested in the lab using environmental data collected in the field. A trial installation of the composite repair is done in the field on a unflawed structure. The information gathered in this test is used to do initial optimization of the design, fabrication and installation of the patch.

2. Phase 2 is the "Repair of Syncrude Structure and Technology Transfer"

In this phase of the project the development and validation of the installation, design, analysis, inspection and quality assurance of the composite doubler repair is finalized for our Syncrude application. In addition the technology is completely transferred to Syncrude through the use of training courses, installation specifications, quality assurance programs and project and technology transfer meetings. Syncrude will have full access to the technology and can transfer it to any group or contractor.

**Phase I: Technology Viability Assessment Tasks**

1. Identification of Repair Applications
2. Load Spectra Monitoring on Candidate Structure(s)
3. Development of Installation Process for Carbon Steel Structure
4. Generalized Testing: Doubler Performance Assessment in the Laboratory
5. Demonstration Repair Installation Including Heat Source/Sink Evaluation
6. Fabrication and Installation Procedures
7. Inspection Procedures

**Phase II: Doubler Installation on Syncrude Structure and Technology Transfer Tasks**

1. Completion of Doubler Designs
2. Analysis of Repair Applications
3. Installation on an In-Service Syncrude Structure and Personnel Training
4. Technology Transfer Activities

## 1.5 Applications Identified

Two trips to the Syncrude site and associated meetings with plant engineers identified the following potential repair applications:

1. Hydraulic and cable shovels – primarily the shovel booms and sticks (see Figures 1-2)
2. Cable shovel revolving frame (body) at window cutout
3. Conveyor belt truss structures (see Figure 6)
4. Mechanical tumbling drums (see Figure 7)
5. Fluid cylinders on tanker trucks
6. Vibrating screens for filtering (see Figure 8)
7. Shovel buckets (see Figure 9 and Section 2.4)
8. Boxes on mining trucks (see Figure 10)
9. Truck frames – stringers and bolsters especially at hinge region (see Figure 11).


**Figure 6: Conveyor Belts Transfer Oil Sands to Cyclofeeder for Hydrotransport**

**Figure 7: Tumblers Initiate the Separation Process in the Extraction Plant**

## 1.6 Downselection to First Repair Target

It was determined that the best, first use of composite doublers is as part of an overall repair method that also includes a weld process. Cracks in structures will first undergo a material removal (gouge) and replacement (weld) process. This is currently the final step in the repair procedure. However, in most instances, fatigue cracks reappear in the weld fill areas. Composite doublers will be installed over these weld regions in order to produce a superior repair with extended fatigue life.


**Figure 8: Vibrating Screen for Filtering Initial Mining Products**


**Figure 9: Hydraulic Shovel Bucket**


**Figure 10: Truck and Truck Box Structure for Oil Sands Mining Operation**

**Figure 11: Mining Truck Frame and Crack Area at Bolster-to-Box ¾" Fillet Weld**

**Cable Shovel Boom** – The Bucyrus-Erie 395B cable shovel boom was chosen as the best application for our initial repair. Figures 12 shows two views of the boom mounted and removed from the cable shovel, respectively. It can be seen that this is a split, two pronged boom. The favorable features of this repair include: manageable wall thickness (7/8" and 1 ¼"), good accessibility, relatively low expected stress levels, and no structural impediments (complex geometry). Figures 13 and 14 show close-up photos of regions repaired with fill welds only. Typical cracks found on the shovel boom are pictured in Figure 15. Figure 16 shows the temporary repair process that uses seam-welded fish plates (steel doublers) to quickly repair boom cracks so that the shovel can continue to operate until planned maintenance can complete the more robust fill-weld repair. Multiple plates are applied as the crack continued to grow across the width of the shovel boom. Figure 17 shows a boom plate crack as it propagates out from under the fish plate and around the corner into an adjacent boom plate.

Other desirable aspects of the shovel boom application are:

- Syncrude maintains an extra boom. This spare boom can be switched with a damaged boom and the shovel can be returned to service. As a result, our repair process will: a) not be rushed, and b) have no adverse effect on Syncrude production.
- The boom can be moved inside Syncrude's shovel maintenance facility. This will eliminate many of the remote, field repair obstacles and substantially reduce the heat sink impediment, especially for Winter repairs.
- Crack history – There is some data available that quantifies the performance of the fill-weld only repairs. In addition, Syncrude is launching a complimentary study to log crack failures at the site, the associated maintenance strategies, and the operational history of the repairs. This information will provide a critical basis of comparison as we evaluate the success of our composite doubler repair method.
- Boom information – The steel plate material has a Canadian specification of CSA-G40.21-92 which is ASTM A633 ($\sigma_u$= 70-90 KSI; $\sigma_y$=50 KSI; elongation = 22-25%). The specific chemical composition that we are trying to match is: $C_{max}$ 0.20,

Mn 1.15/1.5, $S_{max}$ 0.05, $P_{max}$ 0.04, Si 0.15/0.50, and Cb 0.01/0.05. In 6 months of operation, it is estimated that the boom will experience close to 260,000 load cycles.


**Figure 12: Cable Shovel Boom and Split Boom Removed from Shovel**

**Figure 13: Fill-Weld Repair on Boom Side Plate**

**Figure 14: Fill-Weld Repair on Side Plate**

**Figure 15: Typical Cracks Found in the Shovel Boom**

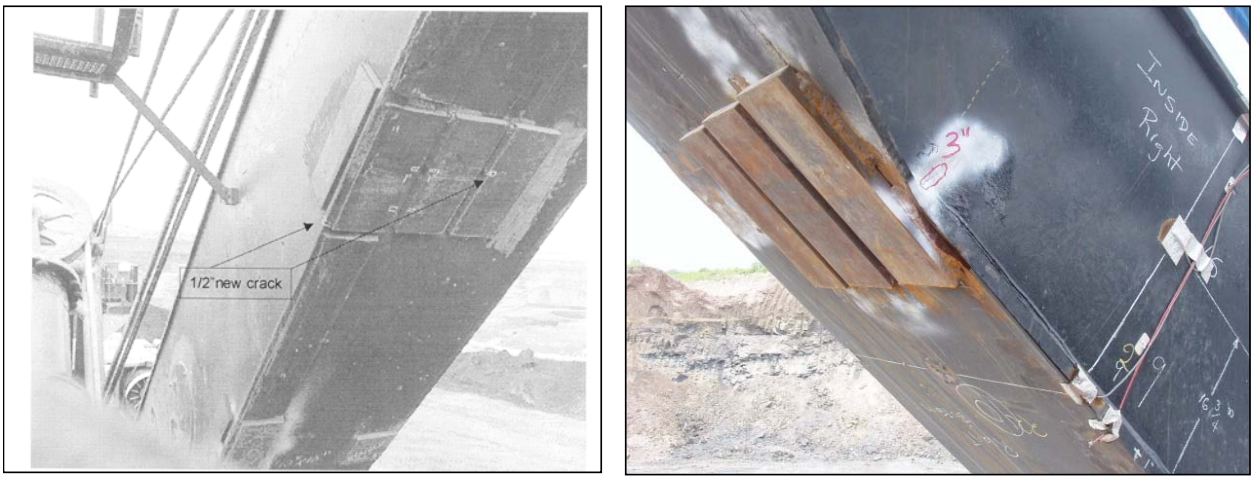


**Figure 16: Series of Fish Plate Repairs to Slow the Growth of a Propagating Crack**

**Figure 17: Crack in Boom Plate Emanating Around the Corner from a Fish Plate Welded Repair**

**This Page Intentionally Left Blank**

## 2.0 COMPOSITE DOUBLER INSTALLATION PROCESS ON CARBON STEEL STRUCTURES

Metal treatment prior to bonding is a key factor for both the initial adhesion of a bonded joint and its long-term environmental durability. Current metal prebond surface preparations are either inconvenient or complex to use, contain hazardous materials (e.g. strong acids), and/or do not provide the performance necessary for successful long-term, durable bonds. Past bond failures, primarily due to inadequate surface preparation, have been a limiting factor in the current use of bonded hardware, especially for primary structure. The portion of the program presented here determined the optimum surface preparation in order to meet both the bond strength and bond durability requirements.

### 2.1 Surface Preparation Options

Before moving into component level and full scale testing on simulated Syncrude repairs it was first necessary to certify a chemical bonding process for steel structure and verify the associated strength of the critical adhesive layer. The prebond surface treatment to which steel is subjected can significantly influence the resultant initial strengths and long-term durability provided by such bonds. The key to structural bonding is that the adherend surfaces must be roughened and free from contamination and weak oxide layers. Proper surface preparation will produce these features on the material and will allow for a reliable joint with sufficient strength and durability [9]. In order to optimize surface preparation, the basic mechanisms of adhesion must be considered. The adhesive must be able to wet the entire surface of the adherend so that there is intimate molecular contact at the joint interface. There are two basic mechanisms of adhesion for structural adhesive bonding: 1) mechanical interlocking of the polymer with the adherend surface, and 2) chemical enhanced bonding of the polymer molecules with the adherend surface layer. Both of these mechanisms were pursued using a tailored set of surface preparation options.

Since this study is aimed at field installation in industrial settings, it is necessary to use simple, repeatable, and economically viable processing procedures. Sophisticated chemical surface treatments are too expensive or complicated to produce repeatable results. Ultra high temperature and high pressure processes are also not feasible in the field. To date, bonded composite doublers have been used on thin aluminum structure and the surface preparation used a phosphoric acid anodize etch. This approach requires a tailored phosphoric acid containment system that is time consuming to apply and potentially hazardous in the repair applications for this program. Another chemical process was developed for the surface preparation procedure on Syncrude carbon steel structures to produce optimum strength in the bond joint. The surface preparation options evaluated in this study were selected on the basis of strength and durability, as well as, their ability to be carried out in heavy industrial settings.

The matrix of surface preparation options is summarized in Table 1. The surface degrease step involved an application of Acetone followed by residue removal using Methyl Alcohol. Surface roughening for mechanical interlocking was provided by grit blasting or a simple oxide removal and sanding process. The surface chemistry was changed in some of the options through the

application of silane, Sol-Gel, or Pasa-Jell. Finally, different primers were applied to assess any durability improvements they might provide in extreme environments. A description of each of these processes follows along with some discussion on several other surface preparation options that were eliminated from consideration prior to any testing.

*Surface Roughening*

Roughening surfaces prior to bonding enhances the strength of adhesive joints. The abrasive process removes contaminated layers, including hard-to-remove oxide layers, and the roughened surface provides some degree of mechanical interlocking with the adhesive. The process also forms a larger effective surface area for the bond and can introduce physical/chemical changes which affect surface energy and wettability. All of these issues must be considered in light of the characteristics of the adhesive and its ability to spread on different surface textures.

Experience has shown that any relatively smooth surface bonded to structural epoxy adhesives will suffer rapid delamination during conditions of high stress and humidity. Rougher surface morphology allows for better adhesion and resistance to the damaging effects of moisture. The task of providing a fine scale, stable, repeatable, rough surface on low carbon steels is difficult due to the surface condition, heat treatment, and metallurgical complexity of the steel materials. For these reasons, along with field installation impediments, chemical etching was eliminated from consideration.

Prior to roughening the surface, Scotch-Brite abrasion was applied to remove any oxide coating and debris. Additional grease and surface residue was removed with an alcohol cleaning. The relationship between surface texture and adhesion is complex and the relative magnitude and interactions of these different mechanisms need to be understood to optimize abrasive surface treatment processes. The grit blast process is used extensively to provide a clean and uniformly roughened surface for high strength bonding applications [10]. In this study, various grit blast energy levels were applied to the carbon steel plates in order to determine the best surface roughening performance for the hardness of our material. Related information from bonded repairs on aircraft was used to select grit type (aluminum oxide) and grit size (50 μm). In addition, the degree of surface roughness (≈50 μinch RMS) was chosen to match the level that produced optimized adhesion tests in aluminum bonds that utilized the same adhesive. This roughness number represents the average departure of the surface profile from the mean plane.

The relationship between the grit blast delivery pressure (energy level) and the corresponding surface roughness was determined. It was found that a 60 psi grit blast on carbon steel (ASTM 572) produced a similar surface roughness as a 40 psi grit blast on aluminum (2024-T3) during aircraft repairs. Filtering and drying systems were added to the compressed air supply line to reduce contamination. Figure 18 shows the test specimen preparation using the portable grit blast system. After blasting, a jet of clean air was blown across the surface to remove loose grit particles. The chemicals listed in Table 1 were then applied generously using brush-on or spray applications such that any contaminating residues were rinsed from the surface. To determine the feasibility of a quicker surface roughening option, hand sanding was included in the test matrix. Zirconium oxide sanding paper was applied in two perpendicular directions to produce a

scratched surface that was sufficiently roughened but much less uniform in appearance. Figures 19 and 20 compare two surfaces that were grit blasted and hand sanded.

| Option | Scotch-Brite Abrade & Degrease | Grit Blast | Blow Off Surface -Oil-Free Air | Post Blast Degrease | Chemical Treatment & Heat Lamp Dry | Primer & Air/Heat Lamp Dry |
|---|---|---|---|---|---|---|
| 1 | ✓ | ✓ | ✓ | - | Sol-Gel | BR-6747 |
| 2 | ✓ | ✓ | ✓ | ✓ | Sol-Gel * | BR-6747 * |
| 3 | ✓ | ✓ | ✓ | ✓ | Pasa-Jell * | BR-6747 * |
| 4 | ✓ | ✓ | ✓ | ✓ | - | BR-6747 |
| 5 | ✓ | ✓ | ✓ | ✓ | - * | - |
| 6 | ✓ | ✓ | ✓ | - | Silane * | BR-6747 * |
| 7 | ✓ | ✓ | ✓ | - | Silane | BR-127 |
| 8 | ✓ | ✓ | ✓ | ✓ | Silane | BR-6747 |
| 9 | ✓ | SAND | ✓ | ✓ | - | BR-6747 |

* Corrosion assessment coupons; 2 at each condition indicated

**Table 1: Surface Preparation Options for Adhesive Bonding**

**Figure 18: Grit Blast of Steel Surface Using 50 Micron Aluminum Oxide Grit Applied at 60 PSI**

**Figure 19: 50X Microscopic View of Grit Blasted Surface at 60 PSI (Surface Roughness = 52 μinch RMS)**

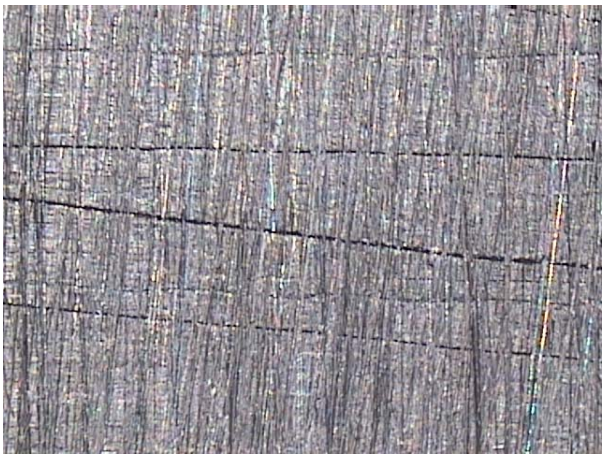

**Figure 20: 50X Microscopic View of Hand Sanded Surface (Nonuniform – no roughness value)**

*Chemical Interlocking*

**Coupling Agents** – Silane chemicals have been used to promote adhesion [11-12]. Use of the silane with a chemically compatible primer provides enhanced durability in hot-wet conditions. Figure 21 shows a schematic of the silane layer being produced on the metal surface to enhance the bonding process. In this study the silane chemical was mixed with distilled water in a 99:1 ratio and then brushed directly onto the grit-blasted steel surface. The silane was applied as follows: 1) 1% diluted mixture was brushed on with a natural hair brush such that the liquid flow was sufficient to check for a water break-free surface, 2) the surface was wetted for 10 minutes with brush applications, 3) the surface silane was blown off with instrument quality air, and 4) excess moisture was driven off via a heat lamp dry (120-150$^{o}$F for 20 minutes). If streaks are noted during the blowing process, it indicates the presence of grit and the silane wetting process is repeated to remove excess grit. Aircraft repairs employ a complete cure of the silane coating at 200$^{o}$F for 60 minutes. In order to cure the composite doubler and adhesive film, the structure must be heated to 225$^{o}$F. Since heating the massive, steel structures more than one time is impractical, this effort evaluated a co-cure process wherein final cure of the silane was achieved simultaneously with the adhesive.

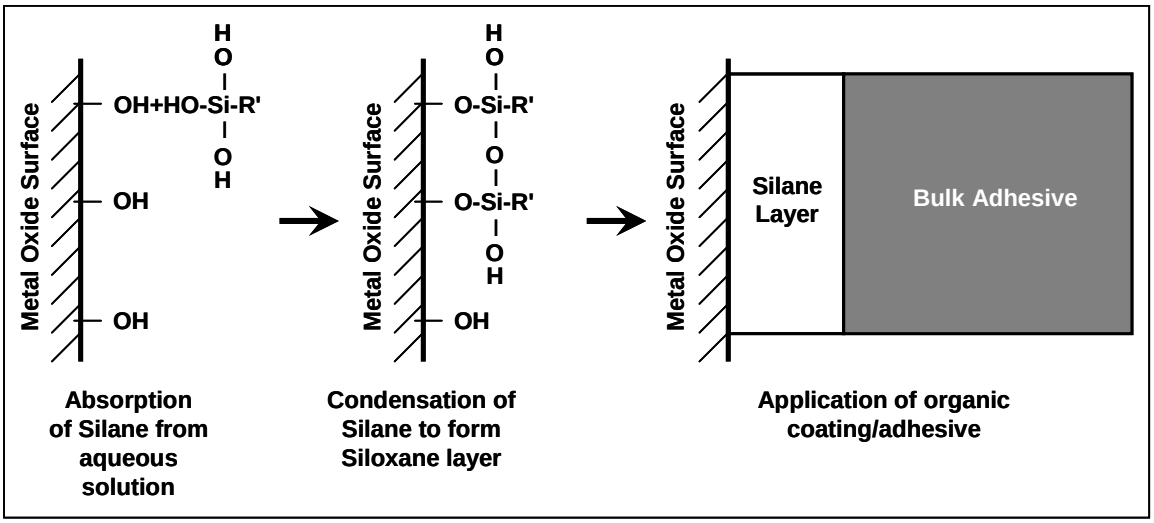


**Figure 21: Schematic of Silane Layer Formed on Steel Surface to Promote Bonding**

Sol-Gel is another prebond surface treatment that facilitates adhesive bonding to metallic surfaces [13]. Sol-Gel formulations developed by Boeing were designed to work optimally with aluminum alloys, however, successful testing has already been completed on stainless steel alloys. This study attempted to extend Sol-Gel use to carbon steel materials. The water based Sol-Gel chemistry develops thin coatings that produce a gradient from the metallic surface, through a hybrid inorganic/organic layer, to the organic epoxy resin (adhesive). Enhanced adhesion is produced by the chemical interaction at the interfaces between the metal and the Sol-Gel and the Sol-Gel and the primer. The Sol-Gel was applied in the same fashion as the silane chemical mixture. It was also co-cured with the epoxy adhesive in a single heat cycle.

**Conversion Coatings** - A number of chemical conversion coatings have been researched as surface treatment alternatives to degreasing, grit blasting, or other coupling agents such as silane or Sol-Gel [11]. These conversion coatings offer the potential for high treatment rates. They produce varying degrees of surface organic material and complex oxide coatings. Zinc and iron phosphate treatment solutions can precipitate crystallites onto the steel surface.

Surface analysis and mechanical joint testing have demonstrated high strength and durability in bonded joints prepared with these chemicals. However, one of the main problems with these chemicals is the formation of a loosely adhering layer of iron oxide "smut" that is difficult to remove before bonding but easily pulls away with the adhesive when the joint is stressed. If the grain size is not carefully controlled, the coating thickness becomes so great that one phosphate crystal precipitates on another and a weak interface is produced. Heat cure epoxies, such as the AF-163 film adhesive used in this study, are especially susceptible to this problem as thermal stresses between the thick conversion coating and the steel substrate can create fractures in the coating. Thus, this steel treatment has a high potential to fail at the metal/metal oxide interface at lower stress levels than expected for the other surface preparation options.

Another major problem with chemical conversion coatings is that the nature of the resulting surface topology is a function of the metallurgy of the substrate. As a result they do not provide

consistent results and, in general, offer no performance enhancement over the more easily monitored and uniform grit blast technique. Because of these application drawbacks and concerns over achieving repeatable results, chemical conversion coatings were eliminated from consideration in the surface preparation test matrix.

**Steel Chemical Etchants** - Effective chemical etching treatments for carbon steels have not been found. Unlike aluminum and titanium, iron does not form coherent, adherent oxides, so it is difficult to replicate the fine microroughness needed for good adhesion found on other substrate materials. Although various chemical etchants have been tried for both low carbon and stainless steels for many years, none has been widely adopted or shown to be superior to grit blasting [14]. One traditional etching chemical for aluminum bonding was considered in this study: Pasa-Jell.

Pasa-Jell is formulated for treatment of aluminum and titanium materials and has been shown to improve bond strength in these alloys by cleaning and producing a surface microroughness. It has a high content of nitric and chromic acids and is used for corrosion removal and surface etching. It also contains chemical activators and inhibitors that can improve the hydrolytic stability of an interface. Pasa-Jell is inorganically thickened to permit application in localized areas and on vertical or overhead surfaces. In this study, the extrapolation of Pasa-Jell to carbon steel materials was evaluated by coating the adherend surface with this paste and removing the residue with a water rinse. However, exposure times well beyond the routine 10-15 minutes failed to produce any appreciable change in the carbon steel surface. In fact, much of the oxide layer was still intact after almost 30 minutes of exposure to Pasa-Jell. These bench top tests eliminated the Pasa-Jell surface treatment (Option 3) before any specimens were manufactured. This was not a highly desirable surface treatment option anyway since it involved the use and disposal of hazardous materials.

*Primers*

To achieve satisfactory bonding with metals, it is often necessary to use primers. Metal surfaces that have been freshly abraded are highly reactive and will undergo rapid interaction with water or organic contaminants. Primers protect surfaces from contamination and improve overall bond performance. Based on their performance in aircraft applications and for both aluminum and steel materials, two different waterborne, chromate primers were evaluated: Cytec Fiberite BR6747 (40-72$^{o}$F storage) and BR127 (0$^{o}$F storage). The BR6747 primer is more easily applied in field applications because: 1) it can be stored at room temperature, and 2) it can be co-cured with the adhesive. The BR127 primer is designed to be cured immediately after application and prior to installing the adhesive. However, due to the reasons cited above the BR127 primer was co-cured simultaneously with the adhesive during this investigation.

*Corrosion Assessment During Surface Preparation*

At various stages of the surface preparation process, test coupons were produced to assess the effects of exposure to atmospheric conditions. The tests were used to determine if corrosion or other bond inhibiting coatings would form on the steel surfaces during any steps of the surface preparation process. Two coupons were produced for each of the six conditions indicated in

Table 1. These conditions cover before and after chemical treatment and before and after primer applications. The coupons were exposed to medium (60%) and high (90%) relative humidity for two days after the steps marked by asterisks in Table 1. During field repairs, it is anticipated that there will be unexpected delays in moving from one installation step to another. These tests evaluated the possible deterioration in a surface that might occur during such delays. However, the humidity chamber tests revealed that there was no degradation in the prepared surfaces nor did any corrosion form in 48 hours of exposure.

## 2.2 Evaluation of Surface Preparation Options

The purpose of mechanical testing of adhesive bonds is three-fold: to provide engineering design data, to serve as a quality control procedure, and to evaluate the performance and relative merits of various bonding processes. The joint strength and durability tests described below provided information on all three of these items, however, the primary goal was to rank the viability and effectiveness of the candidate surface preparation options.

The tests were performed using a series of coupon test specimens that were designed to approximate essential features and test critical elements of our repair. The adherends were mild steel (ASTM A607) similar to the highly weldable steel used in large shovel and truck construction. The specimens were lap shear, wedge-loaded, and cleavage peel coupons as shown in Figures 22 through 24, respectively.

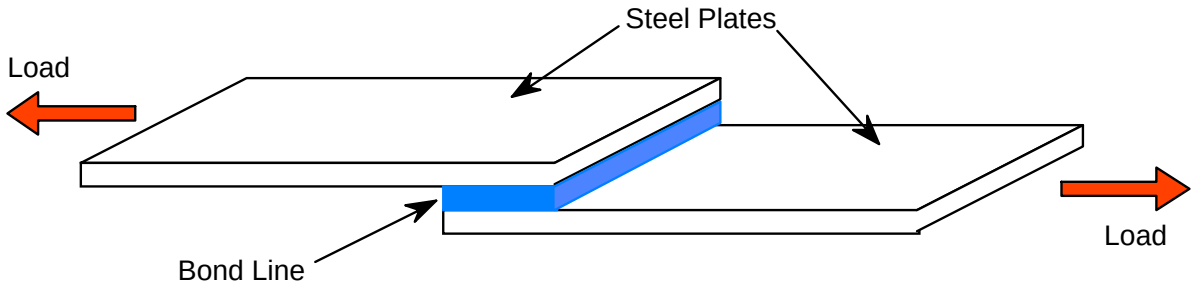


**Figure 22: Lap Joint Shear Strength Test of Bonded Metal Specimens by Tension Loading With Secondary Bending**

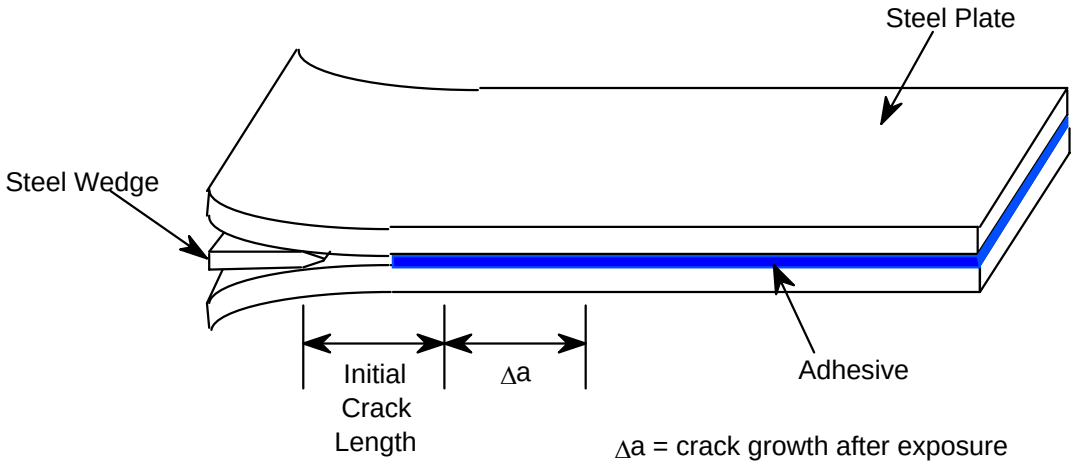


**Figure 23: Wedge Test to Measure Durability of Adhesive-Bonded Surface**

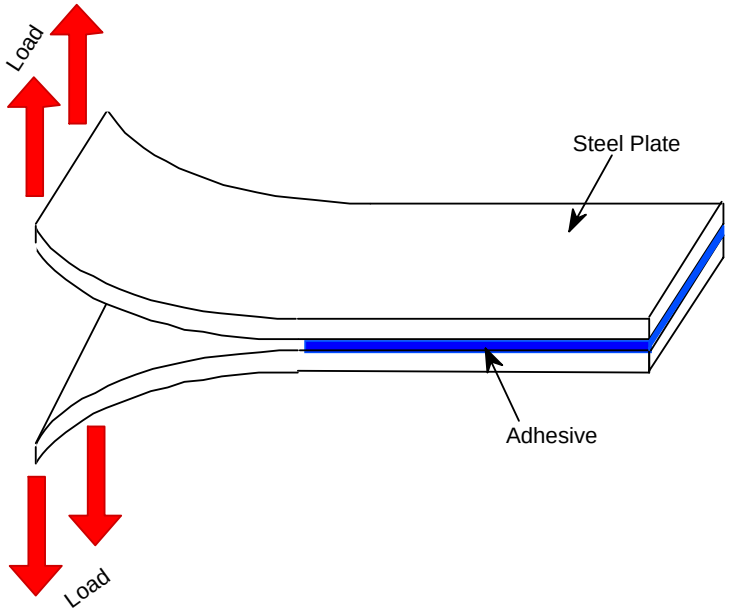


**Figure 24: Cleavage Peel Test to Determine Crack Extension and Arrest Parameters**

A series of coupon tests were conducted to quantify the strength and durability of the bonding process. Similar tests were repeated to evaluate performance in extreme operating environments. Table 2 lists the matrix of coupon failure tests for the specimens shown in and Figures 22-24. Previous studies have shown that water absorption, represented by the hot/wet conditioning, is the primary cause of performance reduction. This environmental conditioning, followed by testing at temperature extremes, is included in all appropriate coupon testing.

| Environmental Durability Tests – Carbon Steel Bonding Process Certification | | | | |
|---|---|---|---|---|
| **Test** | **Test Environment** | **No. of Specimens** | **Minimum Requirement** | **Specimen Figure No.** |
| Lap Shear (0.125" th. adherend; 1" overlap) (0.063" th. adherend; 0.5" overlap) | 75°F | 5 | 4.2 KSI | Fig. 22 |
| | -65°F | 3 | 4.2 KSI | |
| | 180°F | 3 | 3.1 KSI | |
| | hot/wet* @75°F | 5 | $X_{min}$ | |
| | hyd. fluid $^{\Delta}$ @75°F | 3 | $X_{min}$ | |
| | | | | |
| Lap Fatigue (0.125" th. adherend; 0.5" overlap) (0.063" th. adherend; 0.25" overlap) | 75°F | 3 | 500K cycles | Fig. 22 |
| | hot/wet* @75°F | 3 | 500K cycles at 1500 PSI | |
| | | | | |
| Creep Rupture (1600 PSI load for 192 hours) | 75°F | 3 | $\Delta d_{max}$ = 0.015" | Fig. 22 |
| | | | | |
| Adhesive Crack Extension (Fixed Displ., End Bolt Load for $G_{Iscc}$) (Alt. Surface Durability Wedge Test) | 75°F | 5 | $G_{Iscc}$ = 3.5 lb/in | Fig. 23 |
| | hot/wet* @75°F | 5 | 70% of $G_{Iscc}$ unconditioned | |
| | hot/wet* @-65°F | 5 | 70% of $G_{Iscc}$ unconditioned | |
| | | | | |
| Adhesive Crack Extension (Split Pin Test for $G_{Ia}$ & $G_{Ic}$) | 75°F | 5 | $G_{Ic}$ = 8 lb/in | Fig. 24 |
| | -65°F | 5 | $G_{Ia}$ = 6 lb/in | |

* Hot/wet condition represents 30 day exposure to 100% RH @ 120°F or 10% moisture absorption by weight.

$\Delta$ 7 day immersion in hydraulic fluid

$X_{min} = X_q - 3.064S_q$ where $X_q$ and $S_q$ are the mean and standard deviation values from unconditioned tests

$G_{Ic}$ = Critical crack extension force (crack initiation)

$G_{Ia}$ = Arrest crack extension force

$G_{Iscc}$ = Environment crack extension force (crack arrest under aqueous exposure)

**Table 2: Summary of Mechanical and Environmental Durability Tests to Assess Various Carbon steel Bonding Processes**

Lap Ultimate Shear (Fig. 22) - Two bonded plates are pulled apart longitudinally to determine ultimate shear strength of the adhesive.

Lap Tension Fatigue (Fig. 22) - Two bonded plates are cyclically loaded longitudinally in tension to determine fatigue strength of the adhesive bond.

Wedge Crack Growth (Fig. 23) - A wedge is inserted between two bonded steel plates. This test combines the effects of stress and aging environment.

Cleavage Peel & Critical Crack Extension (Fig. 24) - Two bonded plates are pulled apart perpendicularly along one edge until a crack begins to propagate along the bond line.
Cleavage Peel – Crack Arrest (Fig. 24) - Same as above but the crack arrest load is the maximum load that can be exerted on the joint without further crack growth.

The lap tests provided the ultimate shear strength of the adhesive bond as well as the modulus values for the adhesive. In the wedge test, a wedge is inserted 0.75" into a 1" wide by 6" long coupon. The resultant crack growth is measured over time as the bonded joint is exposed to various environmental conditions. Both test series used 3-4 specimens at each condition and the average results are reported.

A single part, heat cured film adhesive (AF-163) was used to bond all of the test specimens. This adhesive has been shown to provide high strength and durability in the extreme hot, cold, and wet conditions experienced by aircraft. The adhesive was cured for 2 hours at 225$^{o}$F and 8 psi (simulating vacuum pressures attainable in the field). Hot-wet conditioning was achieved by 30 day exposure to 100% RH at 140$^{o}$F. In addition, zero degree conditioning was used to study the performance of the bonded joints during winter operation. These environmental exposures were followed by coupon testing at the hot (140$^{o}$F) and cold (0$^{o}$F) temperature extremes. Ambient conditioning and testing was also conducted to complete the range of expected operating conditions and to provide baseline data.

### 2.2.1 Wedge Test

The wedge test specimen combines the effects of stress with aging environments of temperature and humidity. Figures 25-27 show the crack growth as a function of exposure time to the various environments. In most of the samples, a significant percentage of the total crack growth takes place in the first 48 hours when the driving force for the crack is at its maximum. The crack growth tends to stabilize towards a particular value after about 200 hours of exposure. The total crack growth, however, depends upon the surface preparation process used for the joint. The more extensive crack growth in Figure 27 (hot/wet), versus growth measured in the Figure 25 (room temperature) and 26 (cold) conditions, show that water absorption, represented by hot/wet conditioning, is the primary cause of performance reduction.

At ambient conditions, Figure 25 shows that the surface with no chemical treatment (Option 4) performed the best followed by the co-cured silane-primer options (Options 6 & 8). As expected, all of the results are tightly clustered with only a 12% separation between the shortest and longest crack growth. At zero degrees (Figure 26), Option 4 continued to perform the best followed by both the silane and Sol-Gel surface treatment options. It is here that the benefits of grit blasting begin to appear as the hand sanding Option 9 allows for almost twice the crack growth as the other grit blast processes. The primary benefits of grit blasting and the use of primers are seen in the performance of the bonds in hot/wet conditions. Figure 27 contains the largest spread in results with both the silane (Options 6 & 8) and Sol-Gel (Option 2) processes performing the best. Interface durability is a major limitation in the adhesive system. The addition of silane clearly improved interfacial durability. Use of primers – coupling agents that effectively stabilize the iron surface against corrosion – also improved the long term durability of the joint. Surprisingly, Option 4 with no chemical treatment continued to compare well, however, the lap shear results will determine if this good crack mitigation ability is accompanied

by sufficient adhesive strength. The hand sand (Option 9) and non-primer (Option 5) methods performed the worst with crack growth approximately 95% greater than the optimum processes.

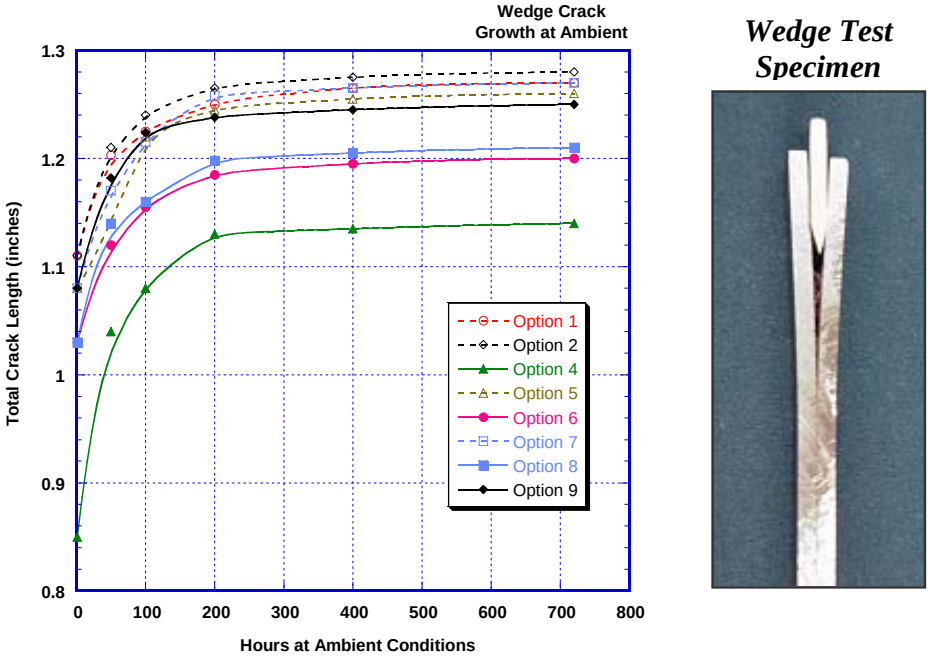


**Figure 25: Comparison of Wedge Crack Extension for Eight Surface Preparation Options - Carbon Steel Bonds at Ambient Conditions**

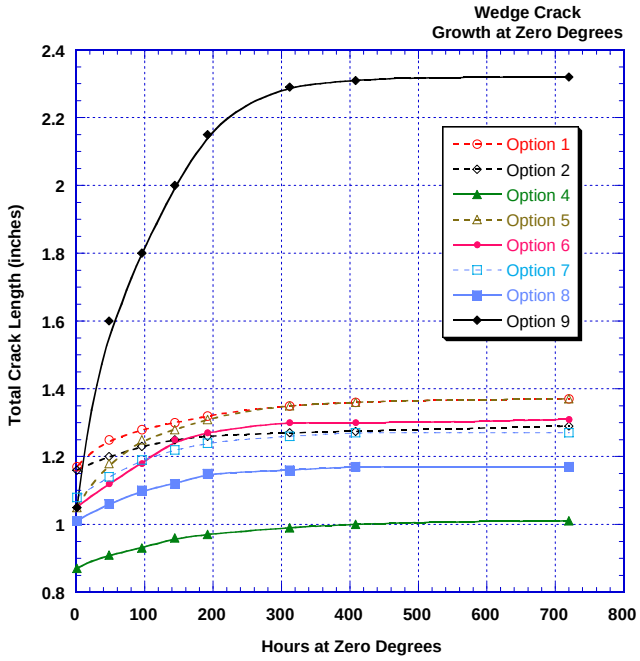


**Figure 26: Comparison of Wedge Crack Extension for Eight Surface Preparation Options - Carbon Steel Bonds at Zero Degree Conditions**

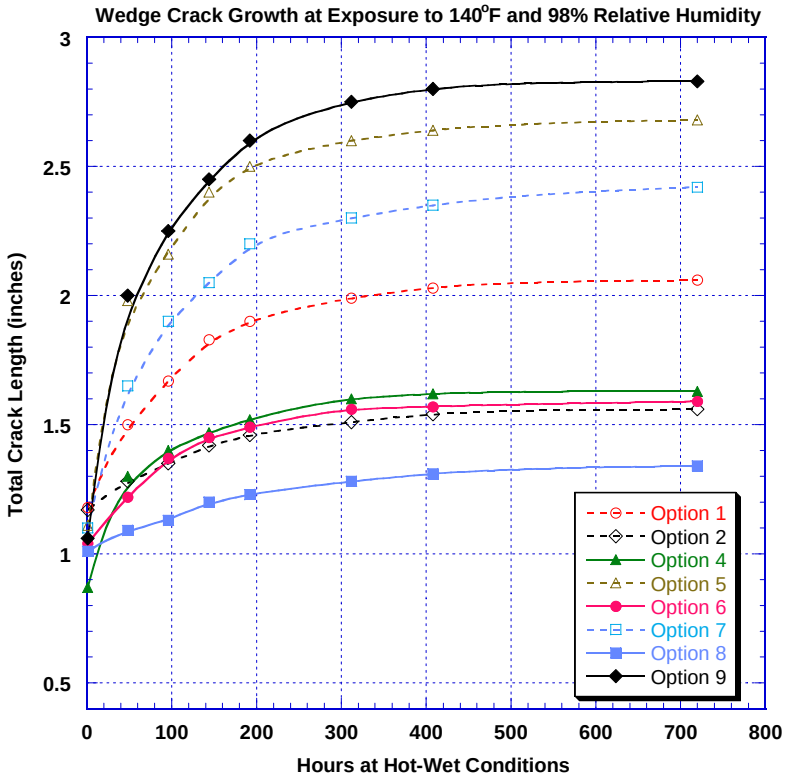


**Figure 27: Comparison of Wedge Crack Extension for Eight Surface Preparation Options - Carbon Steel Bonds at Hot/Wet Conditions**

Figure 28 shows the extreme deformation required to fail the wedge test specimens. Threaded holes were machined into the ends of some wedge tests specimens. Two opposing bolts were then used to produce enough deformation to fracture the adhesive layer. The goal was to demonstrate that adhesive products would appear on each side of the mating steel plates (see lower left photo in Fig. 28). This indicates that the mode of failure was adhesive (vs. cohesive disbonding) and that the full strength of the adhesive material was achieved.

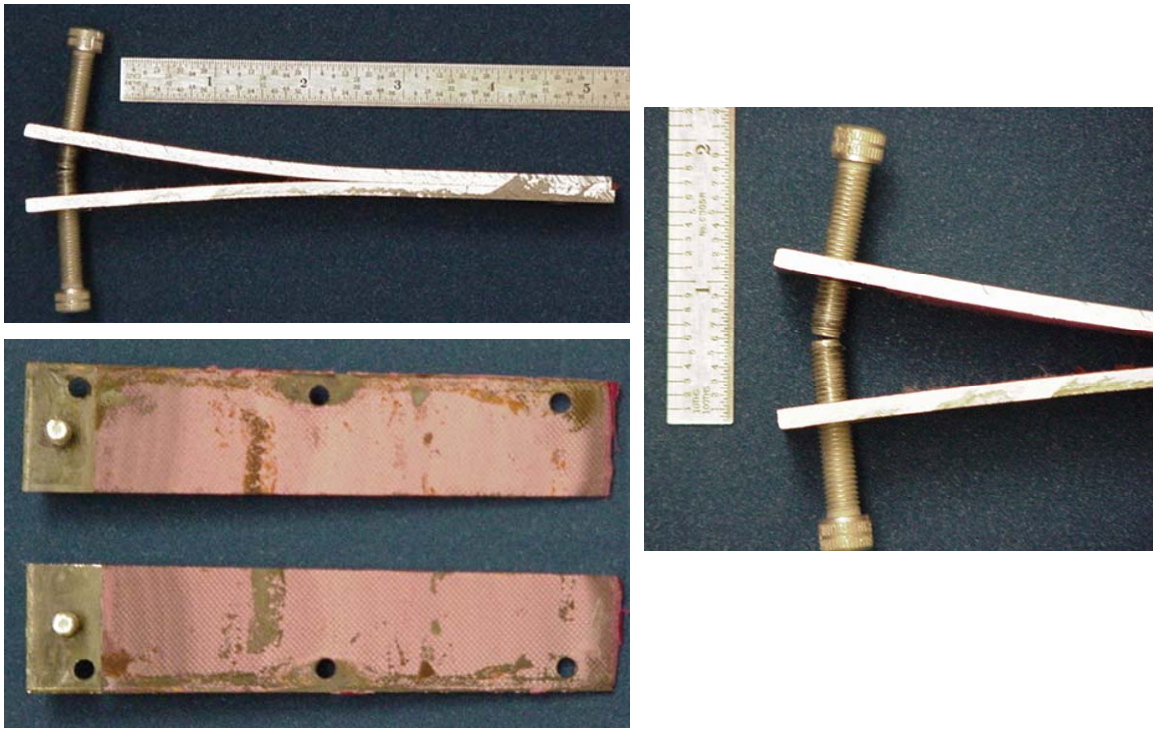

**Figure 28: Extreme Wedge Test Needed to Fail Adhesive and Proof of Optimum Cohesive Failure Mode of the Adhesive**

### 2.2.2 Lap Shear Ultimate Failure Tests

The lap shear results are presented as histograms in Figure 29. This test series used 3-4 specimens at each condition and the average results are reported. At ambient conditions, the Sol-Gel and silane processes were superior with less than a 10% spread in the ultimate shear stress levels ($\gamma_{ambient} \approx$ 5,200 psi). The zero degree exposure tests showed similar results while also revealing that the ultimate shear stress levels are increased at reduced temperatures ($\gamma_{zero} \approx$ 5,00 psi). While the hot/wet conditioning reduced the ultimate shear stress levels in all surface preparation methods ($\gamma_{hot/wet} \approx$ 4,000 psi), processes using silane and Sol-Gel retained most of their initial strength. Options 6 and 8 retained 82% of their shear strength vs. the ambient test specimens while Options 1 and 2 retained 78% of their full baseline strength. In all cases, the simple, primer-only approach that performed well in the wedge tests (Option 4), produced the lowest ultimate shear stress in the test specimens.

The most critical test for bonded joints is durability in humid, high stress environments. Moisture may affect adhesive joints by: 1) hydrolyzing the adhesive, 2) displacing the adhesive at the adhesive adherend interface and, 3) by promoting corrosion at the interface with the steel adherend. Thus the adhesive as well as the surface preparation process must be able to resist this type of degradation. The hot/wet condition tests revealed that mechanical preparations alone do not provide durable bonding substrates. Virgin grit-blasted steel surfaces produced joints with relatively little durability. Figure 27 shows that the untreated steel surfaces (Options 4, 5, & 9) experienced more rapid crack growth during humidity chamber exposure.

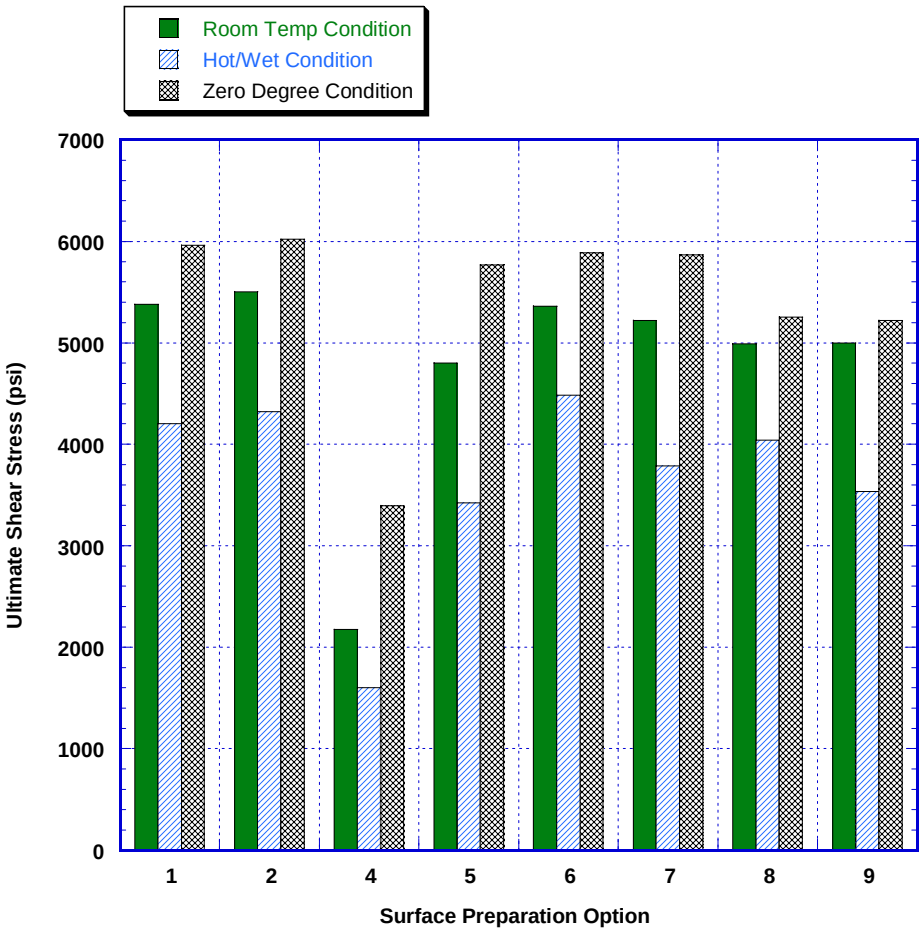


**Figure 29: Ultimate Shear Stress Results for Each Surface Preparation Process**

Clearly, the important parameters include surface roughening and chemical treatment/protection. Results from joints without chemical coupling agents and/or primer are inferior – especially when exposed to hot/wet conditions. Examination of the failure surfaces showed that undesirable adhesive failure (disbonds along bond line) occurred in surface preparation options 4, 5, and 9. Cohesive failure (fracture of the adhesive indicating that the full strength of the adhesive was achieved) was observed in the Sol-Gel and silane surface preparation methods.

Optimum behavior of the bonded joints would cause the failure mode to be cohesive fracture of the adhesive (as opposed to adhesive disbond between the adhesive and the substrate). This would allow the full strength of the adhesive to be utilized in the joint and repairs could be designed using the entire ultimate strength of the adhesive. Since it produces a reduction in processing time, co-curing the primers with the adhesive provides a tremendous advantage over precuring the primer followed by a separate adhesive cure cycle. However, the reduction in processing time is not a benefit if durability is lost. Cohesive failure of the specimens revealed that co-curing the primer did not reduce the performance of the bonded joint.

Cohesive fracture indicates that the bonding interface is stable under the test environment and that the adhesive polymer is the limiting factor in the joint performance. On the other hand, joint failures that are predominantly interfacial (disbond between adhesive and steel surface) indicate unpredictable joint failure which will be dependent on its stress field and environmental exposure history. These results reinforce the previously derived conclusions from the wedge tests about the efficacy of the grit blast-silane-primer surface treatment.

### 2.2.3 Lap Shear Fatigue Durability Tests

In addition to the ultimate shear stress tests, tension-tension fatigue tests were conducted using the lap shear specimens. The two main potential causes of structural failure in composite doubler installations stem from crack growth in the parent steel and adhesive disbonds. When disbonds occur, they may lead to joint failures. By their nature, they occur at an interface and are, therefore, always hidden. A combination of fatigue loads and other environmental weathering effects can combine to initiate these types of flaws. The fatigue tests studied the durability of the bonded joint and the potential for critical failure between the two adherends. The upper end of the applied tension loads was 50% to 55% of the ultimate shear stress values determined by the failure tests. Figure 29 shows that the ultimate shear stress values were on the order of 5,000 psi so the upper tension load was 2,500 lbs. If no failure was observed in the test specimen after 245,000 cycles, the upper load level was increased to 2,750 lbs.

Figures 30-32 show the fatigue results for Room Temperature (70 $^{o}$F), Zero Degree (0 $^{o}$F), and Hot-Wet (140 $^{o}$F) conditioning/testing, respectively. Once again, the Sol-Gel and the silane options (note Options 2 and 6) produced the best results across all operating conditions. In all cases, the simple primer-only (no chemical treatment approaches) that performed well in the wedge tests (Options 4 and 5), produced the least durable joints. When subjected to hot-wet conditioning, these joints could only sustain a relatively few fatigue cycles before failing (see Fig. 32). A significant difference was also observed between the Option 6 silane and the silane processes in Options 7 and 8. These results indicate the affects of different primers and of post grit blast chemical cleaning. It appears that the silane mixture and the BR-6747 primer are the only chemicals that should be applied after the grit blast process. The use of post grit blast cleaning chemicals degrades the joint's durability. Also, the BR-127 primer is usually cured at elevated temperature prior to the bonding process. The co-cure approach used here may have contributed to the poor performance shown in the Option 7 results.

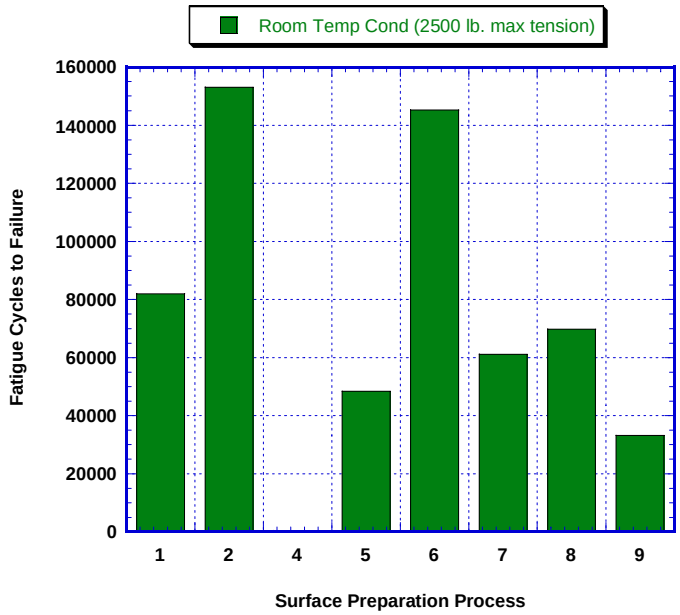


**Figure 30: Cycles to Lap Joint Failure at Room Temperature Testing (tension-tension up to 50% of shear ultimate values)**

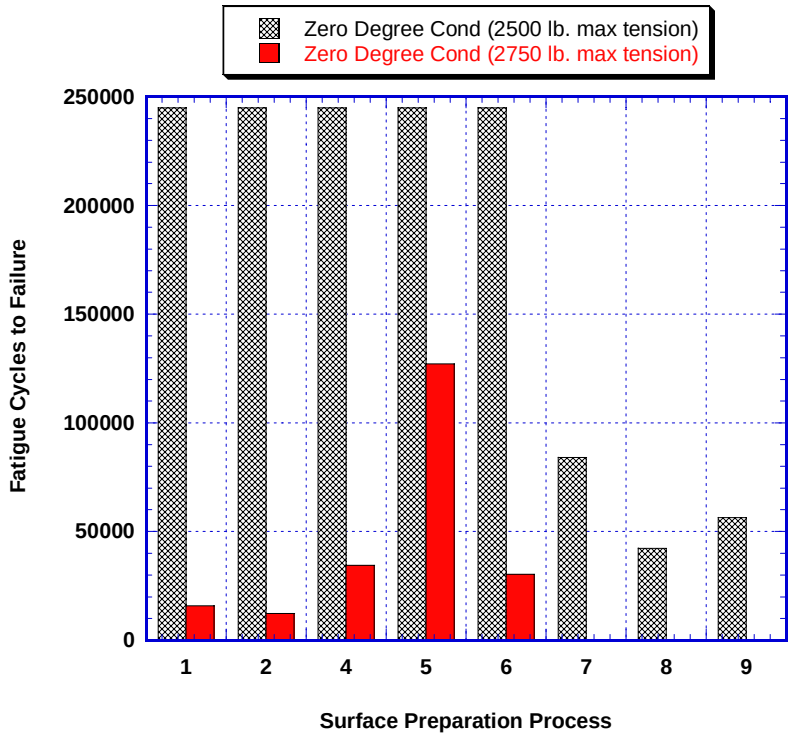


**Figure 31: Cycles to Lap Joint Failure at Zero Degree Testing (2,500 lb. tension-tension followed by 2,750 lb. fatigue)**

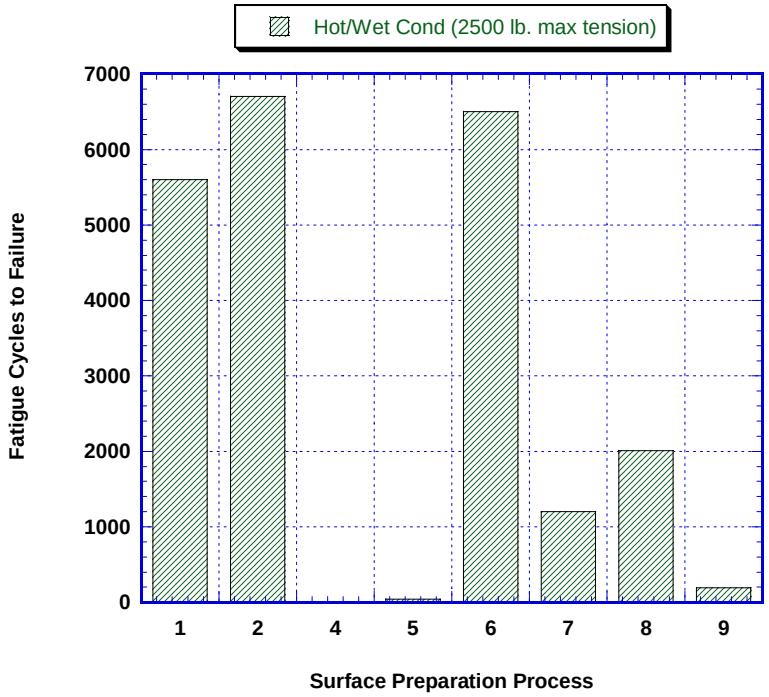


**Figure 32: Cycles to Lap Joint Failure at Hot/Wet Testing (140$^{o}$ F) (2,500 lb. tension-tension fatigue)**

The mechanical interlocking of the hardened epoxy adhesive with the substrate increases the initial bond strength but its real importance is in improving bond durability. With the high strength epoxies used in most structural applications, moisture can completely disrupt the chemical bonds as a result of dispersion forces, leading to catastrophic failure unless interlocking is present.

### 2.2.4 Adhesive Modulus

Adhesives for structural applications must possess high strength and be able to maintain this strength and stiffness under all deteriorating influences. The deteriorating influences may be broadly classified as physical (stresses) and chemical (heat, moisture, foreign contaminants). One important measure of an adhesive's strength is its elastic modulus. Load-displacement data from the lap shear testing was used to arrive at modulus of elasticity values for the AF-163 adhesive. Figure 33 shows the adhesive modulus values for operation in Room Temperature (70 $^{o}$F), Zero Degree (0 $^{o}$F), and Hot-Wet (140 $^{o}$F) conditions. The various surface preparation options did produce some slight differences in adhesive modulus due to microscopic fracture and slippage in the joint during the "elastic" portion of the load response. However, for the most part, the elastic constants derived from these tests were quite similar. The effect of temperature on adhesive modulus – modulus increases as operating temperature decreases – was also evident. The AF-163 modulus values were on the order of 50,000 lbs/in.$^{2}$ at 140$^{o}$F, 55,000 lbs/in.$^{2}$ at 70$^{o}$F and 62,000 lbs/in.$^{2}$ at 0$^{o}$F.

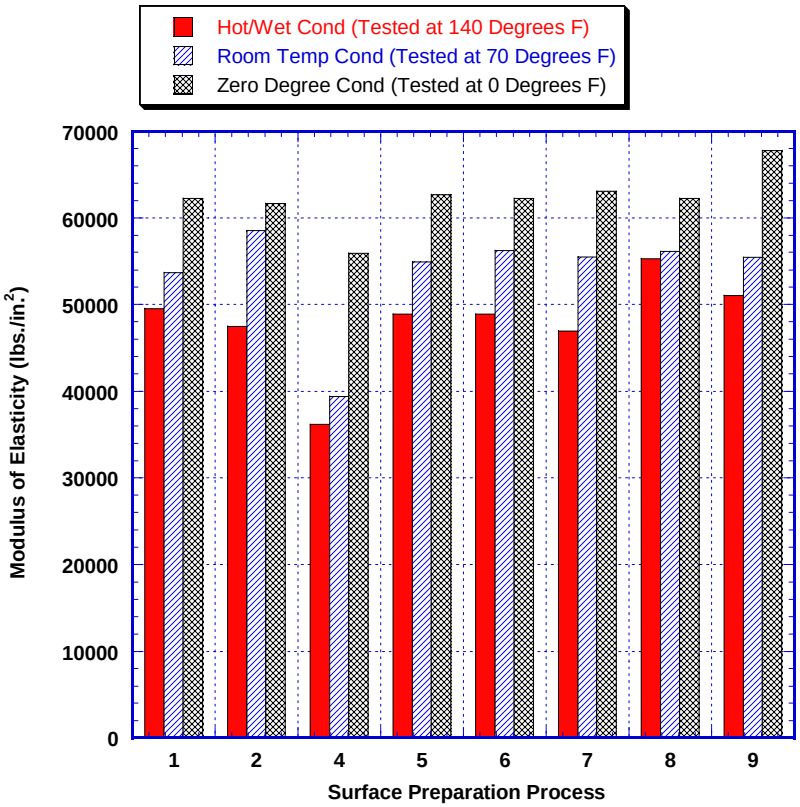


**Figure 33: Affect of Temperature on Adhesive Modulus**

### 2.2.5 Critical Crack Extension and Crack Arrest

A series of other parameters that can be used to study the performance of a bonded joint are the Critical Crack Extension and Crack Arrest properties. To measure these properties, the wedge test specimens shown in Figure 23 are used. However, the specimens are loaded in a cleavage peel arrangement shown in Figure 24. In the cleavage peel tests, the specimen is slowly loaded as per Fig. 24 (displacement control) and the following parameters are measured for each surface preparation option at the various environmental conditions:

$P_c$ = Critical Crack Extension (load producing crack growth)

$P_a$ = Crack Arrest Load (relief level at which crack arrests)

$a_c$ = crack growth caused by critical load

$a_a$ = crack growth that occurs as crack arrests

These parameters were then used to calculate the following crack extension properties:

$G_{Ic}$ = Critical crack extension force (crack initiation)
$G_{Ia}$ = Arrest crack extension force

Critical Crack Extension represents the minimum load required to propagate a crack along the bondline. This separation can be the result of adhesive fracture, disbond growth between the adhesive and adherend, or a combination of the two phenomena. The Crack Arrest Load is the maximum load that can be exerted on the bonded joint without further growth in the adhesion line crack. The tests were conducted at the same temperature as the associated coupon conditioning: $0^oF$, RT, and $140^oF$. Each specimen was loaded until a maximum load level was observed ($P_c$). At that point the machine crosshead was stopped and the load was allowed to drop until an equilibrium was reached (crack propagation stopped at crack arrest level). The initial (pre-test) and final (post-test) crack growths were measured optically using a 50X magnification. In both the Critical Crack Extension and Crack Arrest plots, the goal is to produce the largest load levels (solid portion of the bar charts) while minimizing the degree of crack growth (cross-hatched portion of the bar charts).

Test Procedure:

1. Mount in tensile test machine using eye bolts and clevis arrangement such that specimen is at right angle to the loading direction.
2. Observe load on the specimen while moving crosshead at 0.1 to 0.2 inch/min. When the load peaks (critical load) stop the crosshead movement.
3. With the crossheads stopped, allow the crack to stop propagating and the reducing load to reach equilibrium. Without using any additional force, place a wedge in the opening between the plates as shown in Fig. 2.
4. Record the peak ($P_g$ = critical load) and the equilibrium ($P_a$ = arrest load)
5. Measure final crack length.

The results are plotted in Figures 34-36. In general it can be seen that the hot-wet conditions are the most detrimental to the joint and produce the lowest crack extension and arrest values. Once again, the peel strength of the joint manufactured with the Option 4 process (no chemical treatment with primer) is shown to be quite high. However, the poor shear strength and fatigue performance of this surface preparation process removes Option 4 from consideration. Overall, the results from operation in all environments indicate that the silane surface preparation processes produce the best bondline strengths and crack mitigation. Furthermore, Option 6 performs the best out of the three silane processes. The process with the least resistance to moisture ingress (Option 5 with no primer protection) and the process with the non-uniform surface roughening (Option 9 with hand sanding only) produced the poorest results in the cleavage peel tests.

Ideal adhesive joint designs should utilize adhesives in the mode that makes the best use of their mechanical properties (i.e. they should be used in compression, shear, or tension). Cleavage and peeling forces should be avoided as much as possible. The composite doubler repairs proposed for the Syncrude repairs are predominantly shear joints. In addition, the repairs will be designed to produce joints that provide low average stresses and avoid high local stresses. The doubler taper, overall footprint, and thickness must be balanced to provide sufficient strength while achieving a gradual load transfer from the parent steel structure. Although the peel forces will be

minimized, this is still a good test to differentiate and quantify the capabilities of the candidate surface preparation options.

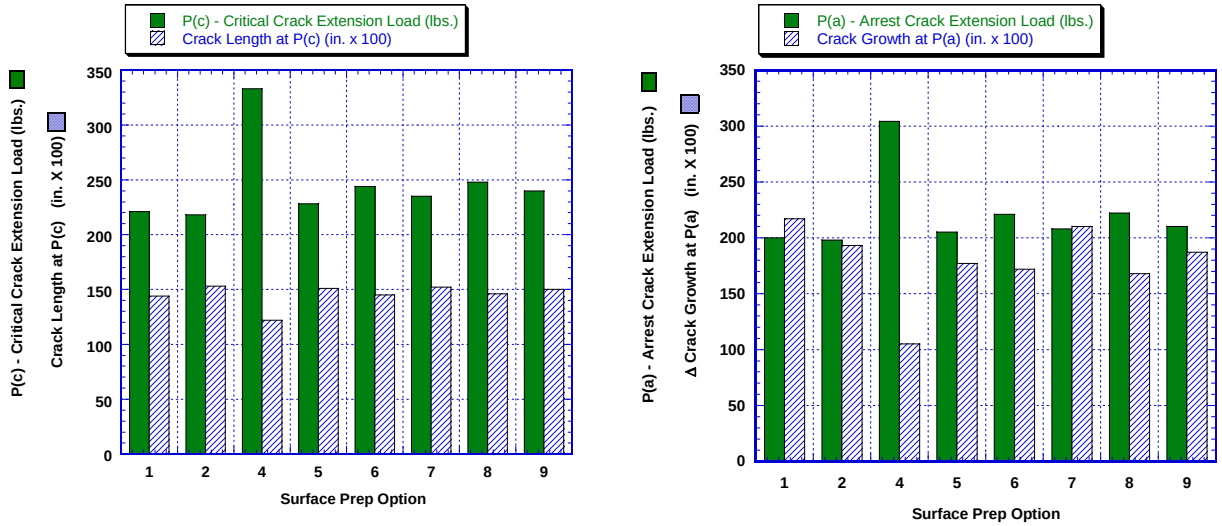


**Figure 34: Critical Crack Extension and Crack Arrest Parameters for Room Temperature Testing (70° F)**

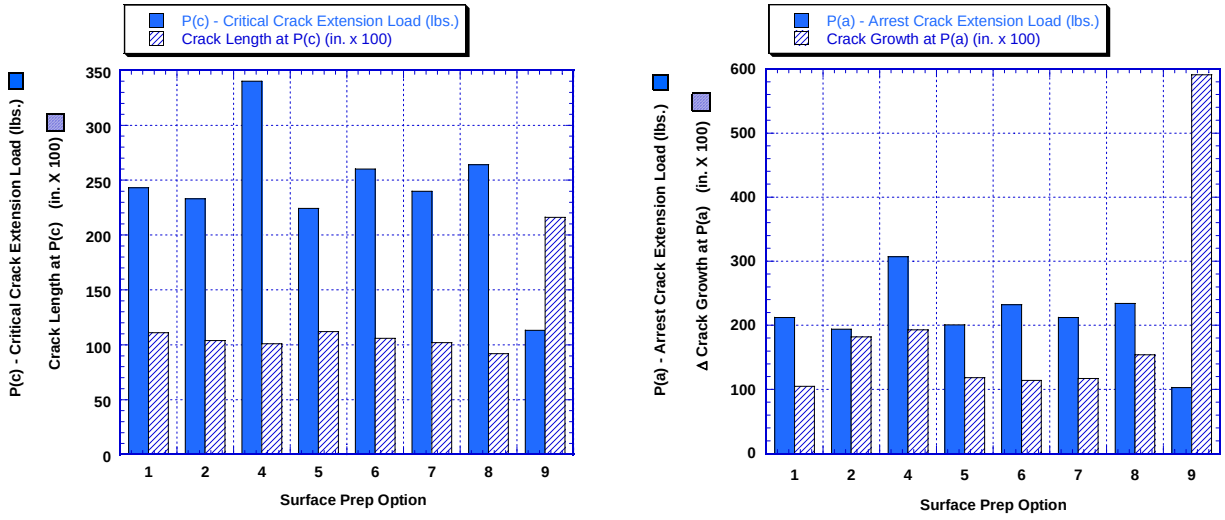


**Figure 35: Critical Crack Extension and Crack Arrest Parameters for Zero Degree Testing (0° F)**

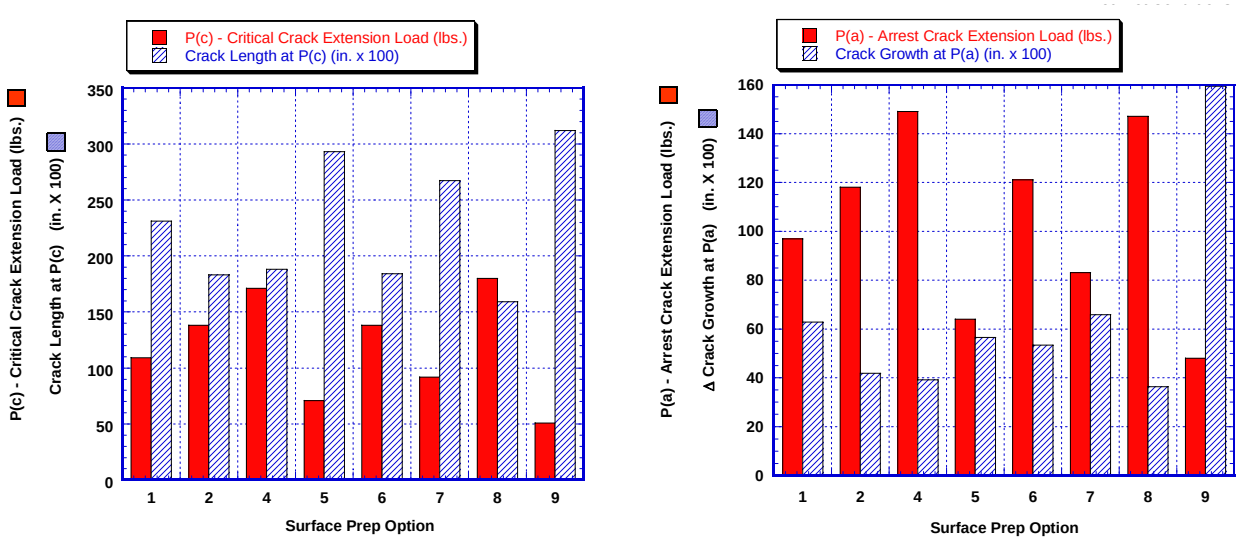


**Figure 36: Critical Crack Extension and Crack Arrest Parameters for Hot/Wet Testing (140$^{o}$ F)**

### 2.2.6 Adhesive vs. Cohesive Fracture Surfaces

Failure of the adhesive joints occur as fracture of the adhesive or as a separation between the adhesive and the adherend. Figure 37 depicts these two failure modes which are defined as follows:

> Adhesive Failure – Joint fails by adhesive film detaching from one or both of the substrates. This is usually caused by poor surface preparation and/or the deteriorating effects of the operating environment.
>
> Cohesive Failure – Adhesive joint fails through fracture of the adhesive film. This provides the highest possible joint strength (full strength of adhesive is achieved).

The strengths measured in the lap shear tests reflect the degree of cohesive and adhesive failure in the respective joints. For example, the low ultimate shear stress values produced by the Option 4 test specimens indicate that a large percentage of the failure surface will show adhesive failures. Conversely, when inspecting Option 6-8 post-failure surfaces, it was observed that the failures did not occur at the steel/silane interface or at the silane/adhesive interface, but rather at the boundary layer region that is strengthened by the presence of the silane coupling agent. The addition of the silane clearly improved the interfacial durability so that cohesive fracture of the adhesive could be reliably produced. By avoiding adhesive disbond failures, the full strength of the adhesive can be achieved. Figure 38 shows the adhesive regions from the failed specimens that used Option 4 (no chemical treatment) and Option 6 (silane treatment) processes. In the photo on the left, note the clear presence of the pink adhesive on both halves of the specimen indicating that the adhesive has fractured. In the photo on the right, note the large number of dark regions which are the exposed portions of the steel surface. These are disbond areas where the adhesive separated from the substrate steel material. The diagonal patterns present in both

photos are created by the scrim cloth that is used to carry the film adhesive. It is estimated that the better surface preparation techniques produced joints with less than 1% adhesive failure while the poor surface preparation techniques produced joints that exhibited 50% to 75% adhesive failure.

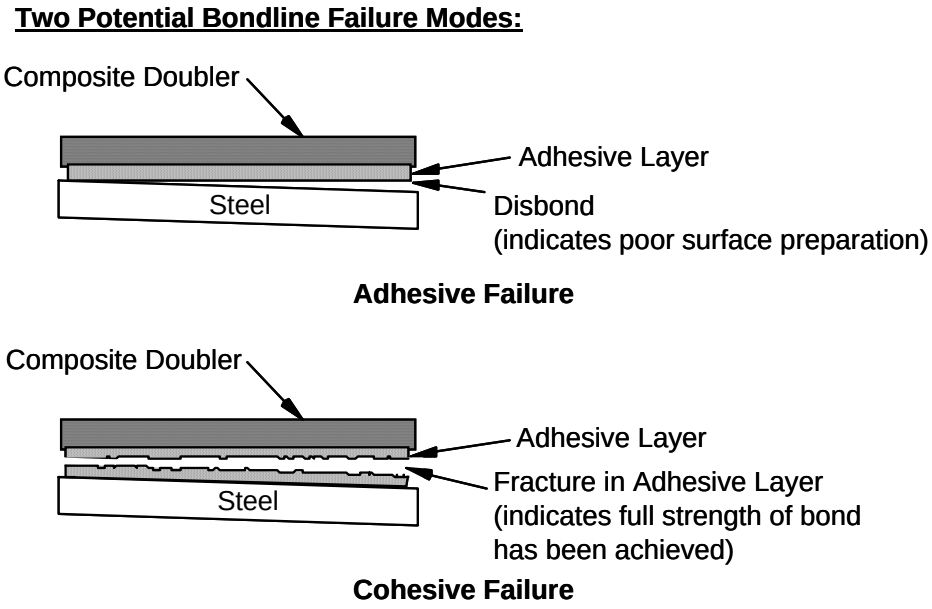


**Figure 37: The Two Primary Failure Modes in Adhesive Joints**

## 2.3 Final Determination of Optimum Process for Bonding Composites to Steel Structures

The variables studied in this effort relate to the three basic methods of surface treatment for good adhesion: 1) removal of contamination or weak boundary layers such as corrosive scale or oxide layers, 2) changing the surface chemistry, and 3) changing the surface texture. By comparing the hand sanded surfaces with the grit blast family of bonds, it can be seen that the uniformity of the roughness provided by grit blasting improves both the ultimate shear strength and crack mitigation capability of the bond. The use of chemical coupling agents and protective primers are also necessary to optimize the performance of bonded joints in carbon steel structures. Conversely, use of timesaving but marginal methods such as hand sanding plus solvent cleaning produces weak bonds with poor environmental durability. The chemical treatment and primer co-cure process validated in this study eliminates the need for two elevated temperature cure cycles. This minimizes complexity and saves installation time.

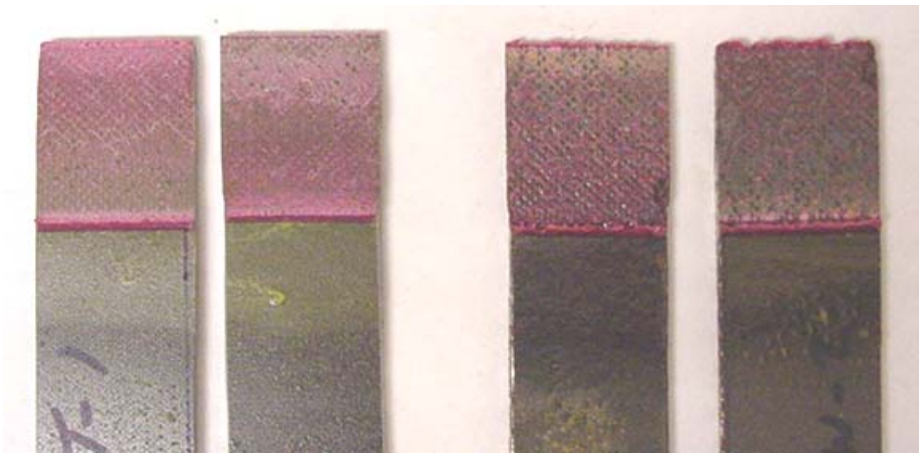

**Option 6 Primarily Cohesive Fracture**

**Option 4 Primarily Adhesive (Disbond) Failure**

**A. Macroscopic View of Failure Surfaces**


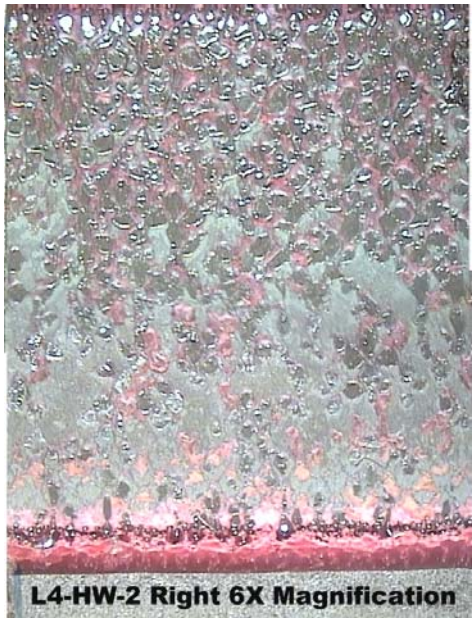


**Cohesive Fracture of Adhesive Film (Option 6 silane treatment)**

**Adhesive Failure at Interface (Option 4 no chemical treatment)**

**B. Microscopic View of Failure Surfaces**

**Figure 38: Photo of Fracture Surface in Lap Shear Specimens**

Table 3 summarizes the overall capability of each surface preparation process by ranking its relative performance in each of the tests described above. While Option 4 produced the best results for all of the peel stress-oriented tests (wedge and cleavage peel), it produced the poorest numbers in the shear stress-oriented tests (lap shear, shear fatigue). Since shear loading is one of the primary features of these composite repairs, it is a major consideration and sufficient reason for rejecting the Option 4 process. The rankings show that both the grit blast-Sol-Gel-primer and the grit blast-silane-primer processes produce the best overall results for bond strength and long-term durability. The results were very repeatable with less than 3% variations observed among common test specimens. The highest ranking across the range of qualification tests was produced by Option 6. For the most part, it is always ranked in the top 3 surface preparation options. When ease of installation and availability of materials are considered, the silane process (Option 6) becomes the obvious surface preparation of choice for this composite doubler repair program. Figure 39 is a schematic summarizing the Option 6 installation process. The process uses a single heat cycle to simultaneously co-cure the Silane, primer, adhesive film, composite doubler and fiberglass cover ply. Figure 40 is a flowchart of the installation steps along with the time required to complete each step. Appendix A contains a photo summary of the surface preparation and composite doubler hot bonding process that has been identified for Syncrude carbon steel structures. Appendix B provides a detailed procedure for installing a composite doubler repair on steel structures.

| Test | Rank of Surface Preparation Option | | | | | | | |
|---|---|---|---|---|---|---|---|---|
| | 1 | 2 | 4 | 5 | 6 | 7 | 8 | 9 |
| **Wedge Crack Growth** | | | | | | | | |
| Room Temp | 7 | 8 | 1 | 5 | 2 | 6 | 3 | 4 |
| Zero Degree | 6 | 4 | 1 | 7 | 5 | 3 | 2 | 8 |
| Hot-Wet | 5 | 2 | 4 | 7 | 3 | 6 | 1 | 8 |
| **Lap Ultimate Shear** | | | | | | | | |
| Room Temp | 2 | 1 | 8 | 7 | 3 | 4 | 6 | 5 |
| Zero Degree | 2 | 1 | 8 | 5 | 3 | 4 | 6 | 7 |
| Hot-Wet | 3 | 2 | 8 | 7 | 1 | 5 | 4 | 6 |
| **Lap Tension Fatigue** | | | | | | | | |
| Room Temp | 3 | 1 | 8 | 6 | 2 | 5 | 4 | 7 |
| Zero Degree | 3 | 4 | 8 | 1 | 2 | 5 | 7 | 6 |
| Hot-Wet | 3 | 1 | 8 | 7 | 2 | 5 | 4 | 6 |
| **Cleavage Peel - Critical Crack Extension** | | | | | | | | |
| Room Temp | 7 | 8 | 1 | 6 | 3 | 5 | 2 | 4 |
| Zero Degree | 4 | 6 | 1 | 7 | 3 | 5 | 2 | 8 |
| Hot-Wet | 5 | 4 | 2 | 7 | 3 | 6 | 1 | 8 |
| **Cleavage Peel - Crack Arrest** | | | | | | | | |
| Room Temp | 7 | 8 | 1 | 6 | 3 | 5 | 2 | 4 |
| Zero Degree | 5 | 7 | 1 | 6 | 3 | 4 | 2 | 8 |
| Hot-Wet | 5 | 4 | 1 | 7 | 3 | 6 | 2 | 8 |


**Table 3: Summary of Overall Performance of the Surface Preparation Options**

The results presented here provide the first step in applying adhesively bonded composite doublers as an alternative to the fusion fillet welding of steel plates to repair trucks and shovels used in the Syncrude mining and oil recovery operation. By combining these test results with composite doubler research from the aviation industry, it appears that the use of heat-cured epoxy resins and fiber-reinforced composites is feasible for replacing fillet welded plates on carbon steel structures. Composite joints can provide sufficient strength requirements while maintaining needed flexibility and improving durability. The limiting factor in bonded composite repairs will probably be their performance in compression stress fields. This will be one of the focus areas for the next phase of this investigation.

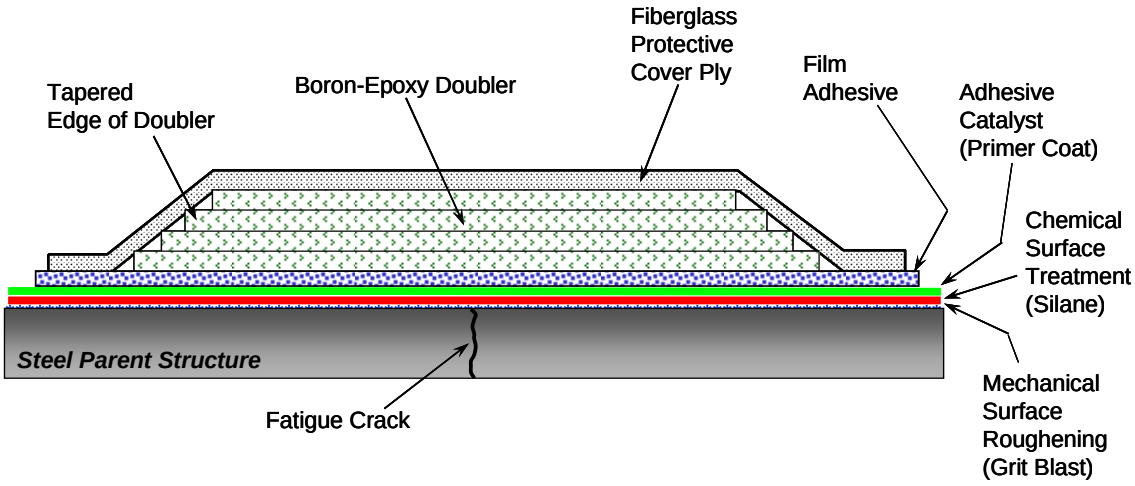


**Figure 39: Summary of Optimum Composite Doubler Installation Process for Steel Structures**

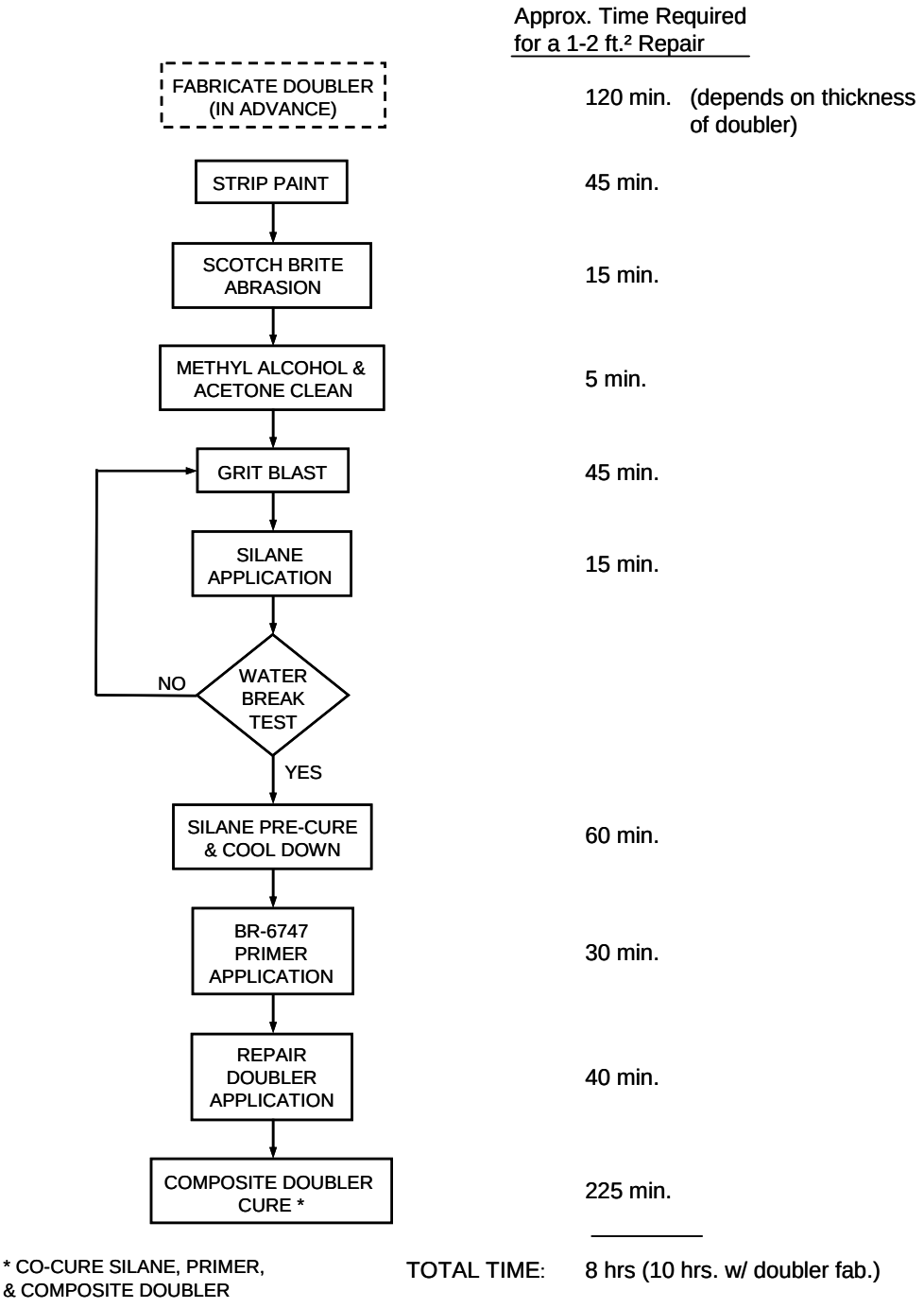


**Figure 40: Flowchart Summary of Composite Doubler Installation on Steel Structures**

## 2.4 Heat Source/Sink Analysis

One of the key issues in assessing the viability of composite repairs for Syncrude structures is the ability to produce sufficient, controlled temperatures in the areas to be repaired. The method of applying the temperature must allow the doubler to be cured within the allowable temperature envelope and avoid any degradation in the surrounding structure or systems. Heating options include the use of traditional rubber/coil heat blankets for composite material cures and/or the use of ceramic heat blankets currently used by Syncrude in its welding process.

With the list of potential repair applications in mind and some idea of the approximate size of the patches, the Syncrude-Sandia team conducted a heat source and heat sink test on a thick-walled Syncrude structure. Figure 41 shows the shovel bucket that was used for this test. The wall of the bucket was approximately 3" thick and the heat sinks included a thicker region immediately adjacent to the zone to be heated and a free edge exposed to open air. It was immediately apparent that the rubberized heat blankets that Sandia has used in its aircraft repairs could not provide the heat necessary to raise the temperature to cure temperatures of 225$^{o}$F. Discussions with Cooper-MQS Canada indicated that the Cooperheat ceramic blankets and associated control system would have sufficient power and control to produce the desired temperature profile. Other advantages include: 1) these are the blankets used by Syncrude, 2) the additional control system is contained in a mobile trailer, and 3) Cooperheat is currently contracted to Syncrude and is familiar with heating these type of structures.

The approach was to mount the Cooperheat flexible ceramic pad heaters around the area to be "repaired" and to induce the temperature in this region using the projection heating method depicted in Figure 42. Numerous rings of heat blankets can be placed around the region to be repaired and placed over large flanges, etc. to counteract the heat sinks. Figure 43 shows several of the blankets and associated thermocouples being installed around the 18" X 18" repair region. Tack welds were used to secure the heaters and thermocouples. Figure 44 shows the final arrangement of ceramic heaters and thermocouples around the test site. The thermocouples around the exposed steel repair region and a close-up of the ceramic heat blankets are shown in Figure 45. Figure 46 is a photo of the complete assembly with insulation placed over the 7 heat blankets.

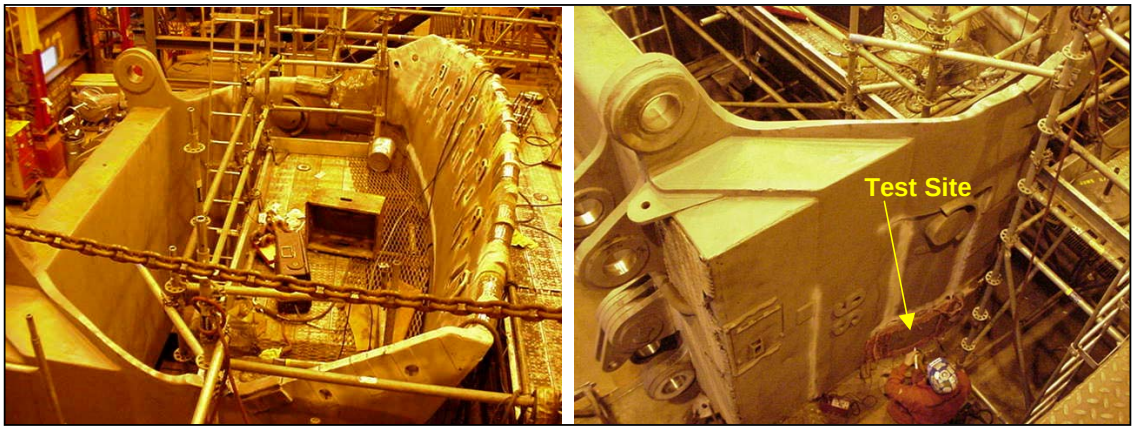


**Figure 41: View of Shovel Bucket and Heat Source/Sink Test Location**

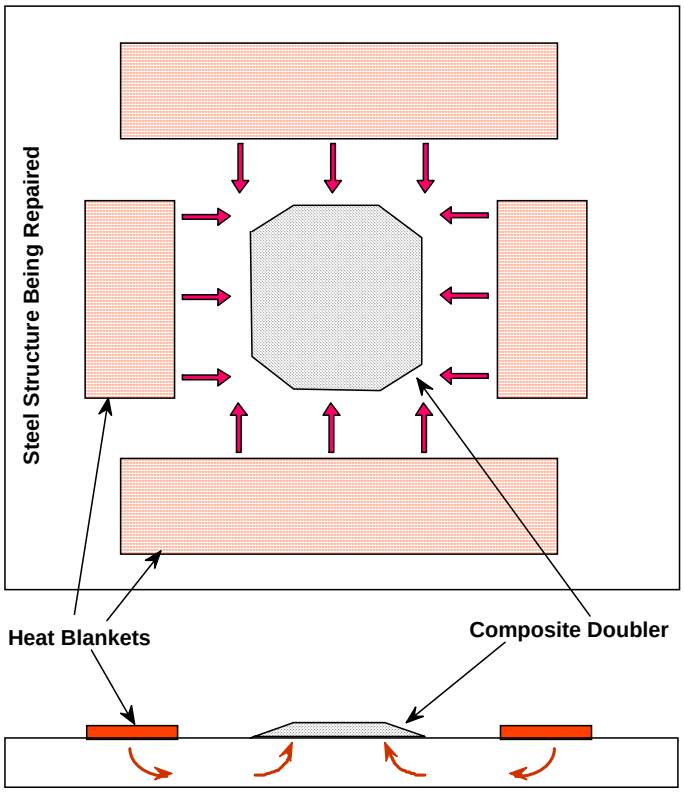


**Figure 42: Basic Concept of Projection Heating**

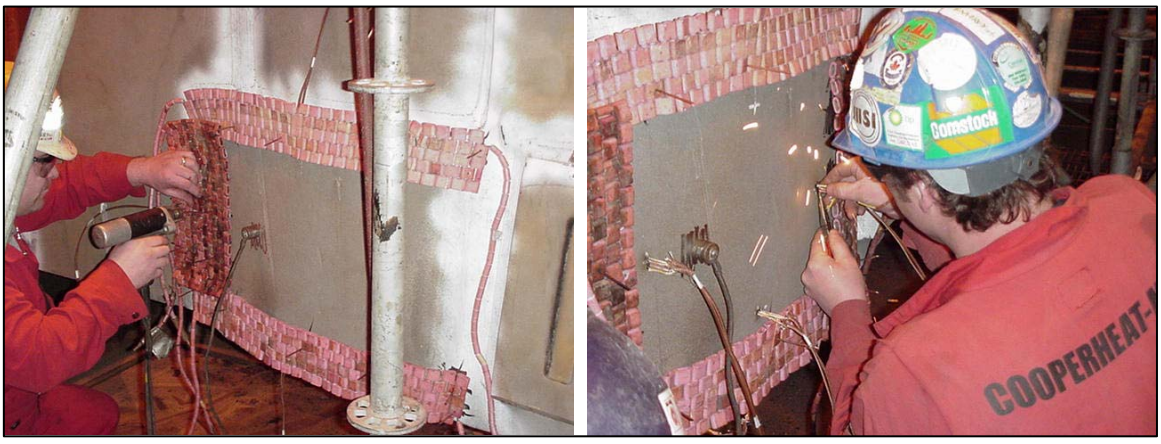


**Figure 43: Placing and Securing Ceramic Heater Pad and Thermocouples Using Tack Welds**

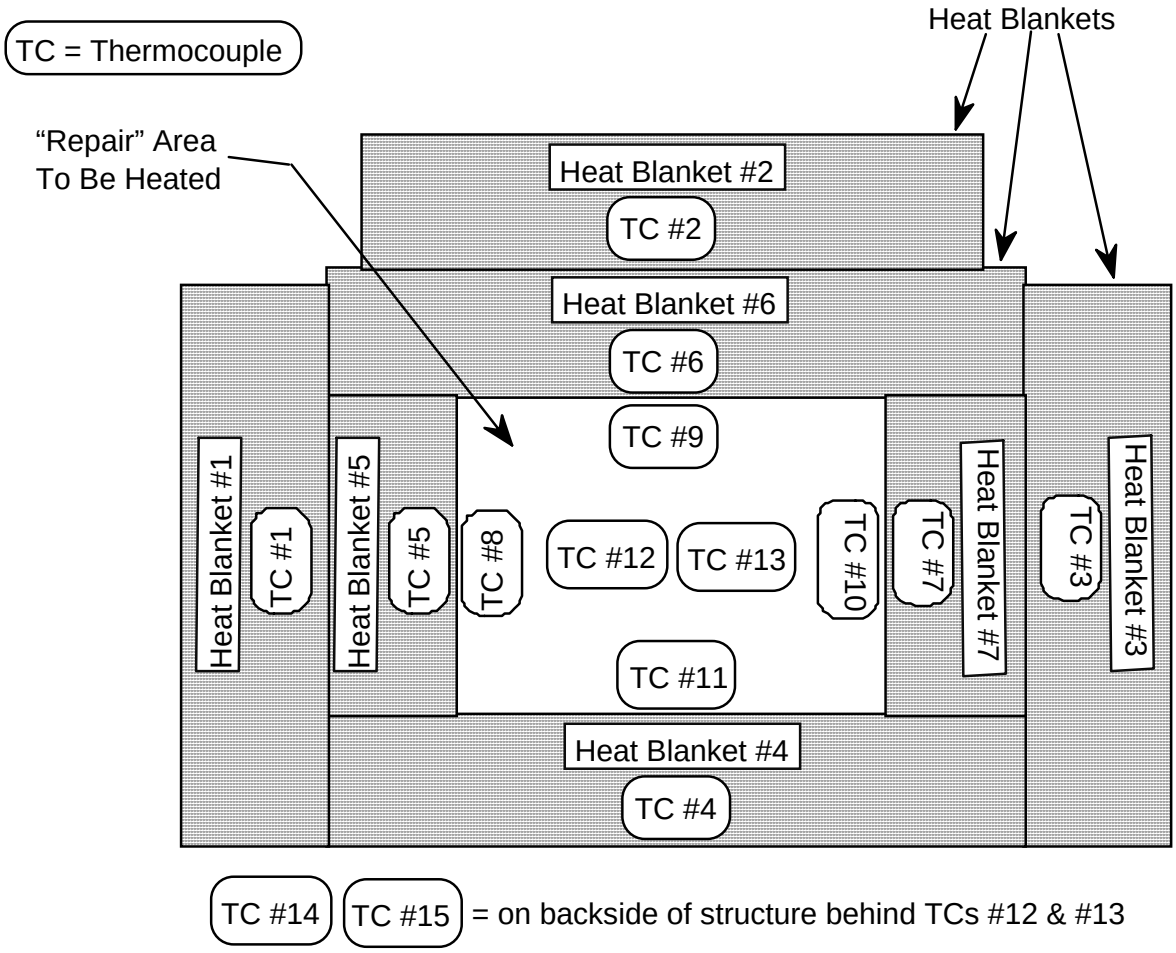


**Figure 44: Heater Pad Placement Around Perimeter of Area to Be Repaired and Thermocouple Locations Used to Monitor Heating Process**

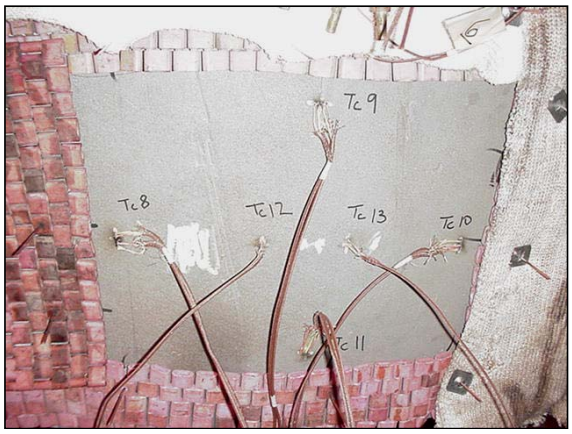


**Figure 45: Thermocouples Placed Inside "Repair" Region (18" X 18")**

**Figure 46: Final Assembly with Insulation Placed Over 7 Heater Pads**

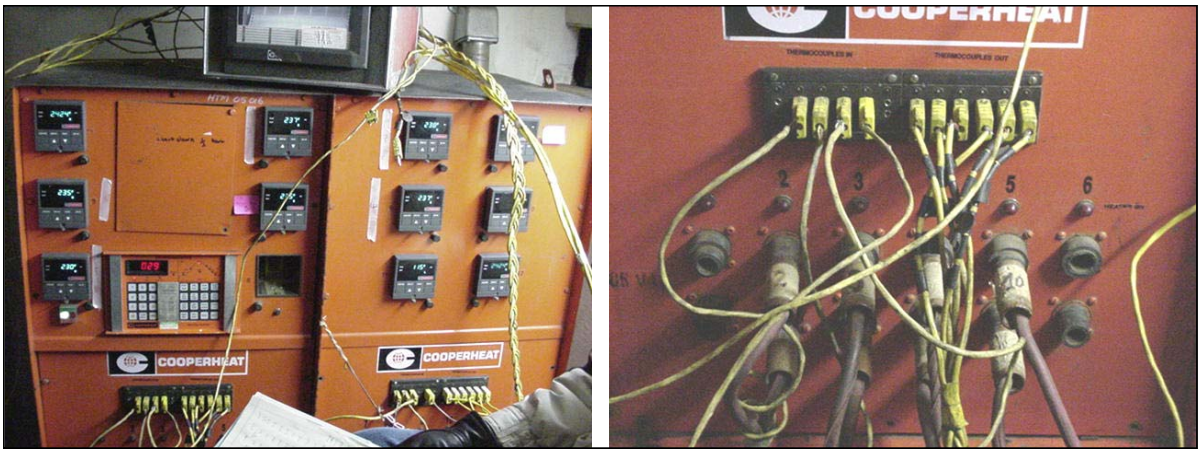


**Figure 47: Cooperheat Controller Showing Input from Thermocouples, Output to Heater Pads, and Temperature Logging**

The Cooperheat control system, shown in Figure 47, was programmed to produce a temperature ramp-up rate of 3°F/minute, a temperature hold at 225°F, and a temperature ramp-down of 5°F/minute. Figure 48 shows this target temperature profile along with the temperatures from all 15 thermocouples. Thermocouples 1-7 were located under heater pads 1-7, respectively, so they can be interpreted as the driving temperatures for the projection heating process. Note that they match the programmed profile quite well. The remaining thermocouples, #8-15, are inside the perimeter of the heater pads and represent the cure temperatures for a composite doubler. As expected, there is some lag in the temperature ramp-up but the slope gradually improves to the 3°F/minute target. As noted in Fig. 48, the set point was adjusted to 240°F to speed up the rise to 225°F. There was some concern that the thermal mass of the structure would cause us to overshoot the 225°F target, however, the temperature in the repair region remained very stable. Once the inner repair region reached the hold temperature (see t= 95 minutes), the temperatures in thermocouples 8-15 remained well within the $\pm$25°F tolerance (min temp. = 222°F; max temp. = 234°F). After the hold temperature was maintained for 20 minutes, the Cooperheat system was shut down. The two data points taken after shut-down showed that the thermal mass does make it difficult to quickly cool the structure. Temperature logs from the strip chart recorder, left on overnight, showed that the structure cooled at about 0.5°F/minute. Although we would like to cool the doubler a little faster than this (cure profile calls for temperature ramp-down of 1-5°F/min), the temperature ramp-down parameter is the least critical aspect of the cure profile. Overall, this was an excellent demonstration of the heating process. While the Cooperheat system shown here may be supplemented by placing rubberized heat blankets over the composite patch itself, there are no other changes needed for this system to properly cure a composite doubler.

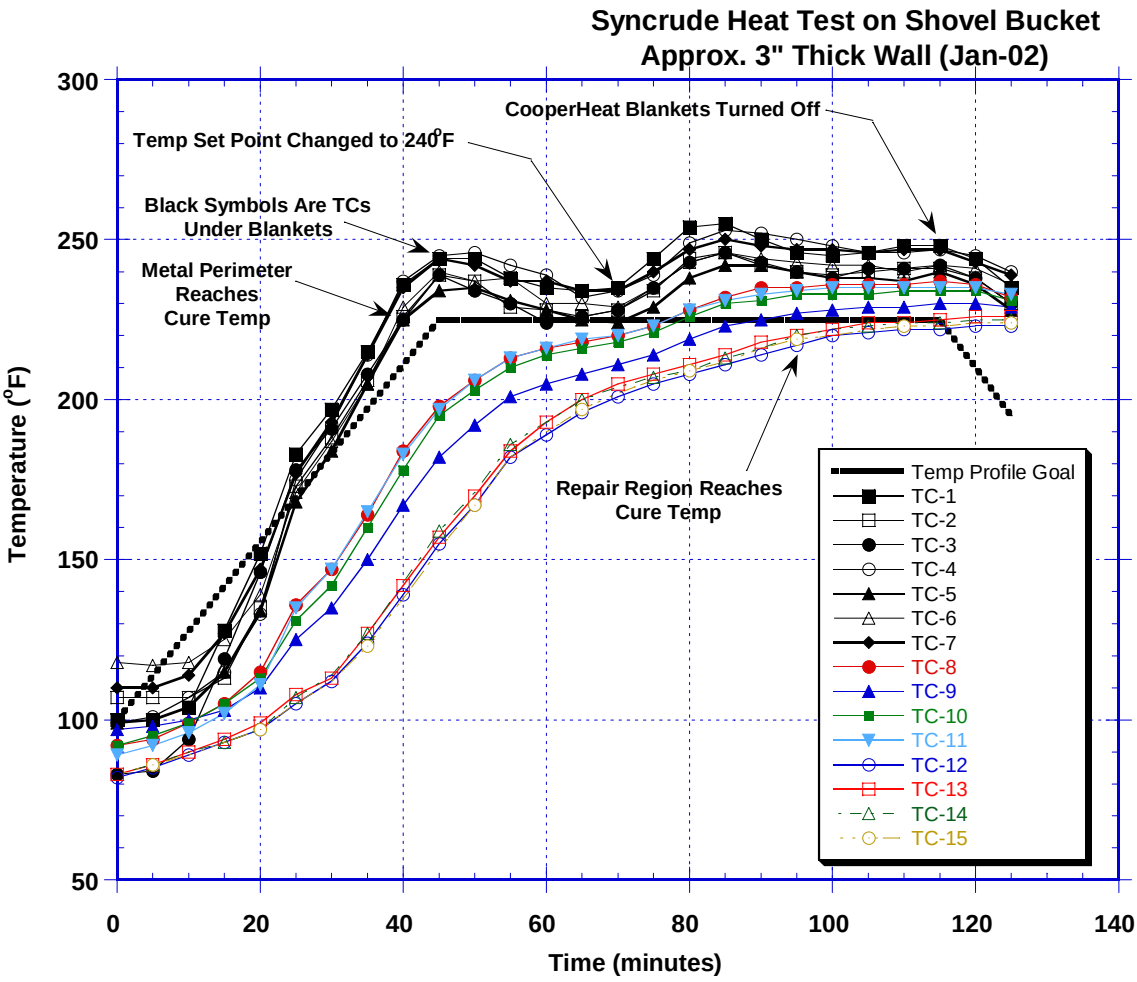


**Figure 48: Temperature Profile of All Thermocouples with Comparison to Desired Heat/Cure Profile**

**This Page Intentionally Left Blank**

## 3.0 COMPOSITE DOUBLER DESIGN GUIDELINES AND VALIDATION FOR REPAIR OF STEEL STRUCTURES

Before arriving at a final family of repair designs for the shovel boom, component level testing was completed to study the response of ultra-thick doublers on thick steel structure. Fatigue and static tests studied flaw initiation and growth, strain fields, residual strength, ultimate strength, and load transfer. In addition, these tests also established the damage tolerance of composite doubler repairs for Syncrude applications. Installation and in-service flaws were engineered into critical regions of the repair to determine if and what detrimental effects they have on the repair. The tests evaluated the critical aspects of the initial Syncrude repair designs: ply lay-up, ply orientation, patch shape and taper, and the bond layer. The thickness of both the doubler and the parent steel structure were representative of the anticipated field repairs.

*Structural Testing Initiative – The purpose of this phase of the study was to assess design options and doubler performance; study flaw initiation and growth, strain fields, residual strength, ultimate strength, and load transfer in realistic composite doubler repairs on carbon steel structure. Fatigue loads were applied to simulate worst-case working environments. NDI & strain gages were used to monitor structural response. Results from the Syncrude stress level monitoring activity were used to determine the appropriate test loads.*

Basic design tenants, established during Sandia Labs' commercial aircraft projects, were used to guide the design of the doubler(s) for these tests. The component level tests addressed general design and installation issues such as: 1) durability of surface preparation and associated strength of adhesive joint, 2) taper ratios needed to transfer the loads and mitigate crack growth while minimizing the doubler footprint, and 3) required stiffness ratios between the parent structure and the composite patch to produce the desired performance. Configurations with assorted loading and boundary conditions attempted to grow engineered flaws and determine load transfer capabilities of composite doublers in the presence of defects. Specimens were tested in a variety of loading modes (shear, tensile, and bending) and stress intensities were measured around cracks to determine critical bonding parameters. The test specimens were produced using the optimum surface preparation determined in the first segment of this study [see Section 2.0].

Exposure to cold, representing worst-case Winter conditions, and heat, representing a weld repair process in an adjacent area, were included to determine if either if these conditions are detrimental to the composite repair installation. The fatigue tests also provided critical crack growth information so that inspection intervals, if necessary, can be related to the degradation rate of the composite doubler under operational service conditions.

### 3.1 Doubler Design Guidelines

The primary issues to be addressed include the optimum location, size, shape, and laminate taper for the patches. The major factors that determine the patch design parameters are the stress levels at the repaired flaw, the stress levels in the composite doubler (maximum allowable fiber stresses), and the stress levels in the adhesive layer between the doubler and the metal skin. The important, fundamental results produced by Jones and Callinan in ref. [15-16] are worth

reviewing in some detail in order to prepare for the damage tolerance discussions later in this report.

The ref. [15] crack repair study used a unidirectional Boron-Epoxy laminate (fiber perpendicular to crack) as a baseline design. The study found that for patches that cover the entire length of the crack, a one ply (0.0057" thick) patch reduces the stress intensity factor to 33.5% of its value for the unpatched crack. Furthermore, the rate of decrease in the stress intensity factor, $K_{1P}$, as the patch thickness increases was found to be quite low. A six layer patch, for example, produced a $K_{1P}$ value of 19.5% of the unpatched value. Thus, an increase in patch thickness by a factor of 6 only produces an additional 14% reduction in the stress intensity factor. Another important finding of the ref. [15] study was that in thin patches, the stresses over the flaw (in both the patch and the adhesive) are critical. However, as the patch thickness is increased, the shear stresses in the adhesive at the edges of the patch footprint become critical and may exceed allowable limits.

The findings summarized above produced a series of design requirements that are necessary to maintaining the structural integrity of a composite doubler repair.

1) Fiber Strain – For a maximum Boron fiber strain of 5,000 με, the stress in the fibers must satisfy

$$\sigma_f \leq 0.005\, E_{11} \qquad (1)$$

where $E_{11}$ is Young's modulus in the direction of the fibers ($28.0 \times 10^6$ psi). When the fiber stress concentration, $K_f$, is considered the governing equation for fiber strain becomes

$$\sigma_f = K_f\, \sigma \leq .14 \text{ lb/in}^2 \qquad (2)$$

Thus, if the applied stress, σ, is known the maximum permissible value of $K_f$ and the minimum permissible patch thickness can be determined.

2) Shear Stress in Adhesive – For a maximum allowable adhesive shear stress of 7 KSI and considering the stress concentrations at the crack and at the edge of the patch, the following design equations must be satisfied

$$\tau_{a(c)} = K_{a(c)}\, \sigma \leq 7{,}000 \text{ lb/in}^2 \qquad (3)$$

$$\tau_{a(e)} = K_{a(e)}\, \sigma \leq 7{,}000 \text{ lb/in}^2 \qquad (4)$$

Equations (2) and (3) can be solved to produce a doubler thickness to satisfy the stress requirements at the crack (for both laminate and adhesive). However, this often produces adhesive stresses at the edge of the doubler that exceed those allowed by eq. (4). Ref. [15] showed that the adhesive stresses at the edge of the doubler can be reduced to admissible levels by stepping the thickness of the doubler from one or two plies at the outer perimeter to full thickness over a taper region. The length of the taper region is normally chosen to produce an

edge taper ratio (taper depth-to-thickness increase ratio) of 10 to 30. Figure 3 shows a typical doubler edge taper used to gradually transfer load from the parent metal skin and reduce the shear stress in the adhesive. An ongoing study at the Sandia Labs AANC regarding the application of composite doublers to DC-10 skin damage encountered this need to balance doubler thickness with an appropriate edge taper [8].

**Damage Tolerance of Composite Doublers** – Inspection requirements (sensitivity and inspection intervals) are driven by Damage Tolerance Analyses (DTA). However, the stack of metal parent material (isotropic), composite lamina (anisotropic), and adhesive layers makes the analysis quite complex and hinders the calculation of an exact DTA. It is difficult to determine the effects of flaw size and the point at which a flaw size/location becomes critical. This is especially true of disbond, delamination, and porosity flaws. Thus, an increased emphasis is placed on quantifying the probability that a flaw of a particular size and location will be detected by a piece of NDT equipment. In addition to this report, detailed discussions on general damage tolerance assessments for structural repairs are presented in references [15-20].

The reference [16] observations mirror one of the primary results obtained in the damage tolerance assessment presented in this report: adhesively bonded doublers are extremely damage tolerant to large disbonds and other detrimental conditions such as impact and hot-wet conditioning. These results are quantified in Section 4 of this report. If, in fact, disbond and delamination flaws do not grow even under extreme environmental conditions, then an acceptable design should be predicated on the fact that the stresses in the adhesive are kept below a limiting or threshold value. As a result, reference [16] introduces an essential design methodology that considers damage tolerance. It uses a fatigue threshold load, $P_f$, and a fatigue threshold strain, $\varepsilon_f$, below which irreversible damage in the adhesive will not occur. The equations used to determine the threshold load and strain values are as follows:

$$P_f = 2\,(t\,W_f\,ET)^{1/2} \qquad (5)$$

$$\varepsilon_f = 2\,(t\,W_f\,E/T)^{1/2} \qquad (6)$$

where,

t = thickness of the adhesive
T = thickness of the adherend (skin)
E = Young's modulus of the skin
$W_f$ = threshold value of the strain energy density of the adhesive

$W_f$ can be determined experimentally [23]. Ref. [16] also describes the maximum load, $P_{max}$, that can be carried by a bond in a symmetrical bonded joint as,

$$P_{max} = 2\,(t\,W_c\,ET)^{1/2} \qquad (7)$$

where $W_c$ is the maximum strain energy density of the adhesive. Thus, composite doubler repair design guidelines are that $P_{max}$ is greater than the ultimate load for the repaired structure and that $P_f$ is greater than the limit load. Ref. [16] also points out that these critical design variables are

affected by the loading rate. A conservative estimate for $P_{max}$ can be obtained by using the value of the maximum von Mises equivalent stress in the adhesive, $\sigma_e$, as measured in high strain rate tests. For AF-163, the adhesive used in this study, $\sigma_e = P_{max}$ = 5,800 psi and the threshold stress $\sigma_{th}$ = 3,600 psi. This analysis approach clearly shows the importance of the adhesive in determining the overall performance of the bonded repair. Ref. [16] goes on to point out the effects of the inelastic strain build-up in the adhesive layer that can accumulate with each load cycle. This hysteresis must be considered when determining the loads and fatigue cycles necessary to reach the maximum strain. Appendix C summarizes the set of basic equations that are used to design a composite doubler repair.

The abilities of nondestructive inspection techniques to meet the flaw detection requirements are presented in Section 5. The fundamental result from the NDI study is that a team of NDI techniques can identify flaws well before they reach critical size. Crack detection in the parent steel material can be accomplished using conventional eddy current and X-ray techniques. Also, ultrasonic and thermography methods have been successfully applied to the problem of disbond and delamination detection.

## 3.2 Load Spectra Monitoring of Cable Shovel Boom

Load spectra monitoring for the shovel boom was performed in conjunction with the Syncrude fatigue crack management research project [21-23]. This joint Syncrude-University of Alberta project seeks to understand how cracks form on Syncrude mobile equipment, develop guidelines to predict fatigue crack behavior, and assess which repair techniques are best suited for various conditions. As part of this program a load analysis, load measurement and finite element model were completed for the BE-395E shovel boom. The boom was monitored while in field operating conditions as shown in Figure 49. Field monitoring of BE 395B shovel 11-77 was conducted for approximately one week. The field test consisted of controlled operation of the shovel under 'simulated' and normal operating conditions. Strains were measured at two cross-sections along the boom (sections A-A and B-B as shown in Figure 50). A total of 32 strain gages were mounted on sections A-A and B-B of the boom as shown in Figures 50-51 [22].

The data from the crack management project were used in this repair study to: 1) determine the primary loading and stress fields that lead to fatigue cracking, and 2) quantify the stress field to allow for accurate design and analysis of composite repairs. The hope was that the load monitoring captured both normal and off-design conditions so that true load extremes could be applied in subsequent design validation tests. The gages determined the loads associated with all phases of use including start-up, shut-down, and routine operation. Other environmental information to be determined includes the number of fatigue cycles (i.e. excursions of $\pm$ 80% of operating stresses) incurred during a normal working day. Areas of uniform strain were instrumented to produce clear and reliable data from which finite element models could be validated. The validated FEMs could then be used to quantify stress risers in the complex geometry regions of the boom.

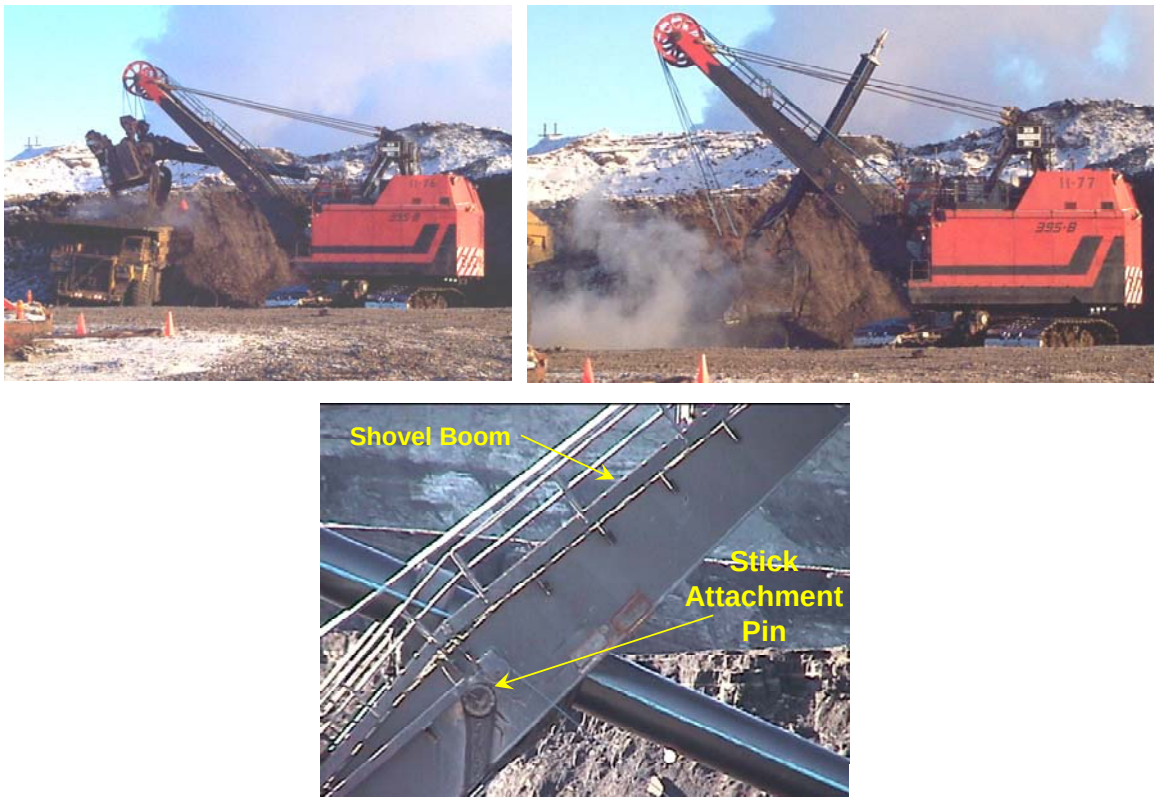


**Figure 49: Typical Operation of Cable Shovel and Close Up of Boom Being Monitored**

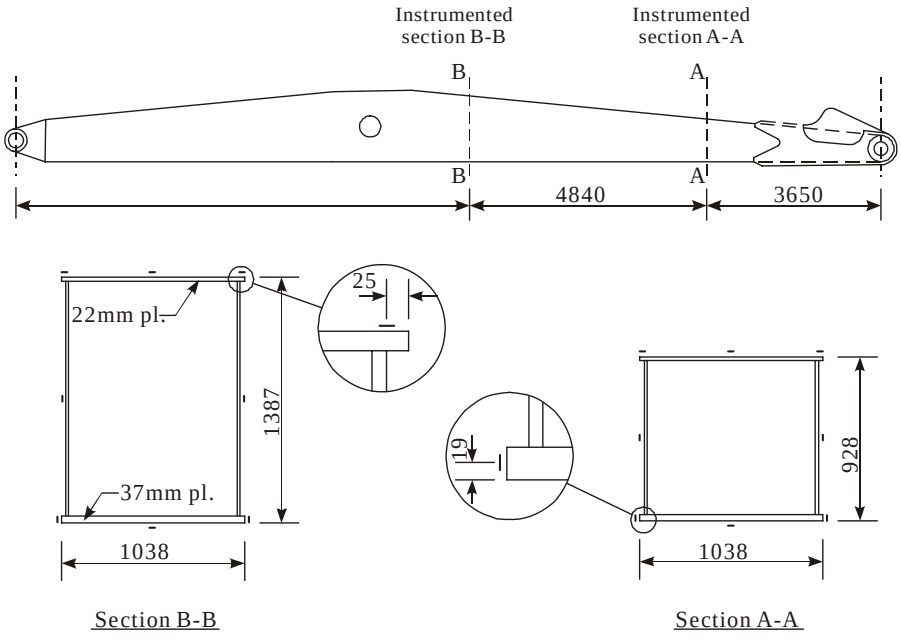


**Figure 50: Shovel Boom Schematic and Strain Gage Layout Used to Monitor Strain Field**

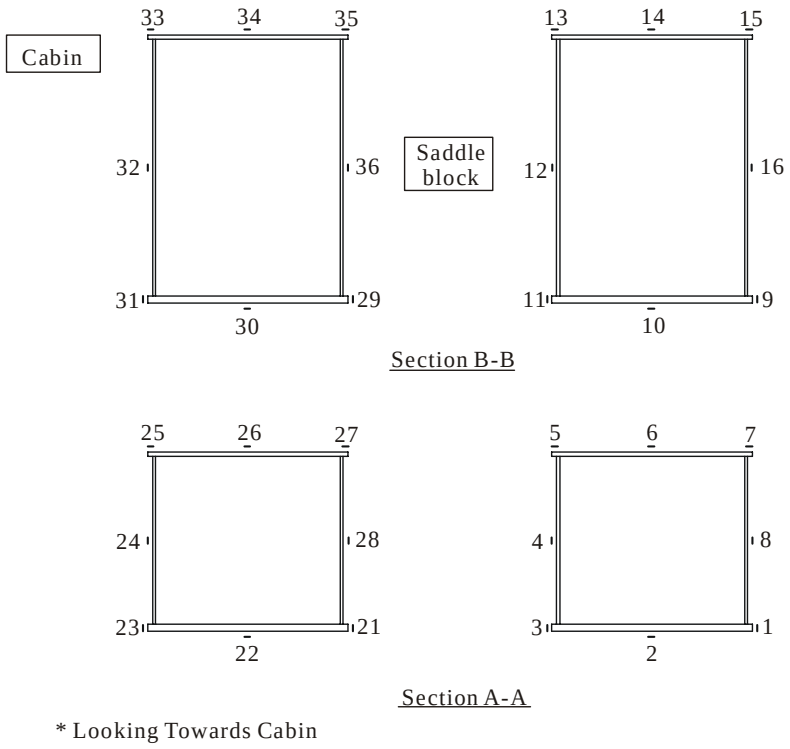


**Figure 51: Strain Gage Layout and Numbering System Used to Monitor Cable Shovel Booms**

The preliminary results from the field measurements and computer model indicated that the loading on the shovel boom was primarily along the longitudinal axis of the boom with very little lateral bending from side to side. In addition, the loading on the bottom section of the boom's box beam is predominately in tension with stress cycles in the range 9.1 ksi - 11.3 ksi (63-78 MPa) with some cycles as high as 14.2 ksi (98 Mpa). It should be noted that these stress ranges do not include any stress concentrations found near the corners, cut-outs, or at the welds.

Overall, the load spectra monitoring and finite element modeling effort produced the following results:

1. Measured $\varepsilon_{max}$ = 400 $\mu\varepsilon$ ($\sigma$=12,000 psi); stress risers around stick attachment could double these stress levels.
2. Twisting, and associated variation in stresses from one side of the boom to the other, is considered minimal.
3. Primary loading stems from bending created when shovel retrieves and carries oilsands while cable restrains (lifts) boom at the end. Measured strains indicated no sign of significant out-of-plane or torsional behaviour of the boom.
4. Over the monitoring period of approximately one week, the data indicated little variation in the strain spectrum, except for the number of cycles at low stress range 1 ksi (7.5 Mpa) or less. A few hundred cycles a day are applied that reach a stress range of around 10 ksi (70 Mpa) away from regions of stress concentration. Monitoring indicates approximately 1,500 cycles per day or 270,000 cycles every 6 months.

5. A preliminary finite element analysis indicates that these stress ranges can more than double in the regions of high stress concentration. It should also be noted that the data collected to date is representative of summer operating conditions. The variation in strain conditions stemming from winter operating conditions should be investigated.
6. A good correlation between field data and finite element predictions indicates that the finite element model is valid and that the method used to load the finite element model is accurate.

### 3.2.1 Modeling of Boom Structure on Cable Shovel

Figure 52 shows a schematic of the shovel boom that includes the internal diaphram plates. Stress risers occur at the welds around each of these plates, as well as at the stick-to-boom attachment point, and act as crack initiation points in the boom. The corresponding FEM of the cable shovel boom is shown in Figure 53. The boom model was discretized using three-node and four-node shell elements implemented in the commercial software ABAQUS [23]. Figures 54 and 55 contain sample analysis results with typical deformation modes and stress levels present in the boom during operation.

FEM results show only minor differences between the principal stresses and the axial stresses. This indicates that the stresses in the boom are primarily axial stresses. The high stress regions, indicated in red, are in areas where fatigue cracks have been detected in the booms. The maximum equivalent stress is 10.4 ksi (72 Mpa). Further mesh refinement is needed to accurately calculate the local stress concentrations expected at the diaphragm welds. *In order to perform the composite doubler evaluations in a conservative manner, the performance testing conducted in this composite doubler repair study will use minimum stress levels of two to four times the stress levels determined in this crack management program. The applied fatigue test spectrums in the performance tests (see Section 3.2.6) were: 24 ksi, 33 ksi, and 41 ksi.*

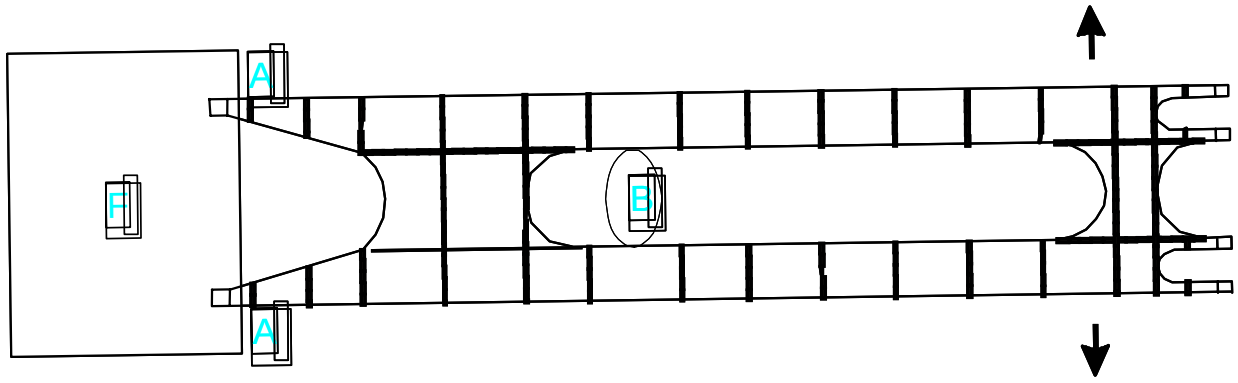


**Figure 52: Top View of Boom Showing Internal Diaphragm Plates**

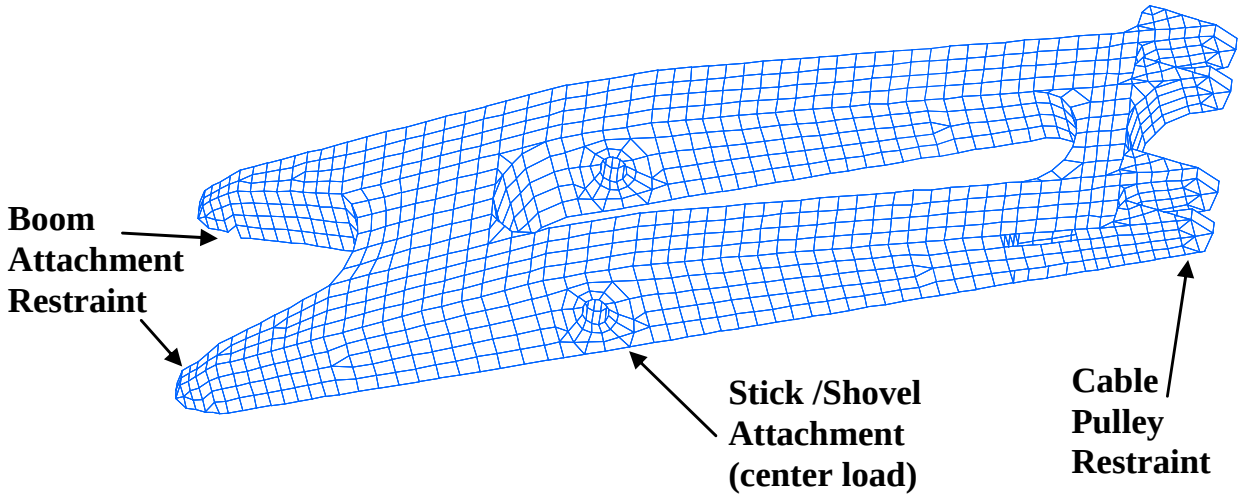


**Figure 53: Finite Element Model of Cable Shovel Boom**

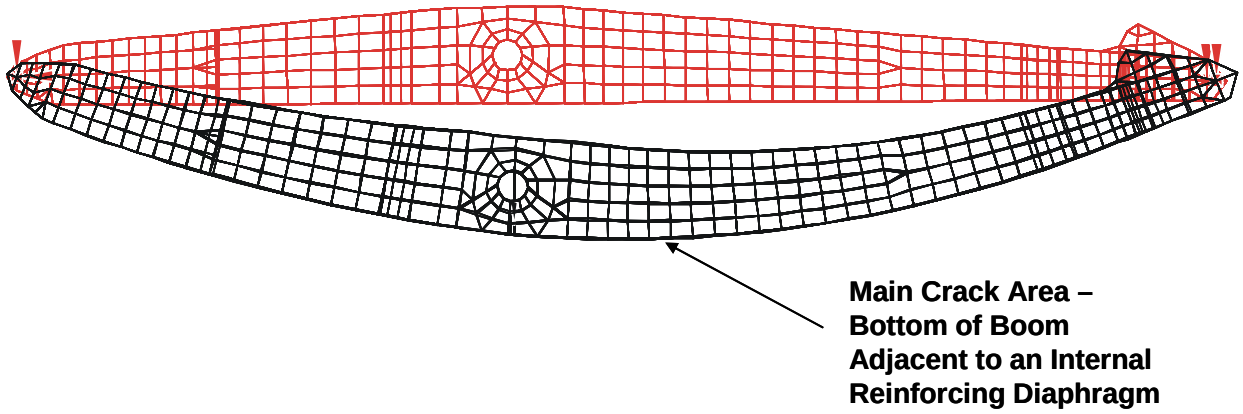


**Figure 54: Primary Deformation During Operation That Causes Boom Cracks**

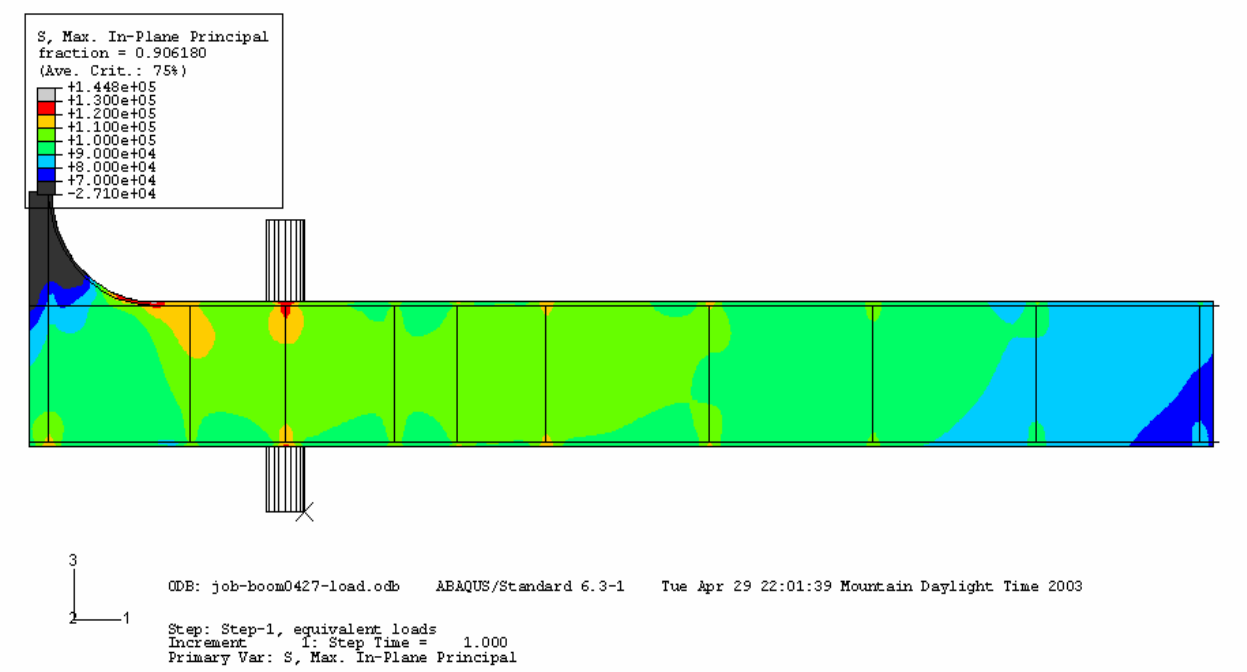


**A. Principle Stresses in Bottom Flange**

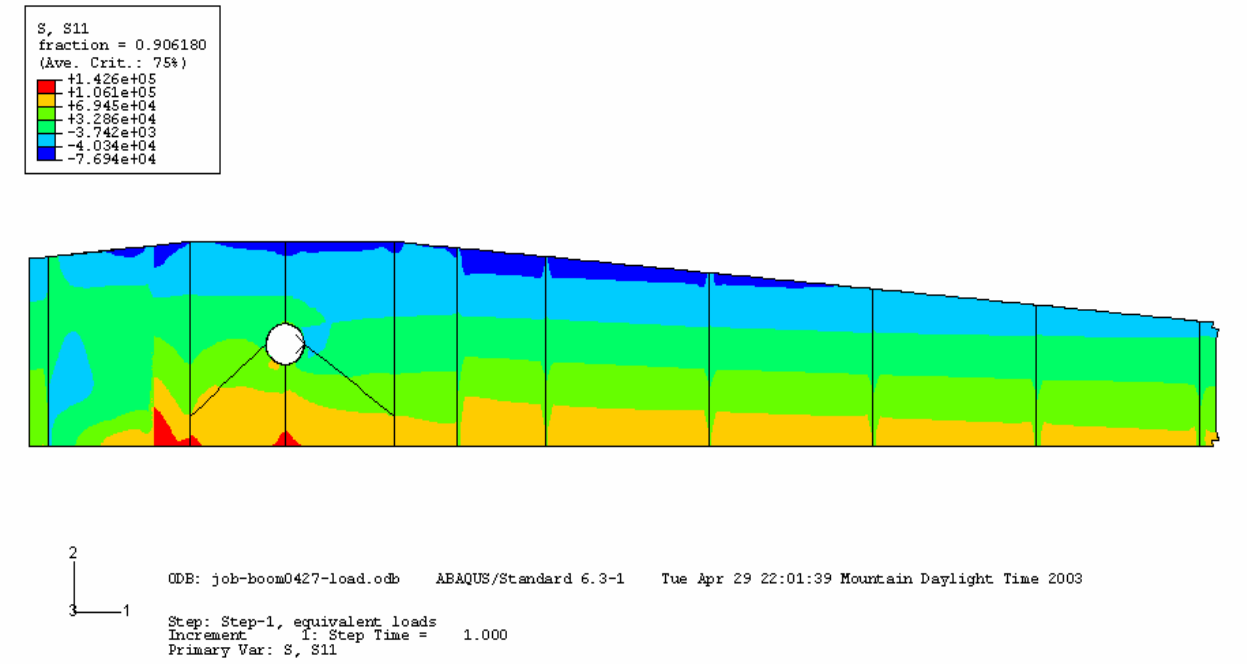


**B. Axial Stresses in Inside Web Region**

**Figure 55: Shovel Boom Stresses Calculated by Finite element Model (Note: stresses shown in the legends are twice the stress range in kPa)**

### 3.2.2 Fatigue Properties of Boom Structure

As part of the crack management program, the Univ. of Alberta and Syncrude conducted crack growth rate tests (specimens produced from representative G40.21 350WT steel plate). The results of six crack growth rate tests conducted at two different stress ranges and two different mean stresses are presented in Figure 56. The results are presented in terms of crack growth rate (m/cycle) versus stress intensity factor range ( $\mathrm{MPa}\sqrt{\mathrm{m}}$ ).

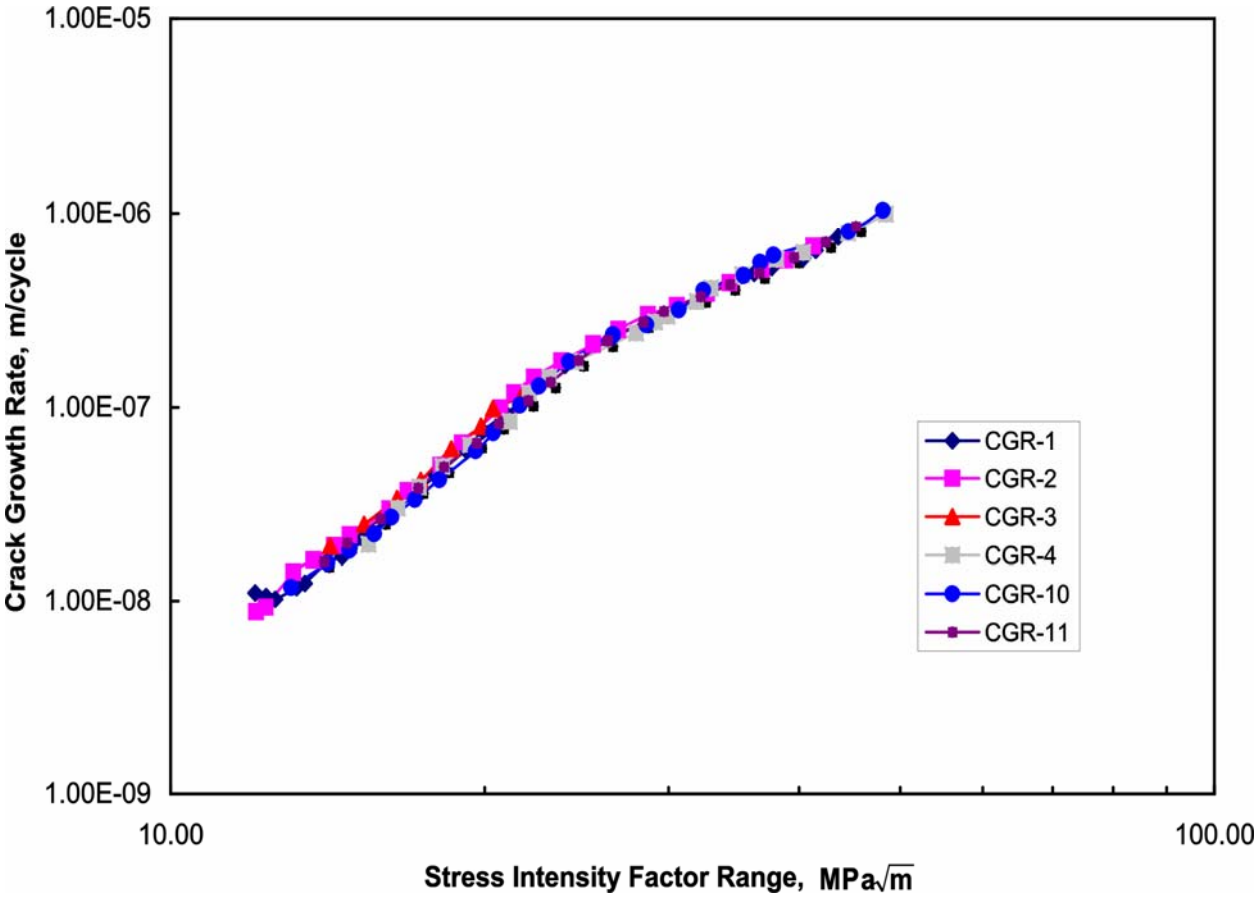


**Figure 56: Results from Crack Growth Rate Tests on Representative Boom Material**

The crack growth rate test results, presented in Figure 56 as the log of crack growth rate versus the log of the stress intensity factor range, indicate that the relationship between crack growth rate and stress intensity factor range is almost linear, as expected. A linear regression analysis was used to obtain the crack growth rate equation required to assess the rate of crack propagation in the shovel boom. The resulting crack growth equation takes the following form:

$$\frac{da}{dN} = 1.55 \times 10^{-12} \left(\Delta K\right)^{3.59} \qquad (8)$$

where, da/dN is the crack growth rate expressed in m/cycle and $\Delta K$ is the stress intensity factor range expressed in $MPa\sqrt{m}$. The data in Figure 56 indicates that a crack might grow anywhere from 0.1" to 10" during a six month operation period (250,000 cycles) depending on the stress intensity factor associated with its location. These crack growth values provide an important basis of comparison when evaluating the crack mitigation capabilities of composite doublers (see Section 4.1).

## 3.3 Damage Tolerance and Crack Mitigation of Composite Doubler Repair Method

### 3.3.1 Tension-Tension Fatigue Panels – Damage Tolerance and Crack Growth Testing

Component level testing was conducted to study the response of ultra-thick doublers on thick steel structure. Fatigue and static tests studied flaw initiation and growth, strain fields, residual strength, ultimate strength, and load transfer. These tests were used to help guide a final family of repair designs for select Syncrude applications and to establish the damage tolerance of composite doubler repairs on steel structure. Engineered flaws were implanted in both the parent structure (cracks) and the composite patch (disbonds and delaminations) to determine if and what detrimental effects they will have on the repair.

Fatigue and ultimate strength tests were performed on specimens with crack, disbond, and impact flaws. Environmental conditions representing temperature and humidity exposure were also included in some of the test specimens. The structural tests were used to: 1) assess the potential for interply delaminations and disbonds between the steel and the laminate, and 2) determine the load transfer and crack mitigation capabilities of composite doublers in the presence of severe defects. A series of specimens were subjected to ultimate tension tests in order to determine strength values and failure modes.

The two main potential causes of structural failure in composite doubler installations are cracks in the steel and adhesive disbonds/delaminations. When disbonds or delaminations occur, they may lead to joint failures. By their nature, they occur at an interface and are, therefore, always hidden. A combination of fatigue loads and other environmental weathering effects can combine to initiate these types of flaws. Inspection of the composite doubler for disbonds and delaminations (from fabrication, installation, fatigue, or impact damage) is essential to assuring the successful operation of the doubler over time.

### 3.3.2 General Fatigue Specimen Description

Figures 57 show the tension-tension fatigue test panels that were used to measure the crack mitigation capability of the proposed repair design. Each specimen consisted of a steel "parent" plate, representing the original Syncrude structure, with a bonded composite doubler. The doubler is bonded over a flaw in the steel. The most severe flaw scenario was an unabated fatigue crack with a co-located disbond (i.e. no adhesion between doubler and parent steel plate) as well as two, large disbonds in the critical load transfer region of the doubler perimeter. Fatigue testing an actual 0.875" or 1.25" thick plate, representing the wall thickness on the cable shovel boom, was not feasible. However, a plate that fits into the thick plate category (3/8" th.)

was used and the proper stiffness ratio between the composite doubler and the parent steel was maintained. The stiffness ratio is defined as:

$$R_x = (E_x t_{laminate})_{BE} / (E_x t)_{St} \quad (9)$$

Where BE represents the Boron-Epoxy laminate properties and St represents the properties of the steel plate. The stiffness ratio should produce adequate stress reduction and crack closure without creating stress concentrations. For the hybrid repair proposed here, the stiffness ratio used was $R_x = 0.3$. Normal stiffness ratios for aircraft repairs with the cracks still present (i.e. not removed by a weld fill process) are on the order of $R_x = 1.0$ to 1.2.

A through-thickness weld repair region was installed in the parent plate before the doubler was installed. This was done by cutting the original plate into two halves and welding them together using the penetration weld profile shown in Figure 58. This process was used to simulate the hybrid repair where a composite doubler is placed over a region where a crack has been removed by a welding process. In order to simulate a worst case condition where the weld process fails to completely remove a crack, a fatigue crack was also added to the weld region of the test specimen prior to bonding the doubler in place. The final test specimen configuration is presented in Section 3.2.4.

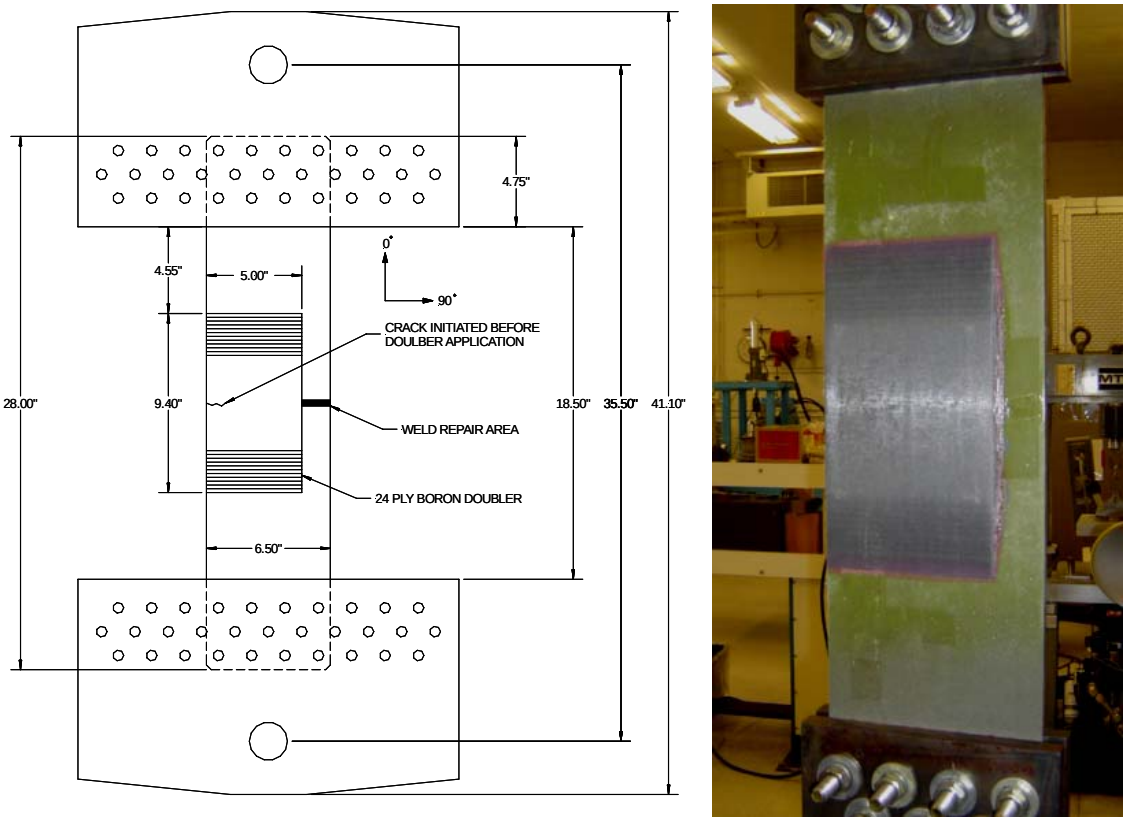


**Figure 57: Fatigue Test Panel with Composite Repair**

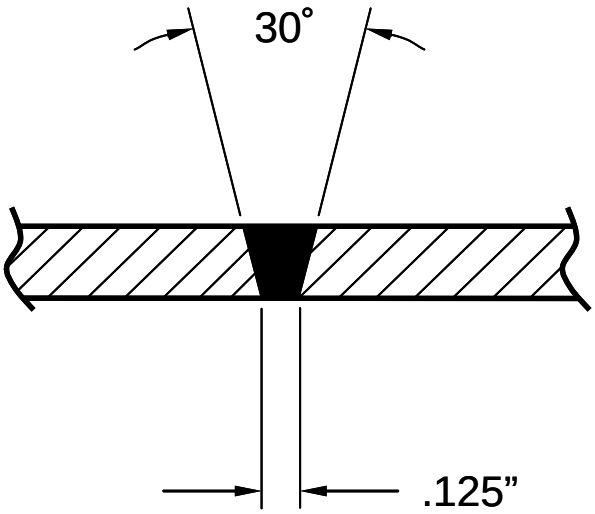


**Figure 58: Crossection of Through-Thickness Weld Repair Installed Over The Entire Width of Steel Plate**

Material - The parent steel plate was ASTM 572-50 material. It was chosen because its chemical make-up closely matches the steel material used in the Syncrude cable shovel boom (Canadian Spec CAN/CSA-G40.21, Grade 50WT). Table 4 summarizes the chemical make-up of the CAN/CSA-G40.21 material used in the shovel booms and compares it to the material available for use in this test series. The plate thickness was 0.375”. The Boron-Epoxy material was type 5521/4. The specifications for production of the Boron-Epoxy material was as follows: 1) SAE Aerospace Material Specification (AMS) 3865C for the Boron fiber, and 2) AMS 3867B and AMS 3867/4A specification for the Boron-Epoxy pre-preg tape material. The adhesive material was AF-163, (0.06 PSF) and the primer was Cytec BR6747. All composite doublers were installed using the process arrived at in Section 2.0 and the procedure listed in Appendix B.

### 3.3.3 Composite Doubler Design for Tension Test Specimens

The Boron-Epoxy composite doublers were a multi-ply, multi-directional lay-up of 24 plies: [0,0,0,0,45,-45,0,0,0,0,-45,0,0,45,0,0,0,0,-45,45,0,0,0,0] with the top ply having the same footprint as the first ply that contacts the adhesive layer. Thus, each composite doubler had a nominal post-cure thickness of 0.140” (approximately 0.0057” per ply plus a nominal pre-cure adhesive layer of 0.010”; the post-cure adhesive thickness is approximately 0.006”). The plies were cut to different lengths in the X (tension load) direction in order to taper the thickness of the resulting doubler edges. This produced a more gradual load transfer between the steel and the doubler (i.e. reduces the stress concentration in the bondline around the perimeter). A ply taper ratio of approximately 16:1 was utilized; this results in a reduction in length of 16 times the ply thickness (approximatley 0.2” step every 2 plies). The number of plies and fiber orientations produced an extensional stiffness ratio of Boron-Epoxy to steel of 0.3:1 $\{(Et)_{BE} = 0.3\ (Et)_{Steel}\}$. The subsections of 3.2.3 below describe how this doubler design was produced.

| Carbon Steel Material Composition Comparisons | | | | | | | | |
|---|---|---|---|---|---|---|---|---|
| **Material Type** | **Yield** | **Tensile Strength** | **Carbon** | **Maganese** | **Phosphorous** | **Sulphur** | **Silicon** | **Cb** |
| CAN/CSA-G40.21, Gr. 50WT | 50K | 70/95K | .22 max | .80-1.50 | .03 max | .04 max | .15/.40 | .10 max |
| ASTM A572 Gr. 50 | 65K | 85K | .23 max | 1.35 max | .04 max | .05 max | .40 max | .05 max |
| ASTM A607, Gr. 50, Class 1 | 50K | 65K | .23 max | 1.35 max | .04 max | .04 max | - | 0.005 |
| 4130 Chromium-Molybdenum Steel | 63K | 97K | .28/.33 | .40/.60 | .035 max | .04 max | .15/.35 | Cr .80/1.1 |
| ASTM A570 Gr. 50 | 55K | 65K | 0.25 | 1.35 | 0.035 | 0.04 | - | - |
| ASTM A569 (ASTM A1011) | 38K | 52K | 0.15 | 0.60 | 0.035 | 0.04 | - | Cu .20 min |
| ASTM A537 | 50K | 70/90K | 0.24 | .70/1.35 | 0.035 | 0.035 | .15/.50 | - |
| ASTM A36 | 36K | 58/80K | 0.25 | - | .04 max | .05 max | .40 max | Cu .20 min |
| Stainless Steel (316) | 30K | 75K | 0.08 | 2.00 | 0.045 | 0.03 | 1.0 max | Cr 16.00 |

**Table 4: Chemical Composition of Syncrude Cable Shovel Steel and the Steel Used in Performance Test Specimens**

#### 3.3.3.1 Calculation of Laminate-to-Steel Extensional Stiffness Ratio

This section describes the method that was used to arrive at the stiffness parameter, $E_x t$, for composite doublers. The calculations used classical laminated plate theory, along with Boron-Epoxy lamina properties, to arrive at the average cured laminate modulus $E_x$ (where $x$ is the direction of the fatigue load).

The Boron-Epoxy lamina properties at room temperature are:

$$E_{11} = 28.0 \text{ X } 10^6 \text{ psi}$$

$$E_{22} = 2.7 \text{ X } 10^6 \text{ psi}$$

$$G_{12} = 0.8 \text{ X } 10^6 \text{ psi}$$

$$\nu_{12} = 0.21$$

$$t_{ply} = 0.0057 \text{ in.}$$

The average laminate properties are calculated using the individual lamina properties listed above along with the following specific lay-up configuration: 1) 24 plies {[0,0,0,0,45,-45,0,0,0,0,-45,0,0,45,0,0,0,0,-45,45,0,0,0,0]}, and 2) laminate thickness t = 0.14" (24 plies X 0.0058"/ply). The resulting laminate properties were calculated:

$$E_x = 25.2 \text{ X } 10^6 \text{ psi}$$

$$G_{xy} = 3.77 \text{ X } 10^6 \text{ psi}$$

$$\nu_{xy} = 0.32$$

Compared to a 0.375" thick, steel plate, the stiffness ratio is,

$$R_x = (E_x t_{laminate})_{BE} / (E_x t)_{St} \qquad (9)$$

$$= \frac{(25.2 \text{ X } 10^6 \text{ psi})(0.14")}{(30 \text{ X } 10^6 \text{ psi})(0.375")}$$

$$R = 0.31$$

This method was used to arrive at the 0.3 extensional stiffness ratio listed in the composite doubler hybrid design plan (Section 3.2.2). By designing the specimens using the nondimensional stiffness ratio, it is possible to extrapolate these results to various parent structure and composite laminate combinations.

#### 3.3.3.2 Fatigue Test Specimen Design Features

The composite laminate design was completed using the repair design methodology described in Appendix C. This process was aided by the use of an Excel-based analysis package [24] that automates the application of the principles presented in Appendix C. The computer program allows the user to input the parameters listed below and to assess how variations in the design parameters will affect the strain fields in and around the composite repair. Laminate design principles were used to determine the $E_x$, $E_y$, $\nu_{xy}$, and $G_{xy}$ for a composite lay-up design. The required number of plies and the transfer length, which defines the overall repair length, were calculated for a one-sided (external) composite repair. An iterative process was then followed whereby specific design parameters were adjusted in an effort to meet general design guidelines. The input data and doubler design results are summarized below.

Design Input Data:

- Parent Plate Thickness = 0.375" th. (ASTM 572)
- Parent Plate Width = 6.5"
- Parent Plate Modulus = 30 X $10^6$ psi
- Doubler (Patch) Thickness = 24 plies X 0.0058" = 0.140" th.
- Doubler Length, $L_r$ = 9.4" (constant thickness length = 5"; taper length @ ea. side = 2.2")
- Doubler Width = 5"
- Doubler Width / Parent Width = 76%
- Stacking sequence - wedding cake stacking sequence (largest ply at the steel interface; sequentially smaller footprint plies are stacked on top)
- Parent Plate Length = 9.4" doubler + 4.55" ea. side for load + 4.75" ea. side for grips = 28" long
- Taper Ratio = 16 (0.2" step every 2 plies). When combined with patch thickness, the taper ratio determines the transfer length, $\beta$.
- Vacuum bag debulk every 4 plies (B-stage cure at autoclave pressure may be option for final design of 65-70 plies)

- Patch shape = rectangular. The doubler edge tapers will be in the X-direction (axial) only as shown in Figures 57 and 59. The doubler will have no taper perpendicular to the axial direction (Y-direction across width of boom) because: 1) it is reinforcing the axial strength of the boom, and 2) it will probably be located along the edge of the box beam plate where full reinforcement strength is needed (i.e. tapered edges do not provde full strength around the perimeter).
- Load constant, N, which is related to the full thickness length of the patch. The overlap length, or one half the doubler full thickness length is equal to N times the transfer length β.

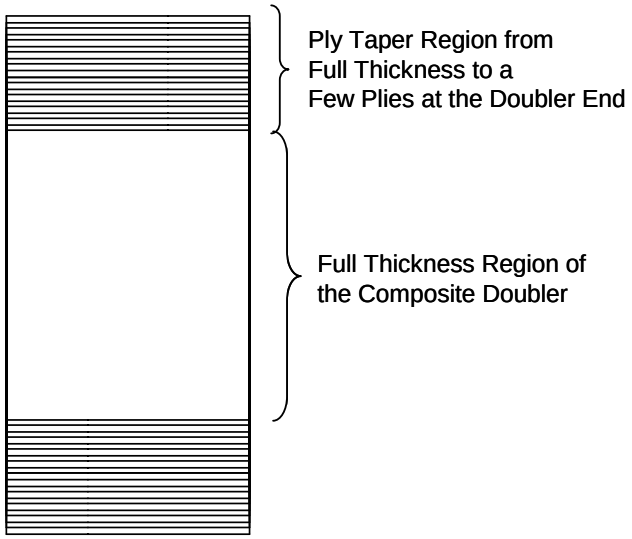


**Figure 59: Composite Doubler for Tension Beam Repair Has Taper in Axial Direction Only (X-direction) and Most Plies Are Oriented in the Axial Direction**

Doubler Design Notes:

- $45^{o}$ plies provide better performance in shear loads.
- Use of corner angle (more difficult lay-up) reduces stress riser in steel-doubler interface – no corner angle used in current designs.
- Adding width improves load transfer into doubler and decreases bypass strain.
- Increasing taper ratio reduces peel stresses – in order to minimize the total doubler length, the taper ratio is purposely selected for the lower end (16); desire is to determine if adequate performance is obtained with this design; higher taper ratios will require longer doublers with more material and more heat requirements.
- No side taper at edge of doubler where maximum reinforcement is needed.
- Twisting of boom (shear loads) is considered minimal – primarily tension loads with occasional reverse compression loading during shovel break-through during digs.

Doubler Design Output:

- Doubler Lay-Up = [0,0,0,0,45,-45,0,0,0,0,-45,0,0,45,0,0,0,0,-45,45,0,0,0,0]

- Stiffness Ratio = 0.31
- Effective Doubler Modulus = 25.2 X $10^6$ psi

#### 3.3.3.3 Doubler Design Analysis - Performance Criteria and Trade-Off Study with Design Prototypes

The input parameters listed above where placed in the spreadsheet program and the doubler lay-up, also listed above, was determined. The repair was optimized by varying the number and orientation of the plies, the taper ratio, the load constant, and the patch geometry. Table 5 shows one of the iterations where trial values are substituted for existing input parameters.

| | Range Tested: | Current Value: | Trial Values |
|---|---|---|---|
| Stiffness Ratio, S | 1.1 - 1.6 | 0.307 | **0.307** |
| Step-off Rate | 15.0 - 50.0 | 20 | **16.000** |
| Patch Width | 1.5 - 5.0 | 5.000 | **5.000** |
| Load Constant, N | 4.0 - 12.0 | 10.000 | **5.000** |
| Adhesive Thickness | 1 | 1 | **1.000** |
| (number of plies) | 2 | | |
| | 3 | | |
| Patch shape | Rectangle | 1 | **1.000** |
| | 30-deg Corner | | |
| | 45-deg Corner | | |
| Stacking Sequence | Wedding Cake | 1 | **1.000** |
| | Reverse Wedding Cake | | |

*Current Value doubler length = 10.5" (taper length = 2.75" so taper ratio is 20)*
*Trial Value doubler length = 9.4" (taper length = 2.2" so taper ratio is 16)*

**Table 5: Iteration on Composite Doubler Design by Varying Input Parameters**

After each iteration, specific guidelines were reviewed to optimize the repair design. The efficiency of the repair was evaluated by studying the resulting strain ratios for the composite doubler repair installation. Figure 60 shows a typical repair under uniaxial loading. Strain locations G1 through G8 pinpoint various regions of the doubler and surrounding parent structure. Table 6 defines the strain ratios that are calculated by comparing the strain levels at each of the various points in Figure 60. In addition, Table 6 lists the goal (design guidelines) for these strain ratios along with a description of the criticality of each strain ratio. The strain ratios listed are in order of importance and the first two items are primary relationships. Therefore, the goal of the iterative design process is to optimize the ratios for the first two or three relationships while producing results that are close to the design goal for the lower few relationships.

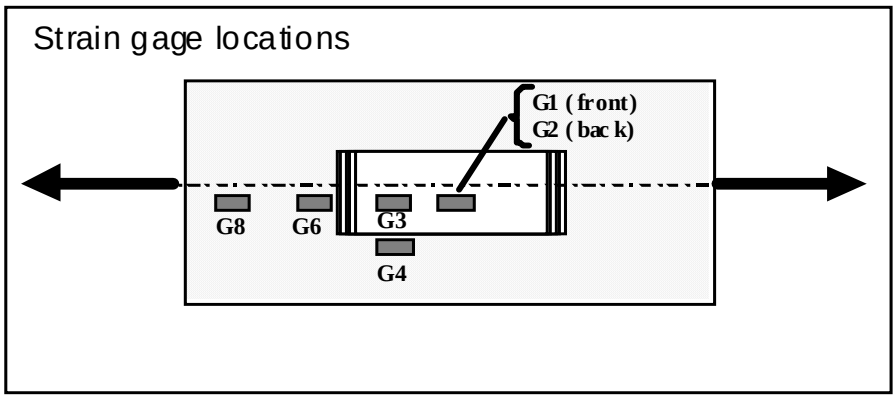


**Figure 60: Strain Locations for Assessing Composite Doubler Designs**

| Strain Gage Ratio | Priority | Minimize or Maximize | Goal | Criticality of the Ratio |
|---|---|---|---|---|
| G2/G8 | 1 | Min | < 0.60 | Lower strain ratio prevents crack growth. |
| G6/G8 | 2 | Min | < 1.15 - 1.30 | Lower peel stresses / stress concentration |
| | | | | at edge of patch |
| G1/G2 | 3 | Max | > 0.75 | Doubler design carries more load than |
| | | | | underlying aluminum substrate. |
| G1/G8 | 4 | Max | > 0.70 | Relationship of doubler strain above notch |
| | | | | to far-field steel strain. |
| G3/G4 | 5 | Max | > 1.30 | Doubler design carries more load than |
| | | | | adjacent steel structure. |
| G3/G8 | 6 | Max | > 0.70 | Relationship of doubler strain in middle |
| | | | | of doubler to far-field steel strain. |
| G4/G8 | 7 | Min | < 0.50 | Lower steel strain near doubler |
| | | | | indicates if is carrying more load. |

| Strain Ratio: | Criteria: |
|---|---|
| G2/G8 | Strain at crack compared to far field strain is most critical ratio to prevent or slow crack propagation by alleviating strain concentration at the crack. Patch width has most effect on G2/G8. |
| G6/G8 | Strain kick in parent metal at end of patch compared to far field strain should be minimized to lessen p stresses at adhesive edge. Requires less stiff, thinner, shorter patch with abrupt taper. N most effecti |
| G1/G2 | Strain on the patch above the notch compared to the strain on the back side of the substrate should be maximum to indicate a patch design efficiently carrying most of the applied load. |
| G1/G8 | Relationship of strain in doubler directly above notch to far field steel strain shows load efficiency |
| G3/G4 | Quarter patch strain on patch to same location on parent |
| G3/G8 | Quarter patch strain to far field |
| G4/G8 | Quarter steel strain or bypass strain to farfield strain |

**Table 6: Performance Criteria for Assessing Viability of Composite Doubler Repairs**

Table 7 summarizes the results from the final two design iterations. The green-filled boxes indicate that the strain ratio goal was achieved. Note that in the second design scenario - which was the final design selected for the Syncrude performance tests - the top three goals were met while the lower four goals are very close to the desired numbers. Finally, Table 8 summarizes the geometry of the composite doubler design to reveal a 24-ply doubler that is 9.4" long, 5" wide, has a 2.2" long taper region (16:1 ply drop-off rate), and a central, full-thickness length of 5". Figure 61 shows the engineering drawing of this repair.

**Design Scenario #1**

| Strain Ratio: | Goal | Current |
|---|---|---|
| G2/G8 | < 0.60 | 0.2140 |
| G6/G8 | < 1.15 - 1.30 | 1.3103 |
| G1/G2 | > 0.75 | 1.3147 |
| G1/G8 | > 0..70 | 0.8706 |
| G3/G4 | > 1.30 | 1.3656 |
| G3/G8 | > 0.70 | 0.7906 |
| G4/G8 | < 0.50 | 0.6181 |

*N = 10; $W_r$ = 5, Taper = 2.75 (TR = 20); $R_x$ = 0.336; Off-Angle Plies = $\pm 30^o$*

**Design Scenario #2**

| Strain Ratio: | Goal | Current |
|---|---|---|
| G2/G8 | < 0.60 | 0.3764 |
| G6/G8 | < 1.15 - 1.30 | 1.1860 |
| G1/G2 | > 0.75 | 1.0373 |
| G1/G8 | > 0..70 | 0.6690 |
| G3/G4 | > 1.30 | 1.2457 |
| G3/G8 | > 0.70 | 0.6223 |
| G4/G8 | < 0.50 | 0.5910 |

*N = 5, $W_r$ = 5, Taper = 2.2 (TR = 16); $R_x$ = 0.307; Off-Angle Plies = $\pm 45^o$*

**Table 7: Comparison of Strain Ratio Evaluations Corresponding to User-Supplied Design Trade-Off Adjustments**

| Patch Design from 'Baker Criteria' sheet: | |
|---|---|
| No. of plies | 24 |
| Transfer Length β (in) | 0.4805 |
| Patch Width Wp (in) | 5.0000 |
| Constant Thickness Length Lr (in) | 5.0000 |
| Step-off Rate of tapered edge | 16 |
| Tapered length Lt [each end] (in) | 2.2000 |
| Total length Lp (in) | 9.4000 |
| Corner Angle (deg) | 0 |
| Stacking Sequence | Wedding Cake |

**Table 8: Summary of Final Composite Doubler Design Dimensions**

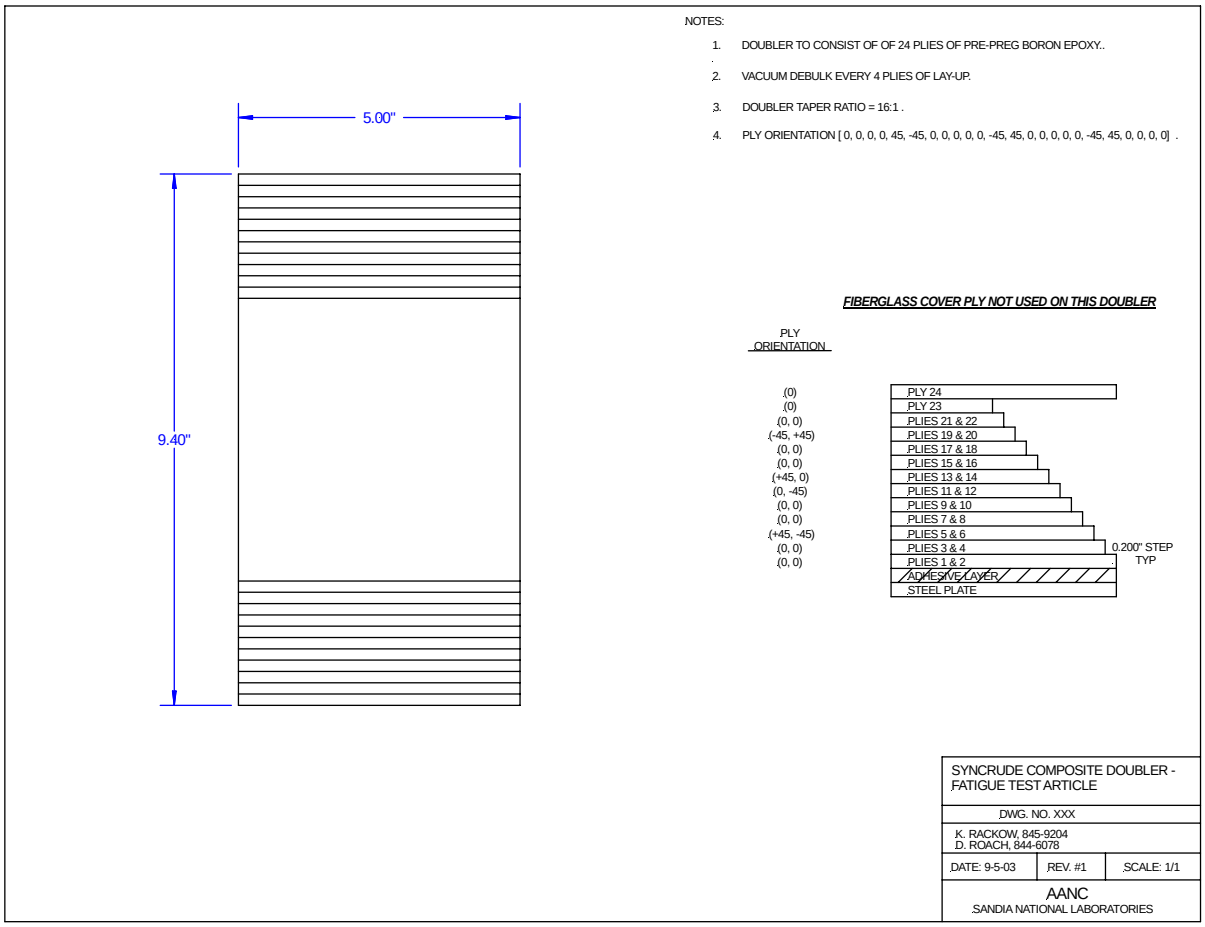


**Figure 61: Final Composite Doubler Design**

### 3.3.4 Test Specimen Configurations

The specimen configurations that were tested are summarized in Table 9. All but three of the 18 specimens consisted of a steel "parent" plate, representing the parent Syncrude structure, with a bonded composite doubler. The doubler was bonded over a unabated crack in the steel structure. The other three specimens contained unrepaired fatigue cracks in the weld region and provided baselines for doubler performance comparisons. Tension-tension fatigue and residual strength tests were conducted on these specimens to evaluate: 1) the composite doubler design methodology, 2) the doubler installation process, 3) the damage tolerance of composite repairs, 4) crack mitigation performance, and 5) long-term durability and strength in the presence of severe environments and off-design conditions.

Figures 62 and 63 show the two basic building blocks for the various test configurations: 1) precracked specimen with optimum composite doubler repair and 2) precracked specimen with a flawed composite doubler repair. The installed flaws consisted of pull tabs in the critical load transfer (tapered edge) region and Teflon inserts placed directly over the crack. Both methods produce disbonds between the composite doubler and the steel structure. Figure 64 shows the flaw inserts placed on a steel panel before the application of the composite repair. It also shows two composite doublers being postioned for final curing and bonding to the steel panels. Note the six thermocouples placed around the perimeter of the doubler installations. These provide temperature feedback to the hot bonder to control the cure temperature profile. The fatigue and ultimate strength test specimen configurations are summarized as follows:

- All 18 specimens contained a full penetration weld simulating a crack fill process (see Fig. 58)
- Total of 18 specimens: 15 with composite doubler repairs, 3 unrepaired baseline specimens
  1. Weld repair only with re-crack (no composite doubler)
  2. Hybrid repair - weld with re-crack and repaired with optimum composite doubler
  3. Hybrid repair - weld with re-crack and repaired with flawed composite doubler
  4. Hybrid repair - weld with re-crack and repaired with optimum composite doubler; specimen conditioned with hot-wet and/or cold exposure
  5. Hybrid repair - weld with re-crack and repaired with flawed composite doubler; specimen conditioned with hot-wet and/or cold exposure
- Three fatigue stress spectrums: 24 ksi, 33 ksi, 41 ksi
- Ultimate failure tests conducted on select panels after fatigue testing

Generation of Cracks in Steel Parent Material - Prior to installing the composite doublers, fatigue cracks were generated in the weld region of the steel substrate plate. Specimen configurations listed in Table 9 with the descriptor "re-crack" were used to simulate welded repairs that subsequently cracked. First, 0.75" length sawcuts were placed in the steel panels to provide starter notches for the fatigue cracks. Second, tension-tension fatigue loads were applied and crack gages with 0.010" resolution were used to monitor 0.25" of actual fatigue crack growth in the specimens. These pre-doubler, crack lengths were recorded and used as the initial crack lengths in the subsequent composite coupon fatigue tests after the composite doubler was installed. Three different fatigue load spectrums were applied to induce stress levels of 24 ksi, 33 ksi, and 41 ksi. Note that the yield stress level for the ASTM572 material is 65 ksi.

| Specimen No. | Condition | Pristine or Flawed | Stress Spectrum (psi) | Specimen Configuration |
|---|---|---|---|---|
| SYN-FAT-10 | Baseline Unrepaired | N/A | 2ksi - 24 ksi | Weld repair only with re-crack (no composite doubler) |
| SYN-FAT-5 | No Conditioning | Pristine | 2ksi - 24 ksi | Hybrid weld & composite doubler repair with re-crack |
| SYN-FAT-9 | No Conditioning | Flawed | 2ksi - 24 ksi | Hybrid weld & composite doubler repair with re-crack and installation flaws |
| SYN-FAT-16 | Hot-Wet Plus Cold | Pristine | 2ksi - 24 ksi | Hybrid weld & composite doubler repair with re-crack |
| SYN-FAT-18 | Hot-Wet Plus Cold | Flawed | 2ksi - 24 ksi | Hybrid weld & composite doubler repair with re-crack and installation flaws |
| SYN-FAT-5A | No Conditioning | Pristine | 2ksi - 33 ksi | Hybrid weld & composite doubler repair with re-crack |
| SYN-FAT-9A | No Conditioning | Flawed | 2ksi - 33 ksi | Hybrid weld & composite doubler repair with re-crack and installation flaws |
| SYN-FAT-14 | Hot-Wet | Pristine | 2ksi - 33 ksi | Hybrid weld & composite doubler repair with re-crack |
| SYN-FAT-16A | Hot-Wet Plus Cold | Pristine | 2ksi - 33 ksi | Hybrid weld & composite doubler repair with re-crack |
| SYN-FAT-18A | Hot-Wet Plus Cold | Flawed | 2ksi - 33 ksi | Hybrid weld & composite doubler repair with re-crack and installation flaws |
| SYN-FAT-3 | Baseline Unrepaired | N/A | 2ksi -41 ksi | Weld repair only with re-crack (no composite doubler) |
| SYN-FAT-4 | Baseline Unrepaired | N/A | 2ksi -41 ksi | Weld repair only with re-crack (no composite doubler) |
| SYN-FAT-7 | No Conditioning | Pristine | 2ksi -41 ksi | Hybrid weld & composite doubler repair with re-crack |
| SYN-FAT-8 | No Conditioning | Pristine | 2ksi -41 ksi | Hybrid weld & composite doubler repair with re-crack |
| SYN-FAT-12 | No Conditioning | Flawed | 2ksi -41 ksi | Hybrid weld & composite doubler repair with re-crack and installation flaws |
| SYN-FAT-13 | No Conditioning | Flawed | 2ksi -41 ksi | Hybrid weld & composite doubler repair with re-crack and installation flaws |
| SYN-FAT-15 | Hot-Wet | Pristine | 2ksi -41 ksi | Hybrid weld & composite doubler repair with re-crack |
| SYN-FAT-17 | Hot-Wet | Flawed | 2ksi -41 ksi | Hybrid weld & composite doubler repair with re-crack and installation flaws |

**Table 9: Specimen Matrix for Composite Doubler Fatigue Panels**

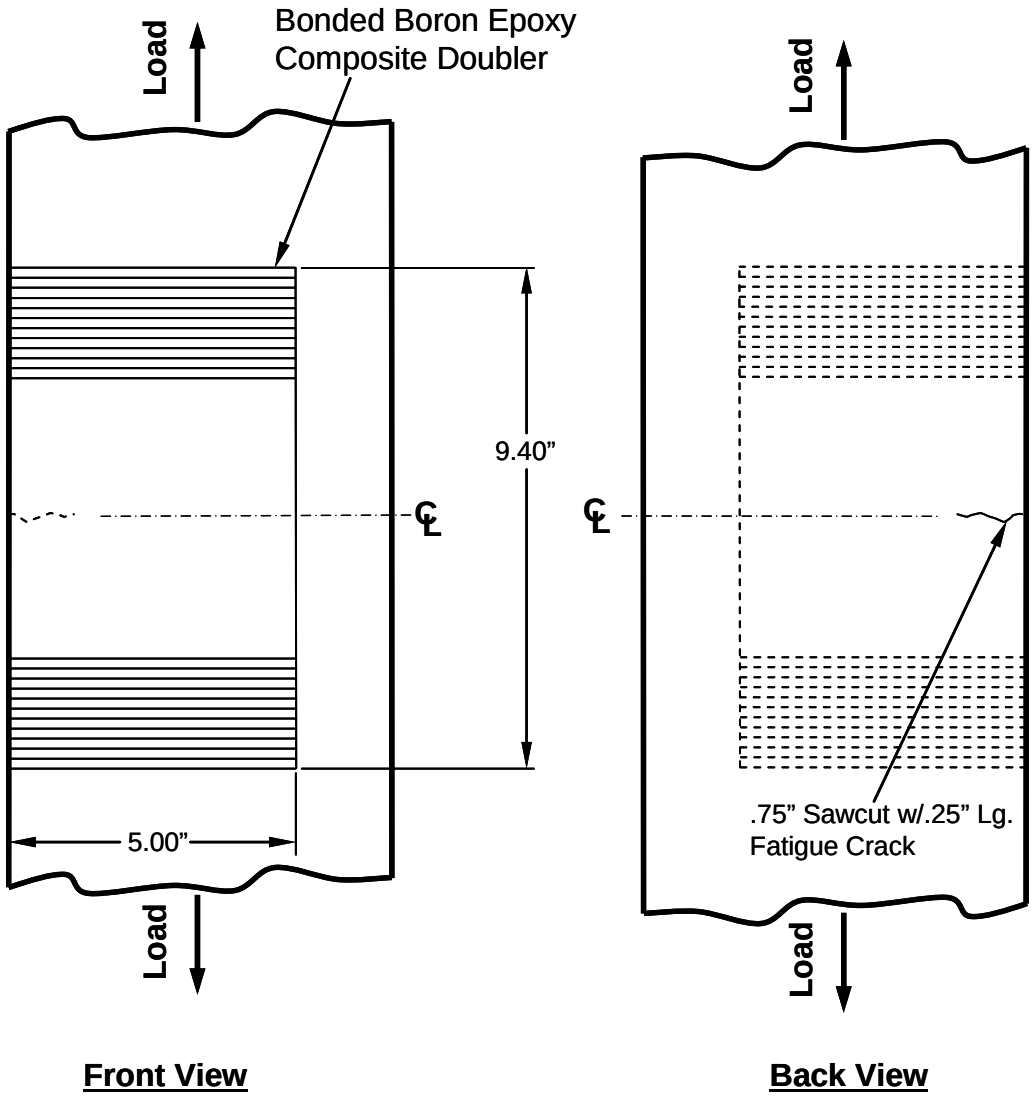


**Figure 62: Tension-Tension Fatigue Panel with Optimum Composite Doubler Repair Installation**

Temperature and Humidity Conditioning – Table 9 also indicates the specimens that were subjected to temperature and humidity conditioning. In order to simulate moisture absorption that may occur during field operations, the specimens were placed in an environmental conditioning chamber at $140^{o}F \pm 5^{o}F$ and 97% ± 3% relative humidity. The specimens remained in the chamber for 30 days to provide a period of time sufficient to achieve saturation moisture content. Some of the test specimens were then subjected to temperatures of $0^{o}F$ to simulate low temperature operating conditions for composite doublers containing a high moisture content. Any trapped moisture could freeze and fracture the composite fibers. Figure 65 shows a photo of the specimen being inserted into the environmental chamber for hot-wet conditioning and the

freezer for 0°F temperature exposure. *Note that this conditioning produces very conservative tests since the normal fiberglass cover plies and epoxy paint coatings, absent in the fatigue test specimens, will almost eliminate moisture absorption in the field.*

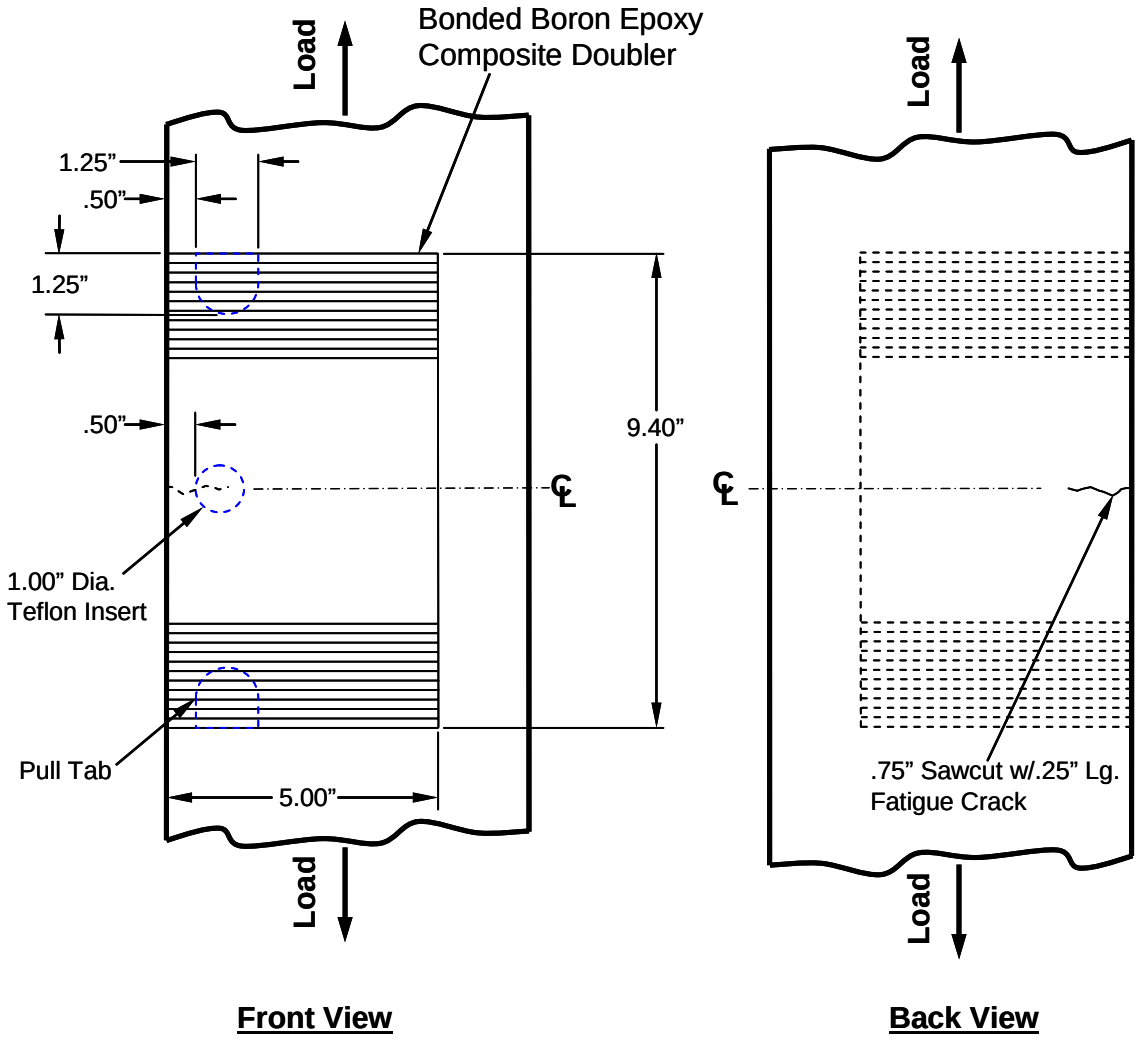


**Figure 63: Tension-Tension Fatigue Panel with Flawed Composite Doubler Repair Installation**

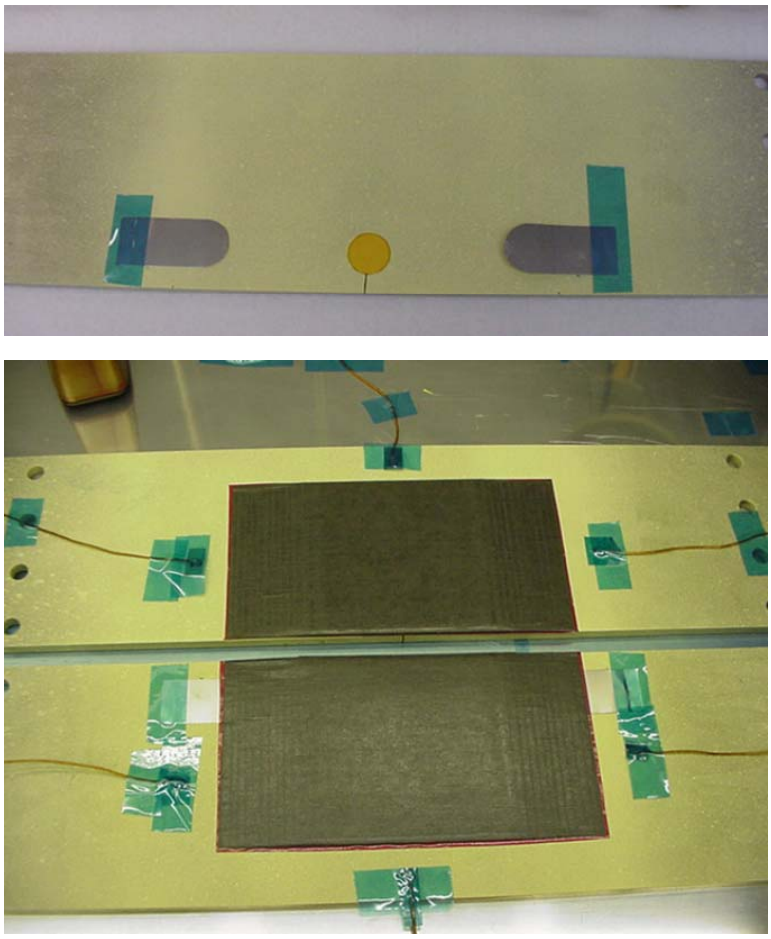

**Figure 64: Flaw Insert Placement On Steel Surface and Cure of Composite Doublers on Steel Coupons**

**Figure 65: Tension Specimens Being Placed into Environmental Chamber and Freezer for Hot/Wet and Cold Conditioning**

### 3.3.5 Load Spectrums and Instrumentation

The lowest stress level for the fatigue tests (baseline stress levels) was 24 ksi to represent slightly more than two times the stress level measured during field monitoring exercises. This allowed us to assess composite doubler repairs in stress riser regions where the stress may be amplified by as much as a factor of two. Additional fatigue tests applied stress levels of 33 ksi (3 times the field stress levels) and 41 ksi (3.7 times the field stress levels) in order to study performance in high stress environments approaching yield levels. These were extremely conservative tests intended to establish safety factors associated with composite doubler repair technology. All fatigue tests were conducted at a test frequency of 3 – 5 Hz. Several specimens that survived the fatigue tests were subjected to ultimate tension tests in order to determine their ultimate/residual strength and to determine failure modes. During residual strength testing, the load was increased, using displacement mode control, at a continuous rate of 0.05 inch/minute. Failure was defined as the point where the specimen was unable to sustain an increasing load.

Strain Field and Crack Growth Monitoring - Load transfer through the composite doubler, stress reduction around cracks, and stress risers around the defects were monitored using the strain gage layouts shown in Figures 67-70. Some biaxial gages were used to measure both the axial and transverse strains in the anisotropic composite material. [In Figs. 67-68, the first number listed represents the axial gage and the second number represents the lateral gage.] Crack growth gages with a resolution of 0.2" per filament were mounted on the back side of the specimen (steel surface) to measure the sequential growth of the seeded fatigue crack. Strain measurements were acquired before and after the fatigue tests and at select intervals during the fatigue tests. These intervals were determined by crack propagation in the test specimen (i.e. after the crack gage indicated additional crack growth).

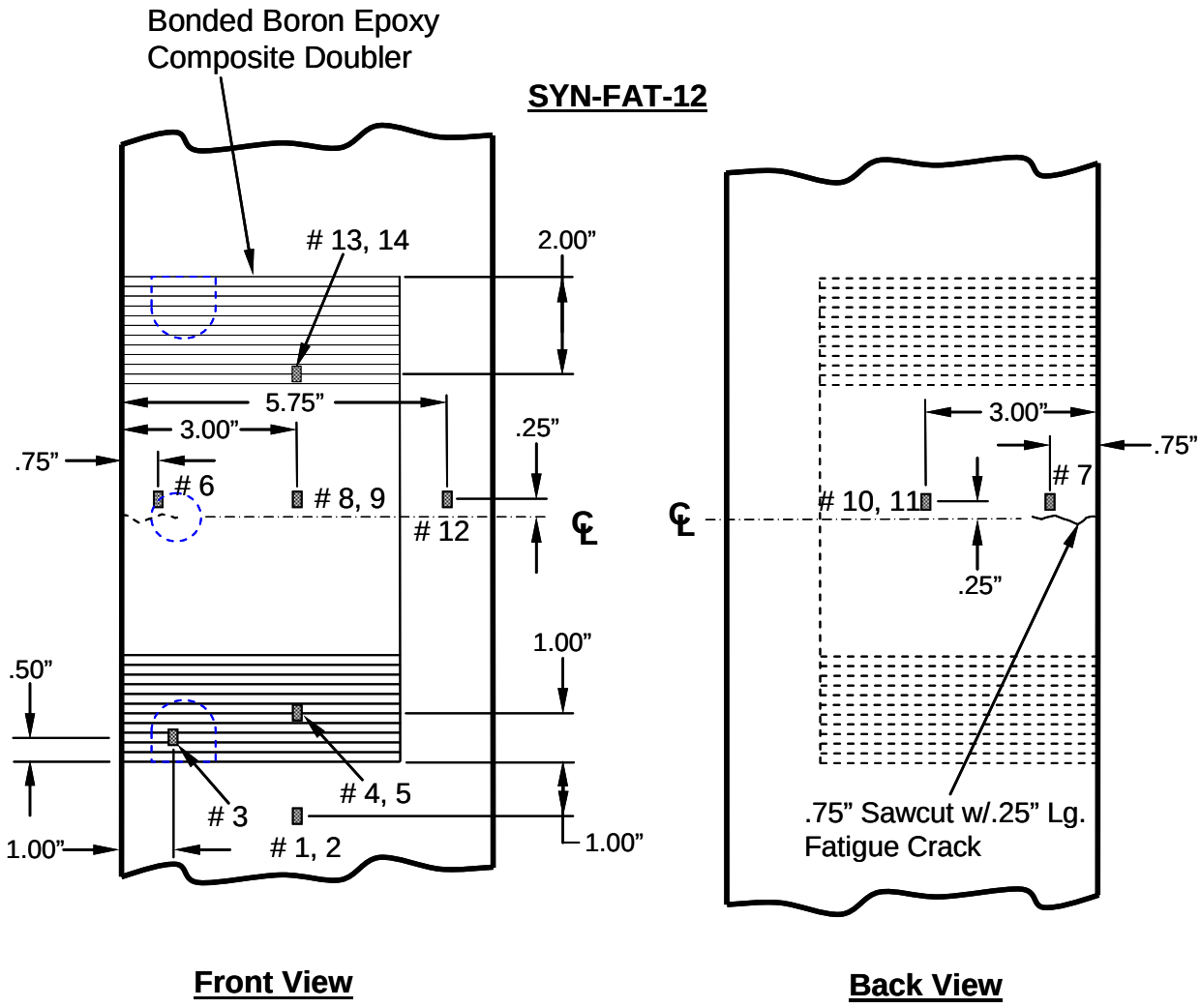


**Figure 67: Strain Gage Layout on <u>Flawed</u> Composite Repair Installation; <u>Unconditioned</u> Specimen SYN-FAT-12**

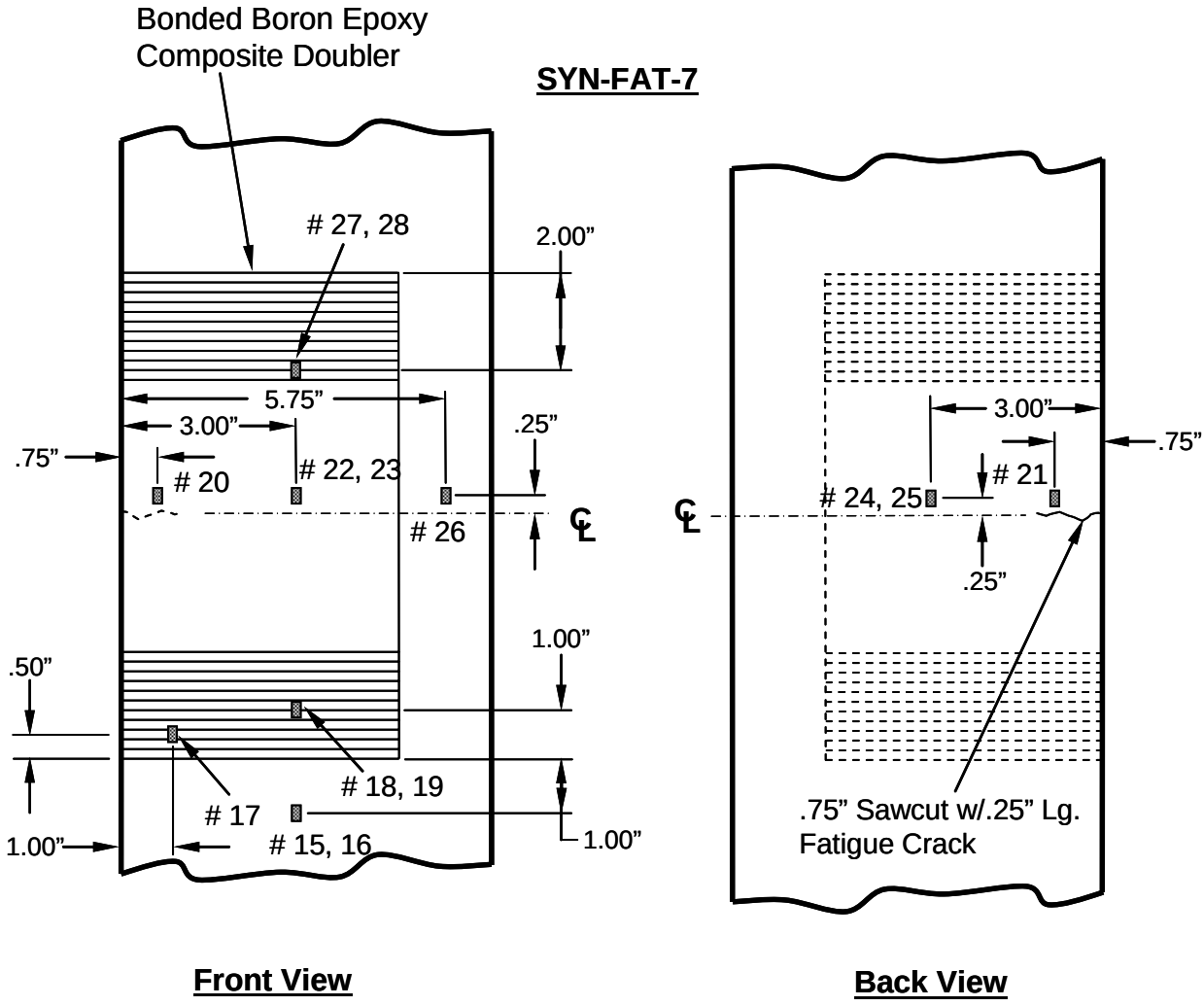


**Figure 68: Strain Gage Layout on <u>Unflawed</u> Composite Repair Installation; <u>Unconditioned</u> Specimen SYN-FAT-7**

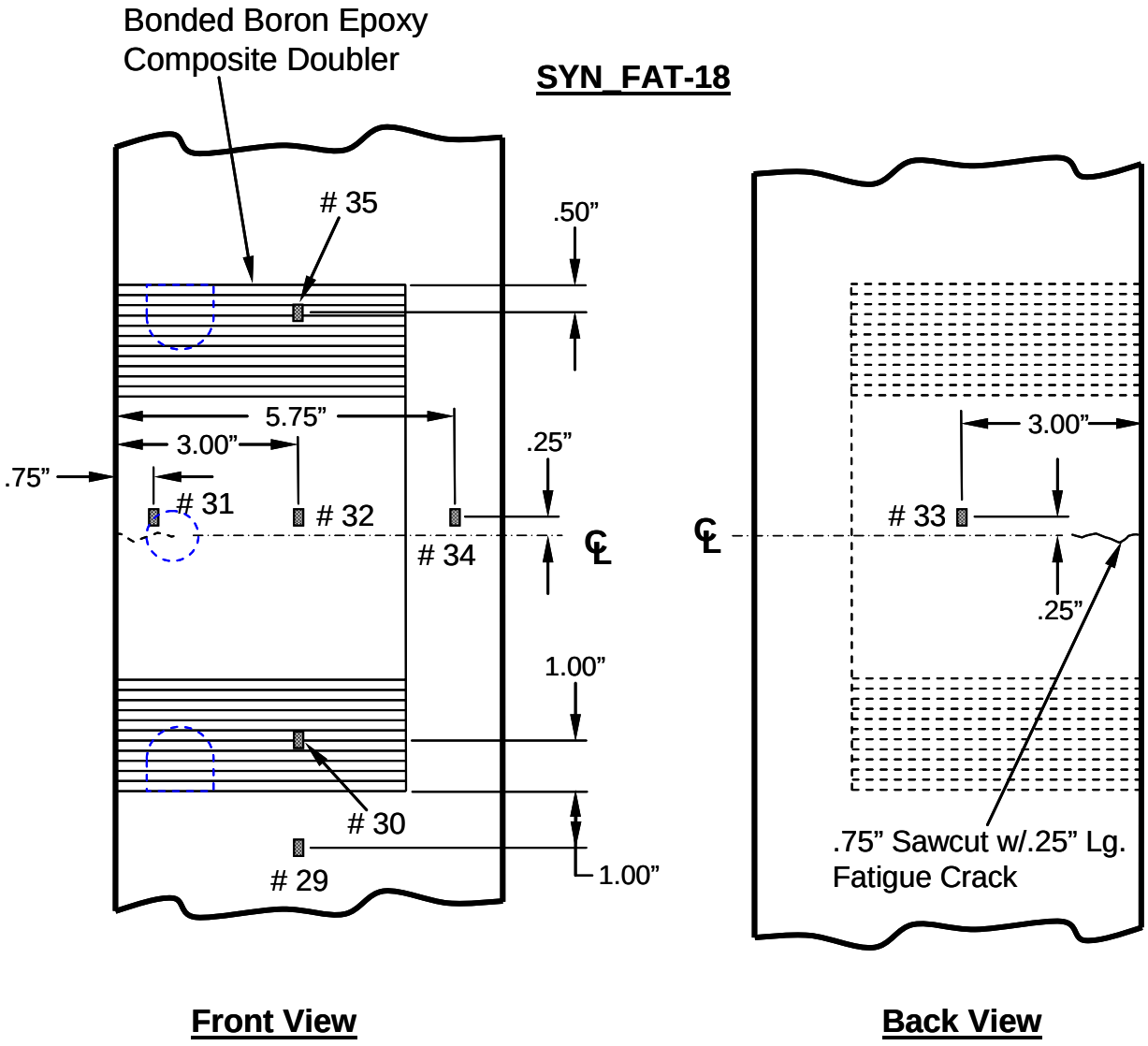


**Figure 69: Strain Gage Layout on Flawed Composite Repair Installation; Conditioned Specimen SYN-FAT-18**

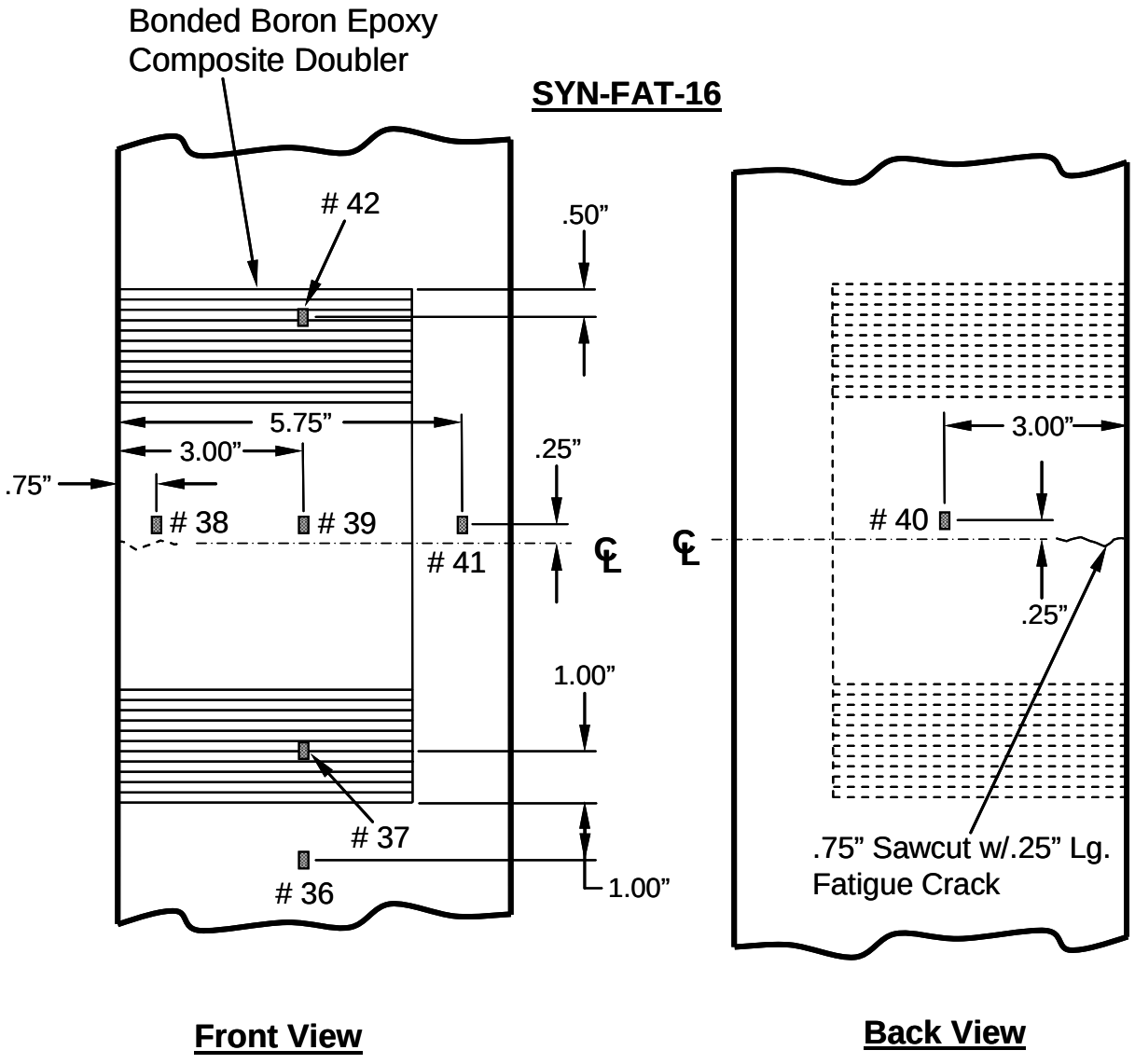


**Figure 70: Strain Gage Layout on <u>Unflawed</u> Composite Repair Installation; <u>Conditioned</u> Specimen SYN-FAT-16**

## 4.0 PERFORMANCE OF COMPOSITE DOUBLER REPAIR METHOD ON STEEL STRUCTURES

The test results supporting this damage tolerance assessment of composite doublers will be presented in three distinct sections: 1) fatigue test results, 2) strain field measurements (evaluation of load transfer), and 3) residual strength tests. Nondestructive inspections, used to relate the above items to flaw initiation and growth, will be discussed in the section on the fatigue test results. The data presented in Section 4.0 provides a comprehensive evaluation of the effectiveness of composite doublers in reducing crack growth in steel substructure. Fatigue and strength tests were performed on specimens with various combinations of crack and bondline flaws. The flaw sizes, locations, and combinations were engineered to produce extreme worst case conditions. Environmental conditions simulating temperature and humidity exposure are also included in the test specimens (ref. Section 3.2). Eighteen specimens representing five different configurations were tested.

*Disbond, delamination and crack sizes used in these damage tolerance tests were at least twice the size of those which can be detected by the NDI requirements. Futhermore, the stress spectrums applied in the fatigue tests were 2 to 3.5 times the stress levels measured in the field. Finally, it should be noted that the cracks are started from free edges so that crack opening during faigue testing is much greater than the displacements that occur in the field. Thus, there is an inherent safety factor built into this crack mitigation and damage tolerance assessment. The composite doubler performance sited here should be conservative.*

### 4.1 Performance Results from Damage Tolerance Tension Tests

Photographs of the damage tolerance test set-up and a close-up view of a composite doubler test coupon are shown in Figure 71. Figure 72 shows the seeded fatigue crack, generated before the composite repair was installed, and the crack propagating through the crack growth gage during testing. The results from all of the fatigue tests are summarized in Table 10 which is broken down into performance for low (24 ksi), medium (33 ksi), and high (41 ksi) stress spectrums. Results from the low stress spectrum tests, which are believed to be the stress levels that are the most representative of those incurred in the field, clearly show the ability of composite doublers to eliminate crack growth when bonded to thick steel structure. The 24 ksi fatigue spectrum specimens are plotted in Figure 73. No fatigue crack growth was observed after 251,000 to 331,000 cycles. Nondestructive inspections, conducted after the fatigue tests, also revealed that there was no flaw initiation or growth in the composite laminate or laminate-to-steel bondline (see Section 4.2). These results were achieved in all specimens, even those containing engineered flaws and subjected to hot-wet and cold conditioning. Note that these performance impediments are anticipated to be extreme worst-case scenarios in that the disbonds removed 20% of the critical load transfer region in the doubler and also eliminated local reinforcement directly over the crack.

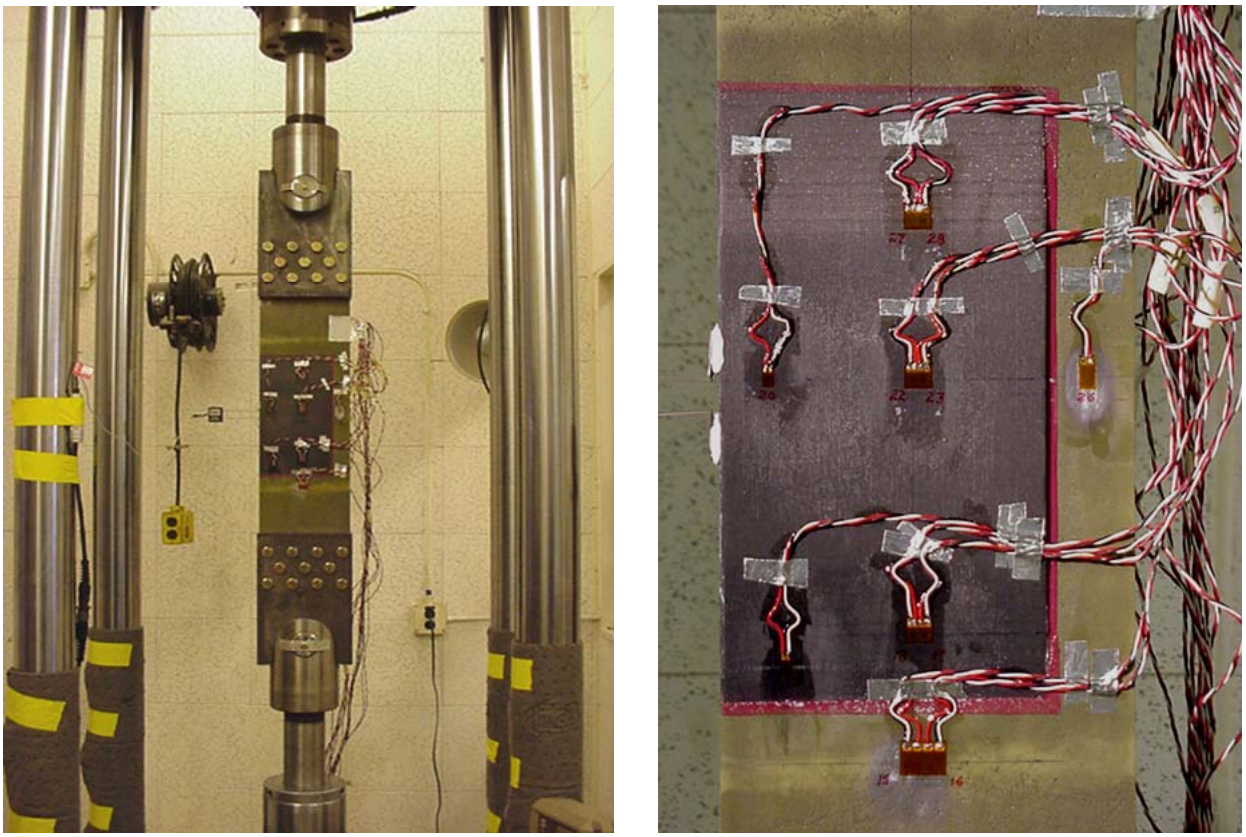

**Figure 71: Fatigue Test Set-Up of Repaired Steel Coupons and Close-Up View of Strain Gage Layout**

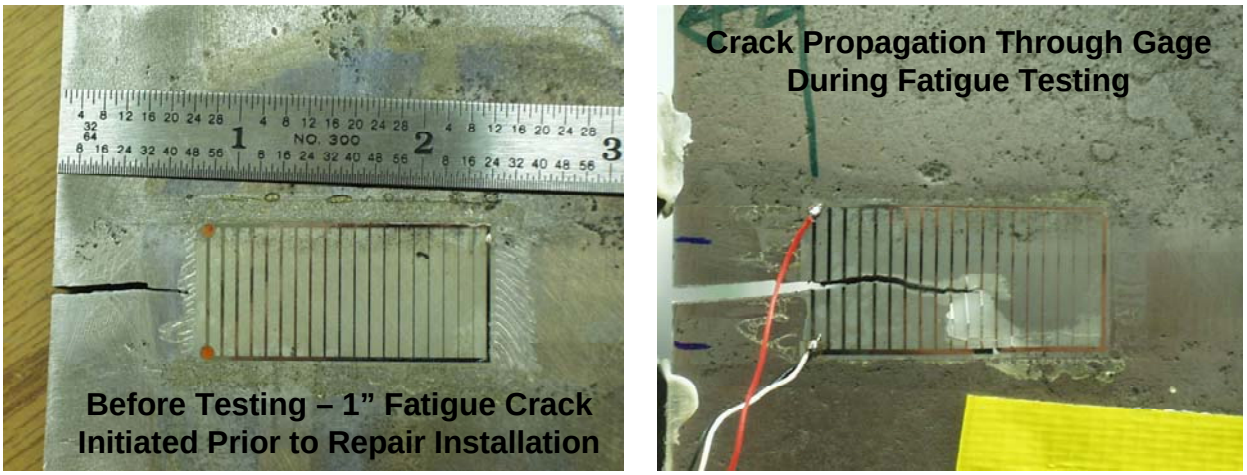


**Figure 72: Crack Growth Gage on Back of Steel Coupon and Crack Status Before and After Fatigue Testing**

| Specimen No. | Condition | Pristine or Flawed | Stress Spectrum (psi) | Number of Fatigue Cycles | Total Crack Growth |
|---|---|---|---|---|---|
| SYN-FAT-10 | Baseline Unrepaired | N/A | 2 ksi - 24 ksi | 129,044 | 1.44" |
| SYN-FAT-5 | No Conditioning | Pristine | 2 ksi - 24 ksi | 251,011 | None |
| SYN-FAT-9 | No Conditioning | Flawed | 2 ksi - 24 ksi | 323,508 | None |
| SYN-FAT-16 | Hot-Wet Plus Cold | Pristine | 2 ksi - 24 ksi | 331,384 | None |
| SYN-FAT-18 | Hot-Wet Plus Cold | Flawed | 2 ksi - 24 ksi | 325,017 | None |
| SYN-FAT-5A | No Conditioning | Pristine | 2 ksi - 33 ksi | 188,703 | .96" |
| SYN-FAT-9A | No Conditioning | Flawed | 2 ksi - 33 ksi | 299,017 | .88" |
| SYN-FAT-14 | Hot-Wet | Pristine | 2 ksi - 33 ksi | 628,422 | .80" |
| SYN-FAT-16A | Hot-Wet Plus Cold | Pristine | 2 ksi - 33 ksi | 208,391 | .64" |
| SYN-FAT-18A | Hot-Wet Plus Cold | Flawed | 2 ksi - 33 ksi | 241,859 | .96" |
| SYN-FAT-3 | Baseline Unrepaired | N/A | 2 ksi -41 ksi | 12,651 | 5.50" |
| SYN-FAT-4 | Baseline Unrepaired | N/A | 2 ksi -41 ksi | 9,743 | 5.50" |
| SYN-FAT-7 | No Conditioning | Pristine | 2 ksi -41 ksi | 109,004 | 1.35" |
| SYN-FAT-8 | No Conditioning | Pristine | 2 ksi -41 ksi | 110,897 | 1.52" |
| SYN-FAT-12 | No Conditioning | Flawed | 2 ksi -41 ksi | 86,500 | 1.42" |
| SYN-FAT-13 | No Conditioning | Flawed | 2 ksi -41 ksi | 70,143 | 1.47" |
| SYN-FAT-15 | Hot-Wet | Pristine | 2 ksi -41 ksi | 42,399 | 5.50" |
| SYN-FAT-17 | Hot-Wet | Flawed | 2 ksi -41 ksi | 23,266 | 1.20" |

**Table 10: Composite Doubler Crack Mitigation and Damage Tolerance Fatigue Test Summary**

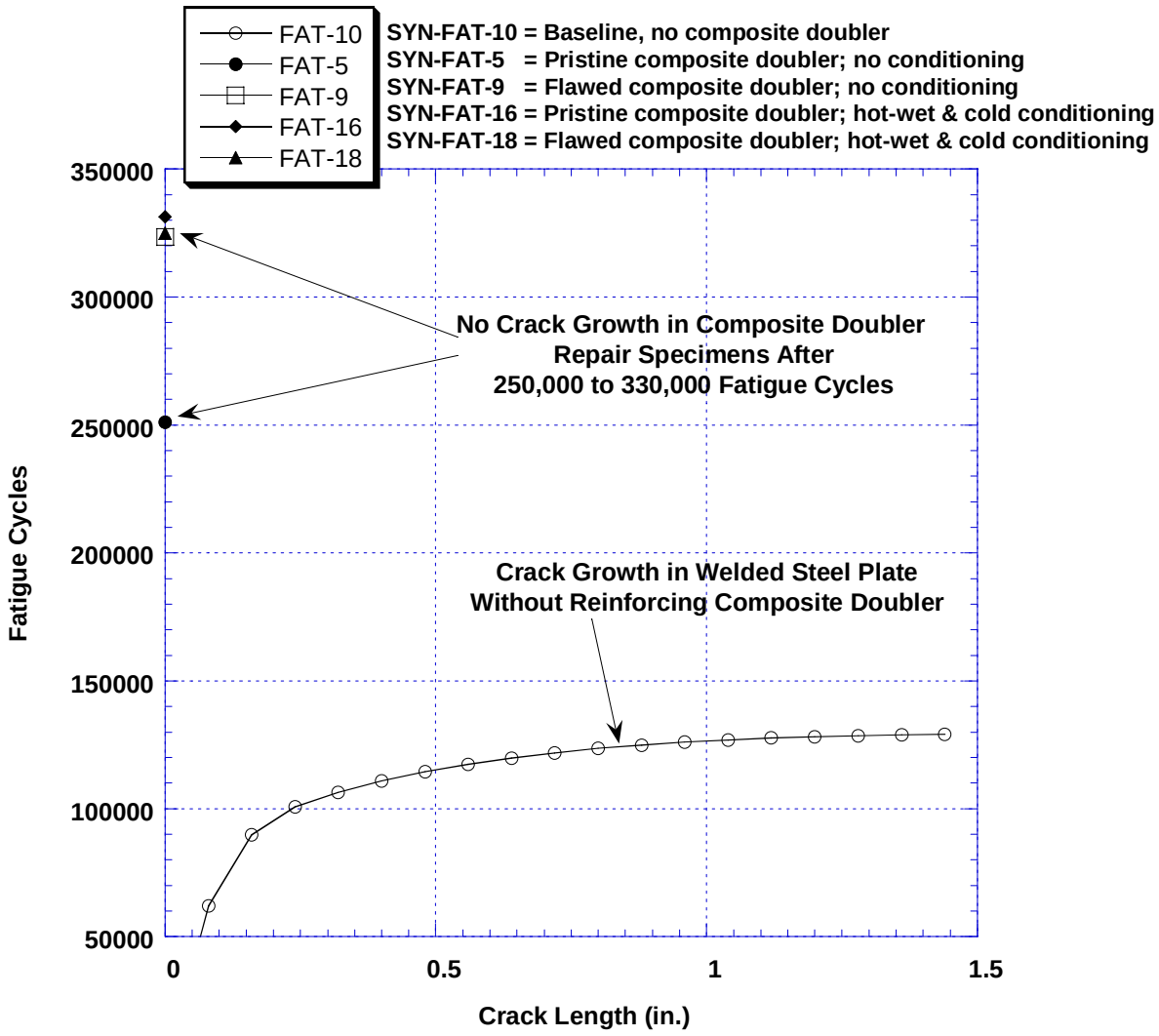


**Figure 73: Fatigue Crack Growth in Steel Plates With and Without Composite Doubler Repairs; 24 ksi Stress Fatigue Spectrum**

Since the initial goal was to survive 250,000 fatigue cycles, the tests were not continued past the 30% overtest. Instead, these same specimens were tested using the medium stress spectrum (33 ksi). The fatigue cycles accumulated in the 24 ksi stress spectrum were translated into equivalent 33 ksi stress cycles using equation (10). Fatigue testing was continued from this point until approximately 1" of crack growth was produced. Calculation of the equivalent number of fatigue cycles at a higher stress spectrum was accomplished using the following equation based on a combination of Miner's Rule and the DOE-B curve.

$$N_{A_{eqv}} = N_{A_1} \left\{ \frac{S_1}{S_2} \right\}^{-4} \quad (10)$$

Where:

$N_{A_{eqv}}$ = equivalent number of cycles for sample A at the specified stress spectrum

$N_{A_1}$ = number of fatigue cycles applied at stress spectrum #1

$S_1$ = stress spectrum #1 (24 ksi)

$S_2$ = stress spectrum #2 (33 ksi)

Table 10 shows that the composite doublers survived 200,000 to 625,000 fatigue cycles before 0.8" to 1.0" of crack growth was produced. The corresponding crack growth plots in Figure 74 show that there is much more scatter in the medium stress spectrum results. This is primarily due to the fact that the medium stress spectrum induces stress levels in the adhesive layer that approach the ultimate capability of the adhesive. This is especially true in the case of hot-wet conditioned specimens where testing has shown that exposure to hot-wet conditions may reduce the adhesive ultimate strength by as much as 20%. However, the overall performance characteristics indicate that the composite doublers still functioned close to the desired 250,000 fatigue cycle goal despite the heightened stress levels of almost 3 times those measured in the field. Note that these results were achieved with specimens, containing worst-case performance impediments of engineered flaws, hot-wet and cold conditioning, and free-edge fatigue cracks.

NDI evaluations and microscopic views of the laminate and steel surfaces revealed that any flaw growth was produced by a cohesive fracture of the adhesive versus the undesirable disbond between the two adherends. This proves that the full strength of the adhesive was achieved and that repair design revisions, not installation process revisions, are needed to improve the fatigue performance in this regime.

Because the highest stress spectrum represents over 3.5 times those measured in the field, results from the 41 ksi tests can best be viewed by comparing the flaw growth in baseline specimens containing no composite repair to the flaw growth observed after a composite repair was installed. Specimens SYN-FAT-3 and SYN-FAT-4 failed completely (5.5" crack growth) after 10,000 to 12,000 fatigue cycles at this level. The optimum composite doubler repairs (SYN-FAT-7 and SYN-FAT-8 with no engineered flaws, no conditioning) improved on this performance by an order of magnitude by only allowing approximately 1.5" of crack growth in 110,000 cycles. The effects of engineered flaws and hot-wet conditioning were much more pronounced in the 41 ksi stress spectrum. Flawed composite doubler installations allowed 1.5" of crack growth in 70,000 to 90,000 cycles, still an improvement of 7 to 9 times over the unreinforced structure. Performance of the hot-wet conditioned specimens was reduced further by the combination of the high stress levels and the reduction in the ultimate strength of the adhesive discussed above. In this latter case, the composite doubler repaired specimens still

survived 23,000 to 42,000 fatigue cycles – an improvement of 2 to 4 times over the unreinforced steel plate.

If the optimum composite repair – protected sufficiently to minimize or eliminate the effects of environmental conditioning – is used as the final performance metric, the results presented above indicate that the fatigue life of steel structures can be extended by a factor of 2 to 10. Bonded composite doubler repairs, if properly installed, can withstand 200,000 to 600,000 fatigue cycles while allowing little or no crack growth in a parent steel structure. These results are obtained for composite laminate designs that are 30% of the stiffness of the structure being repaired.

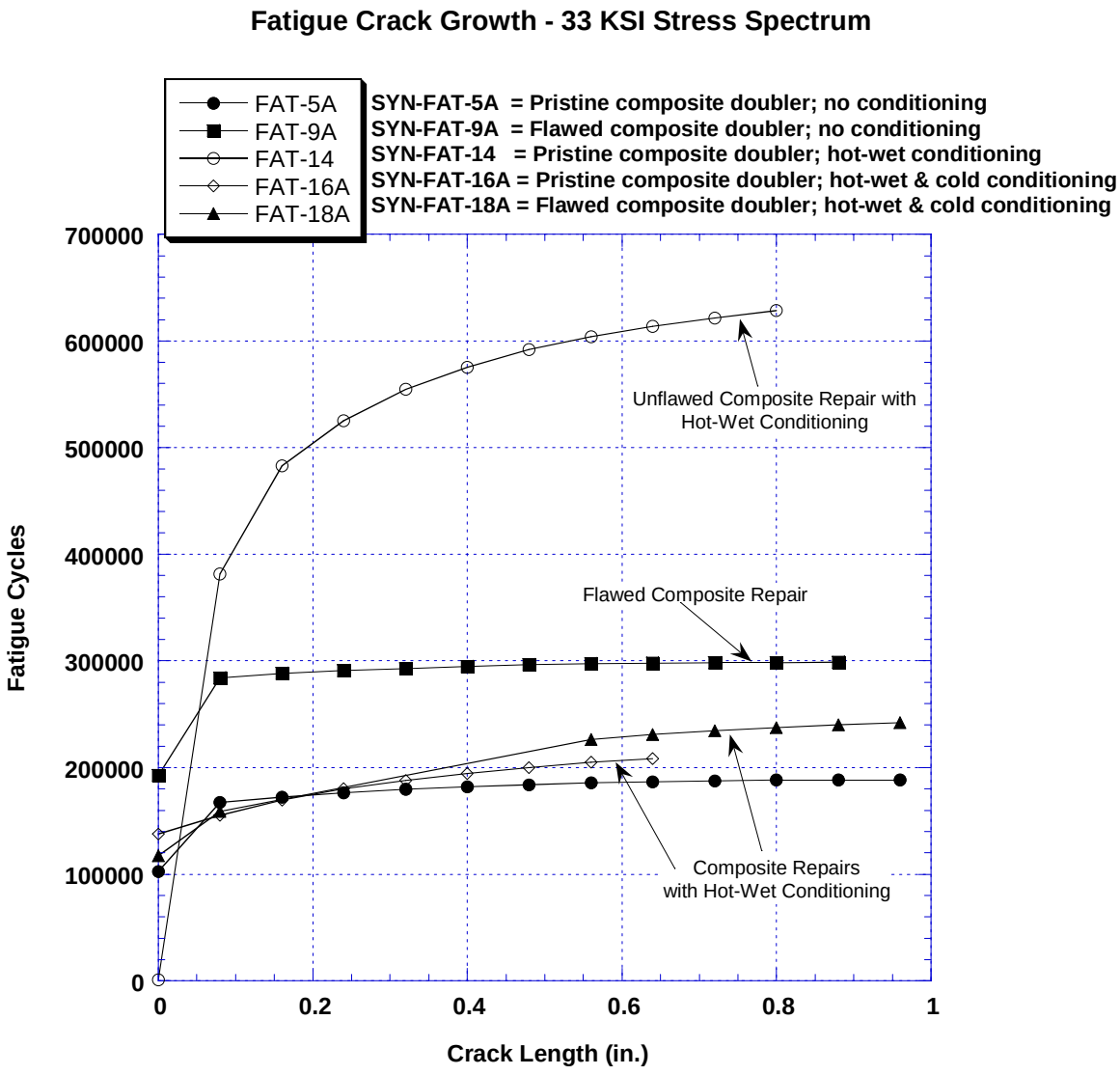


**Figure 74: Fatigue Crack Growth in Steel Plates With and Without Composite Doubler Repairs; 33 ksi Stress Fatigue Spectrum**

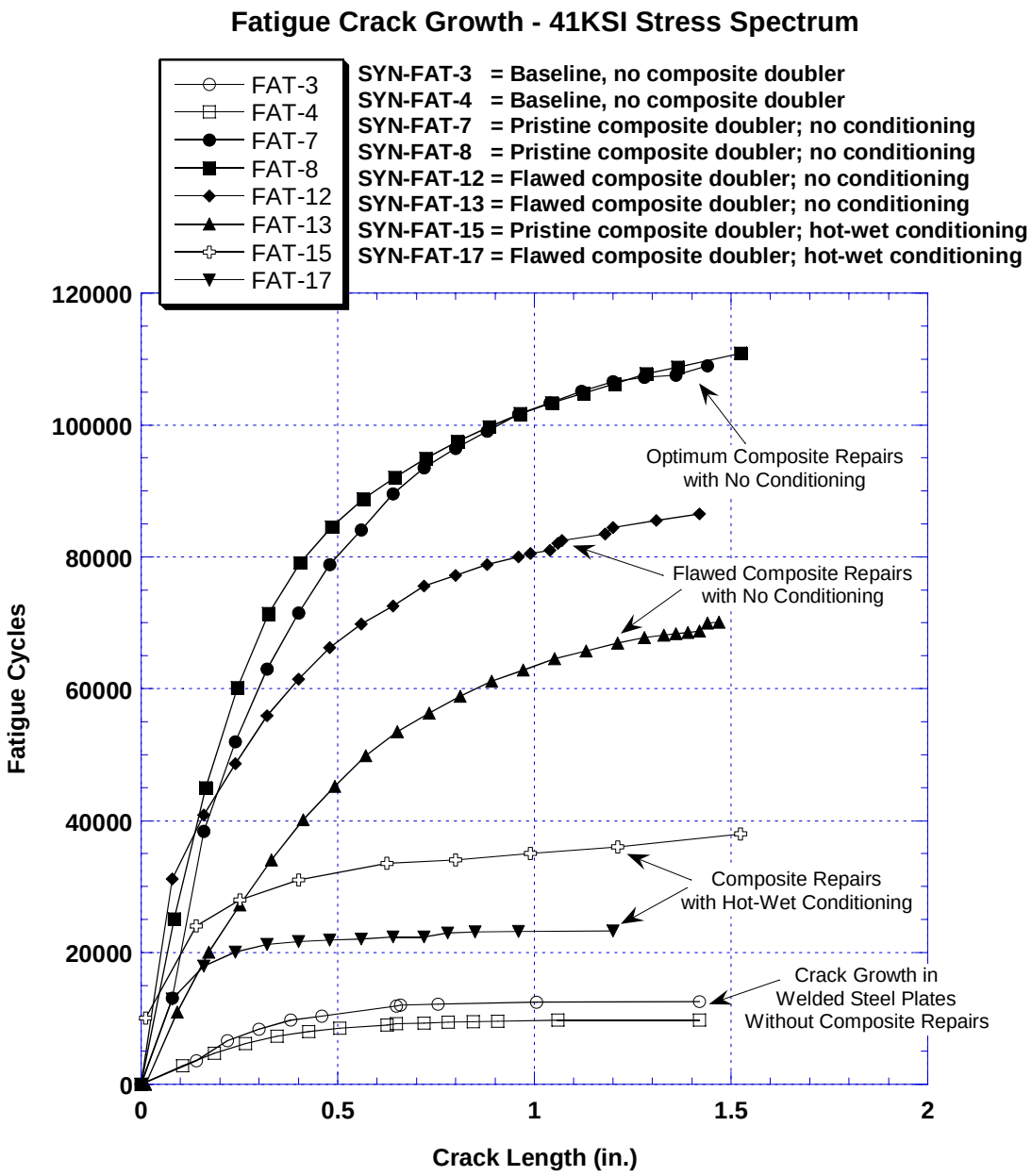


**Figure 75: Fatigue Crack Growth in Steel Plates With and Without Composite Doubler Repairs; 41 ksi Stress Fatigue Spectrum**

## 4.2 Through-Transmission Ultrasonic Inspection of Fatigue Coupons to Assess Pre- and Post-Fatigue Damage

Through-transmission ultrasonics (TTU) passes a beam of sound energy through a component under test and, rather than interpreting the returned wave as pulse-echo UT does, it uses the signals which are transmitted through the test piece. The TTU method requires the use of two transducers, one transmitting the UT wave and one acting as a receiver. Figure 76 shows a schematic of a TTU ultrasonic inspection system. The transducers must be accurately aligned

with each other on opposite sides of the component under test. Disbonds, delaminations, or porosity in the test piece will prevent all or part of the transmitted sound from reaching the receiver transducer. As in pulse-echo UT, the TTU inspection and data interpretation can be improved through the use of C-scan systems. The C-scan records the echoes from the internal structure of the composite doubler as a function of the position of each reflecting interface within the composite material boundaries. A detailed map of the composite doubler and flaws are shown as a plan view. Both flaw size and position within the plan view are recorded, however, flaw depth is not recorded.

To perform an inspection using TTU, both sides of the test piece must be accessible. A water medium is used to provide the UT coupling. Inspections are performed with the test piece immersed in a water tank or positioned between water jets (UT squirter set-up). When using the immersion method, the part and the transducers are submerged in water. The transducers, which are not normally in contact with the inspection surface, are mounted on fixtures that automatically maintain alignment while scanning the entire test piece.

Because of the efficient UT coupling and the associated ability to optimize the amount of energy introduced to the test piece, automated, laboratory TTU immersion tanks are more accurate and sensitive than fieldable, hand scanning devices. The primary disadvantage is the need for parts to be disassembled and immersed in water in order to be inspected. Since this technique requires the sending-receiving transducer pair to be located in front and back of the structure being inspected, accessibility and deployment issues severely restrict the field application of TTU techniques. The motion of the transducer pair must be linked and water coupling to the structure, through complete immersion of the part or through focused water jets, is necessary. TTU is a very accurate NDI technique and was used to establish the degree of damage present in the fatigue test specimens before and after testing.

These damage tolerance tests assessed the potential for loss-of-adhesion flaws (disbonds and delaminations) to initiate and grow in the composite doubler installation. Disbonds can occur between the composite doubler and the steel skin while delaminations can develop between adjacent plies of Boron-Epoxy material. It has been shown in related studies that the primary load transfer region, which is critical to the doubler's performance, is around its perimeter [2, 3-4, 6, 19, 25]. The purpose of the disbonds in configurations SYN-FAT-9, -9A, -12, -13, -17, -18, and -18A were to demonstrate the capabilities of composite doublers when large disbonds exist in the critical load transfer region as well as around the cracks which the doublers are intended to arrest. In this manner, severe worst case scenarios could be assessed and quantitative performance numbers could be established.

The damage tolerance fatigue coupons were inspected using through-transmission ultrasonics. Figures 63 and 64 show the locations of the engineered flaws in the test coupon. Figures 77-78 and 80-83 contain the C-scan results from the TTU inspections conducted before and after fatigue testing. The validation testing revealed ultrasonic resolution and sensitivity for flaw detection less than 1/4" in diameter.

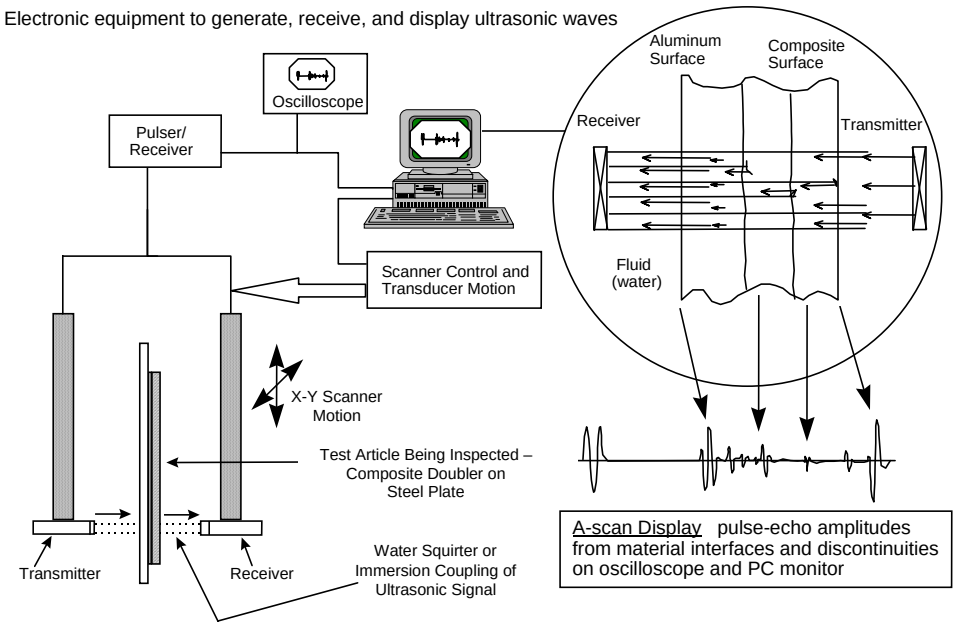


**Figure 76: Thru-Transmission Ultrasonic Test Set-Up**

Figure 77 shows the C-scan images of several unflawed specimens. The scans show that the repair installations were good and that there weren't any unintentional flaws produced during the curing process. The color schemes in SYN-FAT-8 and SYN-FAT-15 specimens differ from the color palette in specimens SYN-FAT-7 and SYN-FAT-16 because different data acquisition settings were used during these inspections. However, there are no flaws revealed in any of the scans. Figure 78 clearly shows the distinct flaw regions identified in the specimens containing the engineered flaws described in Figs. 63-64. The dark regions indicate the three 1" diameter disbonds placed over the center crack and in the critical, tapered, load-transfer region. Large deviations from the norm and the high signal attenuation levels associated with the flaw regions, makes the repair flaws easily identifiable.

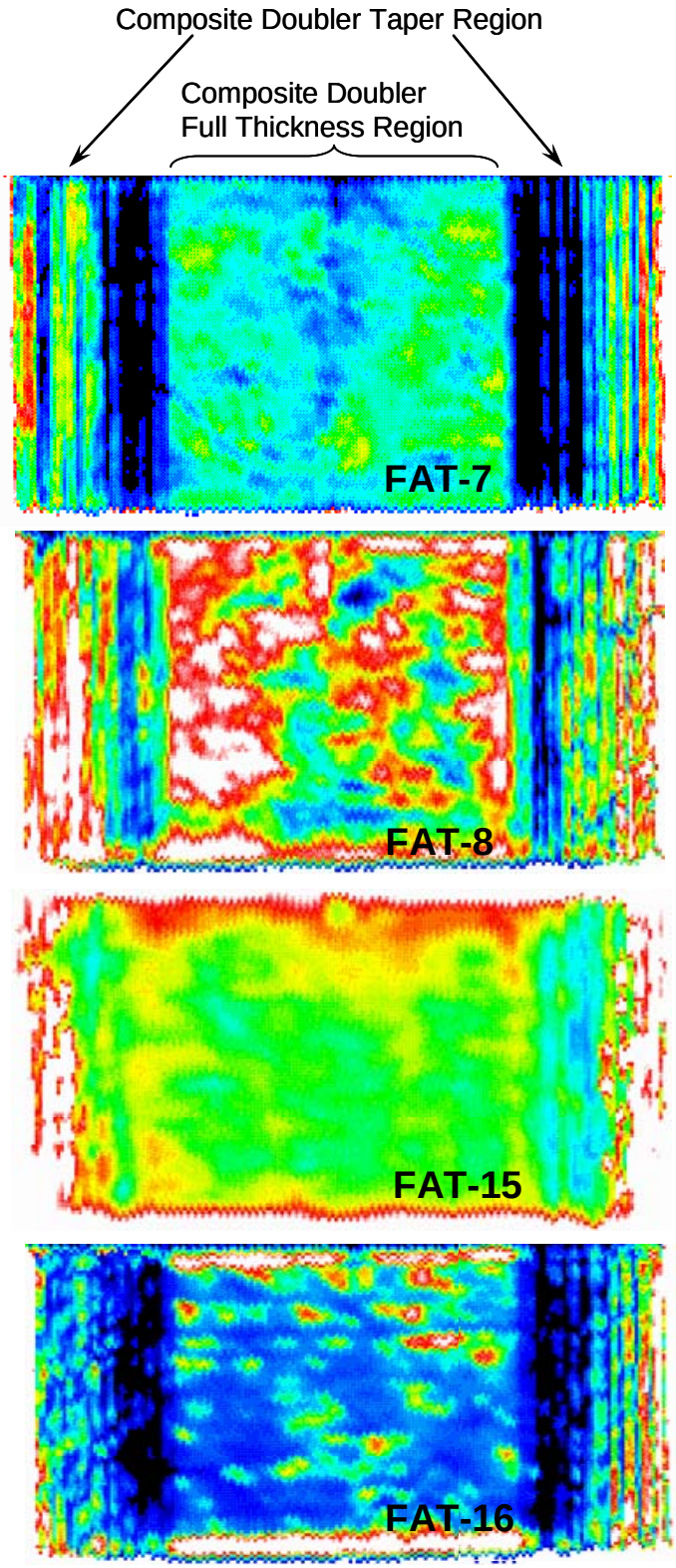


**Figure 77: Through-Transmission Ultrasonic Images of Unflawed Test Specimens Before Fatigue Testing**

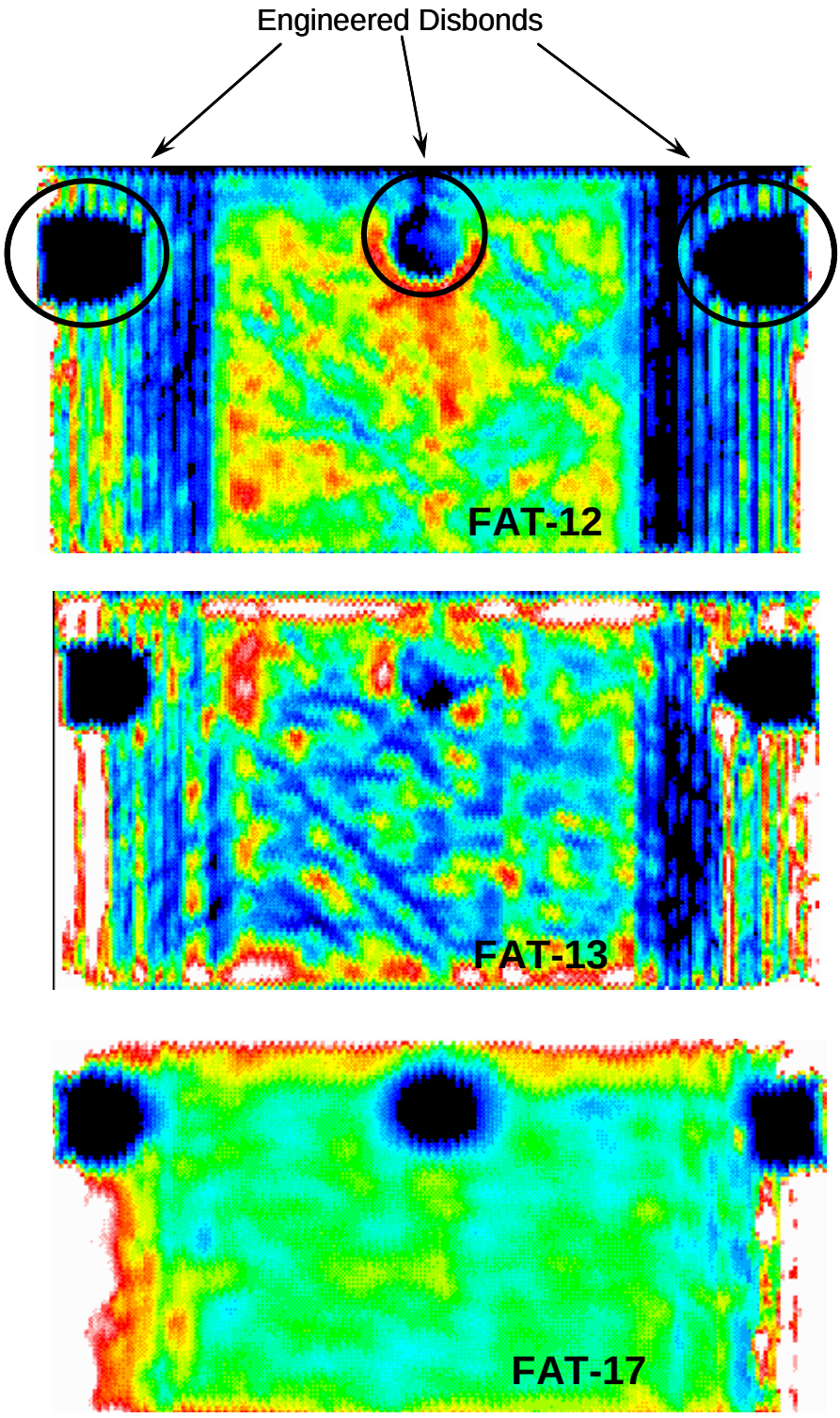


**Figure 78: Through-Transmission Ultrasonic Images of Flawed Test Specimens Before Fatigue Testing**

Views of fatigue cracks at different stages of propagation are shown in Figure 79. The upper left photo shows the starter notch and fatigue crack that was induced before the composite repair. This crack has not engaged the crack growth gage yet. The following three photos show the fatigue cracks generated during cyclic testing and the degree of opening associated with a free-edge crack. The lower photo shows that this crack opening gets extreme – approaching 0.5" – as the crack reaches several inches in length and the test loads are increased to ultimate failure levels. These photos highlight the local displacement in the steel around the crack. This local displacement produces one of the primary forms of degradation in the adhesive layer: cohesive fracture. As the crack opens and closes the adhesive will fracture in the area of the propagating crack. This is not a disbond (i.e. the full strength of the adhesive has been achieved) and the fracture zone is confined to the immediate region of the crack.

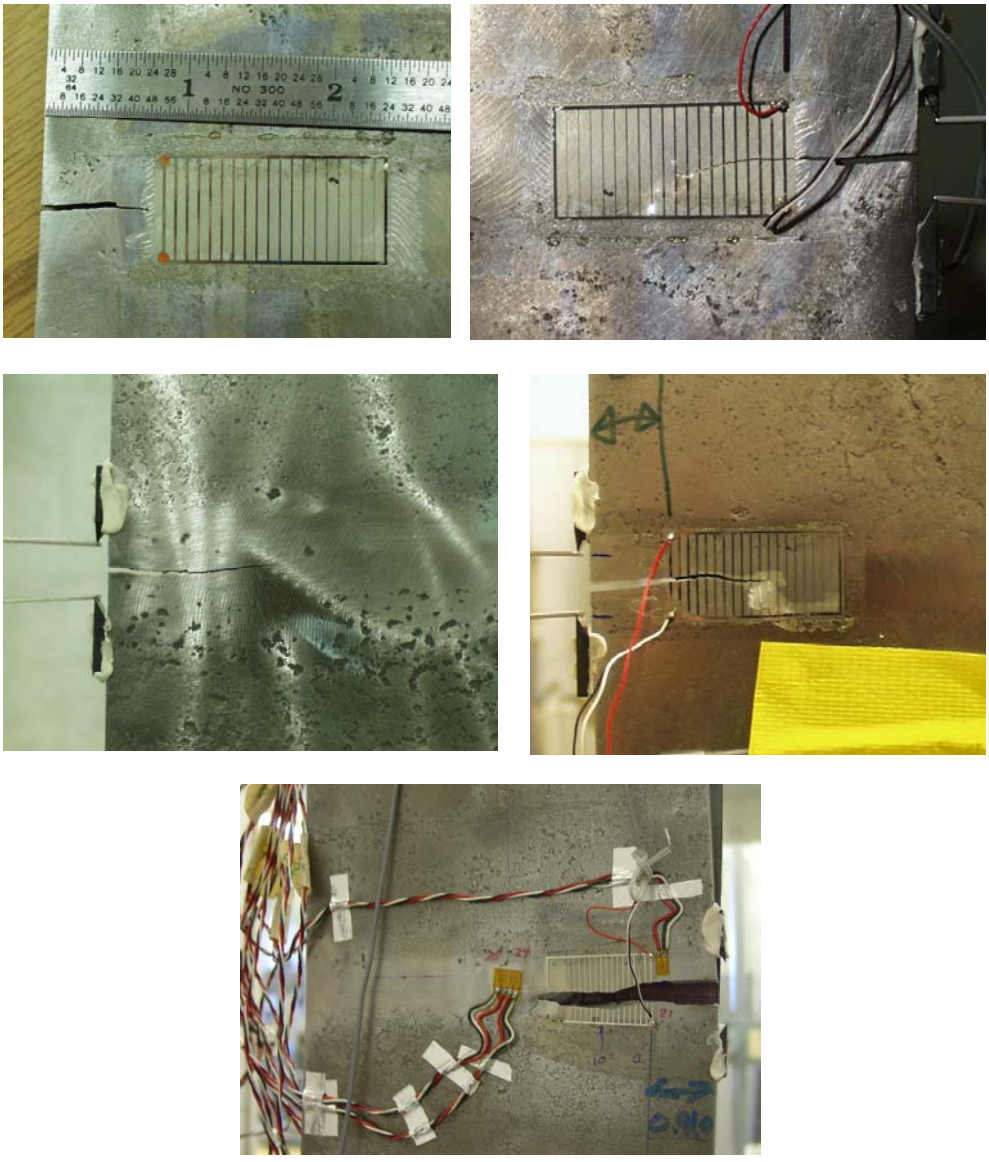

**Figure 79: Photos of Various Stages of Crack Propagation Showing the Local Opening in the Steel Structure**

The effects of this opening and closing phenomenon, and the associated fracture of the adhesive layer, can be seen the Figure 80. The C-scan images in Fig. 80 compare the flaw profiles before and after fatigue testing of specimen SYN-FAT-13. This specimen was subjected to over 70,000 cycles at the highest stress spectrum of 41 ksi (100,000 lbs.). The primary features of note are: 1) there is no growth in the disbond flaws located in the load transfer region, and 2) the adhesive fracture is confined to the immediate region of the crack with minimal impact on the overall performance of the composite doubler repair.

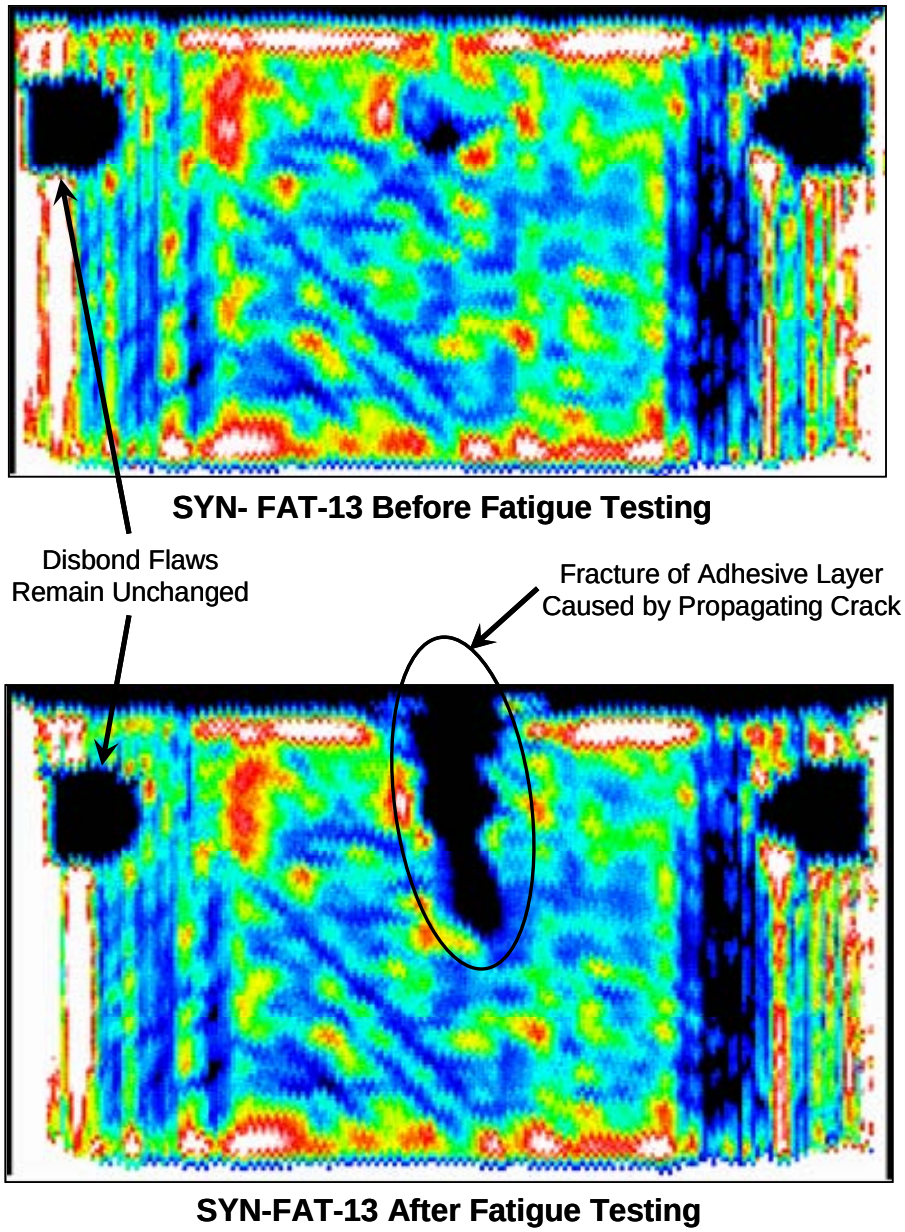


**Figure 80: Through-Transmission Ultrasonic Images Comparing Flaw Profiles Before and After Fatigue Testing (SYN-FAT-13 flawed specimen); High Stress Spectrum = 41 ksi**

Figures 81-83 also show the effects of fatigue loading on composite doubler repairs. Figure 81 compares the flaw profiles in specimen SYN-FAT-14 before and after 628,400 fatigue cycles at the medium stress spectrum of 33 ksi (80,000 lbs.). In these scans, the flaws show up as brighter regions. The primary features of note are: 1) the composite doubler survived over 600,000 fatigue cycles without failing, 2) the edge flaws are adhesive fracture regions versus the undesirable disbonds, 3) adhesive was present on both the composite laminate and the steel surface indicating that the failure mode was optimum, cohesive fracture of the adhesive, 4) the medium (33 ksi) and upper (41 ksi) stress spectrums produce adhesive stress levels that approach the ultimate capabilities of the adhesive film (especially for hot-wet conditioned adhesive), and 5) total crack growth was 0.80" so there was very little fracture of the adhesive layer in the vicinity of the propagating crack.

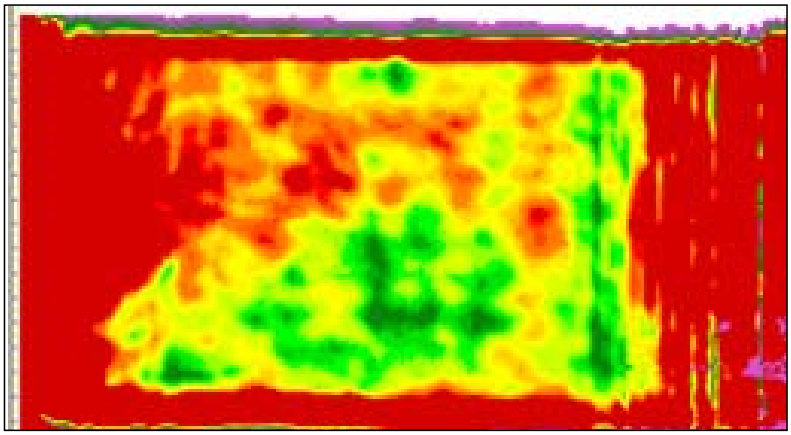

**SYN-FAT-14 Before Fatigue Testing**

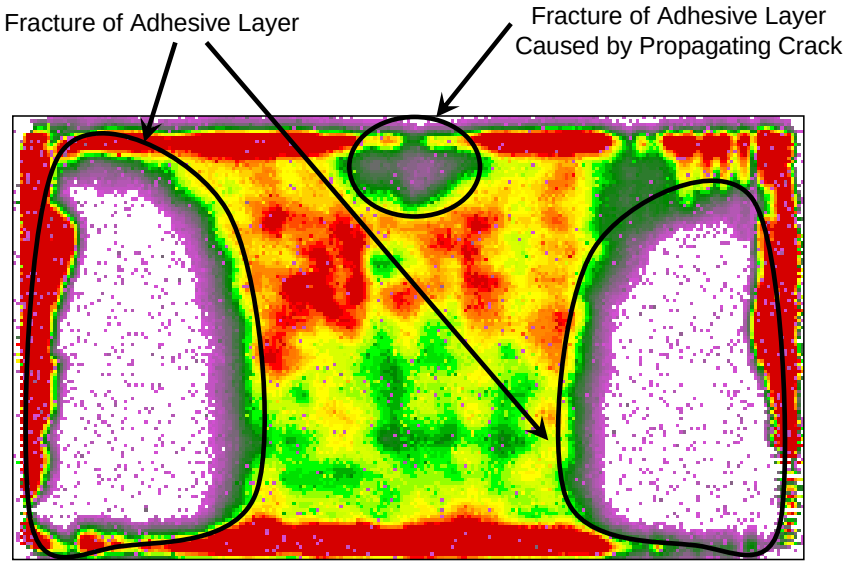


**SYN-FAT-14 After 628,400 Fatigue Cycles**

**Figure 81: Through-Transmission Ultrasonic Images Comparing Flaw Profiles Before and After Fatigue Testing (SYN-FAT-14 unflawed specimen with conditioning); Medium Stress Spectrum = 33 ksi**

Figure 82 compares the flaw profiles in specimen SYN-FAT-18 before and after 325,000 fatigue cycles at the lower stress spectrum of 24 ksi (60,000 lbs.). Again, different data acquisition settings were used in the various inspections so the flaws show up in some scans as dark regions and in other scans as bright regions. In either case, the large deviation from the norm and the high signal attenuation levels associated the flaw regions, makes the repair flaws easily identifiable. The primary features of note are: 1) the composite doubler was subjected to over 325,000 fatigue cycles with no growth in the engineered flaws or initiation of new flaws, and 2) the lower (24 ksi), and probably most realistic, stress spectrum did not produce any flaw growth in the composite doubler repairs or any crack growth in the parent steel after 250,000 to 330,000 fatigue cycles. The latter point is true even in the cases of specimens with seeded flaws and extreme hot-wet and cold conditioning.

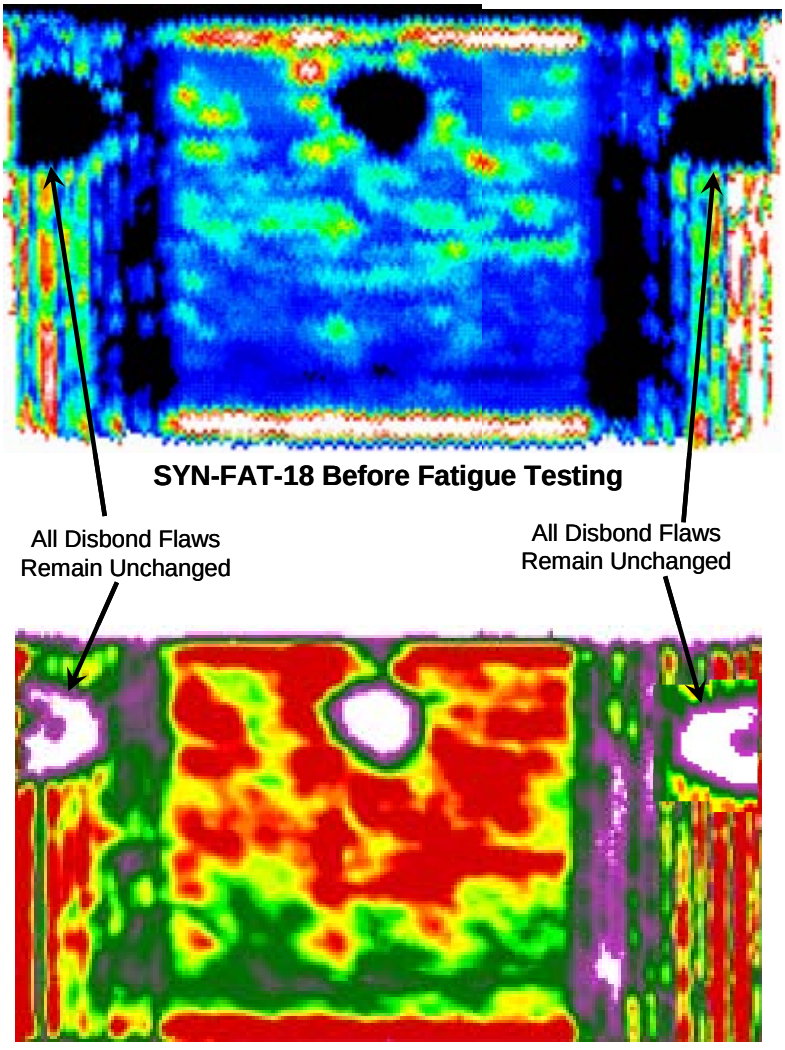


**Figure 82: Through-Transmission Ultrasonic Images Comparing Flaw Profiles Before and After Fatigue Testing (SYN-FAT-18 flawed specimen with conditioning); Low Stress Spectrum = 24 ksi**

Figure 83 returns to the higher stress spectrums to look further into the actual stress field limitations of composite doubler repairs. Figure 83 shows the flaw profile in specimen SYN-FAT-9A after 299,000 fatigue cycles at the medium stress spectrum of 33 ksi (80,000 lbs.). In this scan, the flaws show up as brighter regions. The primary features of note are: 1) the medium (33 ksi) stress spectrum produces adhesive stress levels that approach the ultimate capabilities of the adhesive film and result in the fracture regions shown, and 2) despite the large fracture regions, the composite doubler was able to function to mitigate the crack growth to under 0.90" after almost 300,000 cycles

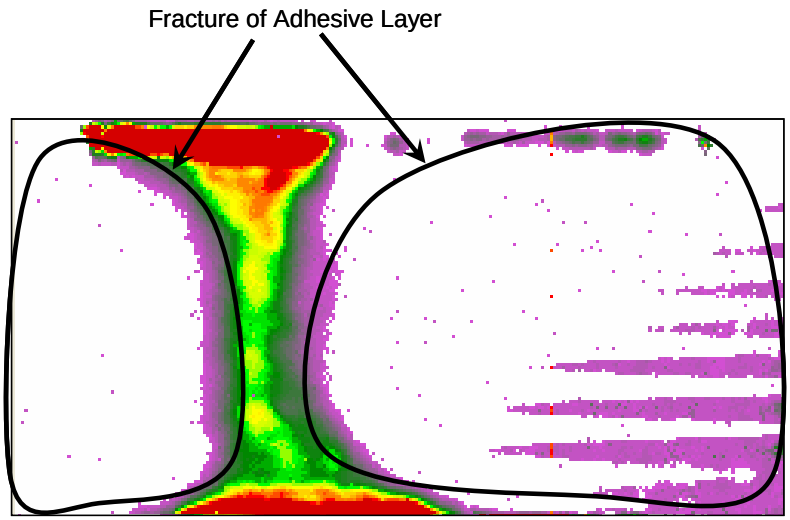


**SYN-FAT-9A After 300,000 Fatigue Cycles**

**Figure 83: Through-Transmission Ultrasonic Image After Fatigue Testing (SYN-FAT-9 flawed specimen with no conditioning); Medium Stress Spectrum = 33 ksi**

## 4.3 Strain Field Measurements

Figures 67-70 show the strain gage layouts that were used to monitor: 1) the load transfer into the composite doublers and, 2) the strain field throughout the composite laminate and steel plate. The stress, strain, and load transfer values presented in this section quantify the doubler performance characteristics discussed above. They provide additional insights into the doubler's ability to: 1) resist crack initiation or mitigate crack growth, and 2) perform acceptably in spite of worst-case installations.

In general, it was observed that all strain responses from the simulated operation stress spectrum were linear. No residual strains were noted when the specimens were unloaded except in the instance where the strain measurement occurred at the fatigue crack. In this latter case, the strain riser associated with the crack caused the strain response to be non-linear (plastic). Subsequent

failure tests (see Section 4.4 below) showed that the strains induced by the fatigue load spectrum were well inside the linear elastic regime for the steel and Boron-Epoxy composite materials.

The maximum doubler strains were found in the load transfer region (taper area) at the ends of the doubler. In all fatigue specimens, the strains monitored in this area were approximately 70% of the total strain in the parent steel plate. This value remained constant over all or most of the fatigue cycles indicating that any bond strength deterioration was minimal and occurred late in the fatigue test cycles. The strain in the steel plate beneath the doubler is reduced in accordance with the strain picked up by the composite doubler. Despite large disbonds which affected approximately 20% of the critical load transfer region, the composite doublers maintained acceptable strain fields in the doubler and steel material. Furthermore, the doublers were able to pick up the strains necessary to accomplishing their intended purpose of strain reduction and crack mitigation in the parent structure. This performance was achieved in spite of collocated flaw scenarios such as disbond flaws and extreme hot/wet conditioning (water absorption/ingress). Note also that these flaws were directly over the cracks which the doublers were intended to arrest.

### 4.3.1 Strain Field Analysis

A summary of the strain fields in the fatigue test coupons can be seen in the series of curves shown in Figures 84-89. The maximum total axial strain in the steel plate (away from the doubler) was always around 900 με (for 24 ksi stress spectrum; test load P = 60,000 lbs.), 1,100 με (for 33 ksi stress spectrum; test load P = 80,000 lbs.), and 1,500 με (for 41 ksi stress spectrum; test load P = 100,000 lbs.). Axial strains in the steel plate beneath the doubler were approximately 50% to 70% of this maximum value while axial strains in the composite doubler ranged from 50% to 70% of the total strain in the specimen. The lateral strains in each of the specimens were produced by the Poisson effect and agreed well with the theoretical relation:

$$\varepsilon_a = - (\nu \text{ X } \varepsilon_l) \qquad (11)$$

where $\nu$ is Poisson's ratio, $\varepsilon_a$ represents axial strain and $\varepsilon_l$ represents lateral strain. Following is a summary of observations regarding the coupon strain fields from the different configurations tested.

Figures 84 and 85 show the axial and lateral strain fields measure in specimen SYN-FAT-7 prior to fatigue testing. The strains were produced by the high stress spectrum (41 ksi) and are representative of an unflawed doubler. Strain reduction in the steel plate and the corresponding strain shedding into the composite laminate is evident. The nonlinear response and strain relief around the crack tip (Channel 21) is also evident. Similar information is obtained from Figures 86 and 87 which plot axial and lateral strains for SYN-FAT-12. These strains were produced by the high stress spectrum (41 ksi) and are representative of a flawed doubler. Note that, for the most part, the strain levels are the same as in the unflawed SYN-FAT-7 specimen. However, strain relief created by the edge disbond is evidenced by the low strain in Channels 3. The higher strains around the center disbond (Channel 6) show that load transfer still occurs through internal disbonds and proves that flaws in these regions are not critical. Finally, a comparison of

strain levels in SYN-FAT-7 and SYN-FAT-12 reveal that the effects of the disbonds are very localized and have very little effect on the overall strain field in the repair.

Figures 88 and 89 plot the strain values for flawed (SYN-FAT-18) and unflawed (SYN-FAT-16) specimens subjected to the low and medium stress spectrums. Observations similar to those sited above can be made. As expected, the load transfer is shown to be the same at the upper and lower taper regions. Overall, the disbonds appear to have minimal effect on the doubler's ability to transfer load and relieve the parent steel plate.

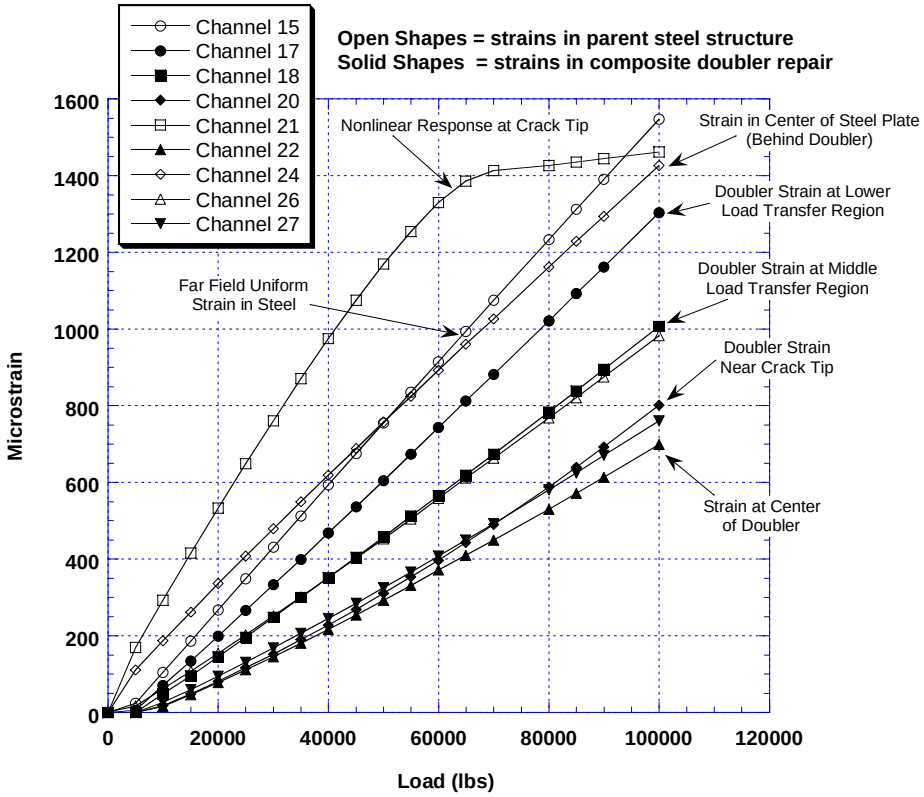


**Figure 84: Axial Strain Field in Steel and Composite for Configuration SYN-FAT-7 – Pristine Composite Doubler with No Conditioning (ref. strain gage locations shown in Fig. 68)**

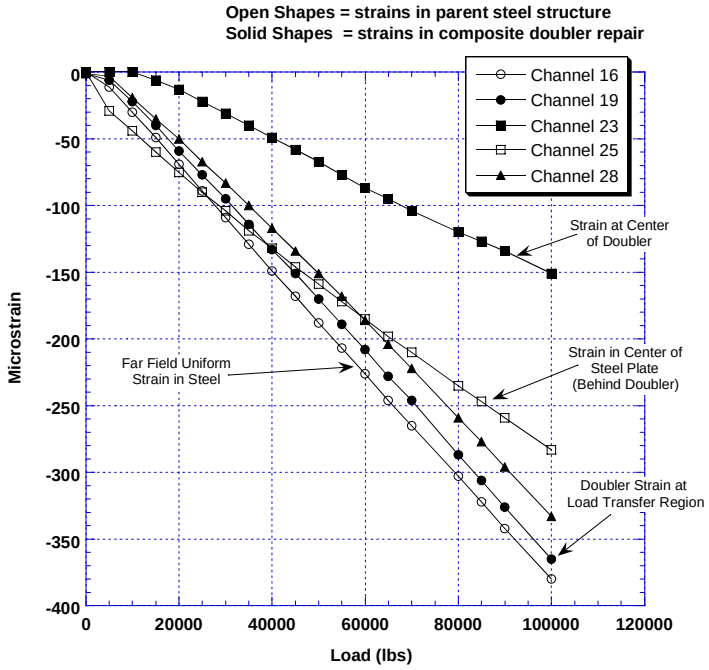


**Figure 85: Lateral Strain Field in Steel and Composite for Configuration SYN-FAT-7 – Pristine Composite Doubler with No Conditioning (ref. strain gage locations shown in Fig. 68)**

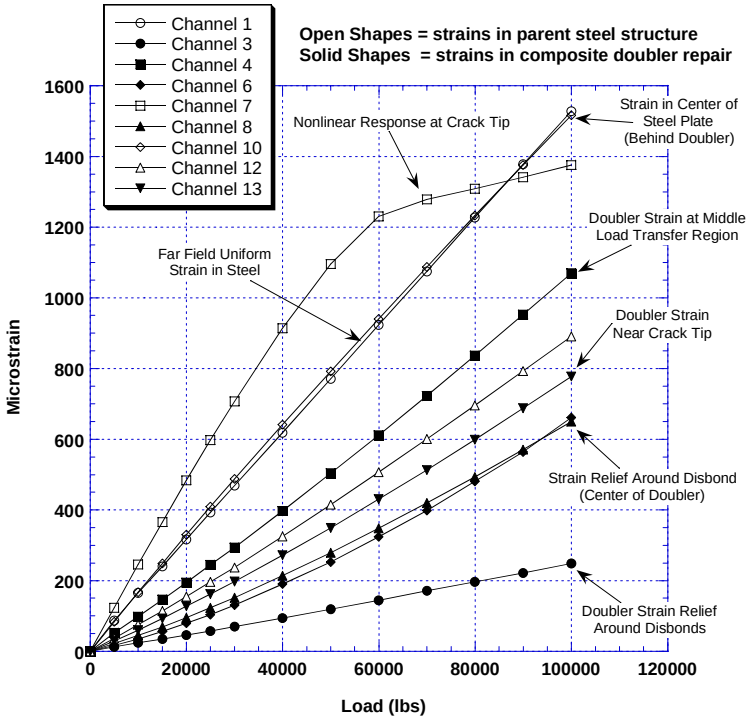


**Figure 86: Axial Strain Field in Steel and Composite for Configuration SYN-FAT-12 – Flawed Composite Doubler with No Conditioning (ref. strain gage locations shown in Fig. 67)**

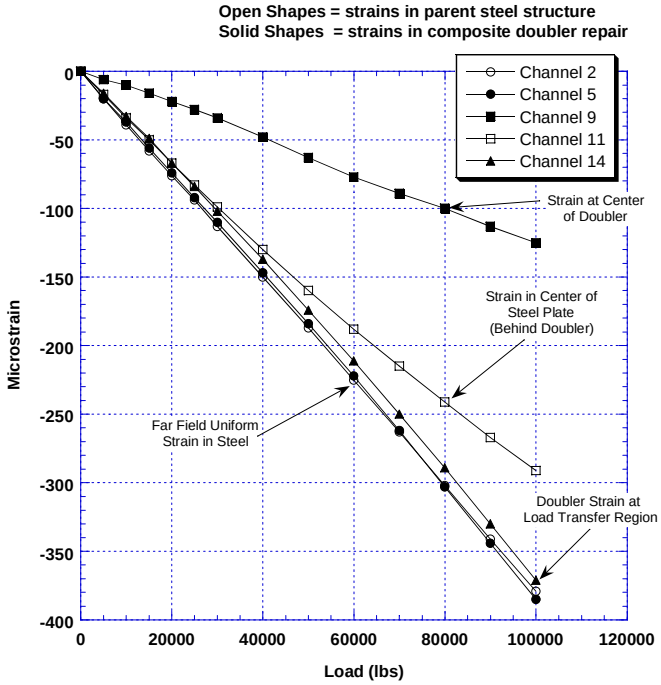


**Figure 87: Lateral Strain Field in Steel and Composite for Configuration SYN-FAT-12 – Flawed Composite Doubler with No Conditioning (ref. strain gage locations shown in Fig. 67)**

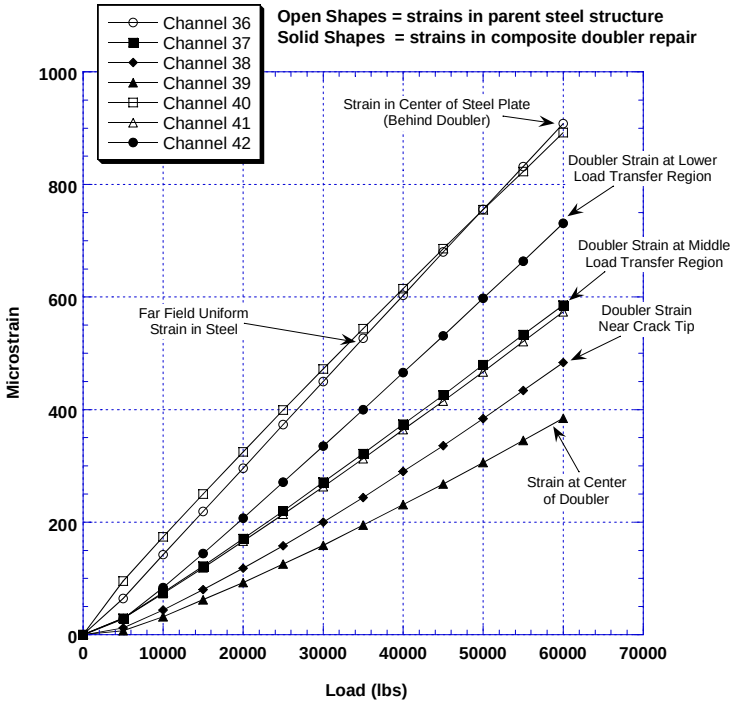


**Figure 88: Axial Strain Field in Steel and Composite for Configuration SYN-FAT-16 – Pristine Composite Doubler with Hot/Wet & Cold Conditioning (ref. strain gage locations shown in Fig. 70)**

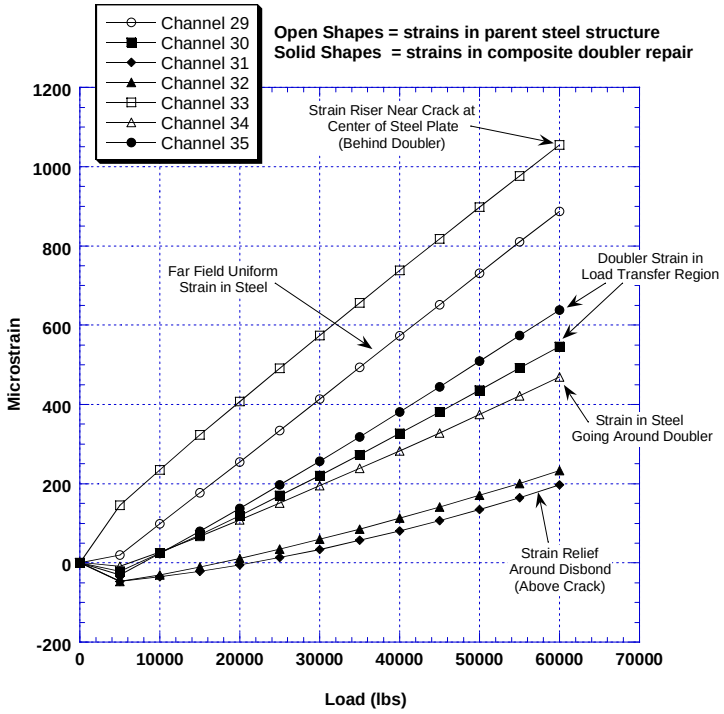


**Figure 89: Axial Strain Field in Steel and Composite for Configuration SYN-FAT-18 – Flawed Composite Doubler with Hot/Wet & Cold Conditioning (ref. strain gage locations shown in Fig. 69)**

### 4.3.2 Stresses in Steel Plate and Composite Doubler

To provide a point of reference for any Boron-Epoxy doubler installation, various stresses sustained by the fatigue test specimens are listed in Table 11. Strain data collected from the biaxial (axial and lateral) gages were used to calculate stresses in the composite doubler and parent steel plate. Strains measured by these gages were used to calculate the corresponding membrane stresses through the following equations:

$$\sigma_a = \frac{E}{1-\nu^2}(\varepsilon_a + \nu\varepsilon_l) \tag{12}$$

$$\sigma_l = \frac{E}{1-\nu^2}(\varepsilon_l + \nu\varepsilon_a) \tag{13}$$

where $E$ is the modulus of elasticity, $\nu$ is Poisson's ratio, $\sigma_a$ is the axial stress in the skin, $\sigma_l$ is the longitudinal (lateral) stress in the skin, $\varepsilon_a$ is the hoop strain, and $\varepsilon_l$ is the longitudinal

(lateral) strain. From Mil-Handbook 5, the modulus of elasticity and Poisson's ratio for ASTM 572 steel are: $E$ =26.5 X $10^6$ psi and $\nu$ =0.26, respectively. As stated in Section 3.2.3, the properties of the Boron-Epoxy laminate are $E_x$ = 25.2 X $10^6$ psi, $E_y$ = 2.43 X $10^6$ psi and $\nu$ = 0.32. In cases where there were no lateral strain gages installed, the Poisson strain levels were calculated using equation (11).

Table 11 shows that uniform stresses of 24 ksi, 33 ksi, and 41 ksi were achieved in the parent skin for each specimen configuration. Away from the fatigue crack, the maximum stresses in the steel beneath the doubler were roughly 60% the yield stress for ASTM 572 steel. Figures 90-91 plot the stress data from the uniaxial tests on specimens SYN-FAT-7 and SYN-FAT-12, respectively, for the 41 ksi stress spectrum (100,000 lb. max load). The maximum stresses in the composite doublers occurred at the edge of the doubler (load transfer region) and were between 70% and 80% of the far field stresses in the steel (16 ksi doubler edge stress for the 24 ksi far field stress; 25 ksi doubler edge stress for the 33 ksi far field stress; 33 ksi doubler edge stress for the 41 ksi far field stress). Stress risers near fatigue cracks, which normally amount to two or three times the uniform strain field away from the flaw, were reduced drastically by the composite doubler. The maximum steel stresses immediately adjacent to the fatigue cracks were less than or approximately equal to, the uniform stress field outside the doubler. A comparison of the stresses at zero and after 100,000 to 325,000 fatigue cycles shows that the doublers picked up additional stresses when the fatigue crack growth reduced the load carrying capacity of the parent steel (i.e. stress relief occurred in steel). This is discussed further in Section 4.3.4 "Effects of Multiple Fatigue Lifetimes on Strain Fields.

| Specimen No. | Strain Chs. | Max. Load for Stress Spectrum (lbs) | Stress at 0 Cycles (psi) | Fatigue Cycles | Stress After Fatigue (psi) | Total Crack Growth | Location on Test Specimen |
|---|---|---|---|---|---|---|---|
| SYN-FAT-7 (Unflawed, No Conditioning.) | 15, 16 | 100,000 (41ksi) | 41,200 | 109,004 | 44,000 | 1.35" | Steel - Far Field |
| | 17 | | 32,850 | | 40,700 | | Doubler Edge (upper taper region) |
| | 18, 19 | | 25,000 | | 32,350 | | Doubler Edge (middle taper region) |
| | 20 | | 20,200 | | 52,000 | | Doubler Above Crack (full thickness region) |
| | 22, 23 | | 18,300 | | 23,400 | | Doubler in Front of Crack (full thickness region) |
| | 24, 25 | | 38,450 | | 66,500 | | Steel - Near Crack Tip |
| | 27, 28 | | 18,400 | | 26,300 | | Doubler Edge (upper taper region) |
| SYN-FAT-12 (Flawed, No Conditioning) | 1, 2 | 100,000 (41ksi) | 40,650 | 86,500 | 44,600 | 1.42" | Steel - Far Field |
| | 4, 5 | | 26,600 | | 35,250 | | Doubler Edge (middle taper region) |
| | 8, 9 | | 17,150 | | 22,100 | | Doubler Above Crack (full thickness region) |
| | 10, 11 | | 41,000 | | 61,850 | | Steel - Near Crack Tip |
| | 13, 14 | | 18,500 | | 24,000 | | Doubler Edge (upper taper region) |
| SYN-FAT-16A (Unflawed, Conditioned, H-W & Cold) | 36, v36 | 80,000 (33ksi) | 32,000 | 208,391 | 31,300 | .64" | Steel - Far Field |
| | 37, v37 | | 20,400 | | 21,250 | | Doubler Edge (middle taper region) |
| | 38, v38 | | 16,900 | | 22,050 | | Doubler Above Crack (full thickness region) |
| | 39, v39 | | 13,400 | | 11,600 | | Doubler in Front of Crack (full thickness region) |
| | 40, v40 | | 31,300 | | 38,300 | | Steel - Near Crack Tip |
| | 42, v42 | | 24,800 | | 26,600 | | Doubler Edge (lower taper region) |
| SYN-FAT-16 (Unflawed, Conditioned, H-W & Cold) | 36, v36 | 60,000 (24ksi) | 24,100 | 331,384 | 24,100 | None | Steel - Far Field |
| | 37, v37 | | 14,800 | | 14,500 | | Doubler Edge (middle taper region) |
| | 38, v38 | | 12,200 | | 12,700 | | Doubler Above Crack (full thickness region) |
| | 39, v39 | | 9,700 | | 9,250 | | Doubler in Front of Crack (full thickness region) |
| | 40, v40 | | 23,650 | | 23,650 | | Steel - Near Crack Tip |
| | 42, v42 | | 18,400 | | 17,900 | | Doubler Edge (upper taper region) |
| SYN-FAT-18 (Flawed, Conditioned, H-W & Cold) | 29, v29 | 60,000 (24ksi) | 23,500 | 325,017 | 23,450 | None | Steel - Far Field |
| | 30, v30 | | 13,800 | | 13,300 | | Doubler Edge (middle taper region) |
| | 31, v31 | | 5,000 | | 5,000 | | Doubler Above Crack (full thickness region) |
| | 32, v32 | | 5,900 | | 5,100 | | Doubler in Front of Crack (full thickness region) |
| | 33, v33 | | 28,000 | | 27,950 | | Steel - Near Crack Tip |
| | 35, v35 | | 16,100 | | 15,450 | | Doubler Edge (upper taper region) |

**Table 11: Stresses in Steel Plate and Composite Doubler at Maximum Test Loads**

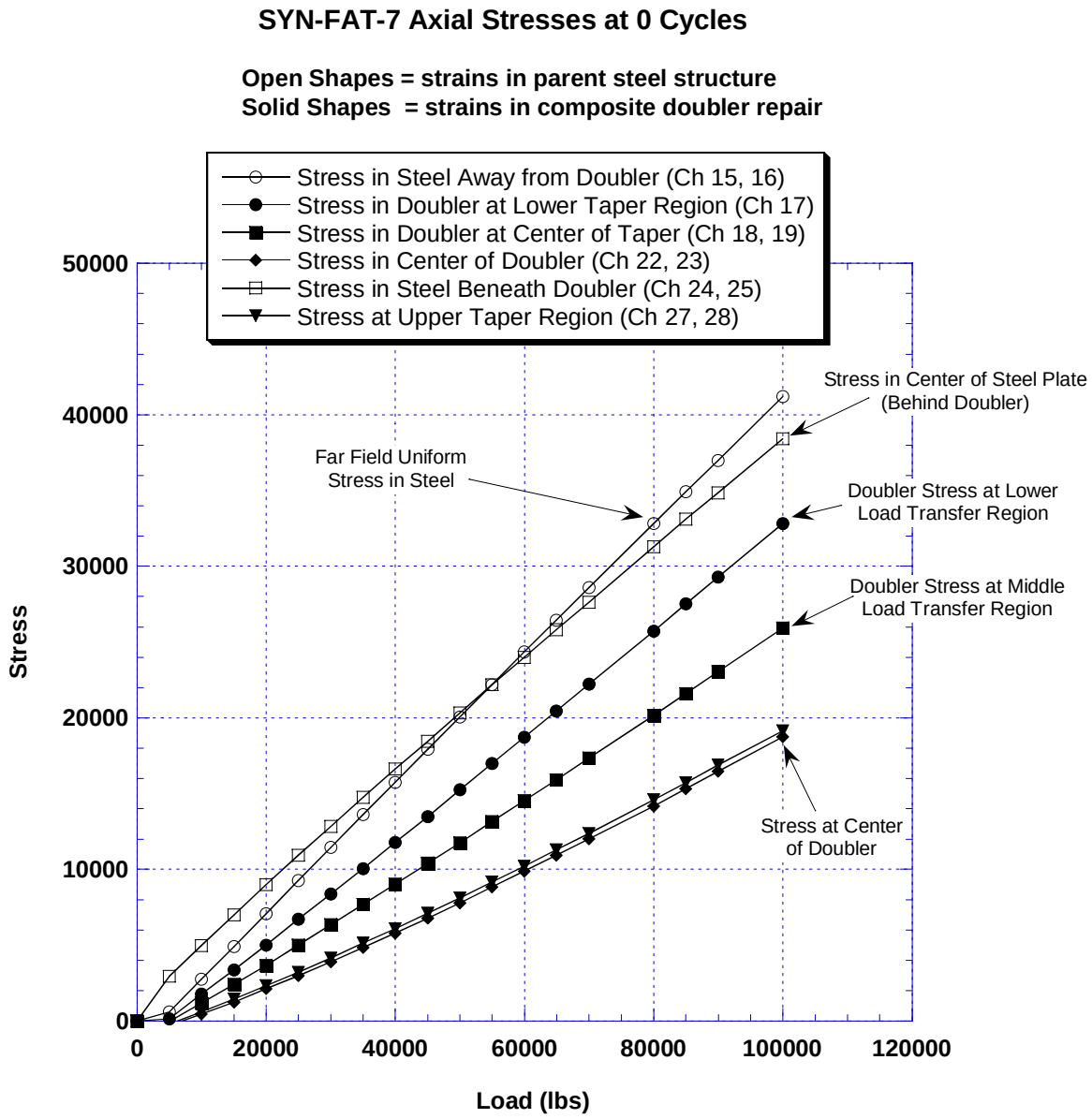


**Figure 90: Stress Levels in Steel and Composite for Configuration SYN-FAT-7 – Pristine Composite Doubler with No Conditioning; 41 ksi Stress Spectrum**

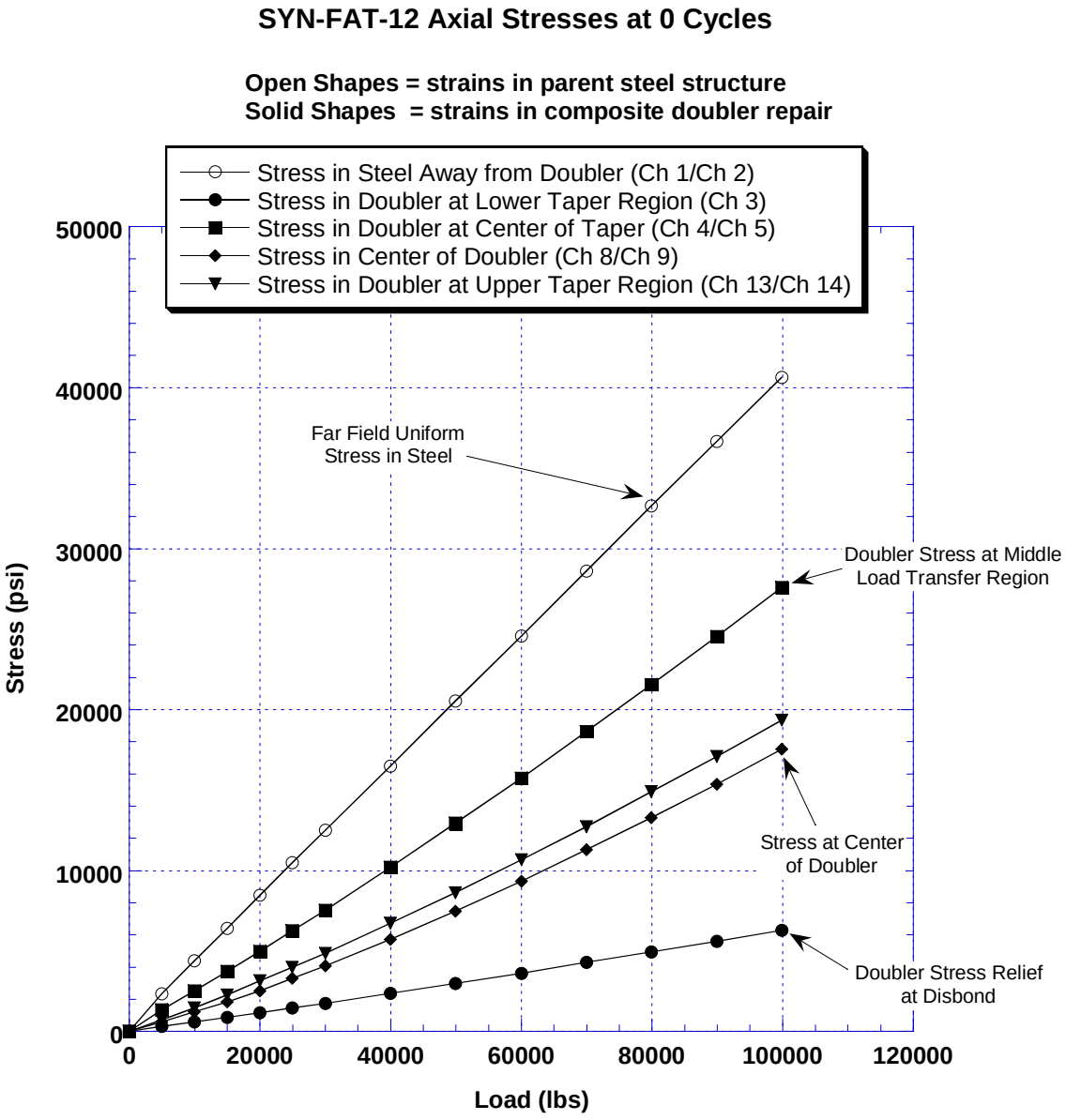


**Figure 91: Stress Levels in Steel and Composite for Configuration SYN-FAT-12 – Flawed Composite Doubler with No Conditioning; 41 ksi Stress Spectrum**

### 4.3.3 Load Transfer

Plots of percent load transfer were obtained by calculating the ratio between doubler strains and strains in corresponding portions of the steel plate. Figures 92-95 show the resulting load transfer plots for various doubler and steel reference channels $\{\varepsilon_{doubler} / \varepsilon_{steel(ref)}\}$ when subjected to the high and low stress spectrums.

*The curves indicate that the load transfer into the doubler - and away from the steel - was similar in all fatigue specimens regardless of the type and degree of damage in the specimen. In*

*the tapered portion of the doubler, the load transfer was consistently in the 40 - 80 % range. In the center, where the doubler reaches its maximum thickness of 24 plies, the load transfer was in the 40 - 60% range.*

The array of fatigue specimens ranged from unflawed (optimum installation) to large, co-located flaws (worst-case scenarios) with hot-wet and cold conditioning. Figures 92-95 show the consistency of load transfer values across the full spectrum of specimens despite the large variations in flaw scenarios. Furthermore, these load transfer values remained constant over much of the fatigue testing. This indicates that there was little deterioration in the bond strength over this time. Normal repair methodologies that utilize doubler stiffness ratios of 0.8 to 1.0, would produce load transfer ratios in the 40-60% range [6, 19, 20]. However, since this repair has a lower stiffness ratio of 0.3, the resulting stresses in the doubler are higher as shown in the graphs. This is an acceptable approach as long as the stress levels in the composite laminate and adhesive layer do not approach ultimate levels.

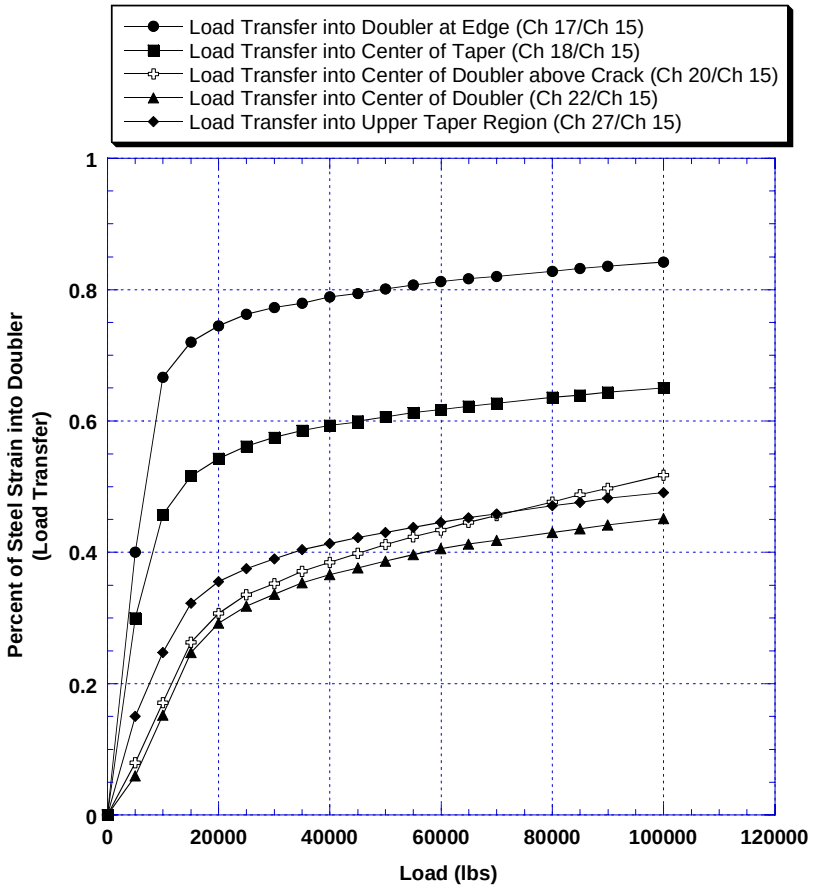


**Figure 92: Load Transfer in Composite Repair SYN-FAT-7 – Pristine Composite Doubler with No Conditioning; 41 ksi Stress Spectrum**

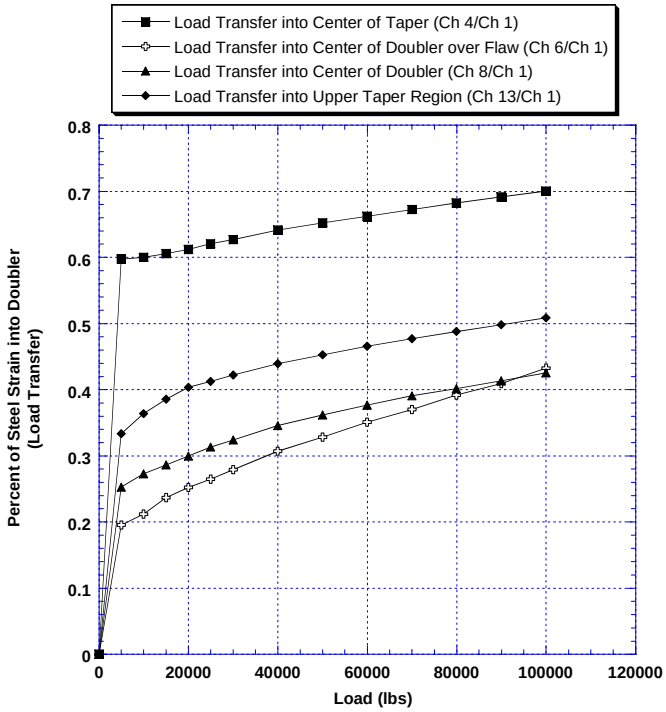


**Figure 93: Load Transfer in Composite Repair SYN-FAT-12 – Flawed Composite Doubler with No Conditioning; 41 ksi Stress Spectrum**

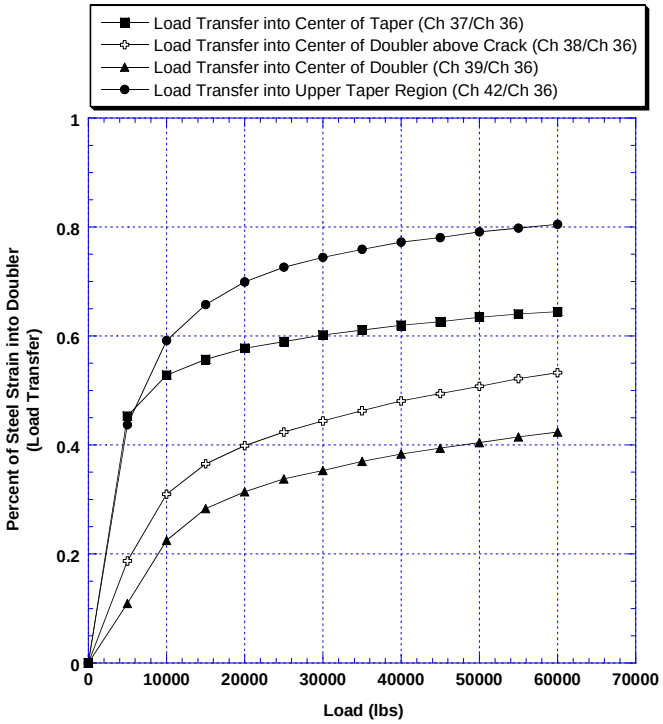


**Figure 94: Load Transfer in Composite Repair SYN-FAT-16 – Pristine Composite Doubler with Hot-Wet & Cold Conditioning; 24 ksi Stress Spectrum**

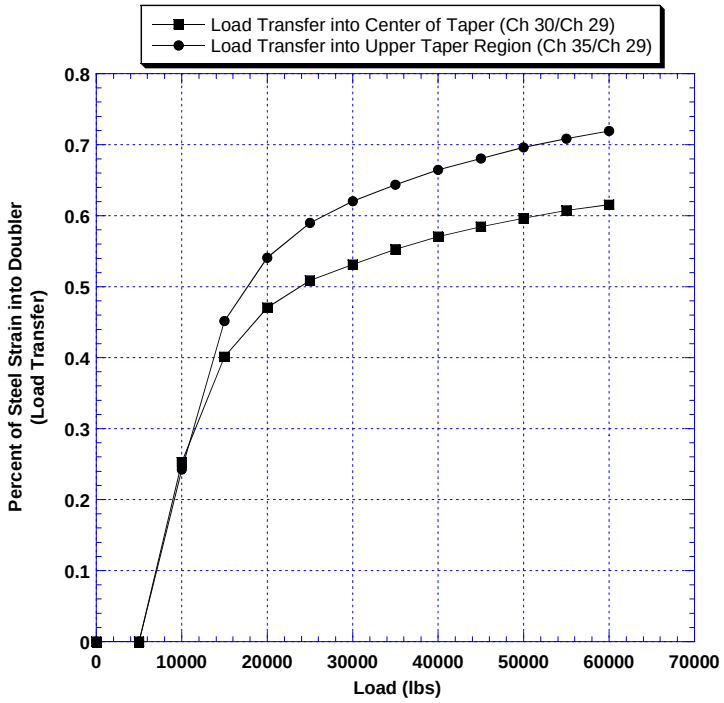


**Figure 95: Load Transfer in Composite Repair SYN-FAT-18 – Flawed Composite Doubler with Hot-Wet & Cold Conditioning; 24 ksi Stress Spectrum**

### 4.3.4 Effects of Multiple Fatigue Lifetimes on Strain Fields

In each of the fatigue specimens, the vast majority of the strain field remained unchanged over the course of the fatigue tests. Several of the specimen configurations showed no change in strain levels from 0 fatigue cycles to 330,000 fatigue cycles. The only strain changes noted in any of the specimens were caused by crack propagation. In these instances, the composite doublers picked up additional strain as the crack propagated across the steel structure.

No Change in Strain Field - Configurations SYN-FAT-5, -9, -16, and -18 exhibited little or no change in strain field during the course of their fatigue tests. No crack growth was measured during the tests that applied 250,000 to 330,000 cycles. The NDI before-and-after results in Figure 82 show that the initial "programmed" flaws in SYN-FAT-18 did not change shape nor did any new flaws develop as a result of the fatigue loads. Quantitatively, the strain gage values acquired before and after fatigue testing substantiate the NDI results. Figure 96 plots the strain field for configurations SYN-FAT-16 before and after 331,000 fatigue cycles. The before-and-after plots lie on top of each other demonstrating an unchanged strain field. Similarly, Figure 97 shows that the strains in the SYN-FAT-18 were undisturbed by 325,00 fatigue cycles. The corresponding stress entries in Table 11 summarize the unchanged stress levels since the stresses in the specimen before and after fatigue cycling are within 5% of each other.

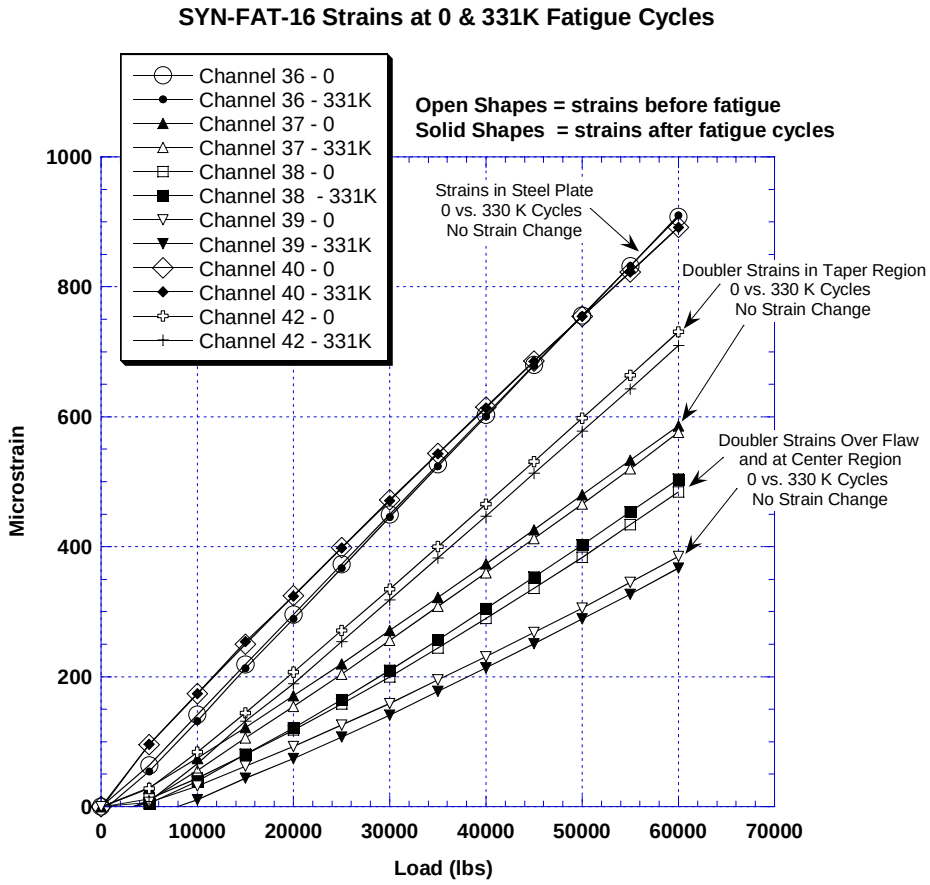


**Figure 96: Strain Field in SYN-FAT-16 Remains Unchanged Over 330,000 Fatigue Cycles – No Crack Growth or Flaw Growth in Doubler Installation; Pristine Composite Doubler with Hot-Wet & Cold Conditioning; 24 ksi Stress Spectrum**

Strain Changes Caused by Fatigue Cracks - In the specimens where crack growth occurred, and especially where the crack grew beyond the perimeters of the implanted disbond flaw, significant strain changes were observed in the immediate area of the propagating crack. The results, however, highlight the ability of the composite doubler to pick up additional load in response to a loss of strength in the parent structure.

The NDI results in Figure 80 show how the propagating crack produced a fracture in the adhesive layer in SYN-FAT-13. Similar changes were observed in SYN-FAT-7, -8, -12, -15, and -17 specimens which all experienced crack growth of 1.2" or more. Once again, the strain gage results quantify and verify the NDI assessments. Although the strains remained constant in the critical load transfer region, Figures 98 - 102 show that there were several localized changes in the strain fields due to the propagation of the crack through the steel plate.

Channel 20 in Figure 98 highlights the increasing load picked up by the composite doubler as the steel crack propagates in SYN-FAT-7. Channel 21 in Figure 99 shows the corresponding reduction in steel strain as the crack grows and eliminates the steel's ability to take any load in

this region. At N= 0 cycles, the strains at the center of the doublers amounted to 50% of the total strain in the steel plates. After N = 109,000 cycles and a crack propagation of 1.4", the same strain gages registered 95% of the total strain in the plate. During the fatigue tests, the Channel 21 strains drop from 90% of total strain to 26% of total strain in plate.

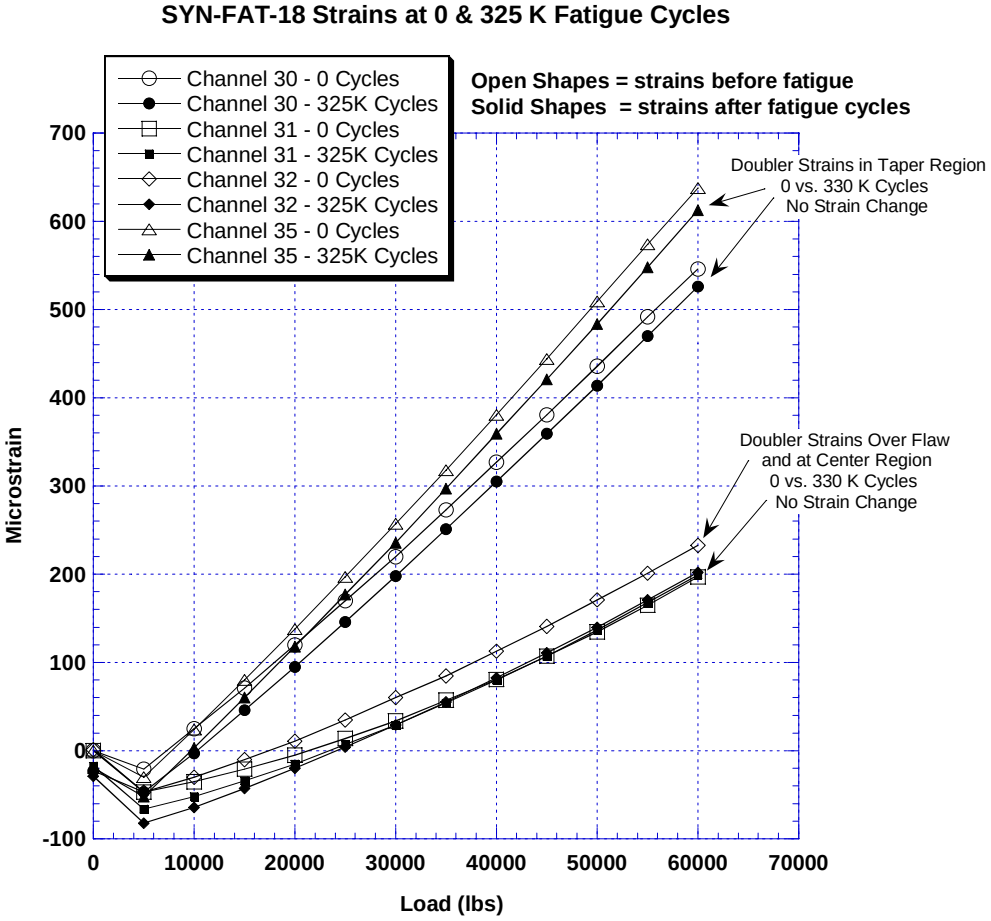


**Figure 97: Strain Field in SYN-FAT-18 Remains Unchanged Over 325,000 Fatigue Cycles – No Crack Growth or Flaw Growth in Doubler Installation; Flawed Composite Doubler with Hot-Wet & Cold Conditioning; 24 ksi Stress Spectrum**

Similarly, Channel 6 in Figure 100 shows how the strain in the doubler center region rises significantly after the fatigue loads grew the crack 1.4". At N= 0 cycles, the strains at the center of the doublers amounted to 40% of the total strain in the steel plates. After N = 87,000 cycles and a crack propagation of 1.4", the same strain gages registered 56% of the total strain in the plate. The central portion of the steel plate (Channel 7 in Figure 101) shows the associated strain reduction (loss of strength) produced by the crack growth. The curves for N = 0 and N = 208,000 cycles in Figure 102 show how the doubler in SYN-FAT-16A picks up more load as the crack propagates and the plate relieves its load (reference Channel 38). These results quantify the ability of bonded composite doubler repairs to increase its reinforcing value as flaws grow and the parent structure losses its ability to sustain normal working loads.

The stress entries in Table 11 quantify the changes in load distribution within the repaired structure. Stress levels in the load transfer (taper) region go up 25% to 40% as the doubler takes on more load. Doubler stress levels in the vicinity of the crack go up 30% to 50%. At the highest stress riser near the crack tip, stress increases of over 100% were measured in the doubler.

*It is important to note three items regarding these change in strain fields: 1) the composite doubler was able to meet its design objectives and absorb additional load as required, 2) the effects were localized about the crack (i.e. the strains around the perimeter - especially in the critical load transfer region - remained unchanged), and 3) the change in flaw shape (ref. Fig. 80) was caused by a cohesive failure of the adhesive, not a growth in the implanted disbond. This latter point is key because the cohesive failure indicates that the installation was good and that the full strength of the adhesive was achieved. Disbonds, indicated by a lack of adhesive on either the laminate or steel mating surface, are undesirable since they can occur at lower loads*

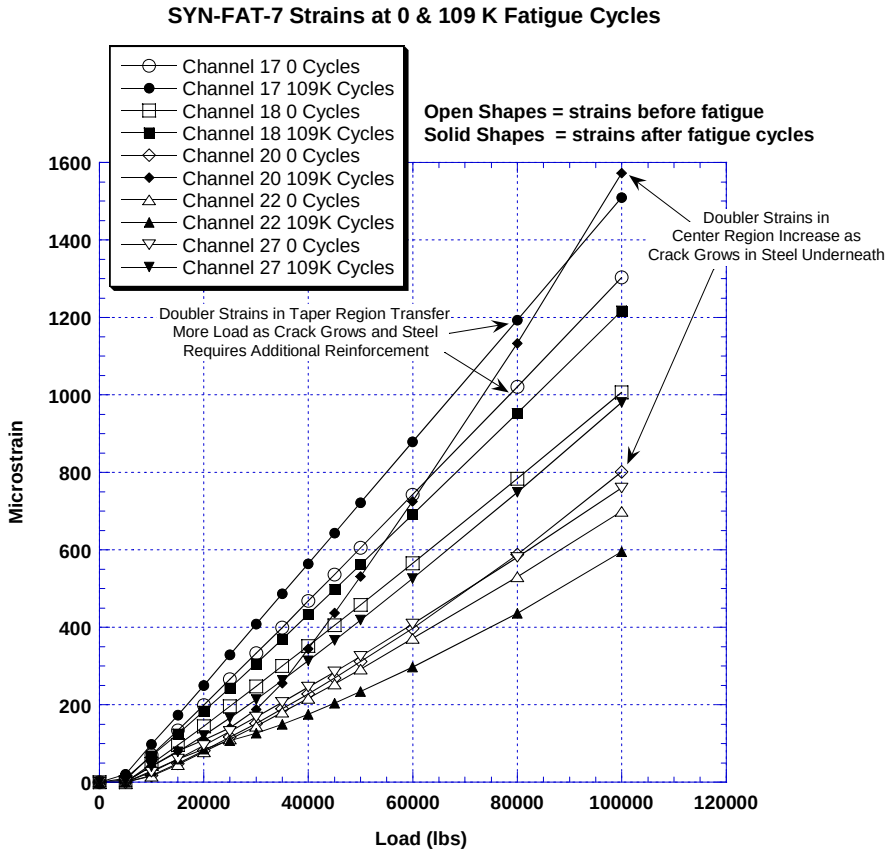


**Figure 98: Strain Field in SYN-FAT-7 Doubler Undergoes Slight Changes Due to Crack Growth in Steel – No Flaw Growth in Doubler Over 109,000 Fatigue Cycles; Pristine Composite Doubler with No Conditioning; 41 ksi Stress Spectrum**

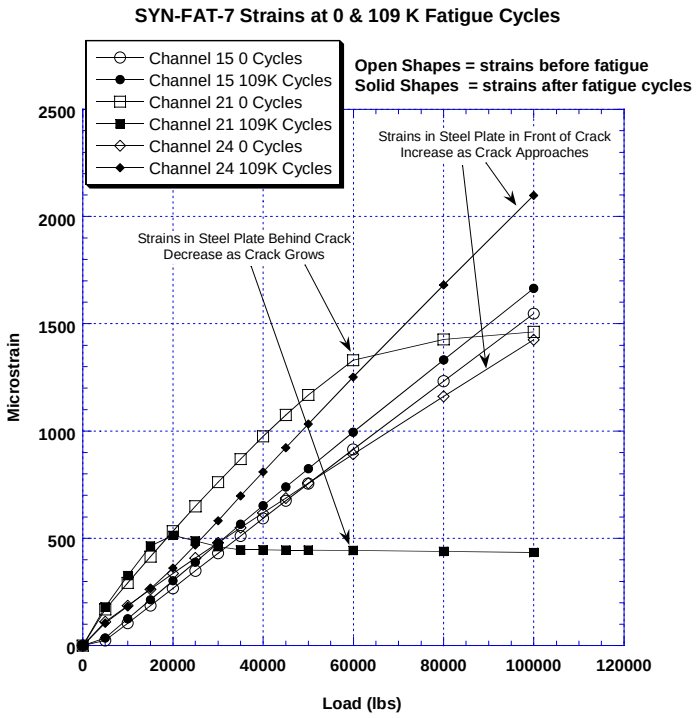


**Figure 99: Strain Field in SYN-FAT-7 Steel Decreases Due to Crack Growth in Plate and Associated Load Shedding; 41 ksi Stress Spectrum**

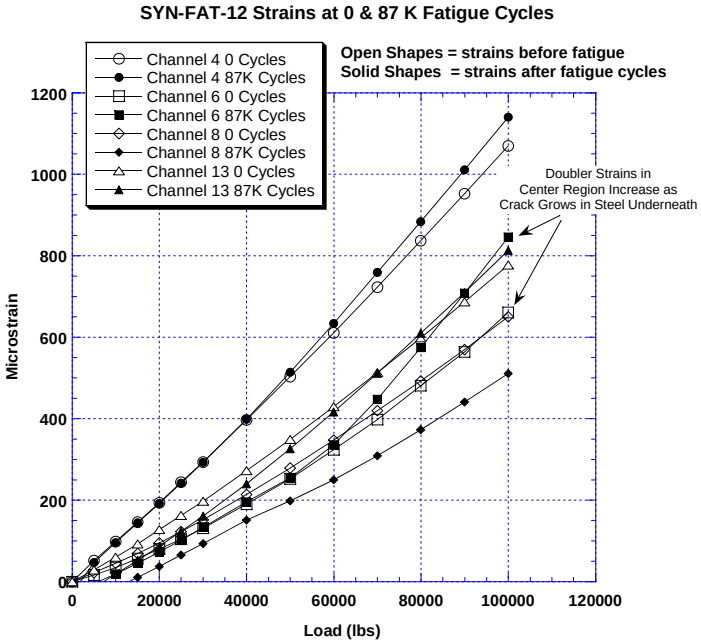


**Figure 100: Strain Field in SYN-FAT-12 Doubler Undergoes Slight Changes Due to Crack Growth in Steel – No Flaw Growth in Doubler Over 87,000 Fatigue Cycles; Flawed Composite Doubler with No Conditioning; 41 ksi Stress Spectrum**

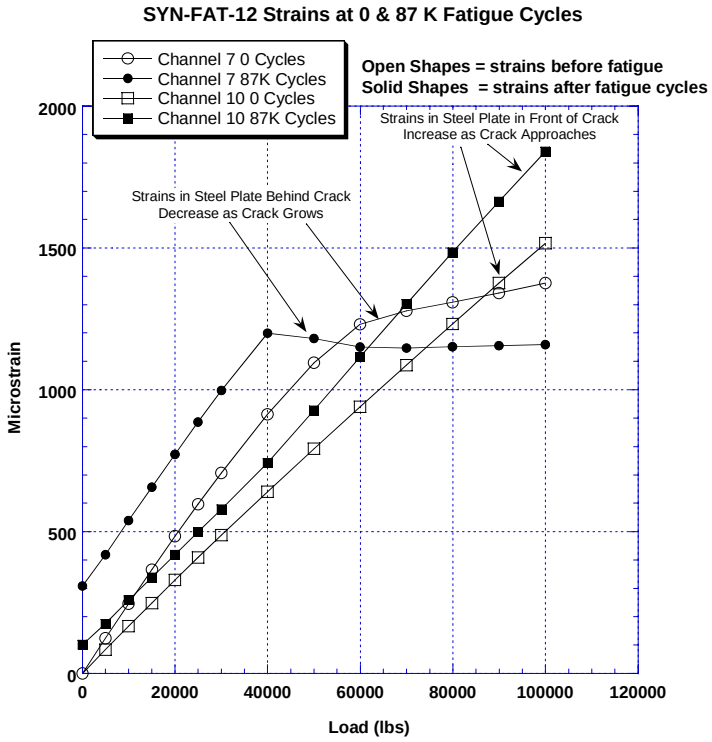


**Figure 101: Strain Field in SYN-FAT-12 Steel Changes Due to Crack Growth in Plate and Associated Load Shedding; 41 ksi Stress Spectrum**

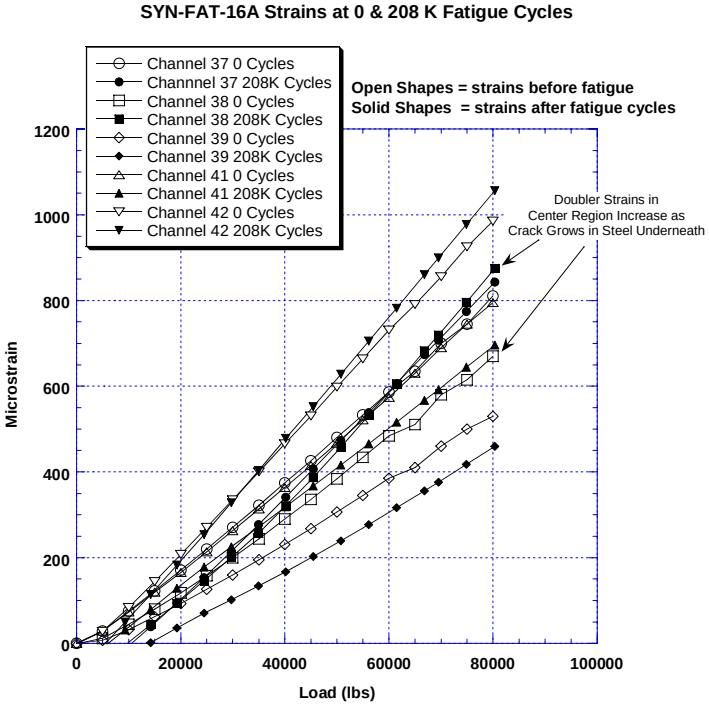


**Figure 102: Strain Field in SYN-FAT-16A Doubler Undergoes Slight Changes Due to Crack Growth in Steel – No Flaw Growth in Doubler Over 208,000 Fatigue Cycles; Pristine Composite Doubler with Hot-Wet & Cold Conditioning; 33 ksi Stress Spectrum**

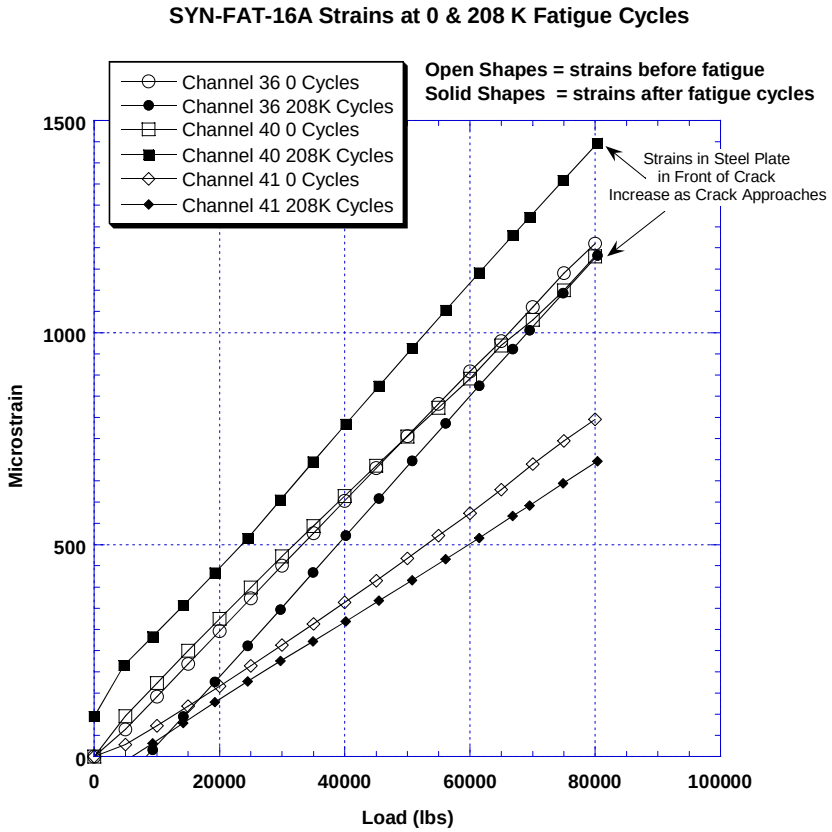


**Figure 103: Strain Field in SYN-FAT-16A Steel Changes Due to Crack Growth in Plate and Associated Load Shedding; 33 ksi Stress Spectrum**

## 4.4 Residual Strength of Damaged Steel Structure with Composite Doubler Repairs

After the fatigue tests were completed, seven of the specimens were subsequently loaded to determine their static residual tensile strength. It is important to note that these were not actually ultimate strength tests since the specimens were tested after flaws were engineered into the specimens and the implanted cracks were grown. By using the maximum load at failure and the original cross section area at the start of the static residual strength test, the resulting "residual tensile strength" numbers are conservative. In the ultimate/residual strength tests, failure was defined as the point where the specimen was unable to sustain an increasing load. The peak load recorded during each failure test was used to calculate the maximum uniform stresses sustained by the flawed specimens (residual strength). Strain gage data was also used to determine the stress values at various locations in the specimen. These locations included the far-field, uniform stress regions, the load transfer regions in the doubler, and the stress riser regions adjacent to the propagating crack.

All seven specimens – SYN-FAT-7, -8, -11, -12, -13, -16A, and -18A – experienced crack growth during the course of their fatigue tests. Their failure occurred in one of two modes: 1) crack propagation and associated cohesive bond failure through the steel plate, and 2) failure of

the composite laminate. In the first failure mode, the doubler separated from the steel plate through a cohesive fracture of the adhesive. Thus, there was no disbond growth and adhesive was found on both the steel and composite laminate. Figure 104 shows this failure mode where the adhesive layer fractures in a cohesive mode.

As the load was increased, the steel beneath the doubler and adjacent to the crack began to yield and elongate. The yield zone expanded to include the tapered edge of the doubler as well as the center of the specimen. This caused the steel to sequentially pull away from the doubler which was not yielding or stretching at the same rate as the parent steel. The result was a rolling wave of cohesive failure in the adhesive layer. *There was no disbond growth in the specimen as evidenced by the presence of adhesive on both the steel and mating composite doubler. This indicates that the installation was successful and the full strength of the adhesive was achieved.* During the course of the test it was possible to hear popping sounds corresponding to the fracture of the adhesive. When this cohesive failure (as opposed to adhesive, or disbond, failure) in the adhesive reached the center crack of the coupon, half of the steel plate was left without doubler reinforcement. At that point, the crack in the steel propagated rapidly across the entire width of the test specimen.


**Figure 104: View of Repair Specimen After Ultimate Failure; Mode of Failure was Cohesive Fracture of the Adhesive Layer Between the Laminate and the Steel**

The second failure mode occurred when the interlaminar stresses in the composite laminate exceeded the ultimate capability of the material. These interply fractures, such as the one shown in Figure 105, always occurred at the interfaces to the $45^o$ plies. This is reasonable since the $45^o$ plies have less strength than $0^o$ plies in the load direction. Figure 105 shows that the ply orientation at the failed interface surface is $45^o$. The fact that either failure mode was possible indicates that the repair design was fairly balanced in its ability to achieve the maximum

allowable stress levels in the laminate and the adhesive layer. Figure 106 shows the extreme crack growth and crack opening that was withstood by the composite repair before failure occurred.

**Figure 105: View of Repair Specimen After Ultimate Failure; Mode of Failure was Interply Fracture of the Composite Laminate**

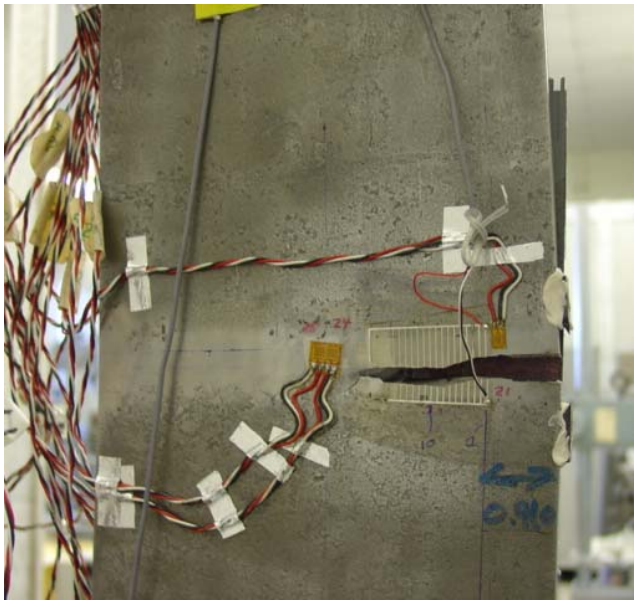

**Figure 106: Extreme Crack Growth/Opening in Structure Before Doubler Failure Occurred**

Figures 107 – 109 show the stress and strain fields in specimens SYN-FAT-7, -12, and -16A up to failure. The steel plate away from the doubler (Channels 15/16, 1/2, and 36) began to yield at approximately 130,000 to 140,000 lbs. (approximately 50 ksi) while the doubler continued to increase its load. Stresses near the crack increased dramatically. Doubler stresses increased in response to stress relief that occurred in the steel plate behind the crack. *Figures 107-109 clearly show a nonlinear response in the composite laminate even though the Boron-Epoxy material alone does not have a plastic regime in its response. This indicates that the composite doubler was able to transmit plastic stresses from the steel structure and that extensive yielding and loading beyond the initial yield level was required to fail the installation.*

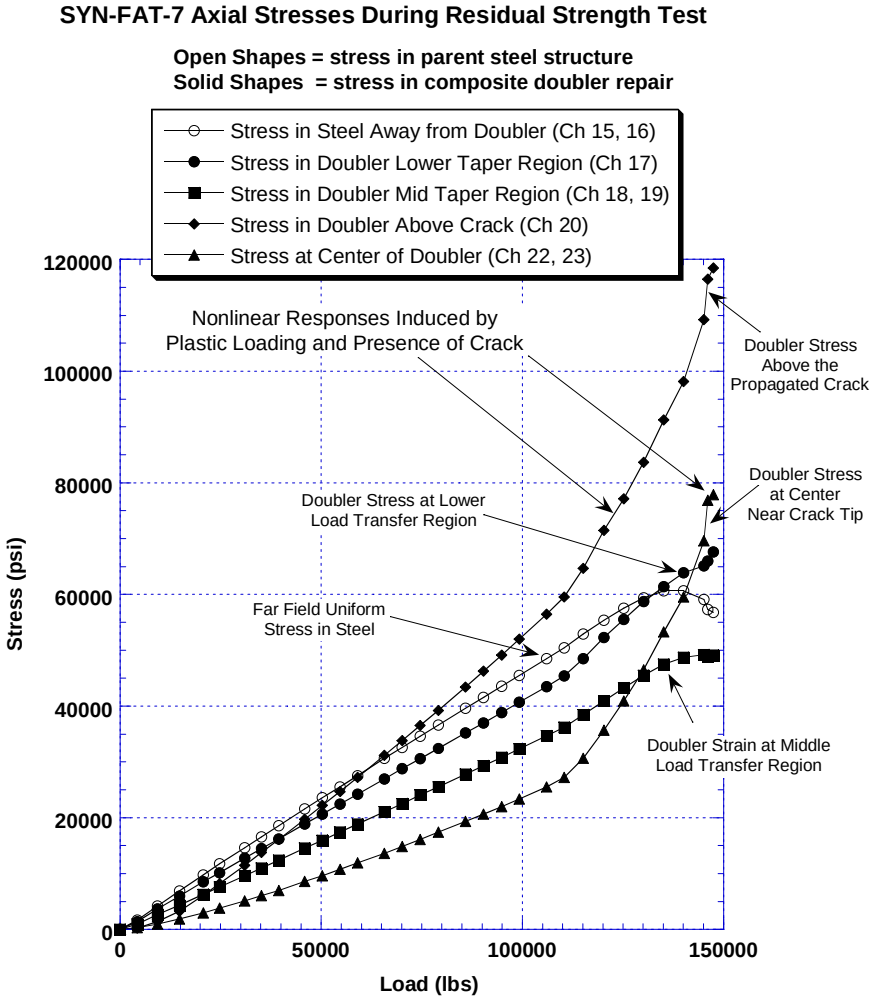


**Figure 107: Stress Levels in Steel and Composite Doubler During Ultimate/Residual Strength Failure Test of SYN-FAT-7 – Pristine Composite Doubler with No Conditioning**

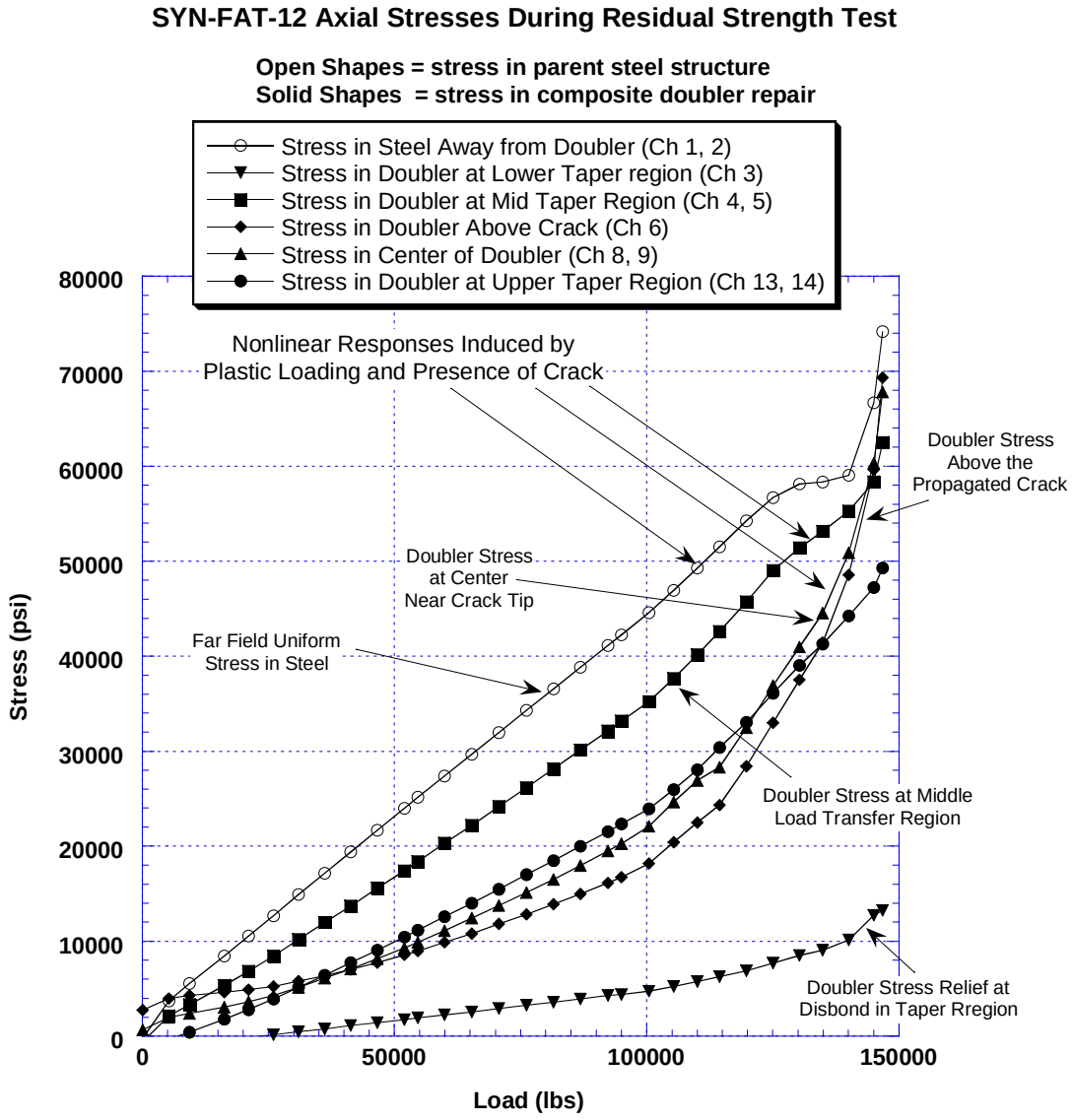


**Figure 108: Stress Levels in Steel and Composite Doubler During Ultimate/Residual Strength Failure Test of SYN-FAT-12 – Flawed Composite Doubler with No Conditioning**

Table 12 summarizes the stress levels in the test specimens at the failure load. While yielding in the parent steel was measured at approximately 50 ksi in these tests, the stress levels in the steel and composite laminate went well beyond this yield level. Maximum stresses around the crack tip even exceeded the 65 ksi ultimate strength value measured in failure tests on the welded steel alone. The residual strength values are listed in Table 13. The residual strength values in all of the specimens were quite similar despite the large differences in the configurations. The baseline for comparison purposes comes from specimen SYN-FAT-11 which contained a welded region without a composite doubler. Ultimate failure of this specimen occurred at 65 ksi. Failure in all six specimens which contained composite doubler repairs exceeded this value and ranged from

77 ksi to 94 ksi. The average residual strength was 89 ksi. It is worth noting that essentially all but one of the specimens exceeded the ultimate strength value for the pristine, unwelded steel material (Manufacturer supplied data on ASTM A572 material tested: $\sigma_{ult.}$ = 85,000 psi). Thus, *even in the presence of severe worst case installations (disbonds amounting to 20% of the load transfer region) and extensive damage growth (fatigue cracks extending through 50% of the specimen width), it was seen that the doubler-reinforced plates were able to achieve residual tensile strengths (i.e. post-damage tensile strength) which exceeded the 65 ksi baseline value for this steel material. Thus, the Boron-Epoxy doubler was able to return the parent structure to its original strength and load carrying capability.*

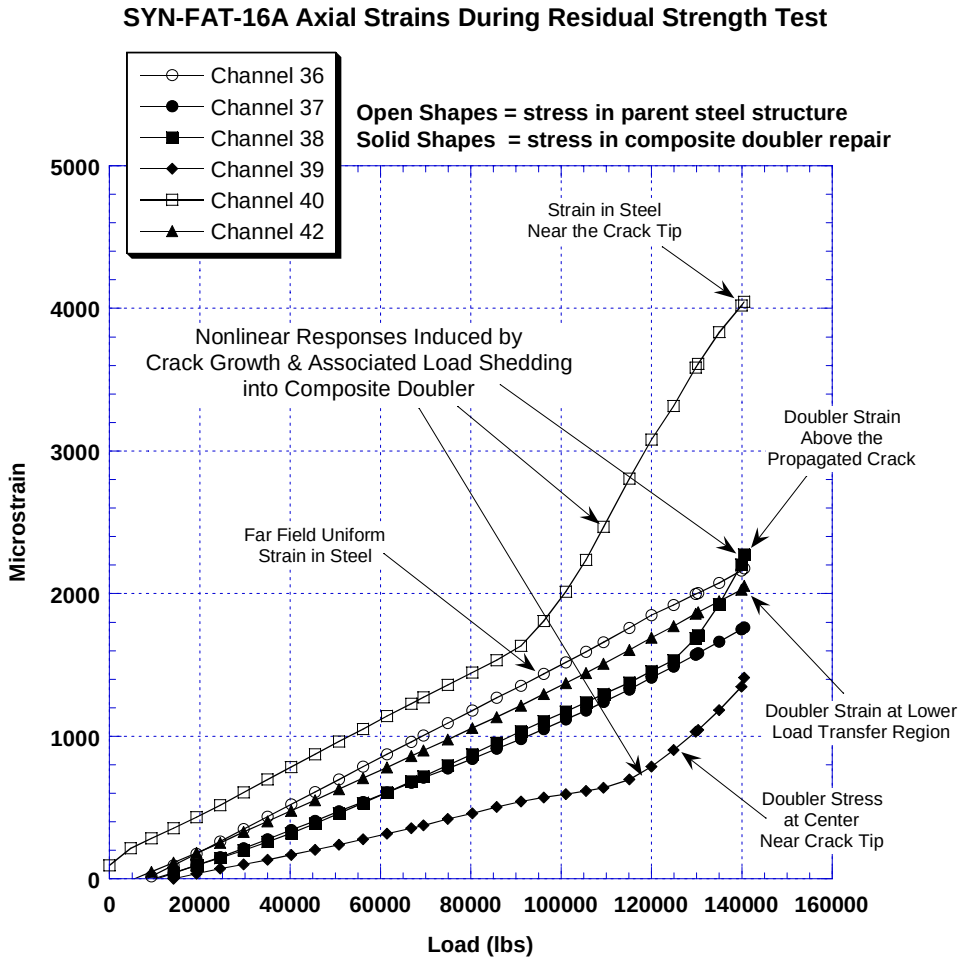


**Figure 109: Strain Levels in Steel and Composite Doubler During Ultimate/Residual Strength Failure Test of SYN-FAT-16 – Pristine Composite Doubler with Hot-Wet & Cold Conditioning**

| Specimen No. | Strain Channels | Ultimate Load | Ultimate Stress | Location on Test Specimen |
|---|---|---|---|---|
| SYN-FAT-7 (pristine composite doubler with no conditioning) | 15, 16 | 147,400 | 56,788 | Steel - Far Field |
| | 17 | | 67,561 | Doubler Edge (upper taper region) |
| | 18, 19 | | 49,131 | Doubler Edge (middle taper region) |
| | 20 | | 118,465 | Doubler Above Crack (full thickness region) |
| | 22, 23 | | 77,907 | Doubler in Front of Crack (full thickness region) |
| | 24, 25 | | 161,820 | Steel - Near Crack Tip |
| | 27, 28 | | 52,640 | Doubler Edge (upper taper region) |
| SYN-FAT-12 (flawed composite doubler with no conditioning) | 1, 2 | 147,000 | 74,162 | Steel - Far Field |
| | 4, 5 | | 62,491 | Doubler Edge (middle taper region) |
| | 6 | | 69,300 | Doubler Above Crack (full thickness region) |
| | 8, 9 | | 67,824 | Doubler Above Crack (full thickness region) |
| | 10, 11 | | 260,780 | Steel - Near Crack Tip |
| | 13, 14 | | 49,275 | Doubler Edge (upper taper region) |
| SYN-FAT-16 (pristine composite doubler with hot-wet & cold conditioning) | 36 | 140,600 | 57,706 | Steel - Far Field |
| | 37 | | 44,402 | Doubler Edge (middle taper region) |
| | 38 | | 57,304 | Doubler Above Crack (full thickness region) |
| | 40 | | 107,272 | Steel - Near Crack Tip |
| | 41 | | 27,321 | Steel - Relief Adjacent to Doubler |
| | 42 | | 51,836 | Doubler Edge (lower taper region) |

**Table 12: Stresses in Steel Plates and Composite Doublers Produced by the Post-Fatigue Residual Strength Tests**

| Specimen No. | Configuration | Max. Stress Measured at Failure (psi) | Residual (Ultimate) Tensile Strength (psi) * |
|---|---|---|---|
| SYN-FAT-7 | Unflawed composite doubler with no conditioning | 161,820 | 93,970 |
| SYN-FAT-8 | Unflawed composite doubler with no conditioning | N/A | 93,300 |
| SYN-FAT-11 | No composite doubler; Weld repair only | N/A | 65,250 Δ |
| SYN-FAT-12 | Flawed composite doubler with no conditioning | 260,780 | 96,100 |
| SYN-FAT-13 | Flawed composite doubler with no conditioning | N/A | 83,400 |
| SYN-FAT-16A | Unflawed composite doubler with hot-wet & cold conditioning | 107,272 | 77,400 |
| SYN-FAT-18A | Flawed composite doubler with hot-wet & cold conditioning | N/A | 86,930 |

* Manufacturer supplied data on ASTM A572 material tested $\sigma_{ult.}$ = 85,000 psi
Δ Baseline residual strength for comparison with composite doubler repair specimens

**Table 13: Residual Strength Values from Specimens After Fatigue Tests Have Propagated Cracks (Post-Fatigue Load to Failure)**

## 4.5 Response of Composite Doublers in Extreme Shear and Bending Environments

### 4.5.1 Three Point Bending Test Description

Objective - The purpose of this test series was to experimentally assess the potential for delaminations and disbonds in a thick composite doubler installation when subjected to extreme bending, compressive, and shear stresses. Bending of the shovel boom, and the associated shear stresses in the adhesive layer, is an important consideration and this test focused on worst case conditions. Three point bending was used to produce high shear stress in doublers and simulate the compression stresses which arise during shovel "break-out" conditions (reverse bending as shovel breaks free from its dig). The loads in this test did not simulate a particular operating condition. Rather, the bending loads were increased until the specimen failed. In this manner, it was possible to assess the design margin and mode of failure associated with high bending and compressive shear strains.

Three Point Bending Test Specimens and Test Set-Up - For this test series, the specimen was a beam comprised of a 24 ply Boron-Epoxy laminate bonded to a steel substrate such that the stiffness ratio between the repair doubler and parent structure was1:3 (30% patch stiffness). The beam was 20″ long and 1″ wide and the doubler design (ply lay-up) was the same as the one used in the fatigue test specimens described on Section 3.3. Figure 110 shows the schematic of the test specimen and Figure 111 is a photo of some test specimens. Six similar specimens were tested so that the repair installation could be evaluated at conditions corresponding to minimal environmental effects and for performance after exposure to hot-wet-cold conditioning. The bend specimens did not contain weld regions

ASTM specifications require hot-wet and cold conditioning to run for a minimum of 40 hours with a 50% relative humidity. The bending specimens for this program were subjected to 98% relative humidity (140$^{o}$F) for 30 days followed by exposure to cold temperatures 0$^{o}$F for 10 days. Since exposure to the 0$^{o}$F temperatures came after the hot-wet conditioning, is was possible for any absorbed moisture to freeze, expand, and create local ruptures in the composite material. The extreme nature of this environmental conditioning was further exacerbated by the omission of any fiberglass cover ply, sealant or epoxy paint over the top of the composite doubler repair. Such protective coatings will be installed in an actual field repair and testing has shown that the fiberglass cover ply and epoxy paint should eliminate the detrimental effects of moisture and associated corrosion.

Prior to testing, NDI was applied to each test specimen. Pulse Echo ultrasonics was used to check for any pre-existing flaws which may affect the test results. Upper and lower load rods were used to support the specimen and transfer the load as indicated in Figures 110 and 112. Figure 113 is a photograph of a test specimen during testing in the uniaxial test machine. Strain gages were used to monitor the stress field in the composite and steel substrates during the tests. Figure 110 shows the strain gage layouts used on one unconditioned and one environmentally-exposed specimen. During the structural tests, the load was uniformly and continuously increased until structural failure occurred. Failure was defined as an inability to sustain an increasing load (i.e. a “knee” in load vs. displacement curve).

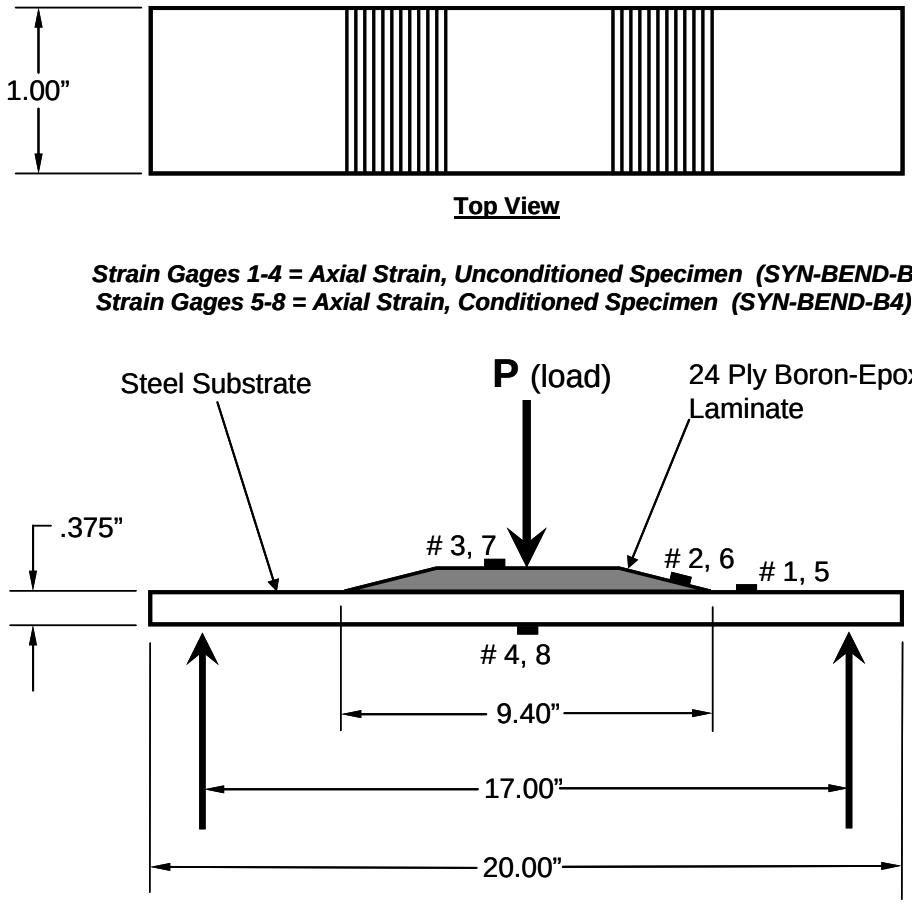


**Figure 110: Composite Doubler Three-Point Bend Specimens for Evaluating Affects of Extreme Shear and Compressive Stresses; Strain Gage Layout Used to Monitor Stress Fields**

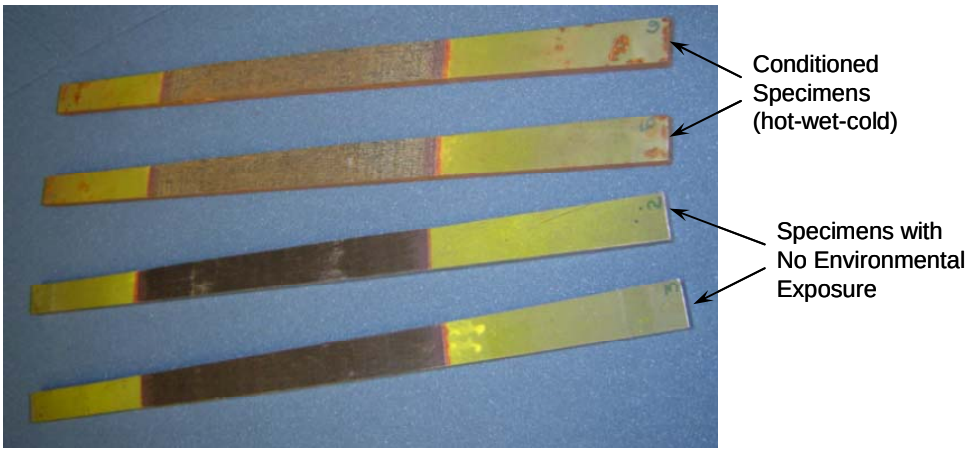


**Figure 111: Conditioned and Unconditioned Test Specimens for Bending-Shear Tests**

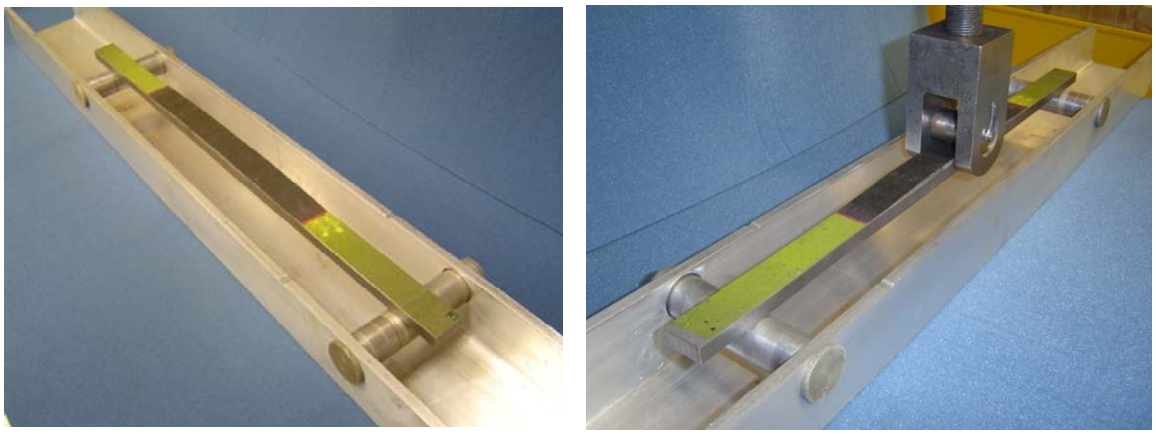

**Figure 112: Three-Point Bend Specimen in Test Fixture Showing Load Application and Boundary Conditions**

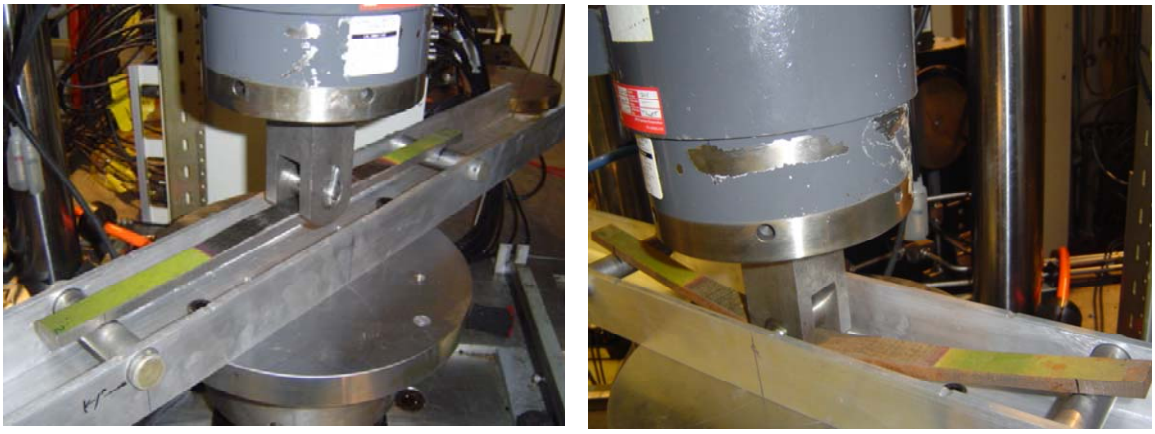

**Figure 113: Three-Point Bend Specimen During Testing**

### 4.5.2 Three Point Bending Test Results

Pre-test inspections did not reveal any flaws in the test specimens. The maximum moment generated in the test specimen is given by the relation:

$$M_{max} = PL/4 \quad (14)$$

The stress produced by this moment can be calculated using the following equation:

$$\sigma = M\,y/I \quad (15)$$

Where:

I = moment of inertia of cross section

M = moment [in.-lbs.]
P = load [lbs.]
L = distance between load supports
y = distance from neutral axis to point of interest
$\sigma$ = stress [psi]

When the beam is supported at two endpoints and loaded at the midpoint and shown in Figure 109, the maximum stress occurs in the outer surface of the test specimen at the midpoint of the beam. This shear stress may be calculated by using equation (14) for the midpoint of the specimen L/2:

$$\sigma_{max} = 3PL/2bd^2 \quad (16)$$

Where:

$\sigma_{max}$ = stress in outer fibers at midpoint [psi]
b = width of beam [in.]
d = depth of beam [in.]

Figures 114 and 115 plot the shear stress values calculated from the strains measured during the 3-point bend tests. Strains in the steel at the bottom of the specimen were tensile while strains in the composite laminate on top were approximately equal in magnitude but were compressive. Tests on steel specimens without composite doublers revealed that yielding in the bend specimens occurs at approximately 55 ksi. Figure 114 shows that yielding in the bend specimens, and the corresponding nonlinear response in the composite repair, began slightly later at 66 ksi. Strain could not be measured in the exact center of the laminate due to the presence of the load application bar. Gages #3 and #7 were close to the center but due to the high strain gradient in this area, equation (16) was also used to make some stress level assessments. Table 14 lists the maximum compressive stress levels produced in the composite repair during the tests. Note the decrease in the stress levels achievable in the hot-wet conditioned specimens. Focused testing has shown that the adhesive strength can be reduced by as much as 20% through exposure to hot-wet conditions. This is the approximate difference between maximum compression stresses in the unconditioned and conditioned specimens. Proven, protective measures will be taken in an actual installation to eliminate these degrading effects. In all tests, the maximum stress levels exceeded the normal yield levels of 55 ksi established for this material. Several of the specimens were able to survive compressive stresses that approached the ultimate strength value for the pristine, unwelded steel material (85 ksi). Once again, these results demonstrate that the composite doubler repair method is able to survive extreme compressive stresses and that the parent structure must go into the yield regime in order to fail the repair.

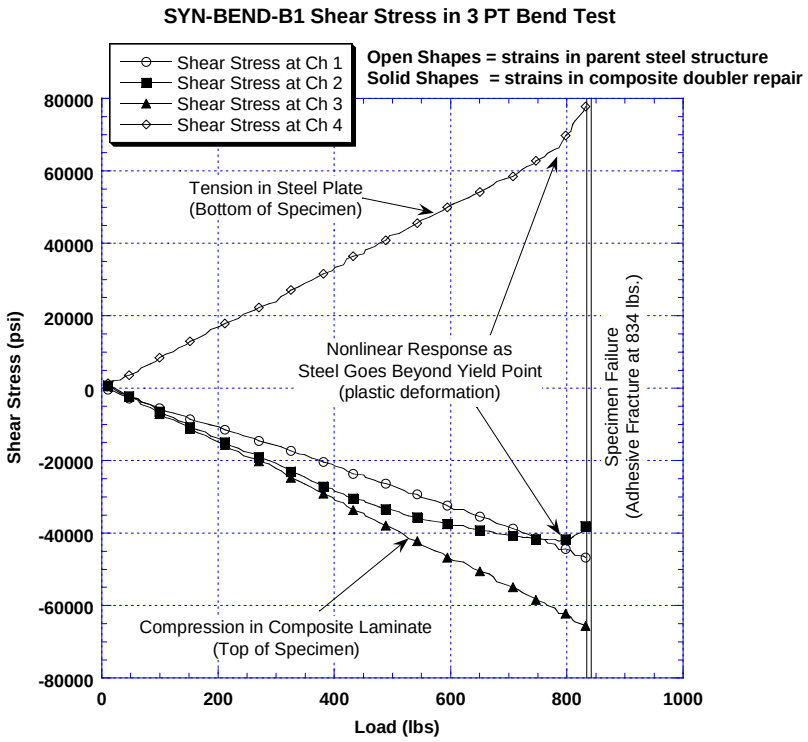


**Figure 114: Shear Stress in SYN-BEND-B1 During Three Point Bend-to-Failure Tests**

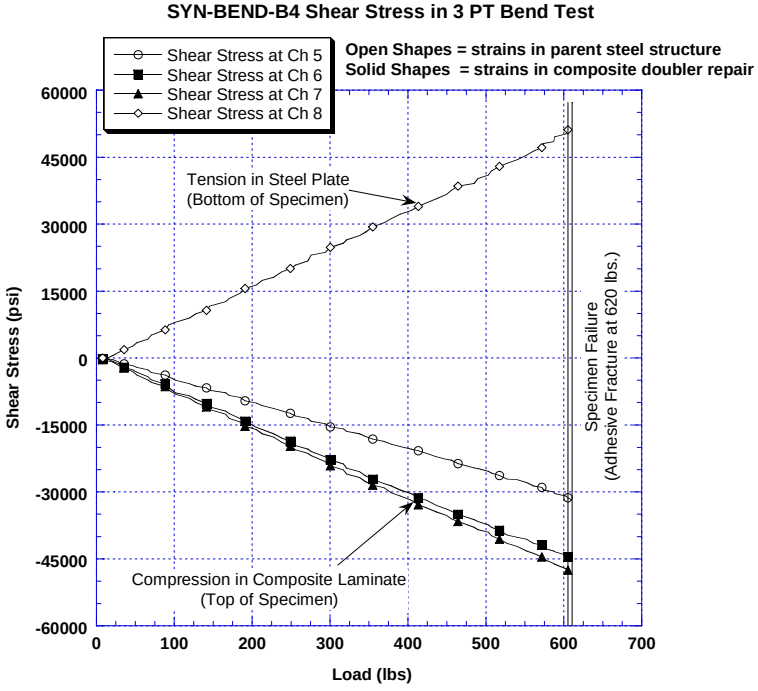


**Figure 115: Shear Stress in SYN-BEND-B4 During Three Point Bend-to-Failure Tests**

| Compression Stresses Sustained in 3- Point Bend Specimens | | | |
|---|---|---|---|
| **Specimen No.** | **Specimen Configuration** | **Condition** | **Max Compression Stress at Failure (psi)** |
| SYN-BEND-B1 | Doubler Repair | No Conditioning | 79,000 |
| SYN-BEND-B2 | Doubler Repair | No Conditioning | 83,600 |
| SYN-BEND-B3 | Doubler Repair | No Conditioning | 73,900 |
| SYN-BEND-B4 | Doubler Repair | Hot-Wet | 58,700 |
| SYN-BEND-B5 | Doubler Repair | Hot-Wet | 64,800 |
| SYN-BEND-B6 | Doubler Repair | Hot-Wet | 61,300 |

**Table 14: Compression Stress Levels in Composite Doubler Laminates Produced by Bending/Compression Tests**

**This Page Intentionally Left Blank**

## 5.0 NONDESTRUCTIVE INSPECTION OF COMPOSITE DOUBLER REPAIRS ON CARBON STEEL STRUCTURES

The two main potential causes of structural failure in composite doubler installations are cracks in the steel, and disbonds at the adhesive layer, and delaminations between adjacent plies in the doubler. When disbonds or delaminations occur, they may lead to joint failures. By their nature, they occur at an interface and are, therefore, always hidden. A combination of fatigue loads and other environmental weathering effects can combine to initiate these types of flaws. Periodic inspections of the composite doubler for disbonds and delaminations (from fabrication, installation, fatigue, or impact damage) is essential to assuring the successful operation of the doubler over time. The interactions at the bond interface are extremely complex, with the result that the strength of the bond is difficult to predict or measure. Although extensive testing has shown this repair method to be extremely damage tolerant, disbonds in critical regions may compromise the integrity of the structural assembly. Therefore, it is necessary to detect all areas of disbonding or delamination, as directed by DTA, before joint failures can occur. The overall goals of the NDI effort was to: 1) utilize suitable NDI techniques to detect cracks in the parent structure, interply delaminations in the doubler, and steel interface disbonds, and 2) generate an inspection method (equipment and procedures) that can be easily deployed by personnel in the field.

### 5.1 Damage Tolerance Assessment and Inspection Intervals

**Establishing Damage Tolerance** - Damage tolerance is the ability of a structure to sustain damage, without catastrophic failure, until such time that the component can be repaired or replaced. In aircraft for example, the U.S. Federal Aviation Requirements specify that the residual strength shall not fall below limit load, $P_L$, which is the load anticipated to occur once in the life of an aircraft. This establishes the minimum permissible residual strength $\sigma_P = \sigma_{L.}$ To varying degrees, the strength of composite doublers are affected by crack, disbond, and delamination flaws. The residual strength as a function of flaw size can be calculated using fracture mechanics concepts. Figure 116 shows a sample residual strength diagram. The residual strength curve is used to relate this minimum permissible residual strength, $\sigma_P$, to a maximum permissible flaw size $a_P$. In the case of the Syncrude structures, field inspection data indicates that many of the structures sited in this report can operate with cracks that are several inches in length. As a result, the goal of this NDI effort was conservatively set to detect cracks of 1" in length which and are concealed beneath a composite doubler that may be as thick as 72 plies (0.40" thick). With the damage tolerance assessment presented in section 4.0, the goal for disbond/delamination detection in the composite doublers was set at a size of 0.5" in diameter.

A fracture control plan is needed to safely address any possible flaws which may develop in a structure. Nondestructive inspection is the tool used to implement the fracture control plan. Once the maximum permissible flaw size is determined, the additional information needed to properly apply NDI is the flaw growth versus time or number of cycles. Figure 117 contains a flaw growth curve. The first item of note is the total time, or cycles, required to reach $a_P$. A second parameter of note is $a_d$ which is the minimum detectable flaw size. A flaw smaller than $a_d$ would likely be undetected and thus, inspections performed in the time frame prior to $n_d$

would be of little value. The time, or number of cycles, associated with the bounding parameters $a_d$ and $a_P$ is set forth by the flaw growth curve and establishes *H(inspection)*. Safety is maintained by providing at least two inspections during *H(inspection)* to ensure flaw detection between $a_d$ and $a_P$ .

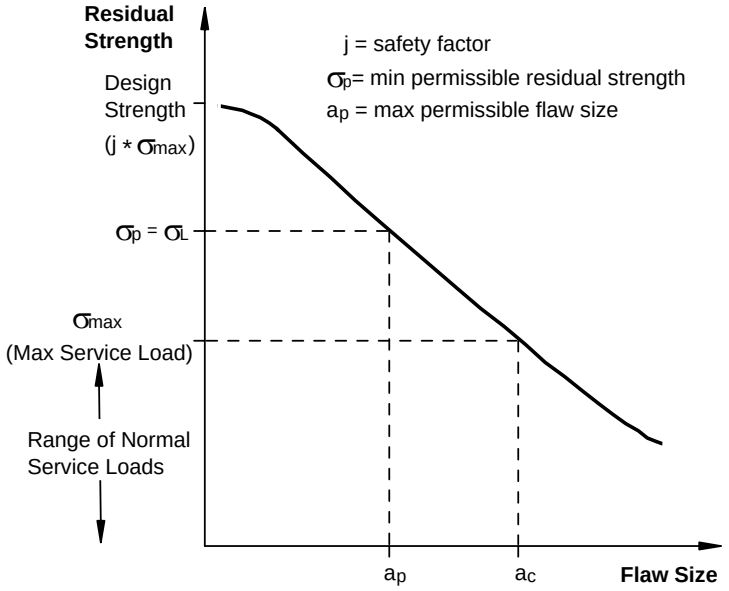


**Figure 116: Residual Strength Curve**

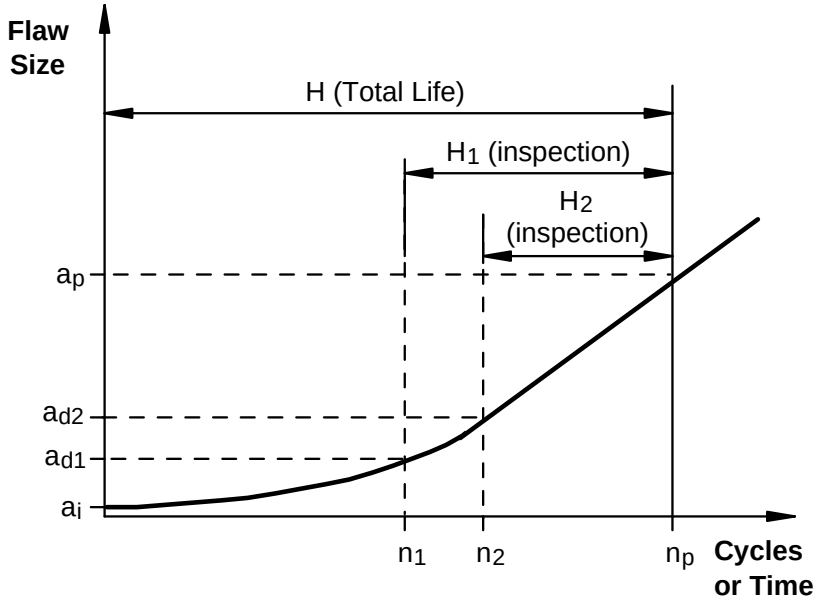


**Figure 117: Crack Growth Curve Showing Time Available for Fracture Control**

**Inspection Intervals** - An important NDI feature highlighted by Figure 117 is the large effect that NDI sensitivity has on the required inspection interval. Two sample flaw detection levels $a_{d\ (1)}$ and $a_{d\ (2)}$ are shown along with their corresponding intervals $n_{d\ (1)}$ and $n_{d\ (2)}$. Because of the gradual slope of the flaw growth curve in this region, it can be seen that the inspection interval $H_1(inspection)$ can be much larger than $H_2(inspection)$ if NDI can produce just a slightly better flaw detection capability. Since the detectable flaw size provides the basis for the inspection interval, it is essential that quantitative measures of flaw detection are performed for each NDI technique applied to the structure of interest. Such quantitative flaw detection measures are presented in the remainder of Section 5.0

## 5.2 Quality Assurance Coupons to Ensure Proper Surface Preparation

Before moving into routine in-service inspections, it is first necessary to ensure that the initial installation was completed properly. Towards that end, quality assurance testing has been developed for certifying the initial installation. The primary QA test utilizes a witness coupon. The witness coupon is a steel strip that is bonded to the prepared surface alongside the composite doubler. After curing, the witness strip is pried off with a wedge. If the adhesive is found on both the coupon and the steel structure, then the surface preparation is good. The full strength of the adhesive is assured since the failure mode was cohesive failure (fracture) rather than adhesive failure (disbond). Figure 118 depicts this surface preparation QA test and the two potential failure modes.

Nondestructive Inspection - It is now necessary to detect any flaws in the installation. Initially, the status of flaws in the doubler and bondline must be ascertained to accept the installation. Thereafter, the flaw status of the doubler, bondline, and parent material must be periodically measured. Nondestructive inspection provides the last line of defense in this regard. NDI is the only means for determining if the structural integrity of the repair area changes over time.

## 5.3 Inspections for Cracks in Parent Material Beneath Composite Doubler

In addition to the normal difficulties associated with crack detection in steel structures, the added complexity of inspecting through a composite doubler to assess the structure beneath introduces new impediments. The two NDT inspection techniques commonly used for crack detection were assessed in this study: eddy current and X-ray.

### 5.3.1 Eddy Current Inspection

Eddy Current (EC) inspection uses the principles of electromagnetic induction to identify or differentiate structural conditions in conductive metals [26, 27]. In this study, it was applied to numerous bonded composite doubler installations in order to assess the ability of EC to detect cracks in steel plates beneath a composite laminate. The presence of a crack is indicated by changes in the flow of eddy currents in the structure. EC signals are physically monitored using

impedance-plane plots which show the reactive and resistive components of a coil as functions of frequency, conductivity, or permeability.

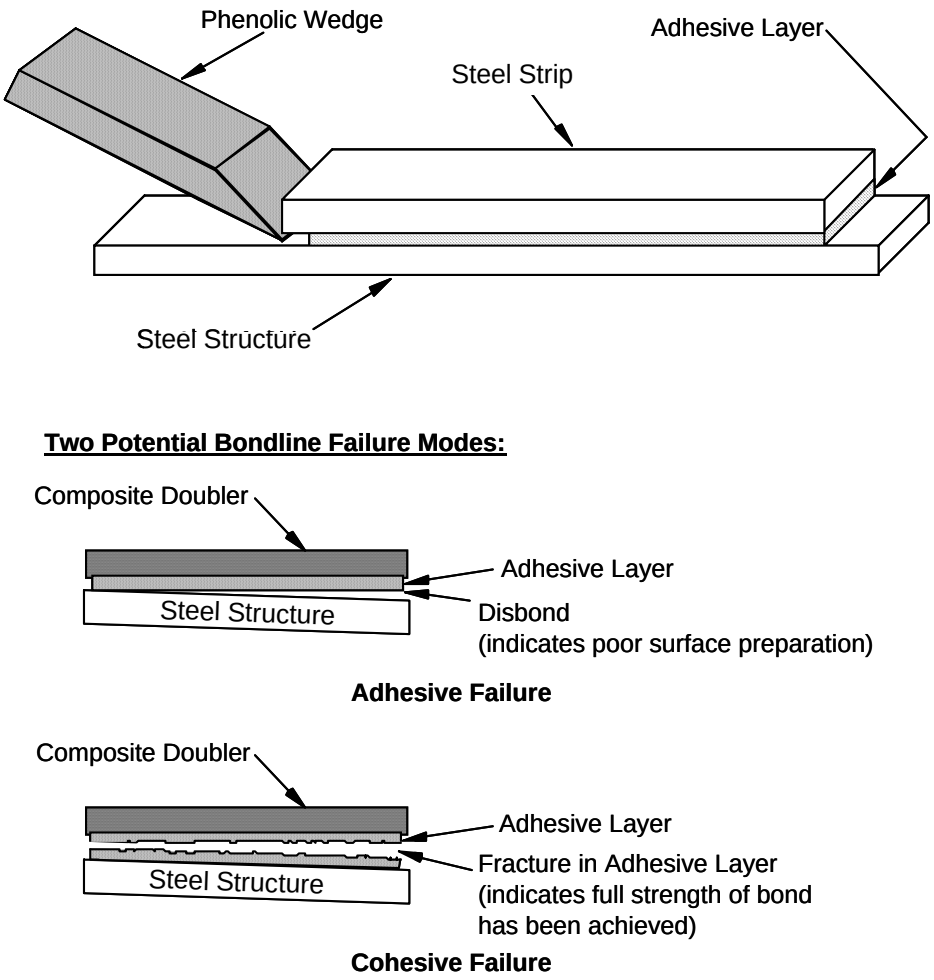


**Figure 118: Quality Assurance Wedge Test for Surface Preparation**

When EC inspections are performed, an electrically conductive material is exposed to an alternating magnetic field that is generated by a coil of wire carrying an alternating current. As a result, eddy currents are induced on and below the surface of the material (see Figure 119). These eddy currents, in turn, generate their own magnetic field which opposes the magnetic field of the test coil. Cracks or thickness changes in the structure being inspected influence the flow of eddy currents and change the impedance of the test coil accordingly. EC instruments record these impedance changes and display them in impedance plane plots to aid the flaw detection process.

The depth of penetration of eddy currents is inversely proportional to the product of magnetic permeability, electrical conductivity, and frequency of the inducing currents. Therefore, eddy current tests are most sensitive to discontinuities on the surface next to the coil, which makes

them very effective for detecting fatigue cracks in the near surface. High frequency eddy current (HFEC) is generally considered 100 kHz and above and is used to detect near-surface flaws. Low frequency eddy current (LFEC) is in the 100 Hz to 10 kHz range and is used to penetrate deeper to detect flaws in underlying structure. As the structure to be penetrated gets thicker, a lower EC operating frequency is required to reach the desired depth. However, the detectable flaw size usually becomes larger as the frequency is lowered. Eddy currents deeper in the material are weaker and lag in phase compared to the currents near the surface. By measuring the phase, it is possible to determine whether the defect is near the surface or at the inner wall. Figure 120 shows an example of an impedance plane display showing phase and amplitudes of EC signals generated by cracks of varying depths.

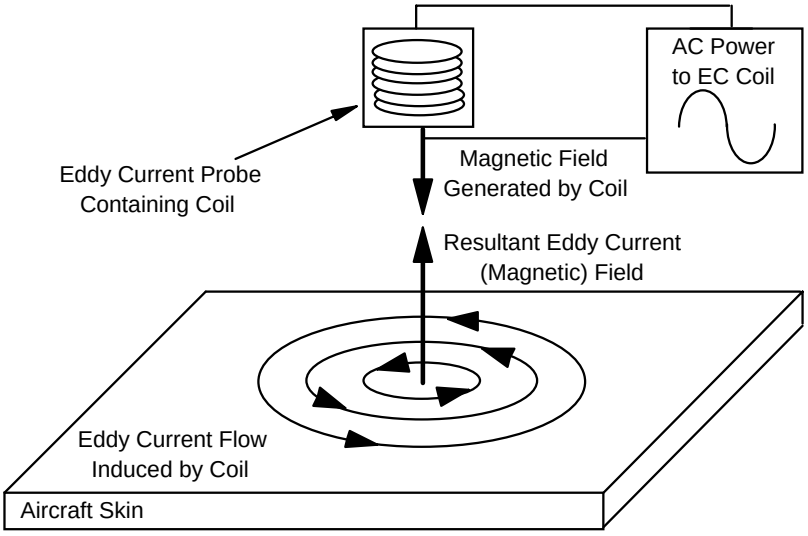


**Figure 119: Induction of Eddy Currents in Conductive Materials**

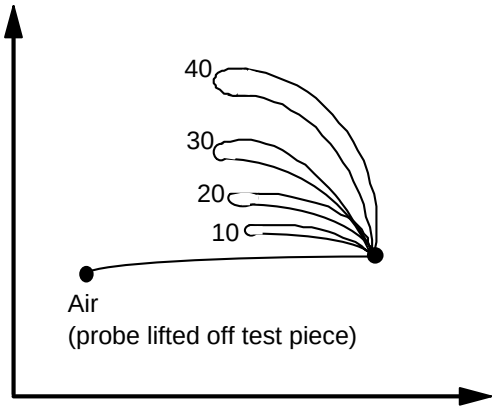


**Figure 120: Impedance Plane Display Showing Signal Traces for Surface Cracks of Different Lengths (shown in mils)**

External surface inspections which may key off visible attributes such as fastener locations (normal origin of fatigue cracks) must now be performed blind since the doubler covers the steel surface. Because eddy currents are created using an electromagnetic induction technique, the inspection method does not require direct electrical contact with the part being inspected. The composite doubler, between the EC transducer and the steel being inspected, does, however, create a lift-off effect which changes the EC signal. This lift-off effect can mask important aspects of flaw detection and must be counteracted by careful equipment set-up, use of suitable calibration standards, and experience in EC signal interpretation. Eddy currents are not uniformly distributed throughout the plate; rather, they are densest at the surface immediately beneath the coil (transducer) and become progressively less dense with increasing distance below the surface. Thus, the inspection sensitivity through composite doublers is decreased by the lift-off effects (equal to thickness of doubler) and associated need to inspect below the surface of the EC transducer. Lower frequency probes can be used to produce a greater depth of EC penetration, however, this is accompanied by a loss in sensitivity versus higher frequency probes. Thus, the thicker the doubler, the greater reduction in crack detection sensitivity. Therefore, EC inspection through composite doublers becomes a balance between signal resolution and the frequency required to inspect beneath a particular laminate.

Structured EC testing was performed in this study in an attempt to quantify EC performance through composite doublers. Both sliding and spot probes were used in this inspection series. Both probes are suited for this type of inspection and have the low frequencies needed to penetrate the doubler layer. Figure 121 shows several of the cracked steel specimens, with and without composite doublers, which were used in this study. Figure 122 shows the Nortec 1000 eddy current device being applied to one of the composite doubler fatigue coupon specimens along with photos of the two EC probes tested.

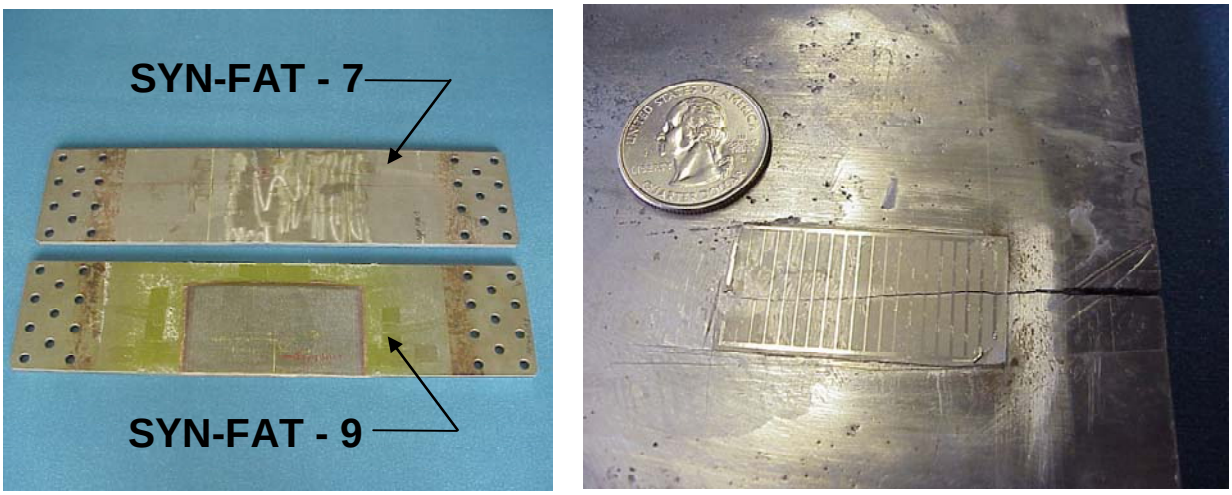


**Figure 121: Panels Used in EC Validation Tests and Typical Fatigue Crack Propagating Through the Crack Gage on the Back of the Specimens**

EC Spot Probe


EC Sliding Probe

**Figure 122: Eddy Current Inspection Set-Up with Nortec 1000 Readout Device Connected to EC Spot probe or EC Sliding Probe**

The first test involved placing the EC probes on a composite repair specimen which contained a fatigue crack under the doubler (SYN-FAT-9). This assessed crack detection through a 24 ply (0.144" thick), non-conductive, composite laminate. Spot probe crack detection occurred ¼" before the probe reached the crack tip. In the case of the sliding probe, crack detection occurred after the crack was under the footprint of the probe. Figure 123 shows representative EC signals generated in cracked structure located beneath the Boron-Epoxy doublers.

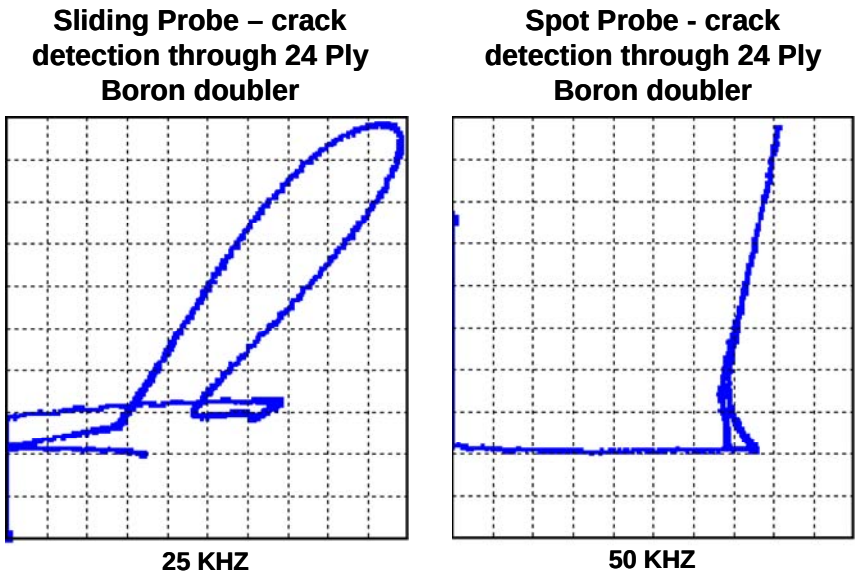


**Figure 123: Large Signals Produced by EC Sliding and EC Spot Probe Indicating Strong Crack Detection Beneath a 24 Ply Composite Doubler**

Figure 124 provides the baseline EC signals associated with no crack in the structure. This is essentially the noise associated with the EC probe, the signal acquisition equipment, and the method used to deploy the transducer. Any deviation from this flat line signal can provide a crack indication. From a reliability standpoint, the desired signal-to-noise ratio is at least 2:1. Comparisons between the signals in Figs. 123 and 124 reveal that the signal-to-noise ratio for crack detection through the 24-ply doublers used in this study is approximately 8:1.

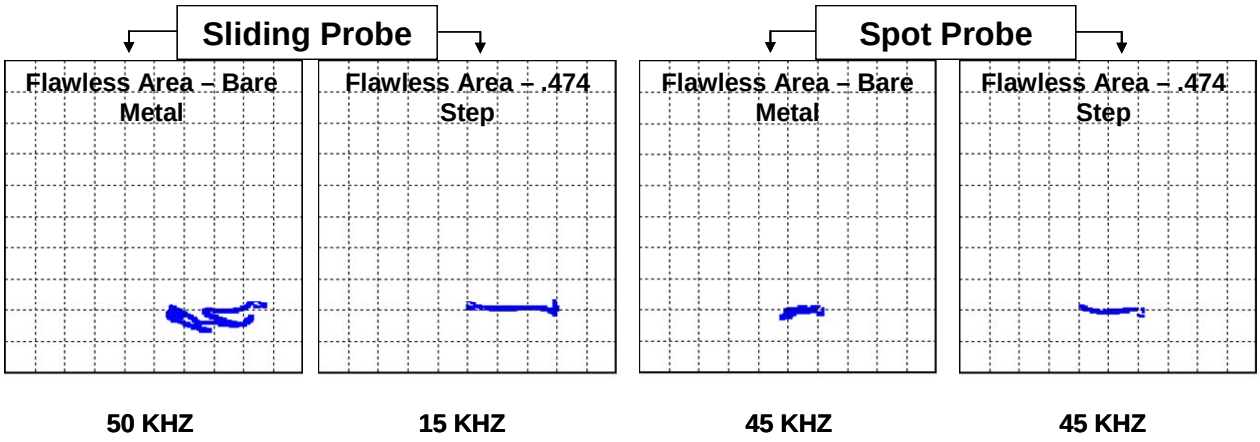


**Figure 124: Signals Produced by EC Sliding and EC Spot Probe When Inspecting an Unflawed Region**

The second test series involved the superposition of a Boron-Epoxy laminate step wedge (see Fig. 125) over a cracked steel structure. The purpose of these tests was to assess crack detection beneath composite doublers of different thicknesses. By placing various step thicknesses of the step wedge over a fatigue crack and studying the eddy current response through this thickness, it was possible to determine any limitations in EC crack detection through ultra-thick composite doublers. For these inspections, the Sliding Probe and Spot Probe were placed on top of the step wedge at each thickness (step thicknesses = 0.016", 0.031", 0.093", 0.143", 0.205", 0.251", 0.307", 0.361", and 0.470"). Then the entire unit (step wedge & probe) was slid towards the crack as shown in Figure 126. Signal characteristics and locations of detection were monitored and documented.

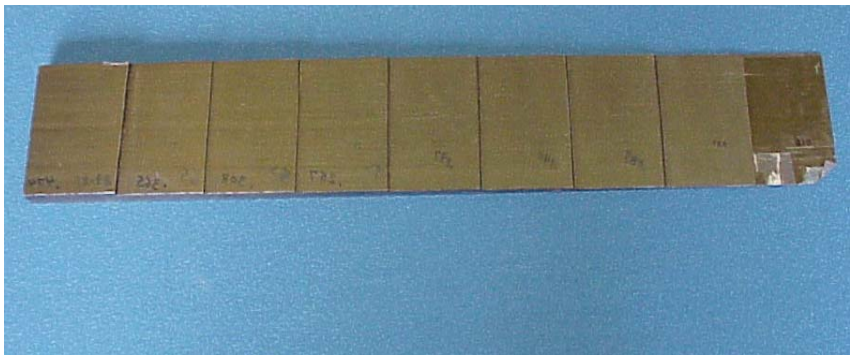


**Figure 125: Boron-Epoxy Laminate Step Wedge Used to Assess Crack Detection Beneath Composite Doublers of Different Thicknesses**

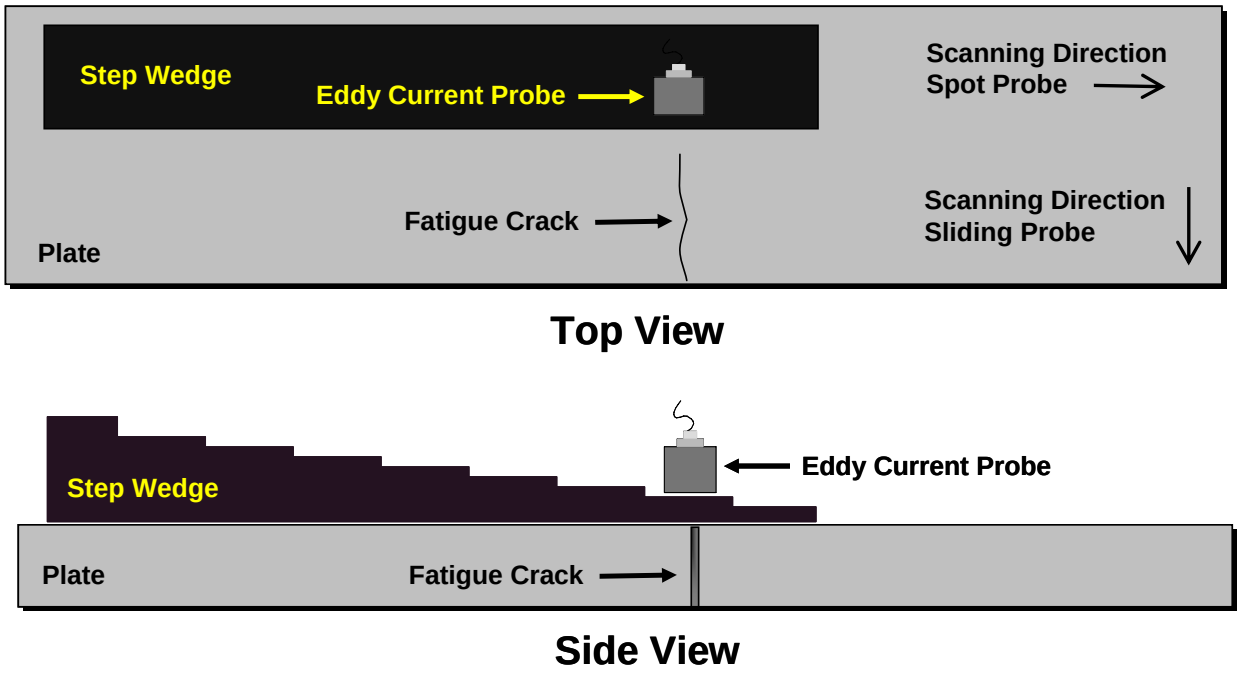


**Figure 126: Inspection with Sliding and Spot Probes Using Step Wedge Over a Cracked Steel Structure**

*It is important to note that because the step wedge was not bonded to the steel plate, highly non-conductive air was located between the wedge and the steel structure. As a result, the signal levels are artificially low. This effect can be quantified by comparing the crack signal from the 0.144" thick bonded doubler (see signal on left side of Figure 123) and to the crack signal from a 0.144" step wedge placed on top of a steel crack (see middle-left signal in Figure 128). For a common gain and doubler thickness, the difference in eddy current signal strength between a bonded and unbonded (air gap) doubler is approximately a factor of two. Thus, the results presented for the step wedge experiments are conservative and the signal-to-noise ratios may be improved by as much as a factor of two for an actual bonded, composite repair installation.*

Figures 127 to 130 show the eddy current signals corresponding to cracks located beneath increasingly thicker composite laminates. The non-conductive composite laminate serves as a lift-off in the eddy current field and produces a reduction in the signal strength. The results shown in Figures 127 and 129 correspond to sliding probe and spot probe inspections through the Boron-Epoxy step wedge placed over the 24-ply doubler. As a result, the thickness (lift-off) of the composite laminate ranges from 27 plies (0.160" th.) to 103 plies (0.618" th.). The results shown in Figures 128 and 130 correspond to sliding probe and spot probe inspections through the step wedge placed over a cracked steel plate with no doubler. As a result, the thickness (lift-off) of the composite laminate for these results ranges from 3 plies (0.016" th.) to 79 plies (0.474" th.). All of the signal plots indicate that crack detection can be reliably achieved through composite doublers. Furthermore, crack detection signals can be obtained through composite doublers in excess of 100 plies and greater than 0.6" thick. For the Syncrude applications identified thus far, it is anticipated that the composite doubler installations will be on the order of 0.3" to 0.5" thick. The eddy current spot probe appears to provide a slightly more repeatable and uniform signal than the sliding probe. The signal-to-noise ratios for the sliding probe ranges from a low of 2:1 to a high of 14:1. The signal-to-noise ratios for the spot probe ranges from a low of 3:1 to a high of 22:1. As discussed above there is some signal loss associated with the placement of the laminate step wedge instead of the more realistic bonding of the laminate. When this unrealistic signal loss is removed, the signal-to-noise ratios for actual composite doublers installations may be twice the values listed here.

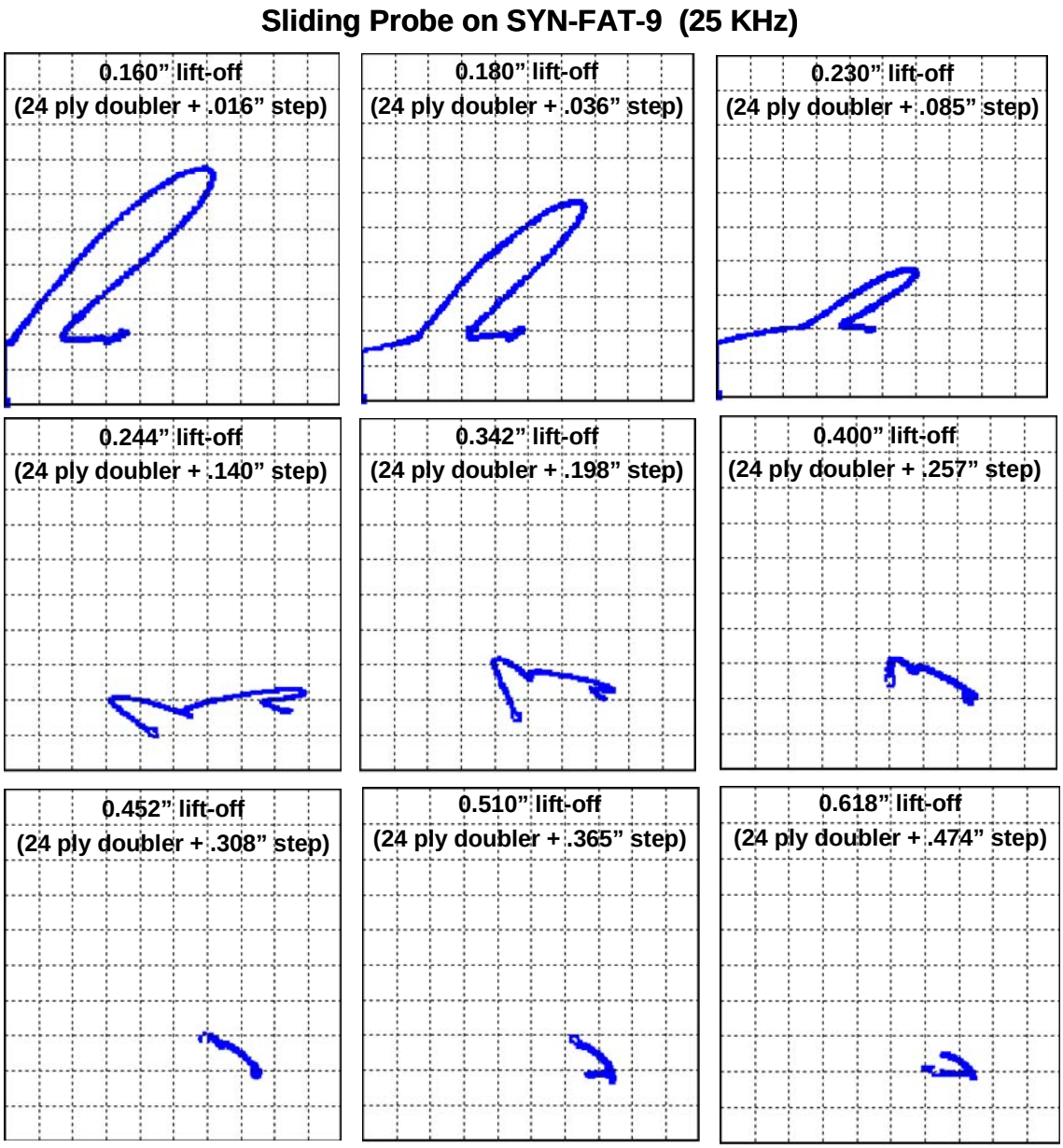


**Figure 127: EC Signals from Sliding Probe Inspection of Composite Repaired Specimen (SYN-FAT-9) with a Fatigue Crack and Step Wedge Placed Over Laminate**

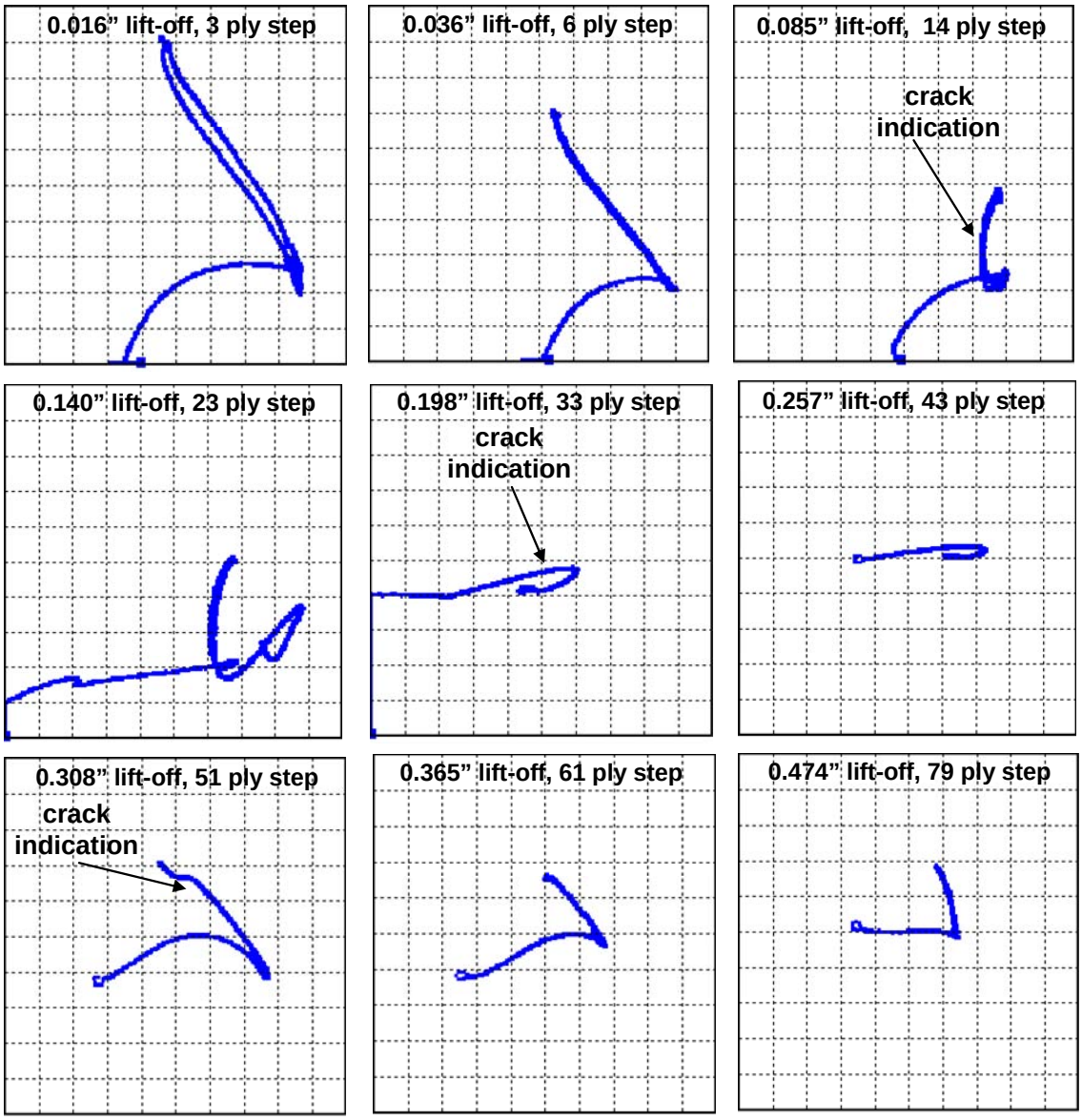


**Figure 128: EC Signals from <u>Sliding Probe</u> Inspection of Unrepaired Specimen (SYN-FAT-7) with a Fatigue Crack and Step Wedge Placed Over Bare Steel Surface**

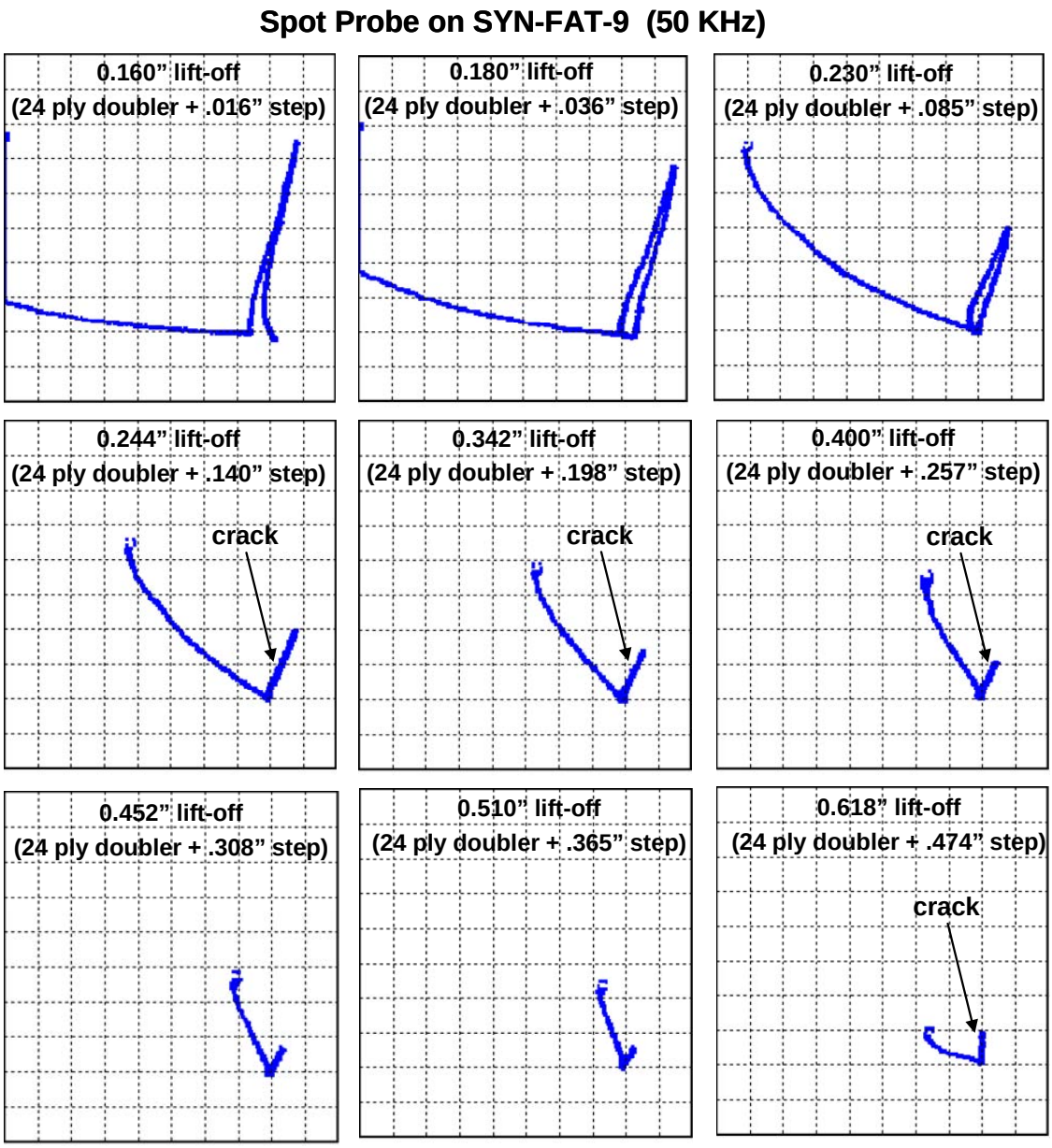


**Figure 129: EC Signals from <u>Spot Probe</u> Inspection of Composite Repaired Specimen (SYN-FAT-9) with a Fatigue Crack and Step Wedge Placed Over Laminate**

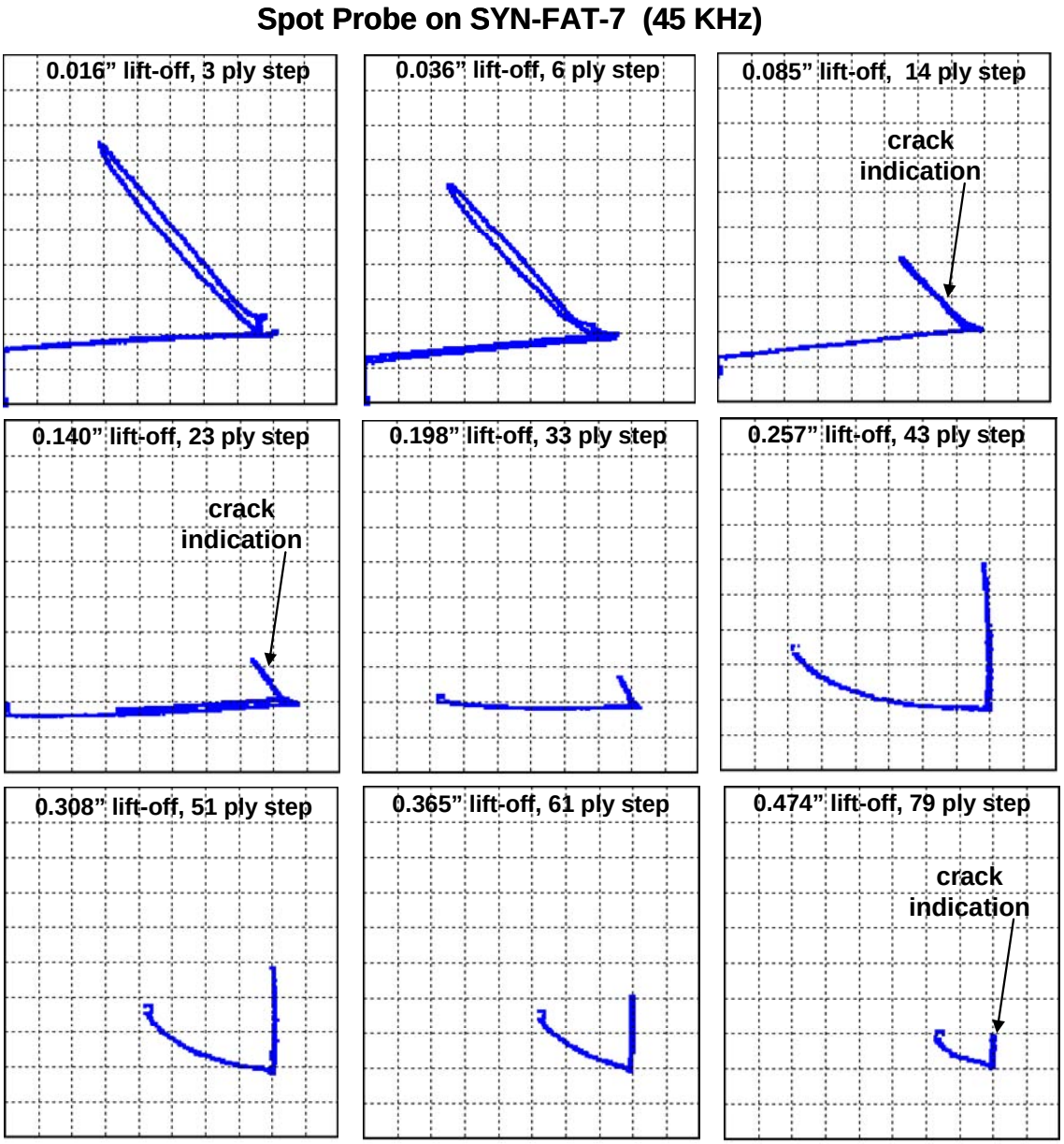


**Figure 130: EC Signals from Spot Probe Inspection of Unrepaired Specimen (SYN-FAT-7) with a Fatigue Crack and Step Wedge Placed Over Bare Steel Surface**

### 5.3.2 X-Ray Inspection

Radiographic inspection is a nondestructive method of inspecting materials for surface and subsurface discontinuities [26]. The method utilizes radiation in the form of either x-rays or gamma rays, which are electromagnetic waves of very short wavelength. The waves penetrate the material and are absorbed depending on the thickness or density of the material being examined. By recording the differences in absorption of the transmitted waves, variations in the material can be detected. Figure 131 shows an application of X-radiography in a field

environment. The most common way of measuring X-ray transmission is with film. After exposure and development, the film will become proportionally darker depending on the amount of radiation which reached the film. Areas that are thinner or lower density will allow more radiation to pass through the part. The greater the radiation transmitted through the part, the darker the film will be.

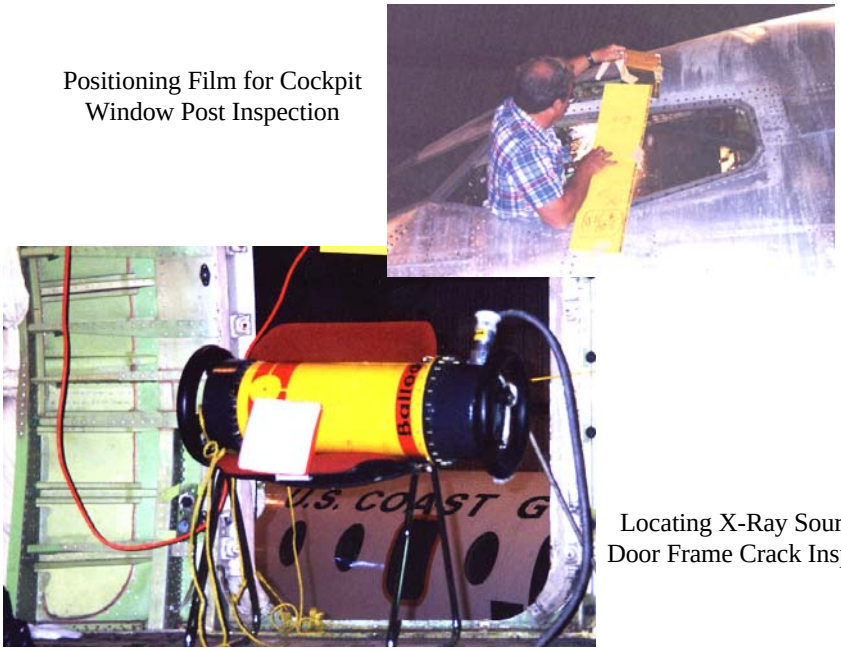


**Figure 131: Aircraft Fuselage Inspection for Cracks Using X-Ray**

*Radiographic Sensitivity (Image Quality)* - Radiographic sensitivity is a function of two factors. The ability to see a density variation in the film, which is "radiographic contrast" and the ability to detect the image outline which is "radiographic definition." Radiographic contrast is the difference in darkness of two areas of a radiograph. If contrast is high, small defects or density changes will be noticeable. Using lower power will result in higher subject contrast. However, lower power requires longer exposure times to obtain the adequate film density. Too low an energy level will not penetrate the part at all.

*Radiographic Definition* - This term is defined as the ability to resolve the defect image on the radiograph. It is affected by the geometric factors of the exposure: size of the radiation source (focal spot size), distance from the target/source to the film, and distance from the part to the film. All of these factors contribute to a loss of geometric sharpness and as geometric sharpness decreases, the ability to see small defects decreases.

*Image Quality Indicators* - Image Quality Indicators (IQI) are used to measure the quality of the exposure and assure that proper sensitivity has been achieved. They measure the definition of the radiograph. By imaging IQI wires of various thicknesses and lengths it is possible to verify the resolution and sensitivity of a radiographic technique/set-up.

*Resolution and Sensitivity - Image Production Through Composite Doublers* - The discussion above provides some background on X-ray inspections and difficulties associated with its use. All of the issues described above exist regardless of whether or not the X-ray exposure takes place through a composite doubler. The primary question to be addressed in this study was: What is the overall effect of a composite doubler on X-ray inspections of structure beneath the doubler? To answer this question, a study was conducted to: 1) demonstrate that composite doublers do not interfere with the ability to perform X-ray inspections for cracks in steel, and 2) identify proper exposure time and power settings to optimize the sensitivity of the X-ray technique when inspecting through thick doublers.

Several fatigue crack specimens were inspected through a 72 ply composite doubler. To form a basis of comparison, X-rays were also taken without the doubler placed over the cracked specimens. The specimens placed beneath the doubler included 1st layer and 2nd layer fatigue crack panels with crack lengths ranging from 0.05" to 1.0". Radiography was found to be a very effective inspection method to interrogate the interior of the parent material covered by a composite doubler. This technique provides the advantage of a permanent film record. To increase the contrast on the film, the X-ray inspection was performed at low kilovoltage (80 kV). Test results showed the ability to detect cracks less than 1" in length. Fatigue cracks on the order of 0.38" in length were found under 0.41" thick (72 ply) Boron-Epoxy doublers. A sample X-ray result of a crack imaged through a 72 ply composite doubler is shown in Figure 132. [Note that significant resolution is lost in translating the X-ray film to a black and white graphic.]

Comparisons with X-rays taken without composite doublers revealed that while the doubler may darken the X-ray image slightly it does not impede the X-ray inspection. Power and exposure times were adjusted in order to restore the desired contract and maintain the specified film density of between 2 and 3. The initial set-up (80 kV, 12 mA, 6 inch source-to-film-distance and 30 second exposure time) on medium speed film produced a film density of 0.98. Increasing the exposure time to 90 seconds produced a film density of 2.64. Image Quality Indicators (IQI), inserted into the field of view, verified the resolution and sensitivity of the radiographic technique. IQI lines with widths of 0.010" and dots with diameters of 0.10" were clearly imaged on the X-ray film. These results showed that X-ray inspections are as effective as before a doubler is installed.

*X-ray Results Summary* - The X-ray tests performed in this study determined that there are no additional impediments brought on by the presence of composite doublers. X-ray inspections were able to achieve high levels of resolution when inspecting through thick composite doublers and the films were very comparable with films acquired on similar structures without doublers. All difficulties associated with X-ray inspections - shadowing from substructure elements, accessibility, and safety issues - are the same as in structures without composite doublers.

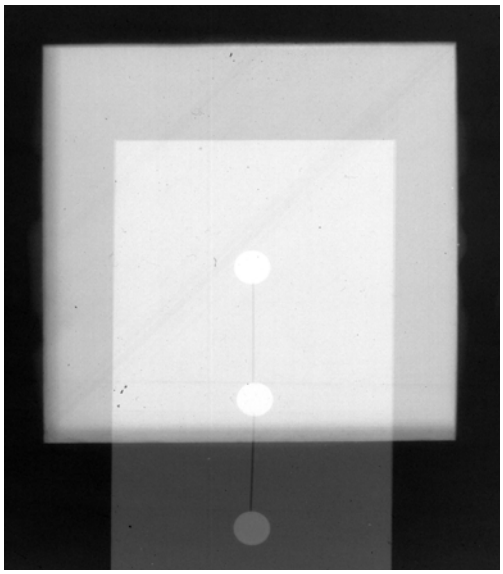

**Figure 132: Sample X-Ray Image of a Cracked Structure Beneath a 72 Ply Composite Doubler**

## 5.4 Nondestructive Inspection Methods for Patch and Bond Integrity

### 5.4.1 Pulse-Echo Ultrasonic Inspection

Ultrasonic (UT) inspection is a nondestructive method in which beams of high frequency sound waves are introduced into materials for the detection of surface and subsurface flaws in the material. The sound waves, normally at frequencies between 0.1 and 25 MHz, travel through the material with some attendant loss of energy (attenuation) and are reflected at interfaces. The reflected beam is displayed and then analyzed to define the presence and location of flaws. The degree of reflection depends largely on the physical state of the materials forming the interface. Cracks, delaminations, shrinkage cavities, pores, disbonds, and other discontinuities that produce reflective interfaces can be detected. Complete reflection, partial reflection, scattering, or other detectable effect on the ultrasonic waves can be used as the basis of flaw detection. In addition to wave reflection, other variations in the wave which can be monitored include: time of transit through the test piece, attenuation, and features of the spectral response [27-28].

The principal advantages of UT inspection as compared to other NDI techniques are: 1) superior penetrating power for detection of deep flaws, 2) high sensitivity permitting the detection of extremely small flaws, 3) accuracy in determining size and position of flaws, 4) only one surface needs to be accessible, and 5) portability.

In UT pulse-echo inspections, short bursts of ultrasonic energy are interjected into a test piece at regular intervals of time. In most pulse-echo systems, a single transducer acts alternately as the sending and receiving transducer. The mechanical vibration (ultrasound) is introduced into a test

piece through a couplant and travels by wave motion through the test piece at the velocity of sound, which depends on the material. If the pulses encounter a reflecting surface, some or all of the energy is reflected and monitored by the transducer. The reflected beam, or echo, can be created by any normal (e.g. in multi-layered structures) or abnormal (flaw) interface. Figure 133 is a schematic of the pulse-echo technique and the interaction of UT waves with various interfaces within a structure. Sometimes it is advantageous to use separate sending and receiving transducers for pulse-echo inspection. The term pitch-catch is often used in connection with separate sending and receiving transducers.

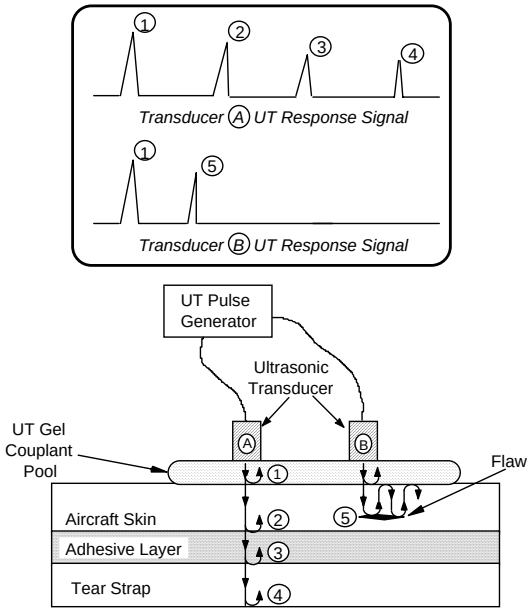


**Figure 133: Schematic of Pulse-Echo Ultrasonic Inspection and Reflection of UT Waves at Assorted Interfaces**

A-Scan Mode - In conventional Pulse-Echo Ultrasonics (PE UT), pulses of high frequency sound waves are introduced into a structure being inspected. A-Scan signals represent the response of the stress waves, in amplitude and time, as they travel through the material. As the waves interact with defects or flaw interfaces within the solid and portions of the pulse's energy are reflected back to the transducer, the flaws are detected, amplified and displayed on a CRT screen. The interaction of the ultrasonic waves with defects and the resulting time vs. amplitude signal produced on the CRT depends on the wave mode, its frequency and the material properties of the structure. Flaw size can be estimated by comparing the amplitude of a discontinuity signal with that of a signal from a discontinuity of known size and shape. Flaw location (depth) is determined from the position of the flaw echo along a calibrated time base. The mechanical vibration (ultrasound) is introduced into the specimen through a couplant and travels by wave motion through the specimen at the velocity of sound. If the pulses encounter a reflecting surface, some or all of the energy is reflected and monitored by the transducer. The reflected beam, or echo, can be created by any normal or abnormal (flaw) interface. Cracks, delaminations, shrinkage cavities, pores, disbonds, and other discontinuities that produce

reflective interfaces can be detected. Complete reflection, partial reflection, scattering, or other detectable effects on the ultrasonic waves can be used as the basis of flaw detection.

Figure 134 and 135 show a Quantum ultrasonic device being used to perform a pitch-catch UT inspection (pulse-echo mode) of a composite doubler bonded to a carbon steel structure. In most pulse-echo systems, a single transducer acts alternately as the sending and receiving transducer. In the pitch-catch inspection mode deployed for this inspection one transducer transmits the UT wave and a second, remotely positioned transducer receives the signal after it travels through the materials being inspected. Figure 136 contains a schematic showing the pitch-catch inspection method and the UT wave travel within the structure during this inspection. During testing, the transmitting transducer was placed on top of the composite doubler and the receiving transducer was placed on top of the parent steel material. If the adhesive bond between the two articles is intact, the ultrasonic signal will pass unobstructed to the receiving transducer.

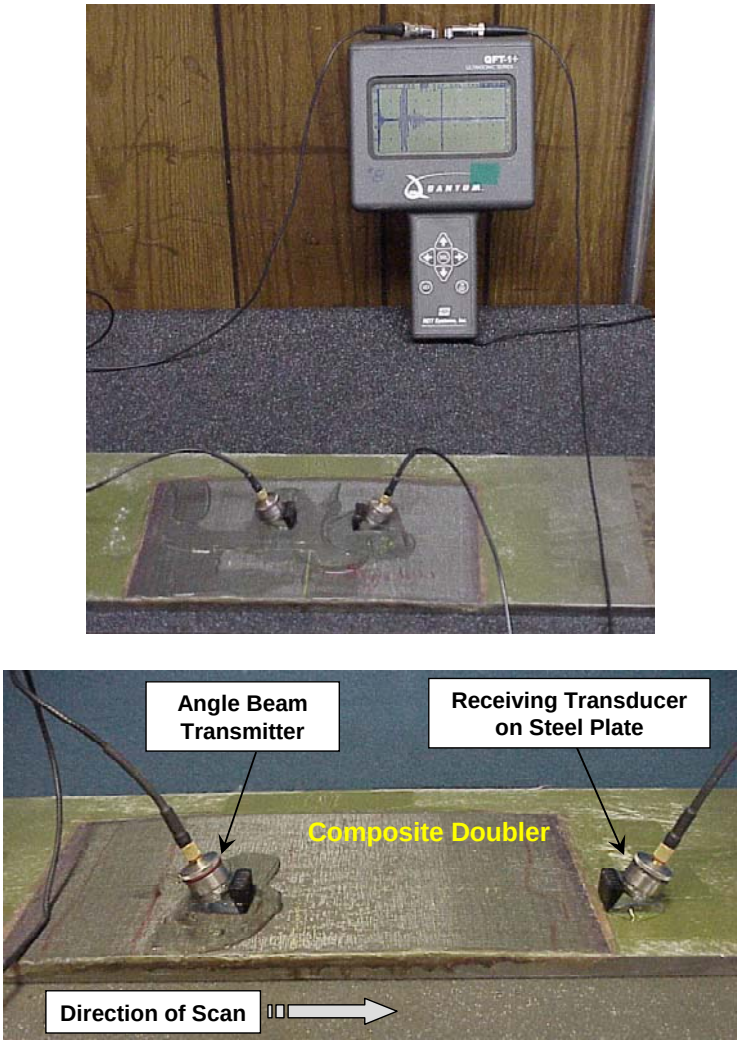


**Figure 134: Pulse-Echo Ultrasonic Inspection of a Steel Structure with a Composite Doubler Installed**

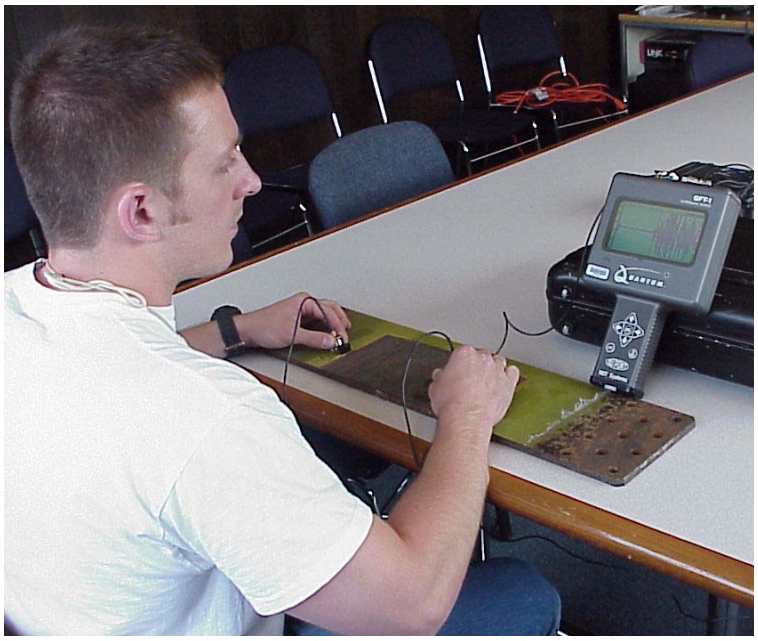

**Figure 135: Inspector Deploying Pulse-Echo Inspection on Composite Doubler Repair**

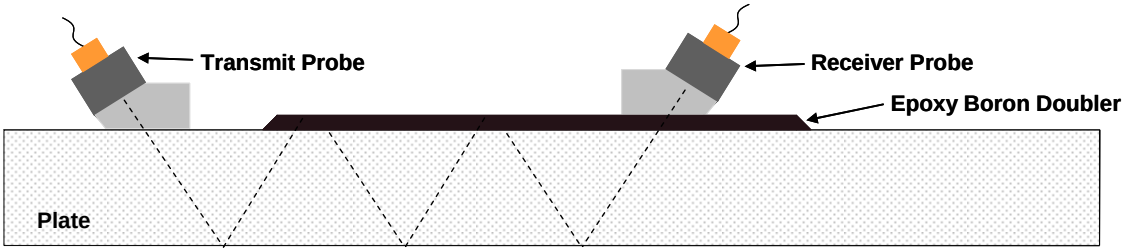


**Figure 136: Schematic of Ultrasonic Wave Travel in a Pulse Echo, Pitch-Catch Inspection of a Composite Repair Installation**

Figure 137 contains a series of A-scan signals produced by the pulse-echo inspection of a doubler specimen that contained intentional, engineered flaws at discrete locations. Changes in the A-Scan signal (i.e. lack of reflected signal from steel back wall), caused by the presence of the disbond or interply delamination, are clearly visible. Key portions of the signal in Figure 137 are identified to highlight how the A-Scan can be used to detect disbonds and delaminations. The primary items of note are: 1) the unique signature of the amplitude vs. time waveform which allows the user to ascertain the transmission of the ultrasonic pulse through various layers of the test article and which indicate a good bond, and 2) the absence of signature waveforms indicating a disbond. The thickness of the composite doubler does not significantly affect the transmission of the ultrasonic signal so similar flaw detection signals can be produced regardless of the doubler thickness. Another important consideration is that this technique can be deployed quickly. A one square foot region can be inspection in around 15 minutes.

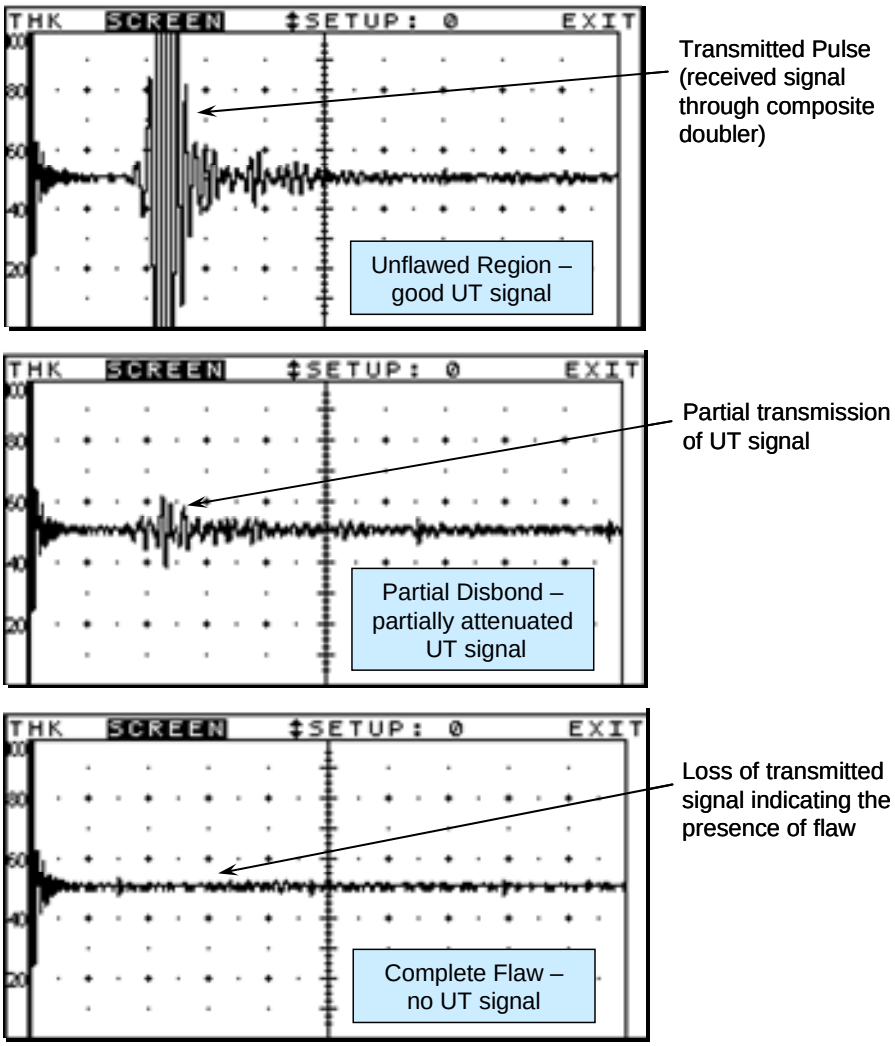


**Figure 137: A-Scan Waveforms from Bonded and Disbonded Portions of a Composite Doubler Repair**

Validation of Pulse-Echo NDI Technique for Disbond and Delamination Detection: Probability of Detection Study - In order to make a valid measurement of the flaw detection capabilities of the pulse-echo ultrasonic inspection method, a Probability of Detection (PoD) study was performed. Flaw detection performance was measured through blind experiments where inspectors had no knowledge of the specimen flaw profiles. A statistically relevant specimen set was used to provide: 1) opportunities for flaw calls over the full range of applicable flaw sizes and locations, and 2) sufficient unflawed sites to assess the Probability of False Alarm (PoFA). Flaw sizes in the test specimens ranged from 0.75" diameter to 0.375" diameter. The results are as follows: 98% of the flaws at or above 0.5" diameter were found. Seventy percent of the flaws less than 0.5" diameter were also found. The NDI techniques worked well with flaw detection including disbond and delamination flaws as small as 1/8" diameter. Damage tolerance thresholds will conservatively require the detection 1" diameter disbond and delamination flaws around the perimeter of the doublers. The inspection intervals for this program are set up to

allow for at least two inspections and two opportunities to find a flaw before it reaches the maximum allowable size. The outcome of this scenario can be simulated by combining the results from two different inspectors. Such a combination produced the following results: 100% detection of all flaws, even those smaller than the required size, and zero false calls. Overall, the test series described above clearly demonstrated that disbond and delamination flaws on the order of 0.5" to 1.0" in diameter can be reliably detected through thick composite doublers.

C-Scan Mode: Use of Scanning Technology - Disbond and delamination detection can be also be achieved by taking the A-Scan signals and transforming them into a single C-Scan image of the part being inspected. C-Scan technology uses information from single point A-Scan waveforms to produce an area mapping of the inspection surface. These 2-D images are produced by digitizing point-by-point signal variations of an interrogating sensor while it is scanned over a surface. C-Scan area views provide the inspector with easier-to-use and more reliable data with which to recognize flaw patterns. This format provides a quantitative display of signal amplitudes or time-of-flight data obtained over an area. The X-Y position of flaws can be mapped and time-of-flight data can be converted and displayed by image processing-equipment to provide an indication of flaw depth. A variety of PC-based manual and automated scanning devices can provide position information with digitized ultrasonic signals. Specific emphasis can be placed on portions of the UT signal - and highlighted in the color-mapped C-Scan - based on user specified amplitude gates, time-of-flight values and signal waveforms. When addressing scanner system capabilities and limitations, key performance factors include: cost (approximately 15 times the cost of a hand-held UT device), design, portability, deployment, articulation and access to enclosed areas, speed of coverage, accuracy, usability (human factors), and computer hardware/software.

Figure 138 shows a C-scan image (based on amplitude) of a thick composite doubler with engineered flaws. The test specimen schematic is also shown to provide doubler lay-up information and the embedded flaws profile. A three-dimensional contour plot is also shown to demonstrate another means of displaying the data and interpreting the results. Disbond and delamination flaws are revealed by continuous and distinct signal loss areas which, depending on the color palette chosen, are either relatively bright or dark compared to the surrounding colors.

The post-fatigue composite repair specimens were inspected using the pulse-echo, pitch-catch method described above. The fatigue-induced fracture of the adhesive was identified by noting the onset of UT signal drop-out. Figure 139 shows the disbond region (actually, adhesive fracture region) that was traced out by the hand-deployed inspection alongside a C-scan image produced by an automated scanner device. Note the similarity in the size and shape of the flaw regions.

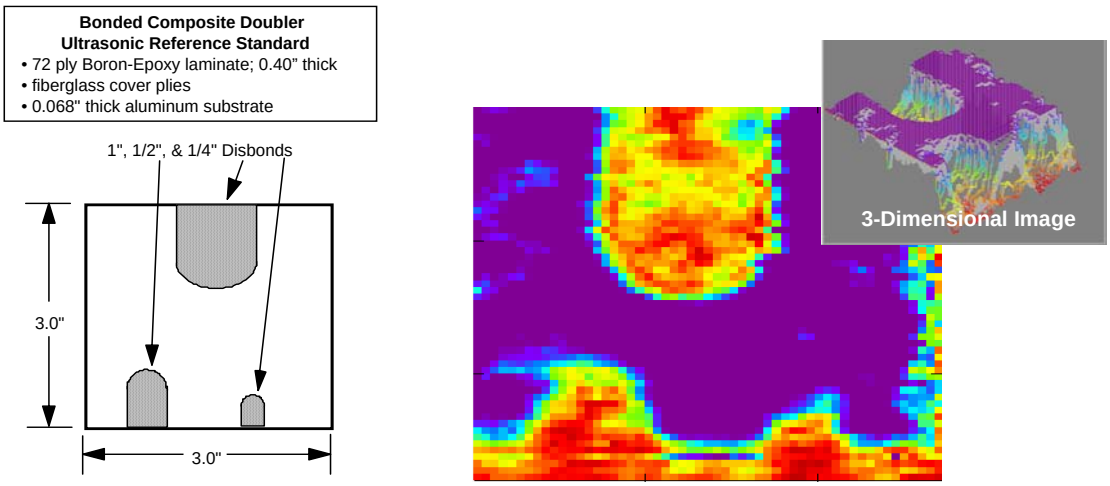


**Figure 138: C-Scan Image Produced by Selective Gating on the Amplitude of All Signals Received by the Transducer**

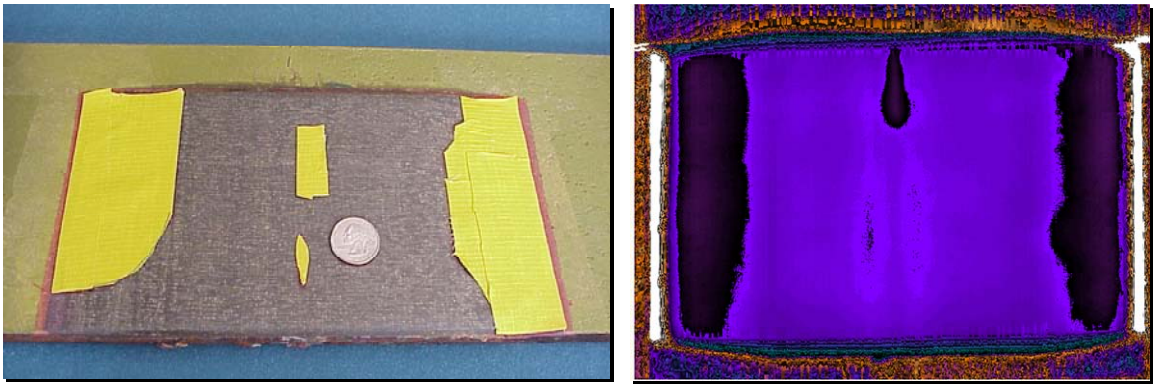

**Figure 139: Comparison of Hand-Deployed Pitch-Catch UT Inspection with Data Produced by an Automated Scanning Device**

### 5.4.2 Thermographic Inspection

Thermography is a nondestructive inspection method that uses thermal gradients to analyze physical characteristics of a structure, such as internal defects. This is done by converting a thermal gradient into a visible image using a thermally sensitive detector such as an infrared camera or thermally sensitive film materials. The temperature distribution on a structure can be measured optically by the radiation that it produces at infrared wavelengths. Many defects affect the thermal properties of materials. Examples are corrosion, disbonds, cracks, impact damage, panel thinning, and fluid ingress into composite or honeycomb materials. By the judicious application of external heat sources, these defects can be detected by an appropriate infrared survey. In this composite doubler study, a turn-key thermography inspection system, the Thermal Wave Imager (TWI), was used to assess the merits of thermography to detect disbonds and delaminations in composite doublers.

Thermal wave imaging is accomplished using high-power flash lamps, an infrared (IR) video camera, and image processing hardware and software, all of which are controlled by a personal computer. The flashlamps put out a short, high-power pulse of light, which raises the surface temperature of the structure approximately ten degrees when it is absorbed by the surface. This temperature pulse propagates into the material as a thermal wave and gets reflected by any defects which may be present in the material. The resulting temperature distribution is then recorded by the IR camera and displayed on the computer monitor. In practice, the computer actually obtains several images at progressively later times after each flash. This method is particularly useful for imaging and determining the depths of disbonds and delaminations in Boron-Epoxy repair doublers. A photograph of the Thermal Wave Imaging System being applied to an aircraft inspection is shown in Figure 140.

Results from Composite Doubler Inspections - Following are results obtained from Thermal Wave Imaging inspections on composite doubler installations which contain engineered flaws. Figure 141 shows a schematic of a composite doubler installed on a metal fatigue coupon. The schematic shows the disbond and crack flaws that were placed in the parent plate and composite doubler installation. The series of images produced at different times during the TWI inspection of this test specimen are shown in Figure 142.

The early time images following the flash clearly resolve the ply drop-off at the edges of composite patch. Beginning at around 0.68 sec, intentionally placed disbonds between the patch and the metal at the left and right edges (where the patch is thinnest) begin to appear. As time progresses, these disbonds begin to show in thicker and thicker layers of the patch. Between 4 and 8 seconds it is possible to see the circular disbond which was implanted over the crack tip and a "tail" extending downward along the induced fatigue crack. The circular disbond is located 13 plies deep in the doubler installation. The disbond tail is also located between the 13 ply doubler and the skin and is associated with a cohesive fracture of the adhesive layer immediately adjacent to the crack growth.

TWI was applied to another Boron-Epoxy doubler which was installed on a DC-9 fuselage section in the AANC hangar. Figure 143 shows a schematic of the 10 ply doubler installation which identifies the size, shape, and location of the embedded flaws. The resultant sequence of images produced by a TWI inspection is shown in Figure 144.


**(a) Close-Up View of TWI Equipment**

**(b) Application of Thermography on 747 Aircraft**

**Figure 140: Thermal Wave Imaging System Inspecting an Aircraft**

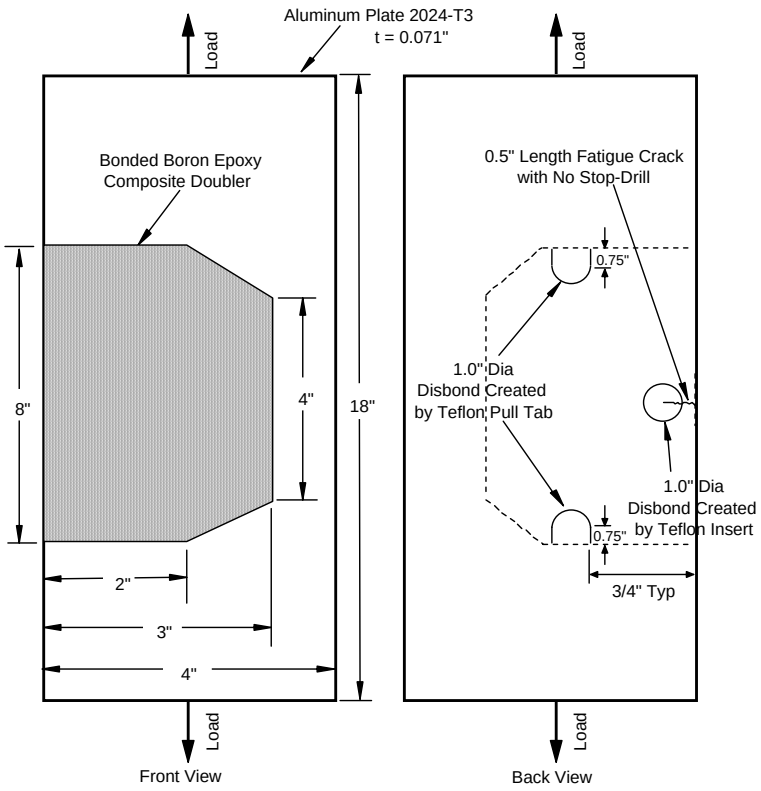


**Figure 141: Composite Doubler Damage Tolerance Test Coupon with Engineered Flaws**

The features seen at early times are defects closest to the outside surface of the patch (note appearance of flaws #1 and #2 in the first few frames). The disbonds, located at the base of the doubler, and the deeper delaminations appear in the later frames corresponding to their delayed effect on the thermal field. All six embedded flaws were identified in the TWI images and flaws smaller than 0.5" in diameter could be detected. Another item of note is that the flaws around the perimeter of the doubler, at its thinnest region, are clearly imaged and do not induce the imaging difficulties.

The advantages of the thermography inspection method include: 1) thermography can be performed without physical contact with the surface, 2) single images can include relatively large areas (1-2 $ft^2$) allowing for rapid inspections of large surface areas, and 3) two-dimensional image of the inspected surface helps the operator visualize the location and extent of any defect. The primary disadvantages of thermography are: 1) it is often necessary to apply a high-emissivity coating during inspections to obtain an acceptable image; steps have been taken to minimize the labor time associated with this task, 2) damage to layers deep within a structure is more difficult to detect than damage in surface layers because the larger mass of material tends to dissipate the applied heat energy; preliminary experiments have shown that TWI can inspect doublers up to 40 or 50 plies (0.25" to 0.30") thick. This latter item, coupled with the cost of a TWI system (over $100K), makes the pulse-echo ultrasonic inspection method a better option for these Syncrude repairs.

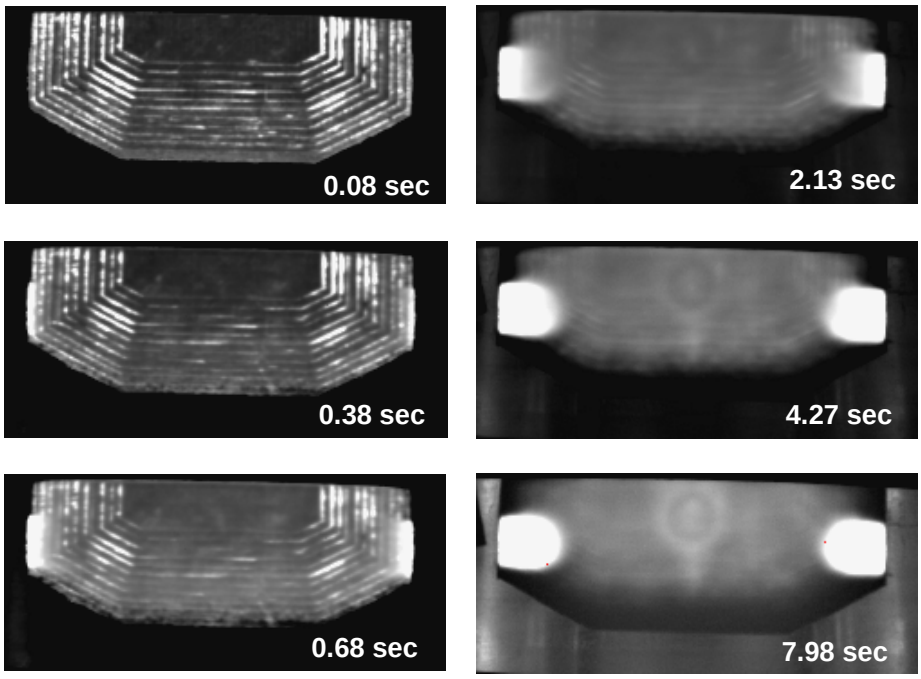


**Figure 142: Sequence of Thermal Wave Images of Composite Doubler Specimen**

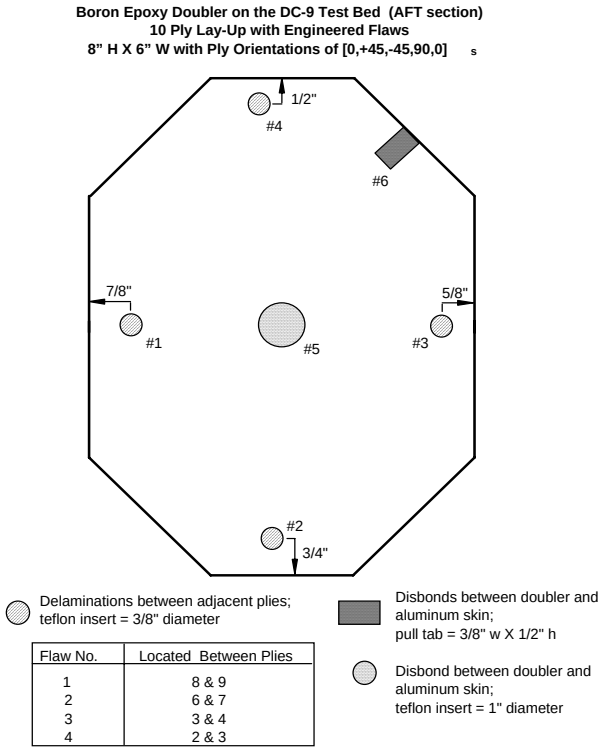


| Flaw No. | Located Between Plies |
|---|---|
| 1 | 8 & 9 |
| 2 | 6 & 7 |
| 3 | 3 & 4 |
| 4 | 2 & 3 |

**Figure 143: Composite Doubler Installation on DC-9 Testbed**

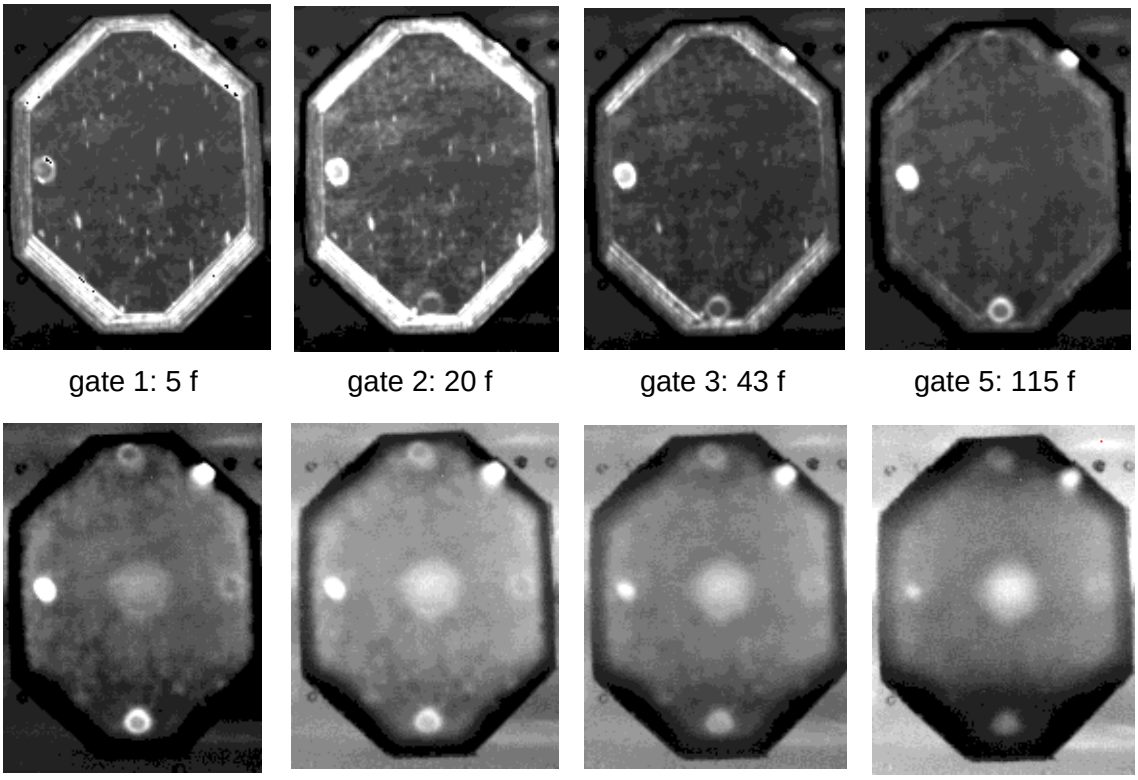


frame time ("f") = 1/60 of a second

**Figure 144: Sequence of Thermal Wave Images from DC-9 Composite Doubler Inspection**

## 6.0 GENERAL ISSUES LEADING TO FIELD REPAIRS

The work described in this report represents the culmination of Phase I of this study: Composite Doubler Technology Viability Assessment. The technology viability tasks included:

1. Identification of Repair Applications
2. Load Spectra Monitoring on Candidate Structure(s)
3. Development of Installation Process for Carbon Steel Structure
4. Generalized Testing: Doubler Performance Assessment in the Laboratory
5. Demonstration Repair Installation Including Heat Source/Sink Evaluation
6. Fabrication and Installation Procedures
7. Inspection Procedures
8. Technology Transfer Activities.

### 6.1 Field Installation and Monitoring of a Composite Doubler Repair

The work outlined above and presented in this report successfully established the installation process and the capability of composite doublers to provide long-term repairs for thick steel structures. The next stage of this work will result in the installation of a field repair. This repair may be preceded by some full-scale testing on an actual Syncrude structure. Alternatively, the data presented in this report may be deemed sufficient to move this technology into the field immediately. In addition, finite element modeling activities, to be undertaken jointly with University of Alberta personnel, have been planned.

In order to assess the installation process alone and to begin accumulating field performance data, a "decal" composite repair could be installed. The structure under this doubler would not contain any flaws so that the composite repair approach could be evaluated in a fail-safe manner. Regardless of the status of the parent structure, any field installation should be accompanied by strain gages to monitor the response of the composite laminate and surrounding steel. Duplicate strain gage sets could be applied to a structure with a composite repair and a similar, unrepaired structure. In this manner, it is possible to infer the performance of the composite doubler repair based on the reduction in the stress field.

### 6.2 Repair Considerations for Syncrude Applications

Following is a description of some issues that will be considered and some follow-on tasks that may be pursued to produce the ultimate goal of a composite repair installation on an operating Syncrude structure. Some additional candidate repair applications are shown in Figure 145.

The items listed below can be pursued to improve and optimize the composite doubler repair process. Completion of these activities is not essential to moving composite repairs to field installations. Consider that the more sophisticated debulk processes and B-stage cure procedures listed below were not used to produce the performance results described in this report.

- Debulk Process – Normally, the doubler laminate is debulked at every 4-6 plies of the lay-up process by using a vacuum bag (approx. 12 psi pressure). The number of plies in the Syncrude doublers will be in the 55-70 range so a global, high-pressure debulk process may be beneficial. It may be possible to improve the debulk process by using a conformable, rubber press that can distribute greater pressure loads over the laminate. Use of an Autoclave would achieve the same end but one is not available at the Syncrude site.

- B-Stage Cure - A B-stage cure may also be applied to the thick doublers ($120^{o}$F and 50-75 PSI) in order to drive out excess resin and minimize porosity in the laminate. It may even be possible to refreeze the doubler after the B-stage cure process so that the doubler can be installed at a later date.

- Use of Alternate Materials – If cost becomes a consideration, carbon-graphite pre-preg plies may be an option. However, the strength of the carbon-graphite material is only 70% (uniaxial tape) or 40% (cloth/weave) of the Boron-Epoxy material. There are other materials, such as Silicon-Carbon, to explore and any design limitations, cost trade-offs, and material availability issues should be addressed.

- Heating Process and Thermal Surveys - Although the results from the initial heat source/sink assessment were very good, this activity will be revisited using the exact structure to be repaired. Then it can be determined if the Cooperheat ceramic heat blankets need to be supplemented with additional heat sources. This process will also characterize the repair region so that the temperature dwells and set points necessary to produce the desired cure profile can be determined.

- Use of Alternate Adhesives – A room temperature adhesive may allow for installation of pre-cured patches. Strength requirements may be hard to meet with low temperature adhesives. Paste adhesives are able to fill undulations in uneven surfaces better than film adhesive, however, limited pot life of two part adhesives can produce reliability problems.

- High-Wear Applications - Future work in high-wear applications (i.e. shovel buckets) and high temperature applications (upgrading) may provide areas of growth once the technology has been established.

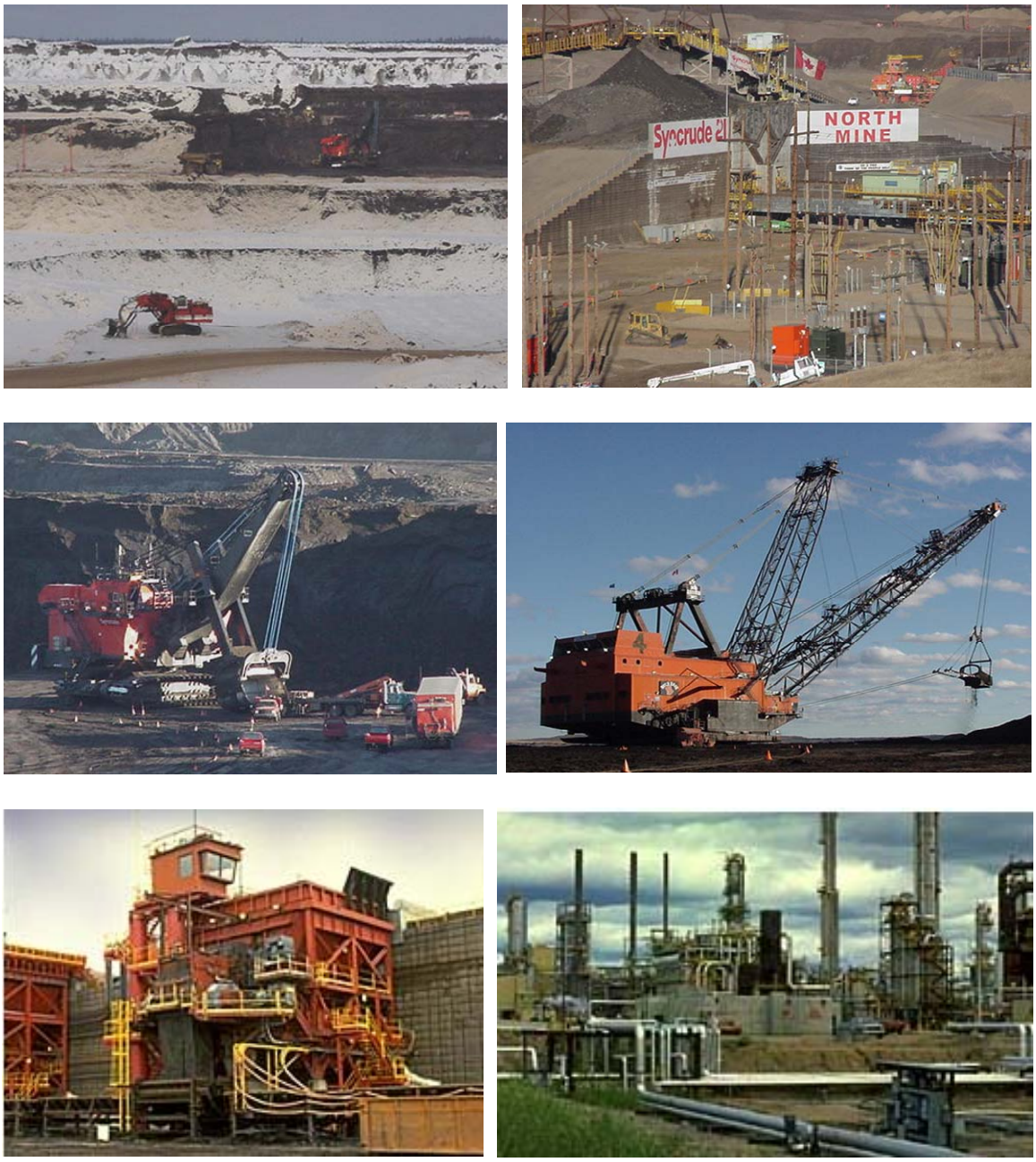


Rock Crusher

Upgrading Plant

**Figure 145: Sample Syncrude Equipment that Could Utilize Composite Doubler Repair Technique**

**Figure 145 (continued): Sample Syncrude Equipment that Could Utilize Composite Doubler Repair Technique**

## 6.3 Large-Scale Testing of Composite Doublers in the Laboratory

For the example of the shovel boom application, a proposed, large scale test article is shown in Figure 146. In lieu of testing an actual welded box beam from a cable shovel, the response of thick composite doublers could be studied using a simulated box beam structure. Loading will be applied by a multi-actuator system to produce representative and extreme shear (payload weight), side bending (movement to transition payload to trucks), and torsion (non-symmetric payloads and dynamic operation) loads. The purpose of this test is to: 1) verify composite doubler analysis techniques for thick-walled structures, and 2) experimentally assess the limit loads in extremely thick composite doubler installations in highly-stressed, representative structure. The specimen and load configuration can be designed to provide stress levels which exceed the design limit loads. Strain gages will be used to measure the applied stresses, stress intensity factors at critical regions, load transfer into the doubler, and stress relief in the parent steel structure. NDI will also be integrated into this test to quantify any flaw onset and growth. Since the weld regions, especially those near the diaphragms, are the critical crack locations a welded box beam will provide a better test. Welded, steel plates can be used to produce a box beam with representative geometry and material properties. Holes can be added to the plates to simulate the stick-to-boom attachment point. Reinforcement plates can also be added inside the box beam to simulate the diaphragms and produce associated stress risers near the doubler. Finally, the repaired portion of the beam can contain a gouge weld region in order to create an uneven surface.

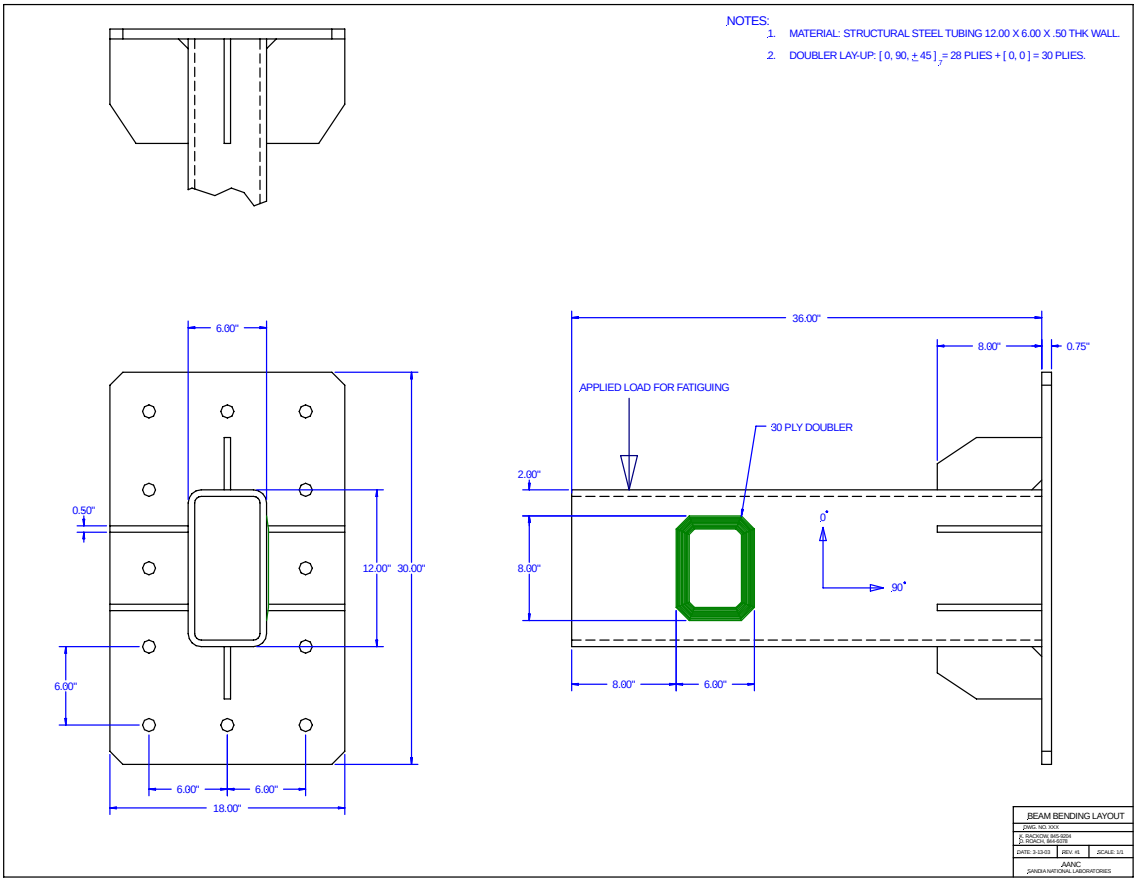


**Figure 146: Box Beam Structure to Simulate Cable Shovel Boom - Loaded with Representative Shear, Torsion, and Bending**

## 6.4 Living Infrastructure Concepts

### 6.4.1 Smart Structures - In-Situ Distributed Health Monitoring Sensors

A "smart structure" is one which is sufficiently instrumented so that the data can be synthesized to form an accurate real-time picture of the state of the structure in all its critical aspects. In this case, the absence of disbonds and delaminations indicates that the doubler is able to perform its duty. The absence of cracks indicates that the structure is able to safely continue to operate.

The current state of nondestructive inspection – as proposed in Section 5.0 – involves the manual application of ultrasonic and eddy current NDI methods. While the data presented in this report indicates that manual inspections provide a reliable health monitoring approach, less labor intensive and more frequent structural assessments can be performed via distributed sensor systems. Such health monitoring systems utilize a network of leave-in-place sensors that can assess a structure on a frequent, or even continuous, basis. By positioning sensors along the critical regions of the doubler and surrounding steel structure, as shown in Figure 147, it is possible to detect the onset or growth of cracks and disbonds in real time.

The costs associated with the increasing maintenance and surveillance needs of aging structures are rising. The application of distributed sensor systems can reduce these costs by allowing condition-based maintenance practices to be substituted for the current time-based maintenance approach. Through the use of in-situ sensors, it is possible to quickly, routinely, and remotely monitor the integrity of a structure in service [29]. This requires the use of reliable structural health monitoring systems that can automatically process data, assess structural condition, and signal the need for human intervention. Prevention of unexpected flaw growth and structural failure can be improved if on-board health monitoring systems exist that could continuously assess structural integrity. Such systems would be able to detect incipient damage before catastrophic failures occurs.

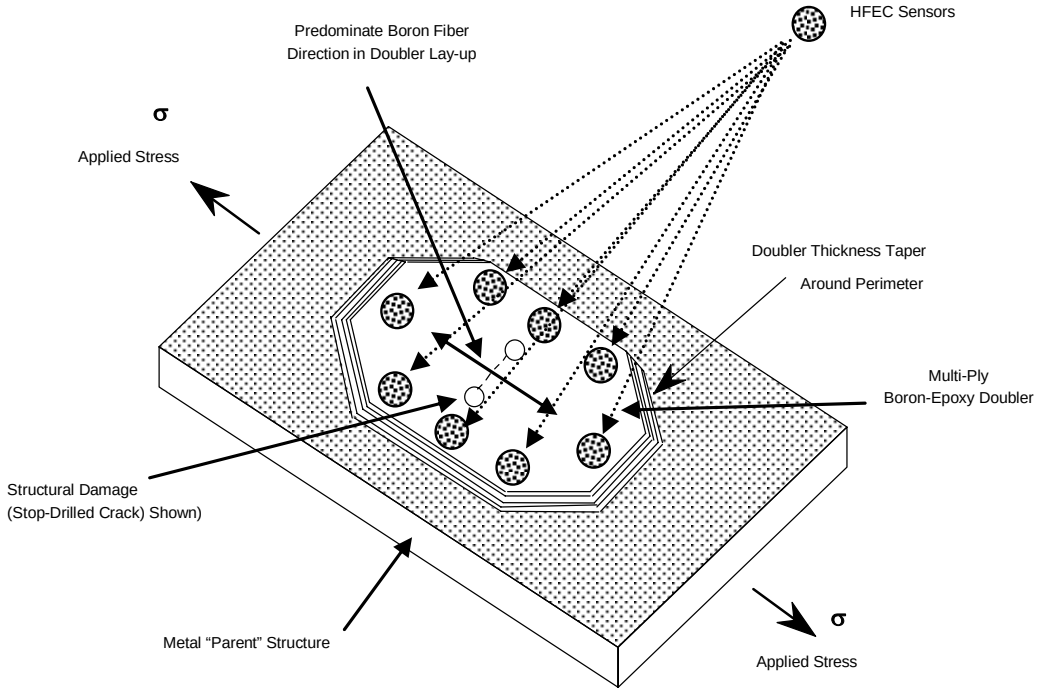


**Figure 147: Distributed Sensor System to Continuously Monitor the Health of Composite Doubler Repairs and the Parent Steel Structure**

Internally-sponsored R&D at Sandia Labs, is developing a variety of miniature sensors and studying the deployment of these sensors in distributed networks for continuous, real-time health monitoring. The by-products of this study will be directly applicable to Syncrude field use whether it is for monitoring pristine or repaired structures. Four different sensor designs are being pursued: 1) Fiber-Optic Bragg Grating sensor, 2) micromirror fiber optic sensor, 3) piezoelectric transducer, and 4) high frequency eddy current sensor.

Fiber-Optic Bragg Gratings consist of index of refraction discontinuities intentionally placed in the core of an optical fiber with periodic spacing. Several Bragg gratings can be implemented into a single fiber with multiple different grating values to form a distributed sensing network. A

broadband light source is injected into the fiber and the absorption spectrum is measured using a monochromator or similar instrument.

The transmission spectrum will have regions of missing energy that correspond to the grating period. Thus, a stress measurement can be performed by observing the wavelength shift while distorting the periodicity of the grating via application of stress. Thus, the Bragg approach provides both strain magnitude and strain position measurements. These can be calibrated to provide information on structural flaws. Fiber breakage, corresponding to crack growth in the structure can also be easily observed. While the cost of equipment to monitor Bragg gratings is prohibitive for dedicated inspections on a single repair, this approach is ideal for periodic monitoring of multiple structures as a transportable field instrument and has superior sensitivity to strain over Optical Time Domain Reflectometry. Innovative multiaxis fiber grating sensors have been produced with both extensional and lateral strain sensitivity. This approach intends to demonstrate that strategic measurement of multidimensional strain fields can be used to track the onset of damage in composite repairs. FOBG sensor systems have been installed on two composite doubler repair specimens as shown in Figure 148 (one flawed and one unflawed repair). The sensors encompass the entire perimeter region of the doubler so that they are able to detect the onset of any flaws within the footprint of the repair. Fatigue tests will be completed to evaluate these sensors.

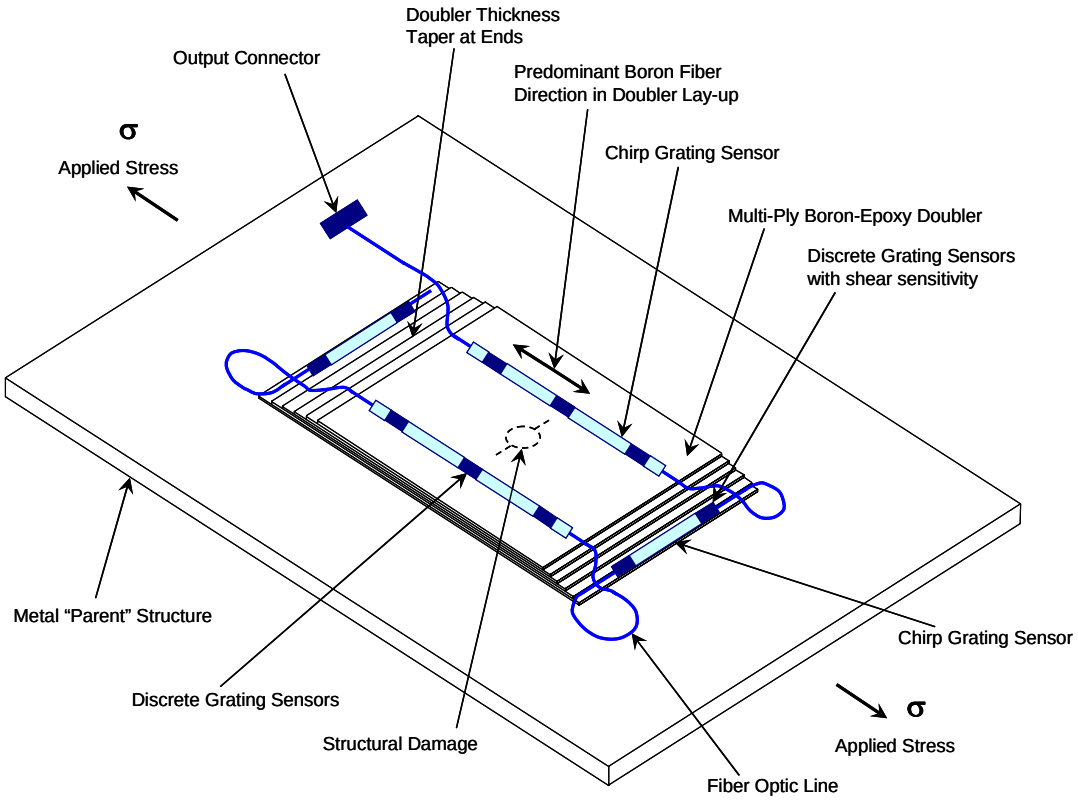


**Figure 148: Fiber Optic Bragg Sensors Installed on a Composite Repair Fatigue Specimen**

Fiber Optic Micromirror Sensor - A simpler, low-cost sensor has been produced that relies on a single fiber with a reflective end that can be used for crack monitoring. This fiber optic micromirror sensor functions by placing a modulated optical signal on the fiber and then measuring the intensity of the reflected signal from the fiber end. The propagation loss of the fiber is sensitive to strain and breakage allowing production of a low cost monitor that is ideal for permanent monitoring of crack propagation past a boundary. Figure 149 is a drawing of the system that has been constructed and tested and illustrates the sensing approach. Light from the LED optical source is passed through an optical coupler to a detector for intensity reference. The rest of the light probes the reflectivity of the fiber network that is rigidly connected to the structure under test. If the crack propagates across the fiber, which is rigidly connected to the structure under test, the breakage occurs and is observed at the second optical detector. Currently work is determining the level of strain that can be measured using the same technique. Figure 150 is a plot of the reflectivity measured as a function of time as a thin Au film is deposited on the fiber end. Clearly, a break in the fiber reduces the reflectivity significantly since the reflectivity difference between the pristine Au end and a bare fiber is on the order of 190 mV. The measured signal-to-noise ratio of this system will allow one part in $10^4$ variation in reflectivity to be measured offering the promise of strain measurement using this technique.

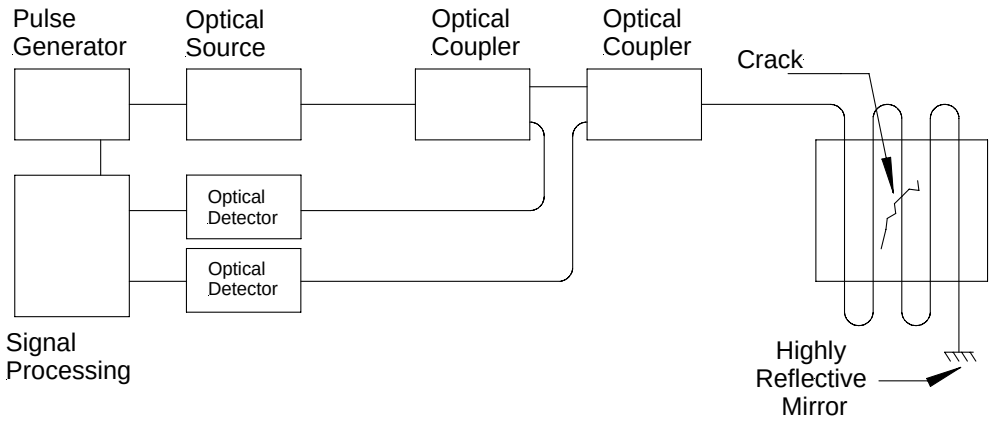


**Figure 149: Diagram of Micromirror Sensor Illustrating the Application as a Crack Monitor**

Piezoelectric Transducers (PZT) were built by embedding PZT materials in a thin dielectric carrier film. The spacing of the active PZT elements and the shape of the film were determined by the need to monitor local and global damage in the composite laminate and steel substructure. The PZT sensor network (see Fig. 151) was designed for active sensing whereby each PZT generates a diagnostic signal and alternately acts as a sensing element to interpret signal anomalies for damage detection and location. The PZTs range in size from 0.125”-0.50” in diameter with a thickness of 0.01”-0.03”. They can be laid out in custom configurations to detect damage in critical regions and provide an image of the structure in the area of the sensor network. A time-varying electrical signal is input to any of the actuators/sensors. This causes a propagating stress wave to emanate from the actuator and travel through the material for detection by the neighboring sensors. These signals can be compared with previously recorded

baseline test signals to identify the location and extent of damage or other structural anomaly. Both electro-mechanical impedance and wave propagation methods can be used for signal analyses.

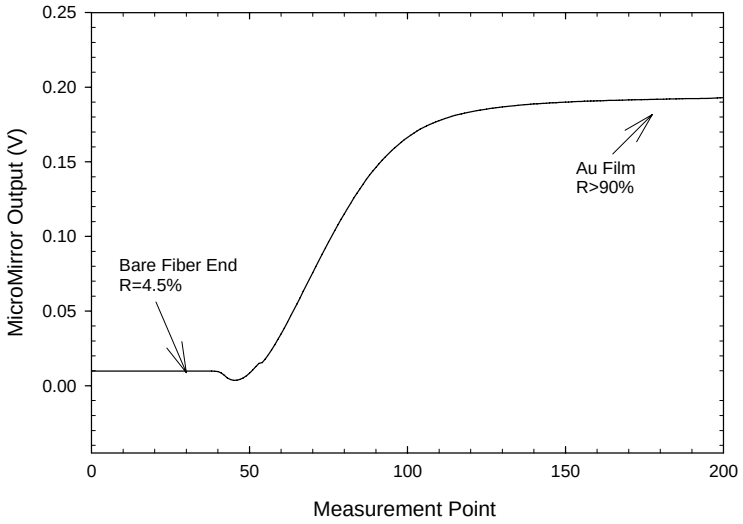


**Figure 150: Plot of Relative Reflectivity Measured by the Micromirror System as a Function of Time for Au Deposition on the End of the Fiber**

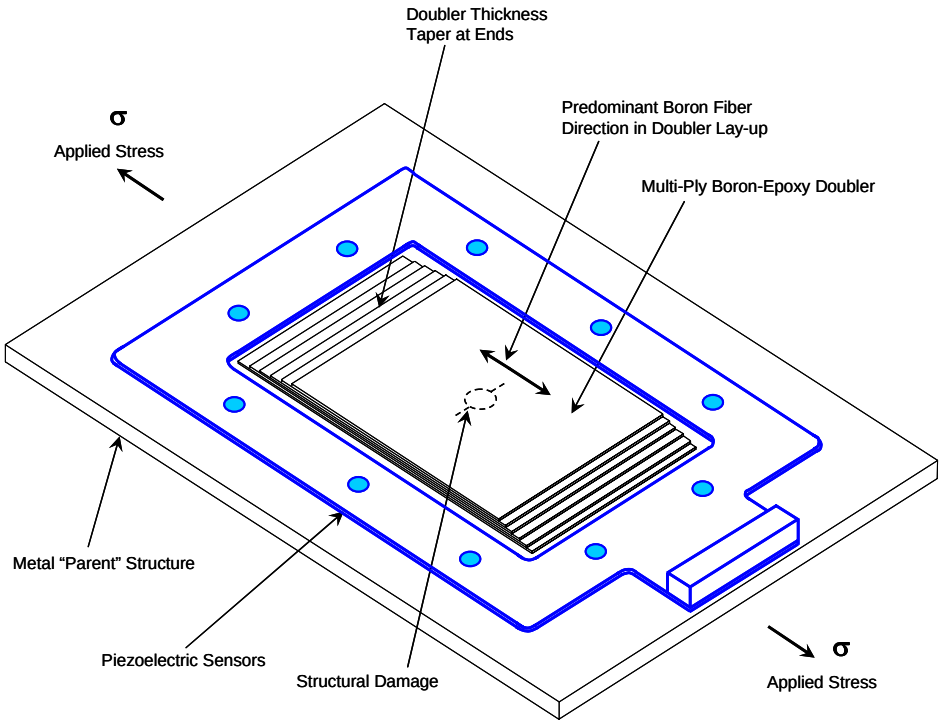


**Figure 151: Piezoelectric Sensors Installed on a Composite Repair Fatigue Specimen**

High Frequency Eddy Current (HFEC) Sensors - Another subtask is investigating high frequency eddy current sensors to detect disbonds in the doublers and crack growth in the parent structure. By positioning sensors around the critical regions of the doubler it is possible to establish an in-situ network for continuous, real-time health monitoring. Initial EC images produced with a robotic scanner indicated that EC techniques can detect cracks in the parent steel while also identifying disbonds between the composite laminate and the steel structure. In the area of crack detection, impedance bridge and other differential circuits were explored to maximize the magnetic flux density and corresponding eddy current strength. Several EC sensor prototypes have been produced and tested. Successful crack detection was achieved with a dual coil configuration that combines a pancake, excitation inductor with a co-located pickup coil to produce a transducer that requires very little drive current (75 mA) and operates in the desired 10 KHz range. Figure 152 shows the prototype sensor along with the large signal it produced when it was scanned over a crack. Excellent crack detection was achieved even when inspecting through composite repairs approaching 0.5" thick (EC lift-off impediment).

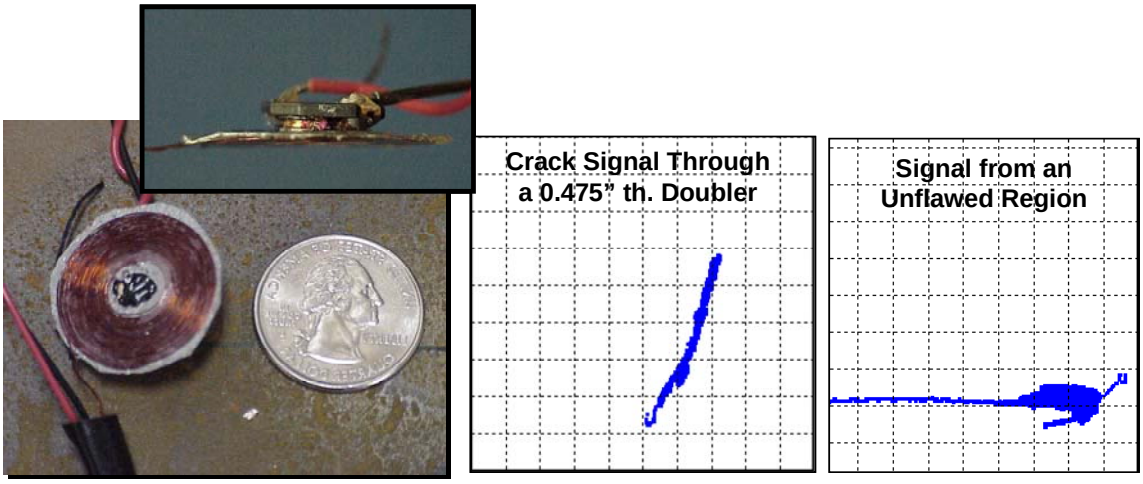


**Figure 152: Sandia Pancake EC Sensor and Large Signals Showing Crack Detection Through Composite Doublers**

Sensor Development Efforts - Performance testing has been planned to evaluate the health monitoring capabilities of the fiber optic and piezoelectric sensors, optimize their design, and lead to distributed sensor networks for continuous, remote assessment of structural integrity. This will include redesign of the detection hardware to produce a low-power, highly portable system that can be operated autonomously and will provide a log of sensor readings and a catastrophic failure alarm. The investigation will also determine the level of strain that can be measured using the micromirror technique. In the eddy current arena, ongoing activities are developing a more sophisticated electronics package - including digital signal processing to filter and detect phase shifts - to further increase probe sensitivity. Another activity is improving the dual coil configuration by incorporating conditioning electronics, shielding and packaging for the sensor. Focused testing will determine the spatial sensitivity of the optimized probe and the minimum detectable feature size. Packaged, distributed sensor networks can then be designed,

mounted, and evaluated. Miniaturization of the sensors using on-board power supplies and electronics for signal conditioning and data acquisition is necessary to allow for quick, reliable, autonomous, and unobtrusive installations. Figure 153 shows some internal circuitry and an integrated sensor and package design proposed for the HFEC probe pictured in Figure 152.

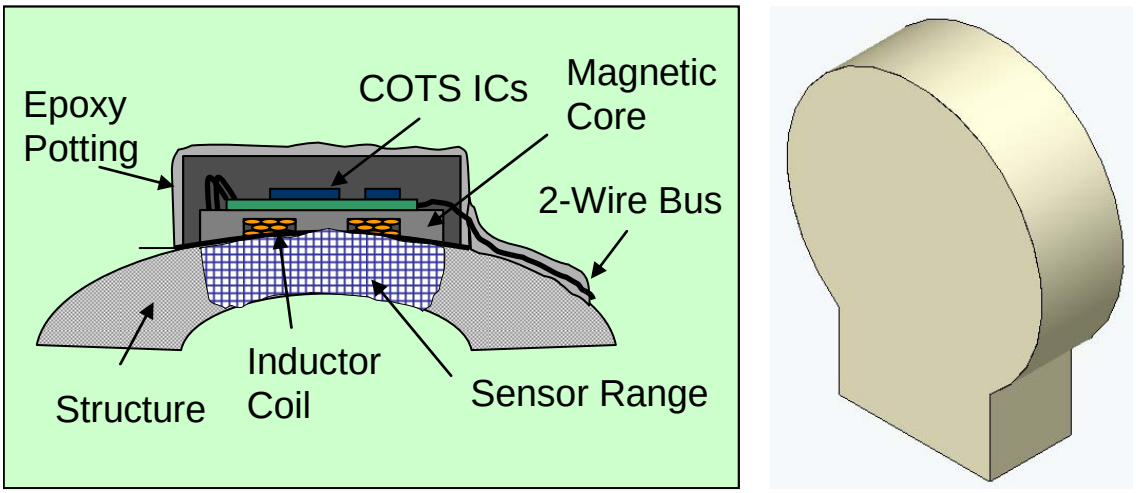


**Figure 153: Internal Circuitry and Packaged Sensor for Mounting on Structures in the Field**

Deployment of Health Monitoring Sensor Networks – Distributed sensor networks can be deployed in any of the three approaches listed below. These options are listed in the order of increasing complexity, however, less labor is required to monitor the systems as they become more complex.

1. *In-Situ Sensors Only* – The sensors are the only items permanently installed on the structure. At the desired inspection intervals, power, signal conditioning, and data acquisition electronics are manually transported to the structure to be monitored. The sensors are linked to the monitoring electronics via an electrical connector and flaw detection is completed by an inspector at the site.
2. *Sensor Network with In-Situ Data Acquisition* – In this system, miniature, packaged electronics is also placed in-situ with the sensor network. The electronics contains the necessary power, memory and programmable circuitry for automated data logging. The data is periodically downloaded to a laptop through manual hook-ups at the site.
3. *Sensor Network with Real-Time Data Transmission to a Remote Site* – This approach is similar to item #2 with the addition of a telemetry system that allows for continuous, wireless transmission of data to a web site. The web site can be programmed to interrogate critical aspects of the data and use pre-set thresholds to provide continuous green light/red light information regarding the health of the structure. The web site can even be programmed to automatically send an e-mail to Syncrude personnel if the condition monitoring process indicates the need for repairs or other maintenance.

The latter approach allows for true condition-based maintenance in lieu of maintenance checks based on time of operation. A series of expected maintenance functions will already be defined, however, they will only be carried out as their need is established by the health monitoring system. The use of condition-based maintenance coupled with continuous on-line structural integrity monitoring could significantly reduce the cost of inspection, maintenance, and repair.

### 6.4.2 Self-Healing Composite Structures

Self-healing materials are inspired by living systems, in which minor damage triggers an autonomic healing response. Figure 154 illustrates the self-healing concept. Healing is accomplished by incorporating a microencapsulated healing agent and a catalytic chemical trigger within a polymer matrix. Damage in the form of a bond dislocation serves as the triggering mechanism for self-healing. The approaching dislocation ruptures the embedded microcapsules, releasing a healing agent into the crack plane through capillary action. Polymerization of the healing agent is triggered by contact with the embedded catalyst, bonding the crack faces. As with biological systems, this triggering mechanism provides site-specific control of healing. An additional unique feature of our healing concept is the use of *living* polymerization catalysts (*i.e.*, having non-terminated chains), thus enabling multiple healing events. Repair of damage is accomplished automatically and without human intervention, improving performance and service-life.

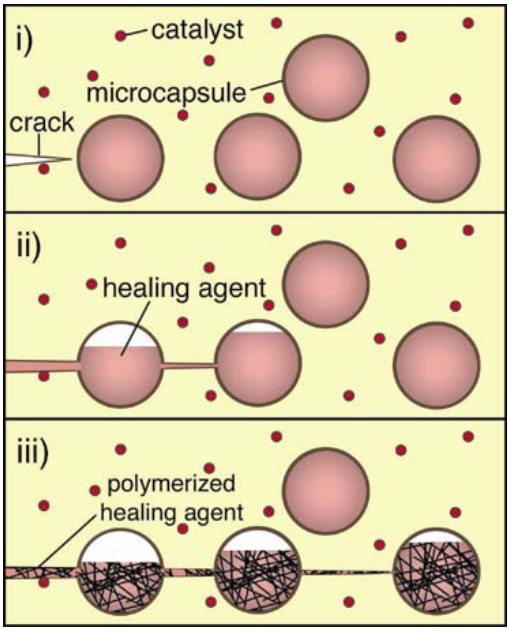


**Figure 154: Self-Healing Concept in Which Microcapsules of a Healing Agent are Dispersed to Rebond a Dislocation in a Composite Laminate**

Ongoing activities at Sandia Labs are developing self-healing laminates suitable for bonded repair of metallic structures. Research to date has focused on selection of the appropriate

chemistry, perfecting the triggering mechanism, and developing an effective protocol to assess healing efficiency. Tasks completed to develop the self healing material specifications include: 1) identifying materials and requirements for composite doubler adhesive system, 2) surveying potential failure modes for adhesive and identify self-healing strategies, 3) exploring ring-opening metathesis polymerization (ROMP-based) healing agents for adhesive systems, and 4) conducting screening studies of candidate self-healing materials systems to meet requirements for composite doubler adhesive system. The healing efficiency of candidate resin systems is being measured by carefully controlled fracture experiments. The most critical issue for the laminate fabrication task is to identify the processing window for compaction pressure in which the microcapsules remain structurally intact throughout cure while ensuring full compaction of the laminate stack. Fracture toughness recovery will be measured to assess the efficiency of healing in the composites laminates.

In preliminary testing, successful healing was accomplished by incorporating a small volume fraction of microcapsules in an epoxy resin along with a transition metal catalyst. The embedded microcapsules were shown to rupture in the presence of a crack and release the healing agent into the crack plane where polymerization was initiated. Double cantilever beam and lap shear specimens were tested to evaluate the performance of the healing agents and the method of deploying them in the adhesive layer. The efficiency of crack healing in both static and cyclic loading regimes is summarized in Figure 155 and 156. Over 90% recovery of virgin fracture toughness is achieved along with significant life extension during fatigue loading.

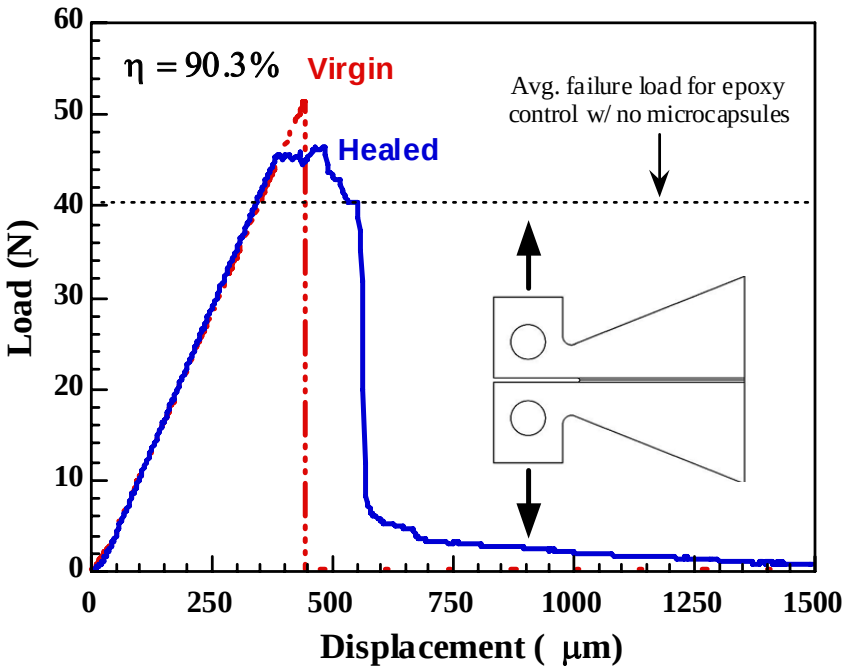


**Figure 155: Self-Healing Performance: Load-Displacement Data for a Virgin and Healed Epoxy Fracture Toughness Specimen**

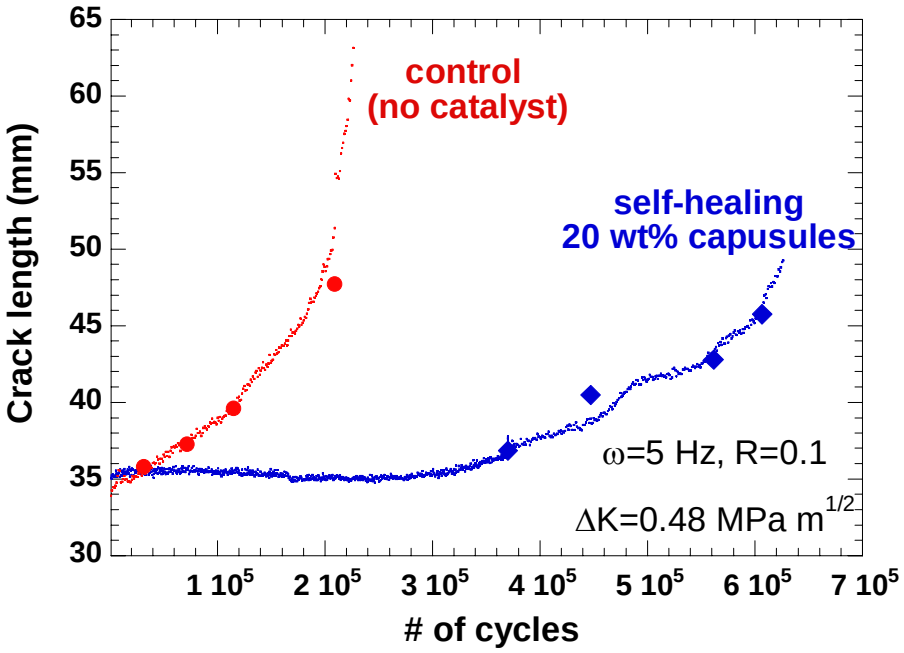


**Figure 156: Self-Healing Performance: Fatigue Crack Length vs. Number of Cycles for Self-Healing Epoxy and Epoxy Control Samples**

## CONCLUSIONS

An unavoidable by-product of a metallic structure's use is the appearance of crack and corrosion flaws. Economic barriers to the replacement of these structures have created an aging infrastructure and placed even greater demands on efficient and safe repair methods. This report presents the results from a study into the application of composite patches on large steel structures. The initial focus was on trucks and hydraulic shovels typically used in Syncrude mining operations. Extreme fatigue, temperature, erosive, and corrosive environments induce an array of equipment damage. The current weld repair techniques for these structures provide a fatigue life that is inferior to that of the original plate. Subsequent re-cracking must be revisited on a regular basis. Mechanically fastened repairs involve the addition of new holes with associated stress risers and new crack initiation sites. In addition, the time and labor involved to attach such repairs can be prohibitive. The use of bonded composite doublers has the potential to correct the difficulties associated with current repair techniques and the ability to be applied where there are no rehabilitation options. It promises to be cost-effective with minimal disruption to the users of the structure. This study has shown that bonded composite repairs have crack mitigation capabilities that are superior to bolted and welded repairs.

The goal of this project was to establish bonded composite doublers as a reliable and cost-effective structural repair method for civil structures and to develop adequate real-time monitoring and to ensure the long-term integrity of such structures with minimal need for human intervention. This investigation established the effectiveness of composite materials to strengthen damaged or deficient steel structures. The general issues investigated to establish the performance of composite doubler repairs in complex environments were: 1) patch installation (surface preparation, tooling, heat sinks, effect of underlying structures, field work), and 2) patch design (strength, damage tolerance, durability, reliability, flaw containment, optimum adhesive properties, and critical patch parameters.

Performance tests established the viability of composite doubler repairs to reinforce steel structures and minimize/eliminate the effects of cracks, corrosion or other flaws. Fatigue and ultimate strength tests evaluated the overall effect of composite doublers on stress intensity, crack growth, and strength characteristics of steel structure. The structural tests determined: 1) the potential for interply delaminations and disbonds between the steel and the laminate, 2) the load transfer and crack mitigation capabilities of composite doublers in the presence of severe defects, and 3) an optimum composite doubler design philosophy. The study included flawed installations (poor installations) and extreme environmental conditioning in order to assess the damage tolerance of these composite doubler repairs and to prove their ability to operate in off-design conditions.

This report presents a comprehensive assessment of different mechanical and chemical surface preparation techniques. An optimum, and field installation-friendly process was established that uses grit blasting, Silane chemical, and steel primer to produce a strong and durable bonded joint. The factors influencing the durability of composite patch installations in severe field environments were determined. Results from this study show that the fatigue life of steel structures can be extended by a factor of 2 to 10 through the use of composite patches. Bonded

composite repairs can withstand 200,000 to 600,000 fatigue cycles while allowing little or no crack growth in a parent steel structure. Data acquired during failure tests showed that the composite doubler was able to absorb stresses in the plastic regime and that extensive yielding of the steel was required to fail the installation. Residual strength failure tests demonstrated that the doubler-reinforced plates were able to achieve residual tensile strengths (i.e. post-damage tensile strength) which exceeded the 65 ksi baseline value for this steel material. Thus, the Boron-Epoxy doubler was able to return the parent structure to its original strength and load carrying capability. Nondestructive inspection techniques were developed to adequately monitor the health of the patch and the parent structure. Ultrasonic methods can be used to reliably detect disbonds in a composite doubler repair well before the flaw reaches critical size. Eddy current methods were produced to detect cracks in the steel structure beneath the composite laminate. Cracks of less than 1” in length can be detected through doublers in excess of 0.5” thick.

In summary, an in-depth performance assessment of composite doublers for repair of civil, steel structures was completed. The factors influencing the durability of composite patches in severe field environments were determined along with related laminate design and installation issues. By encompassing all "cradle-to-grave" tasks - including design, analysis, installation, structural integrity and inspection - this study firmly established the capabilities of composite doubler repairs. The goal of this project was to establish bonded composite doublers as a reliable and cost-effective structural repair method for steel structures and to develop adequate real-time health monitoring to ensure the long-term integrity of such structures with minimal need for human intervention. Although an initial application was targeted – repair of a cable shovel boom – the tests were conducted such that the results are applicable to a very wide range of steel repair scenarios. The results provided in this report prove that the use of composite doublers, which do not have brittle fracture problems such as those inherent in welds, will help extend the structure’s fatigue life and reduce the equipment downtime.

## REFERENCES


1. Roach, D., “Joint Syncrude and Sandia National Labs Project: Development of Bonded Composite Repair of Oil Recovery Equipment”, Syncrude Canada Ltd Internal Consultants Reports, April 2003.
2. del Valle, V., Johnson, S., “Syncrude Sandia National Labs: Composite Patch Program Report 01”, Syncrude Canada Ltd., Research Department Progress Report 31, 2003.
3. Roach, D., "Development Program to Certify Composite Doubler Repair Technique for Commercial Aircraft," First DoD/FAA/NASA Conference on Aging Aircraft, July 1997.
4. Baker, A.A. and Jones, R., *Bonded Repair of Aircraft Structures*, Martinus Nijhoff Pub., The Netherlands, 1988.
5. Roach, D. and Walkington, P., “Full Scale Structural and NDI Validation Tests on Bonded Composite Doublers for Commercial Aircraft Applications," Sandia National Laboratories/ Dept. of Energy Report No. SAND98-1015 , February 1999.
6. Roach, D., "Damage Tolerance Assessment of Bonded Composite Doubler Repairs for Commercial Aircraft Applications," Sandia National Laboratories/ Dept. of Energy Report No. SAND98-1016 , August 1998.
7. Roach, D. and Walkington, P., "Development and Validation of Nondestructive Inspection Techniques for Composite Doubler Repairs on Commercial Aircraft", Sandia Report SAND98-1014, May 1998.
8. Roach, D., "Commercial Application of Composite Doublers for DC-10 Fuselage Repairs," Int'l SAMPE Symposium on Composites in Engineering, May 2001.
9. Brewis, D., “Factors Affecting Bonding of Metals,” *Materials and Technology*, Vol. 2, August 1986.
10. Bockenheimer, C., Valske, B., and Possart, W., “The Influence of Mechanical Pretreatment on the Polymer Structure of Adhesive Bonds,” 5th European Adhesive Conf., September 2000.
11. Critchlow, G. and Webb, P., “Chemical Conversion Coatings for Structural Adhesive Bonding of Plain Carbon Steels,” *Int’l Journal of Adhesion*, Vol. 20, Aug. 2000.
12. Arnott, D., “Bond Durability Performance – The Australian Silane Surface Treatment,” Int’l Council of Aero Sciences Congress, September 1998.
13. Blohowiak, K., et al., “Bonded Repair Techniques Using Sol-Gel Surface Preparations,” DOD/FAA/NASA Conf. on Aging Aircraft, September 1998.
14. Clearfield, H., McNamara, D. and Davis, G., “Adherend Surface Preparation for Structural Adhesive Bonding,” *Adhesive Bonding*, Cambridge Scientific, 2002.
15. Jones, R. and Callinan, R., “A Design Study in Crack Patching,” Fibre Science and Technology, Vol. 14, 1981.
16. Jones, R., Chiu, C., Paul, J., “Designing for Damage Tolerant Bonded Joints,” *Composite Structures*, Vol. 25, 1993.
17. Roach, D.P., and Walkington, P., “Full Scale Structural and NDI Validation Tests on Bonded Composite Doublers for Commercial Aircraft Applications", Sandia National Laboratories/ Dept. of Energy Report No. SAND98-1015 , November 1998.
18. Baker, A.A., "Fatigue Studies Related to Certification of Composite Crack Patching for Primary Metallic Aircraft Structure," FAA-NASA Symposium on Continued Airworthiness if Aircraft Structures, Dept. of Transportation Report No. DOT/FAA/AR-97-2,I, July 1997.

19. Rice, R., Francini, R., Rahman, S., Rosenfeld, S., Rust, S., Smith, S., and Broek, D., "Effects of Repair on Structural Integrity", Dept. of Transportation Report No. DOT/FAA/CT-93/79, December 1993.
20. Chiu, W.K., Rees, D., Chalkley, P., and Jones, R., “Designing for Damage Tolerant Repairs,” ARL Aircraft Structures Report 450, August 1992.
21. Obaia, K., Radke, C., “Crack Management of Mobile Equipment”, Syncrude Canada Ltd., Research Department Progress Report 31 (5) 266-275 (2002).
22. Yin, Y., Grondin, G., Obaia, K., “Crack Management of Mobile Equipment,” Syncrude Canada Ltd., Research Department Progress Report 31 (7), 2002.
23. Yin, Y., Grondin, G., Elwi, A., Obaia, K., “Fatigue Crack Management in Heavy Mining Equipment,” Syncrude Canada Ltd., Research Department Progress Report 32 (07), 2003.
24. Fiebig, J., “Composite Doubler Design and Optimization Handbook Tool,” Warner Robins Air Logistic Center, June 1999.
25. Callinan, R.J., Rose, L.R., and Wang, C.H., “Three Dimensional Stress Analysis of Crack Patching,” Proc. Of Int’l Conf. Fracture, ICF-9, April 1997.
26. Metals Handbook Ninth Edition “Volume 17 Nondestructive Evaluation and Quality Control”, ASM International, 1989, pp 241 - 246.
27. Ansley, G., et. al., "Current Nondestructive Inspection Methods for Aging Aircraft," U.S. Dept. of Transportation, FAA Report No. DOT/FAA/CT-91/5, June 1992.
28. Roach, D., Moore, D., and Walkington, P., “Nondestructive Inspection of Bonded Composite Doublers for Aircraft”, SPIE Int’l Conf. on NDI of Aging Aircraft, December 1996.
29. Roach, D., “Use of Distributed Sensor Systems to Monitor Structural Integrity in Real-Time,” Quality, Reliability, and Maintenance in Engineering, Professional Engineering Publishing Ltd., Oxford, UK, 2004.

# APPENDIX A

## Photo Summary of Laminate Fabrication and Installation Process for Bonding Composite Doublers on Carbon Steel Structures

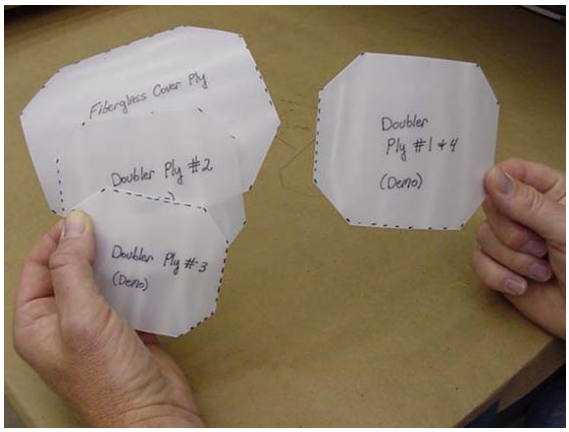


**Figure A-1: Mylar templates for B-E Plies, Adhesive and Fiberglass Cover Ply**

**Figure A-2: Cut Roll of B-E Tape into Doubler Plies**

**Figure A-3: Use Template for Proper Sizing and Ply Orientation**

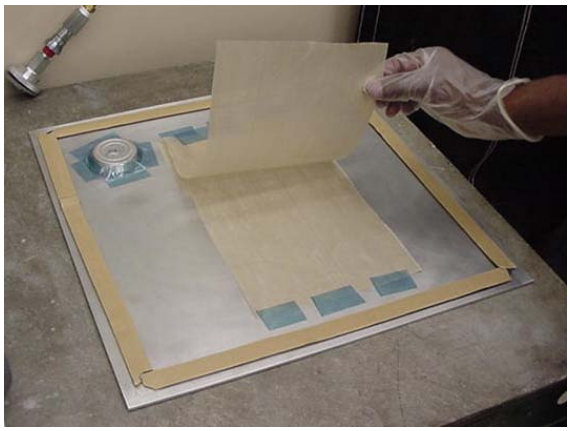

**Figure A-4: Sandwich of Armalon Release Fabric on Doubler Debulk Tool**

**Figure A-5: Lay Up B-E plies in Proper Stack (1st ply goes face down)**

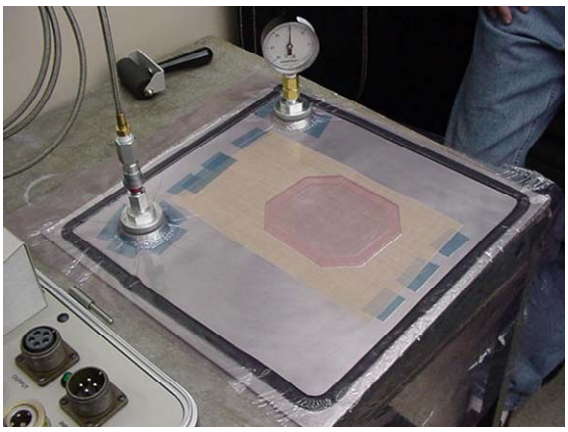

**Figure A-6: Vacuum Bag Debulk of Doubler Every Four Plies**

**Figure A-7: Coarse Scotchbrite Grind to Remove Excess Scale/Oxide**

**Figure A-8: Degrease with Acetone Followed by Methyl Alcohol**

**Figure A-9: Grit Blast Device Uses 50 µm Aluminum Oxide Grit**

**Figure A-10: Grit Blast Steel Surface**

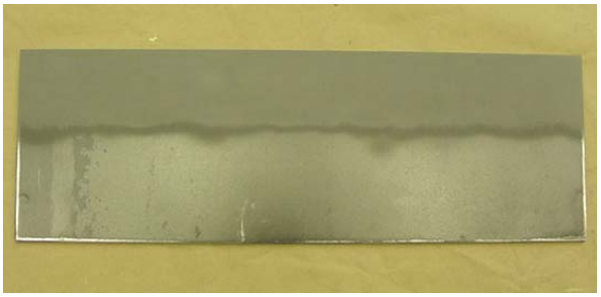

**Figure A-11: Grit Blast Surface Along Top**


**Figure A-12: Mix Silane Solution (99:1 ratio of distilled water to Silane)**

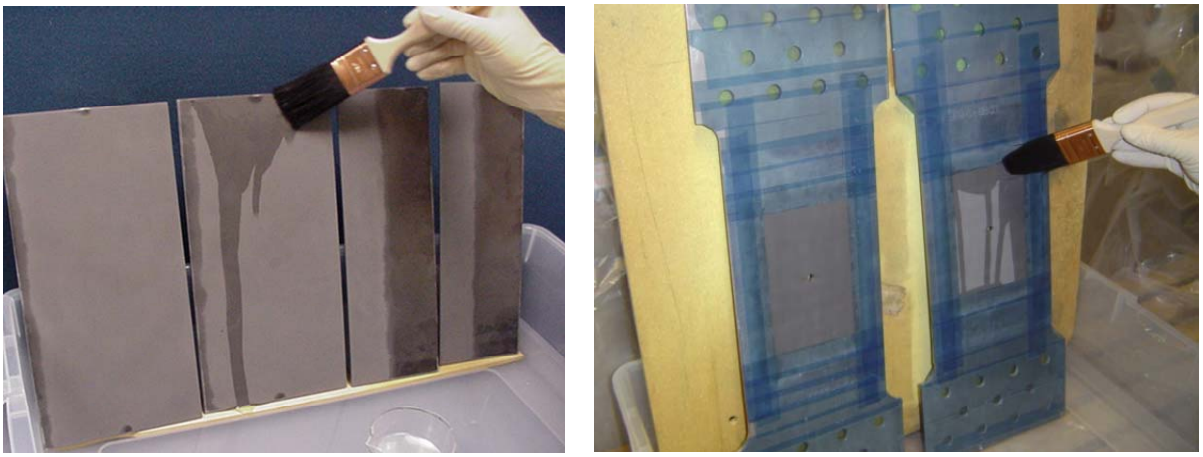

**Figure A-13: Brush-On Application of Silane Mixture to Steel Surface**

**Figure A-14: Wet Surface with Silane Solution for Ten Minutes**

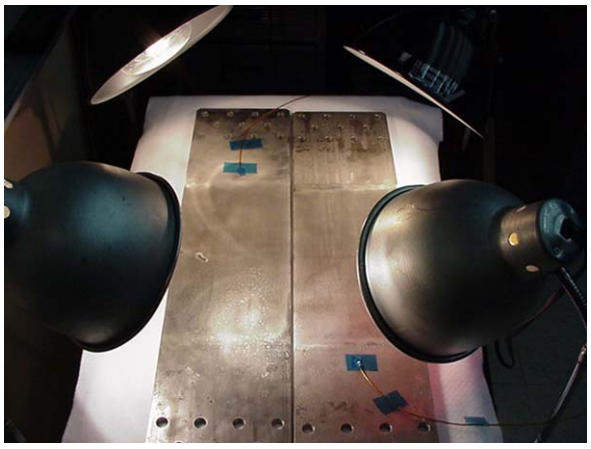

**Figure A-15: Drive Off Silane Moisture (Pre-Cure) Using Heat Lamps**

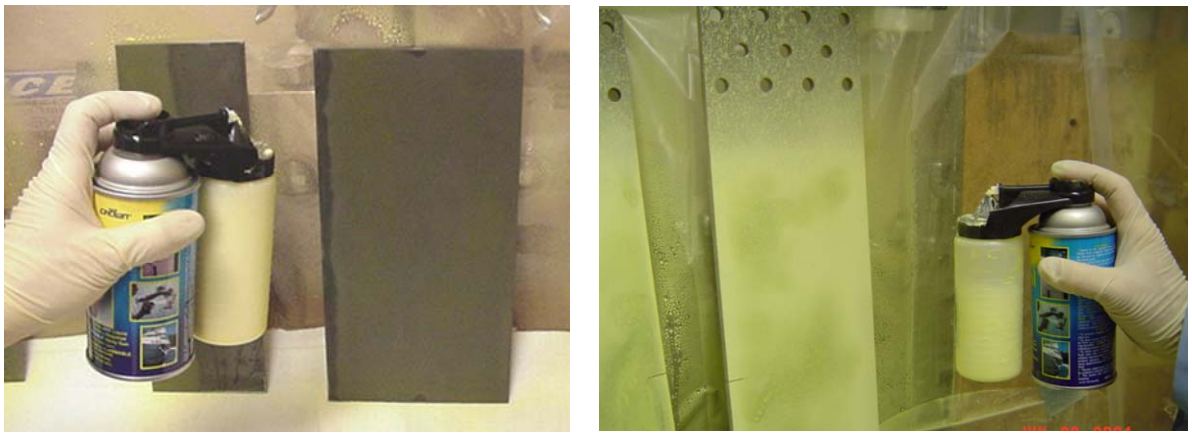

**Figure A-16: Spray BR6747 Primer on Steel Surface**

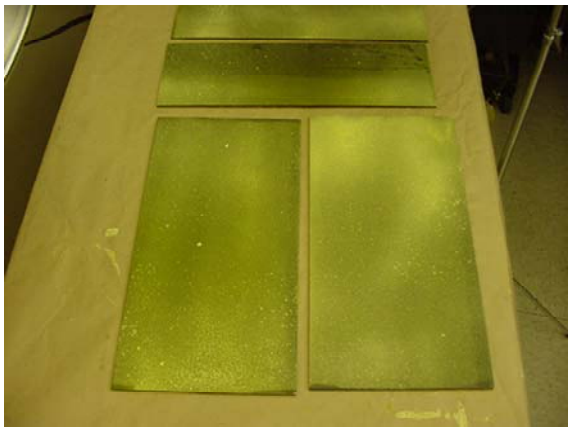

**Figure A-17: Drive Off Primer Moisture Using Heat Lamps**

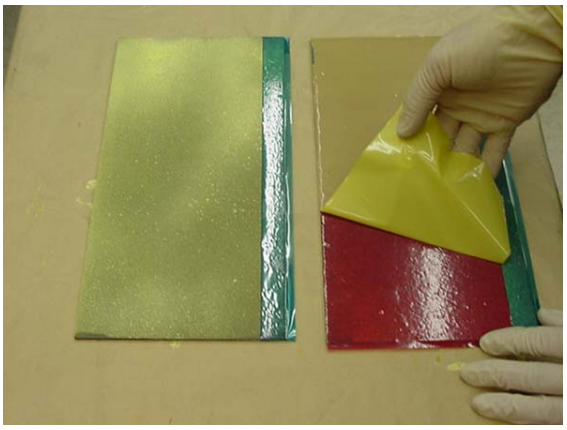

**Figure A-18: Apply Adhesive Film to Composite Doubler Laminate**


**Figure A-19: Cut Two Witness Coupons from Steel Plate and Prepare Surface for Bonding Process**

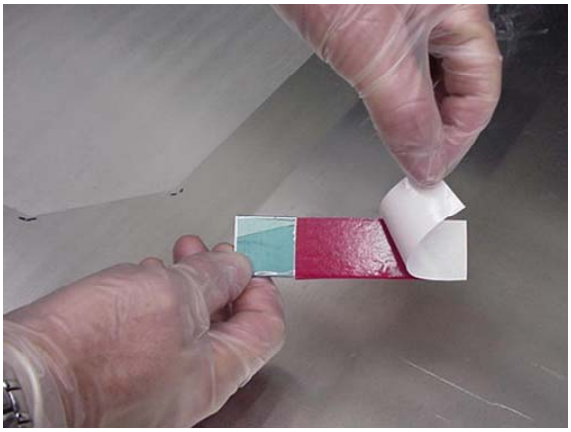

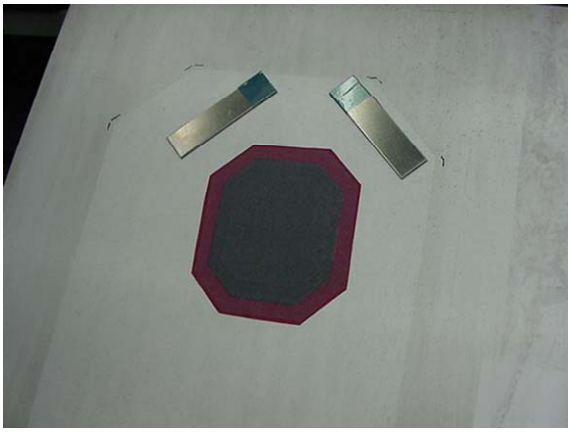

**Figure A-20: Place Adhesive Strip on Back of Witness Coupons and Place Doubler and Witness Strips on Prepared Surface**

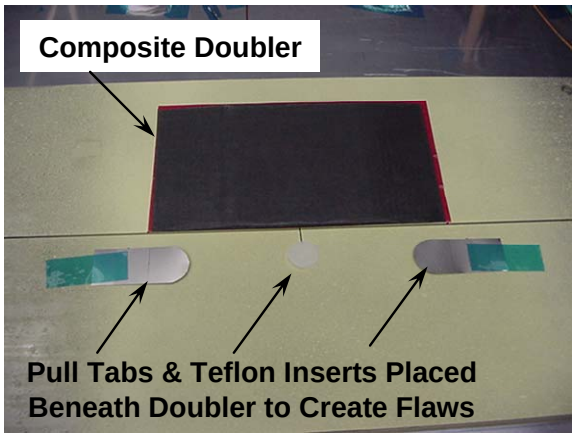


**Figure A-21: Place Doubler on Prepared Steel Surface**

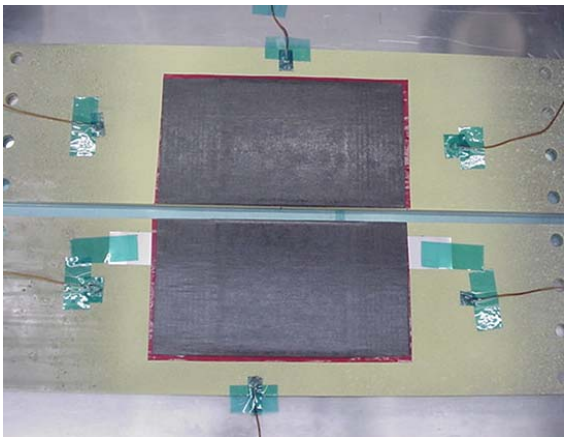

**Figure A-22: Two Composite Doublers in Place; Six Thermocouples Placed To Control Cure Temperatures**

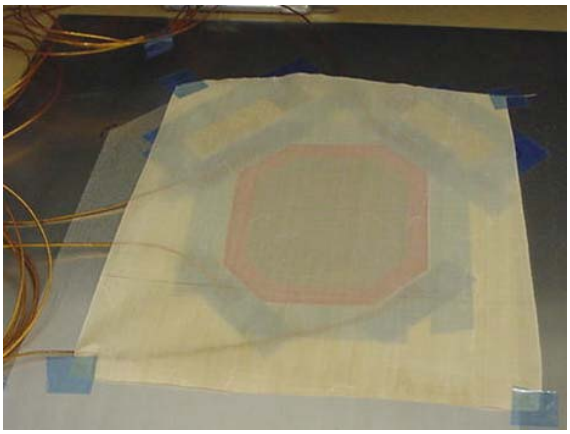

**Figure A-23: Place Armalon Release Fabric**

**Figure A-24: Place Multiple Plies of Bleeder Cloth**

**Figure A-25: Place Non-Perforated Release Film**

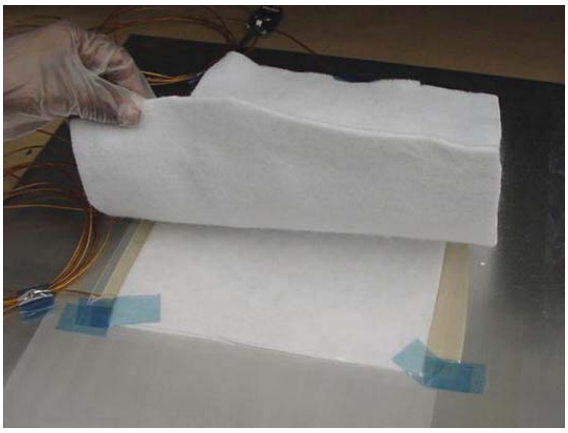

**Figure A-26: Place Breather Mat**

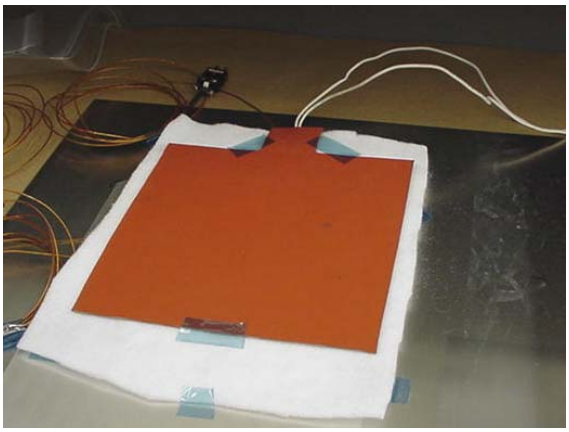

**Figure A-27: Place Heat Blanket**

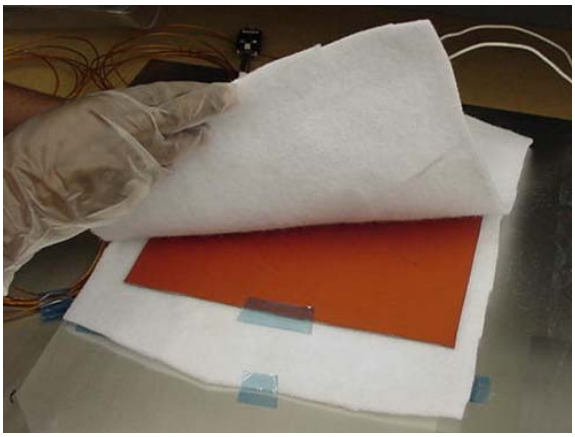

**Figure A-28: Place Breather Mat**

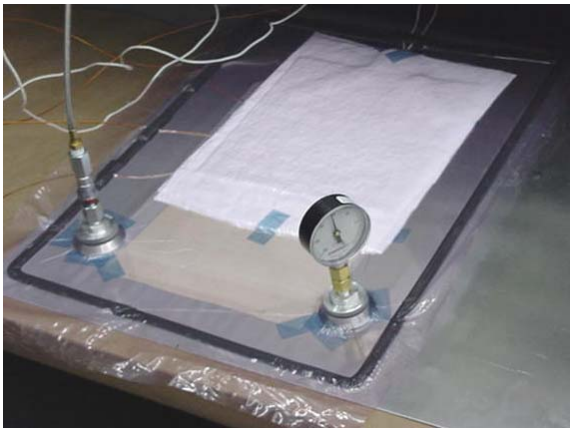

**Figure A-29: Install Vacuum Bag**


**Figure A-30: Program the Heat Control System for Cure Cycle**

**Figure A-31: Hot Bonding Process - Vacuum Bag Pressure with Heat Blanket; Bleeder Cloths for Controlled Resin Bleed; Co-Cure of Primer, Boron-Epoxy Doubler, and Adhesive; Heat Lamps Used to Adjust Local Temperatures**

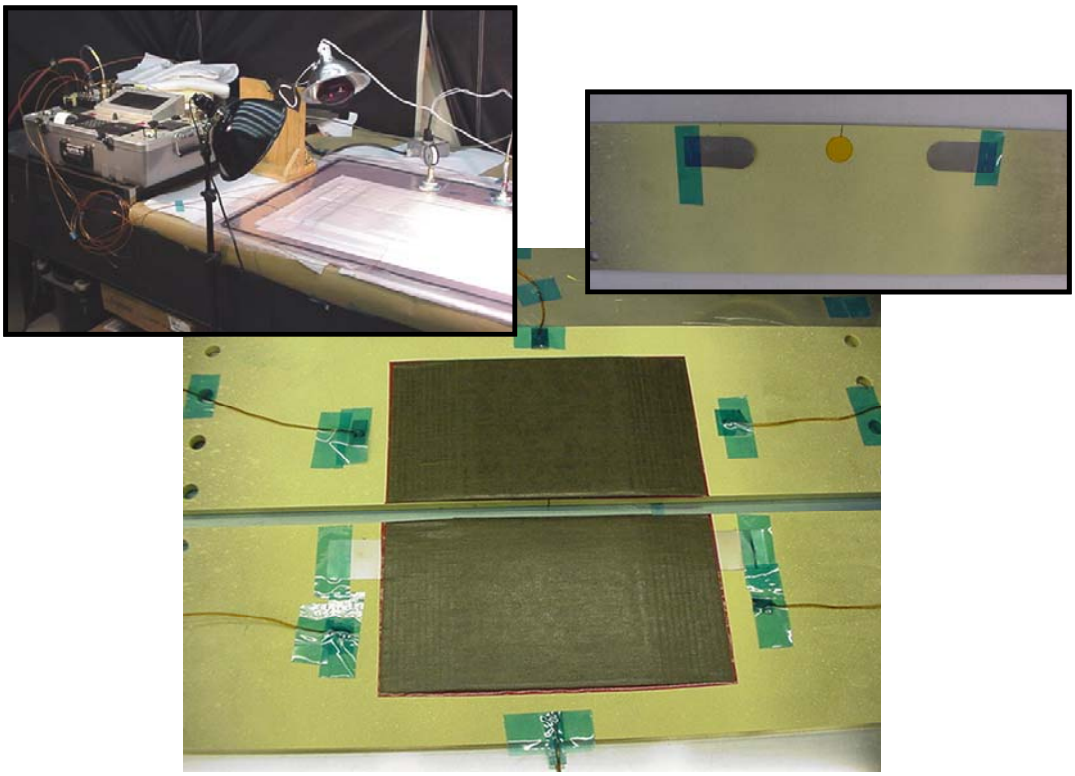

**Figure A-32: Completed Specimens with Composite Doublers Installed; Heat Application (left inset), Flaw Inserts Placed Under Doublers (right inset)**

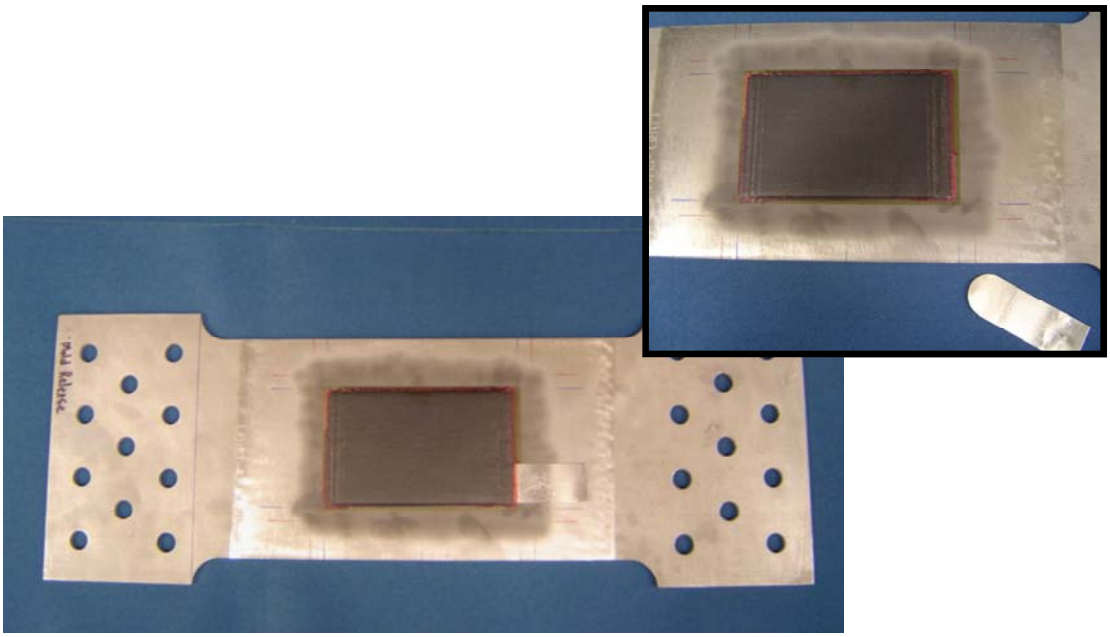

**Figure A-33: Composite Doubler Fatigue Specimens After Installation and with Pull Tab Removed to Create Engineered Disbond Flaw (inset)**

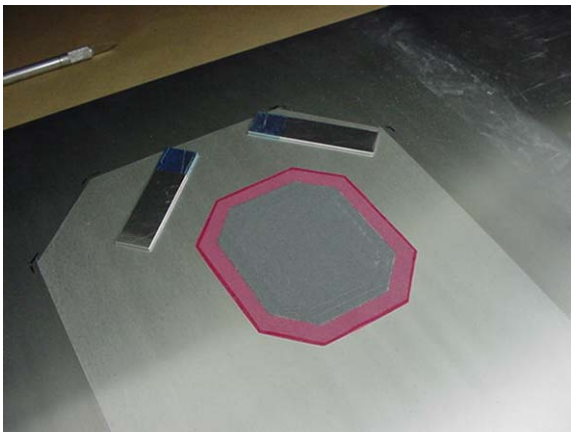

**Figure A-34: Finished Product - Red Color is from Adhesive Layer**

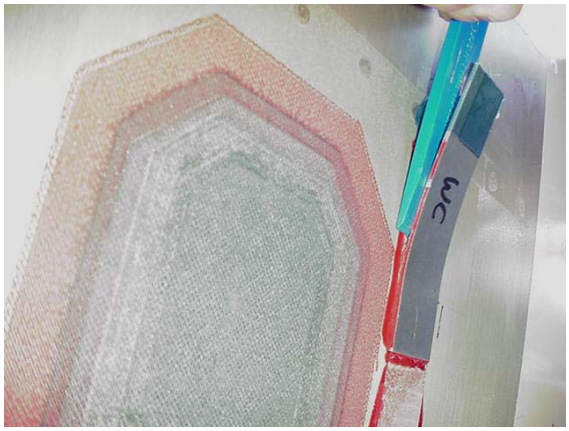

**Figure A-35: Remove Witness Coupon Using a Plastic Wedge; Beige Color is From Fiberglass Cover Ply**

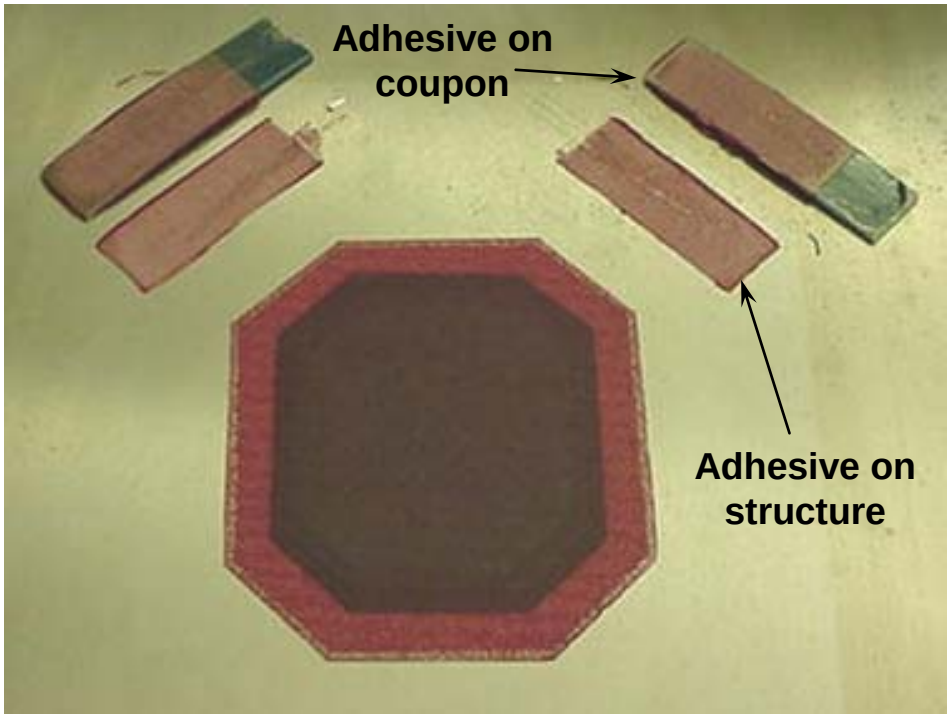


**Figure A-36: Witness Coupons Removed - Note Adhesive on Both Coupon and Parent Skin Indicating That Full Strength of Adhesive Has Been Achieved**

**This Page Intentionally Left Blank**

# APPENDIX B

## Installation Process for Repairing Carbon Steel Structures Using Bonded Composite Doublers

# Installation Process for Repairing Carbon Steel Structures Using Bonded Composite Doublers

## Table of Contents


**1.0 GENERAL……. 185**

**2.0 REPAIR CONSIDERATIONS AND PROCESS FLOWCHART…… 186**

**3.0 TOOLING, EQUIPMENT, AND FACILITY REQUIREMENTS…..… 188**
**3.1 Equipment……..… 188**
**3.1.1 Pressurizing Devices…..……..….. 188**
**3.1.2 Heating Equipment……..…. 188**
**3.1.3 Temperature Control……. 190**
**3.2 Prohibited Materials…….. 191**

**4.0 REPAIR MATERIALS AND SUPPLIES……..… 192**

**5.0 DAMAGE ASSESSMENT…… 193**

**6.0 INITIAL SURFACE PREPARATION – REMOVAL OF ORGANIC SURFACE FINISH……..… 194**
**6.1 Paint Removal…….……..……..….. 194**
**6.2 Basic Surface Cleaning and Preparation……..... 195**

**7.0 MECHANICAL SURFACE PREPARATION BY GRIT BLASTING… 196**

**8.0 CHEMICAL SURFACE PREPARATION: SILANE TREATMENT METHOD FOR ADHESIVE BONDING…….…… 199**
**8.1 Silane Preparation Process…… 199**
**8.1.1 Silane Mixing…….……. 199**
**8.1.2 Silane Application…….……..…….. 200**
**8.1.3 Silane Pre-Cure Process…… 200**
**8.2 Application of Bond Primer (Post Silane)…….……..….... 201**
**8.2.1 Removal of Moisture from Primer..……..……..…. 201**

**9.0 FABRICATE WITNESS COUPONS (Peel-Proof Strips)……..... 201**

**10.0 BORON/EPOXY DOUBLER REPAIR……..… 204**
**10.1 Preparation of Boron/epoxy Doublers……. 204**
**10.2 Preparation of Film Adhesive……..… 206**
**10.3 Doubler Installation……..… 206**
**10.3.1 Co-Cured Doublers……..... 206**
**10.3.2 Preparation for Cure……..….. 207**
**10.3.3 Process for Doubler Cure to Steel Structure……..… 208**

**11.0 POST-REPAIR INSPECTION..……..… 211**

# Installation Process for Repairing Carbon Steel Structures Using Bonded Composite Doublers

## 1.0 GENERAL

This section establishes the procedures for the repair of steel structures using adhesively bonded Boron/epoxy co-cured doublers. This procedure utilizes a 225°F-cure Boron/epoxy structural material. The surface preparation is critical for metal bond repairs. The procedure involves a grit blast surface roughening to enhance mechanical adhesion, followed by the application of silane & primers to chemically enhance the bonding process.

**Typical Composite Doubler Installation** - Figure B-1 shows a typical bonded composite doubler repair over a cracked parent steel structure. The doubler consists of a series of Boron/epoxy composite plies that are stacked and debulked to produce a cohesive laminate repair patch. The number of plies and fiber orientation are determined by the nature of the reinforcement required (i.e. stress field and configuration of original structure). The taper at the edge of the doubler is used to produce a gradually increasing stress gradient in the area of primary load transfer. A top ply of fiberglass is installed to supply mechanical and environmental protection for the installation. Surface preparation is the most critical aspect of the doubler installation. This consists of paint removal, solvent clean, light abrasion, grit blasting and chemical treatment (silane/primer) to ensure proper adhesion. Since the doubler must be installed in the field, vacuum bag pressure and in-situ heat sources (e.g., heat blankets, ceramic heaters) are used to simultaneously cure the composite laminate and adhesive layer.

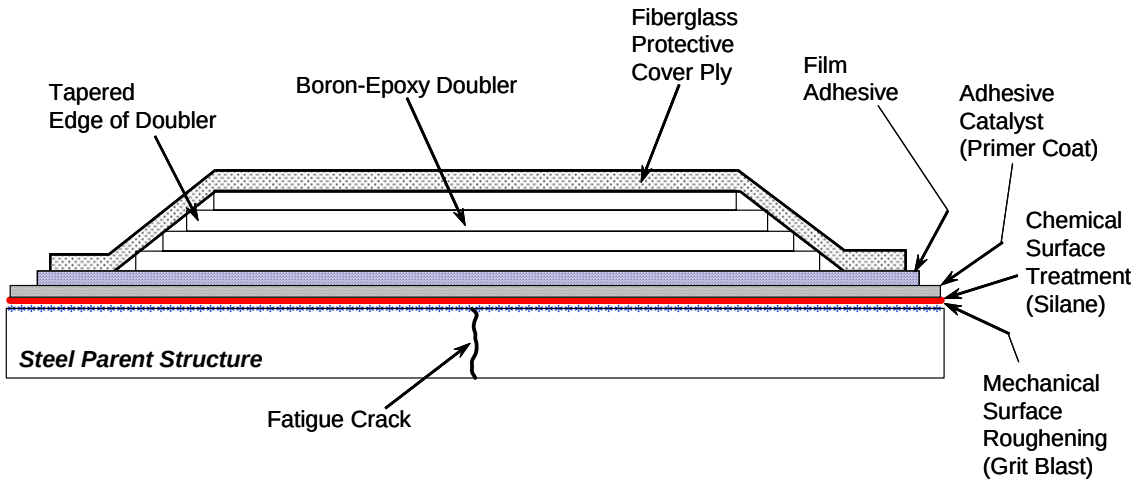


***Single heat cycle: co-cure of Silane, primer, adhesive, composite doubler and fiberglass cover ply***

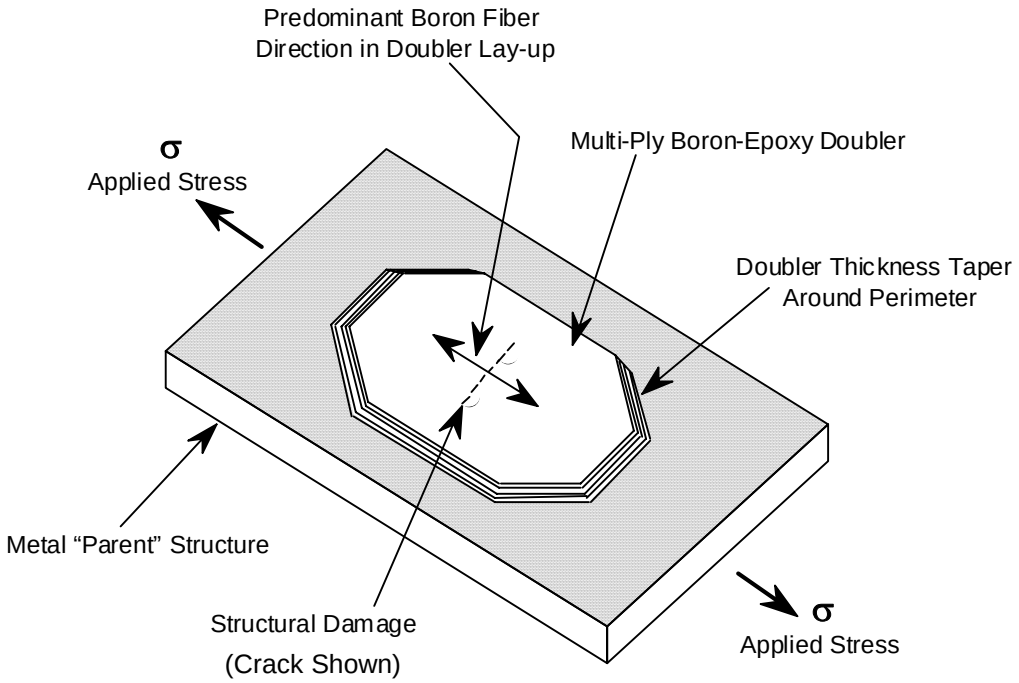


**Figure B-1: Schematic and Isometric Views of a Bonded Composite Doubler Repair**

## 2.0 REPAIR CONSIDERATIONS AND PROCESS FLOWCHART

1. Contour of repair shall not be excessive for the thickness of the repair doubler chosen. The application may require a caul plate or special tooling.

2. Repair area surface should have a relatively even surface with local surface anomalies not to exceed .010 inches deep for abrupt thickness changes & 0.25" deep for gradual undulations of the surface.

3. Radius of curvature should not be less 0.5 inches.

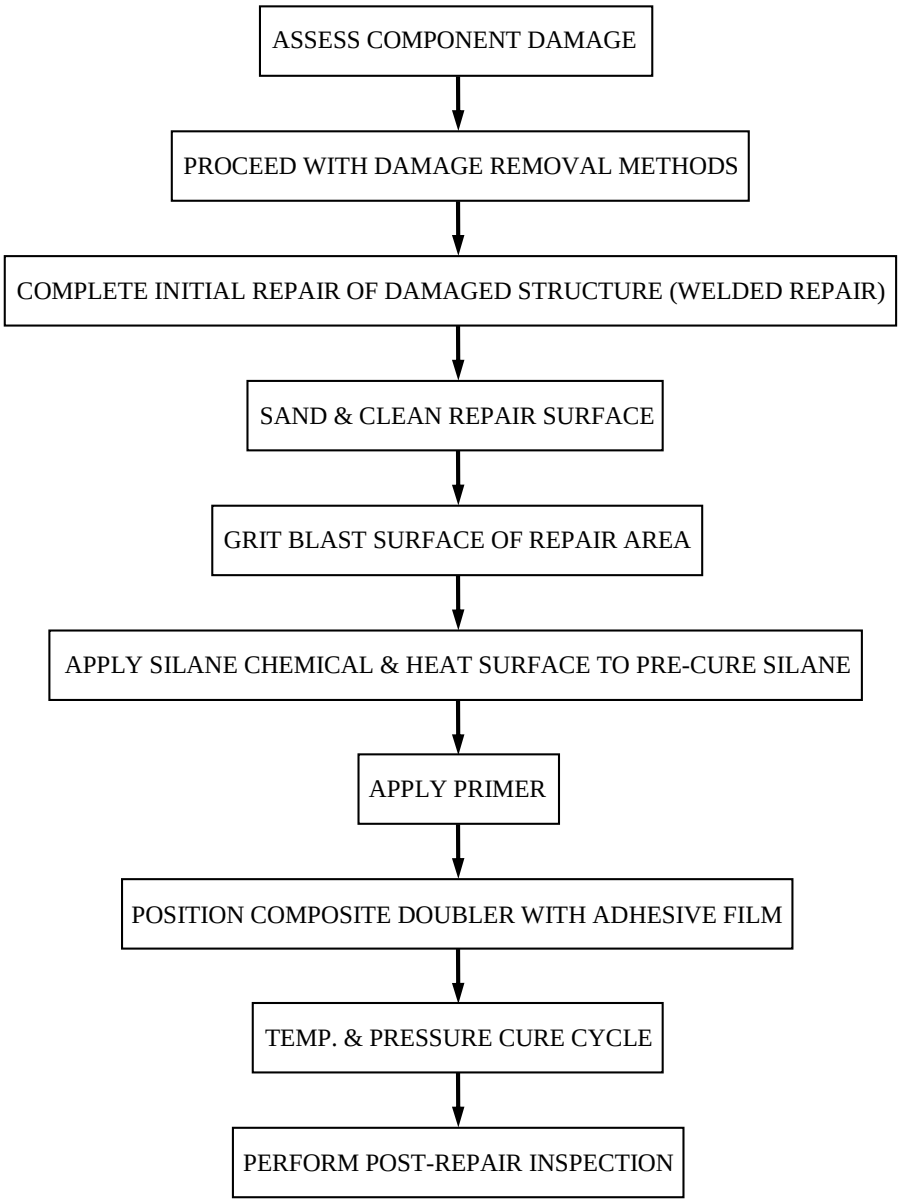


**Figure B-2. Repair Flowchart for Installing Composite Laminate on Steel Structure**

## 3.0 TOOLING, EQUIPMENT, AND FACILITY REQUIREMENTS

Processing procedures outlined herein are for preparation, lay-up, and cure of Boron/epoxy repairs. They are to be used only in areas of reasonable cleanliness when temperatures at the repair surface are between 32°-85°F. Protect all bond surfaces from oil mist, exhaust fumes, and gases, soot, rain, dust, and other particulate matter. All equipment requiring calibration shall only be used if it is still within its calibration date.

### 3.1 Equipment

#### 3.1.1 Pressurizing Devices

A vacuum bag is used to maintain the 17 in.Hg. pressure required to debulk and bleed out excess resin in the Boron/epoxy repair. It is also used to assist in holding repair items, such as heat blankets, insulation layers, and thermocouples in contact with the repair area.

#### 3.1.2 Heating Equipment

Required power and type of heating equipment will be determined by the thickness of the parent structure along with other geometry features of the repair area. Heating equipment shall be compatible with the pressurizing devices. Heating equipment to cure the primer, adhesive and doubler includes:

A. Heat Lamps – Either tungsten filament or quartz tube.

B. Electric Heating Blankets – Electric heating blankets (shown in Figure B-3) are an efficient means of heating the bondline. The direct heating approach achieved with the heat blanket is shown in Figure B-4. The blanket should have 5 Watts/square inch minimum capability and provide continuous heating across the cure area.

C. Hot Bonder – Used for the control of the cure cycle during the bonding of the doubler. It controls the vacuum pressure and the temperatures of the heat blanket and monitors the corresponding thermocouples during the cure cycle. This item must be kept within calibration in order to use for the bonding application.

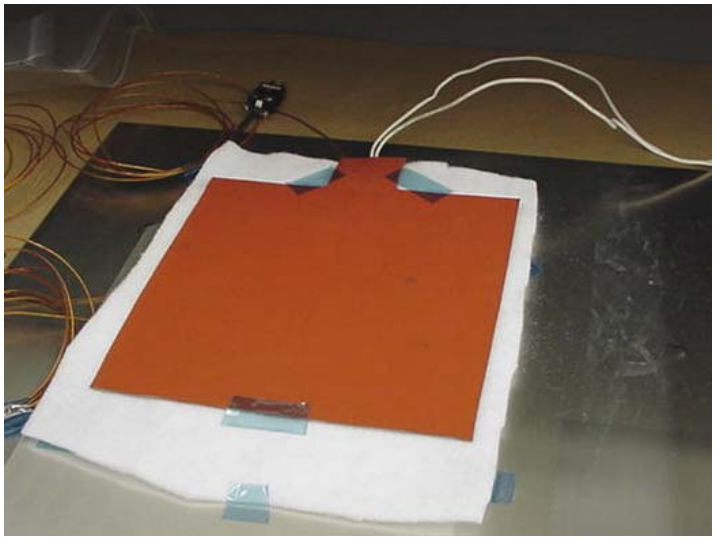

**Figure B-3 Heating Blanket with Insulation on Underside**

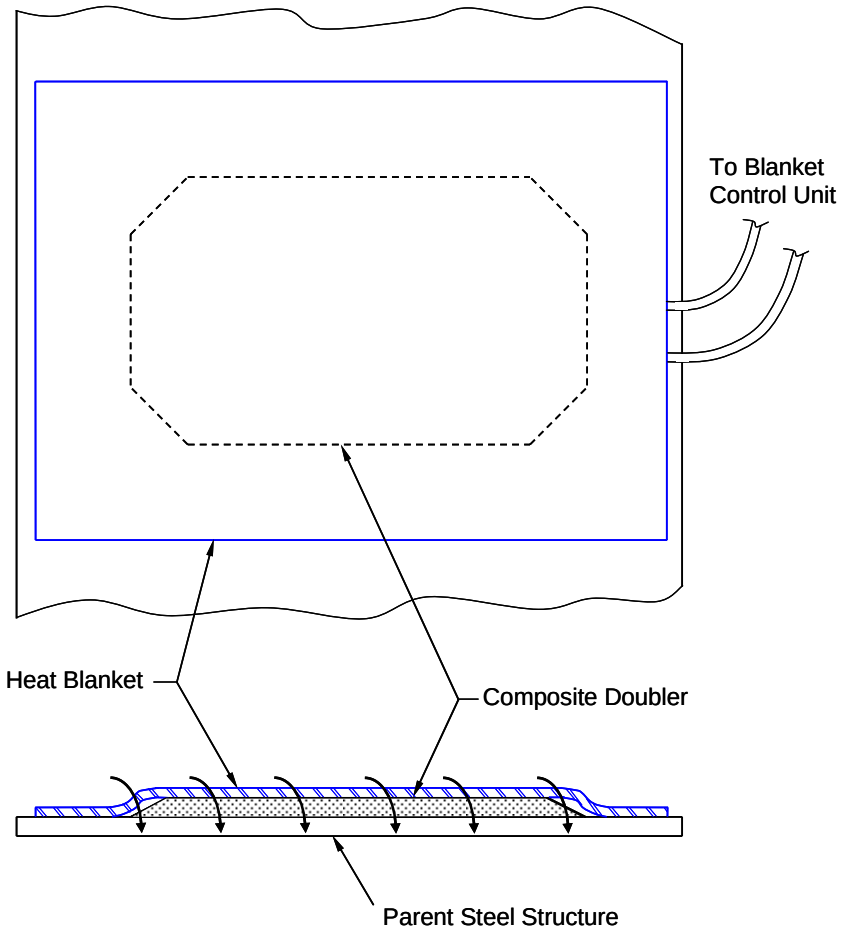

**Figure B-4 Basic Concept of Direct Heating Using Heat Blankets**

D. Ceramic Heating Elements – Flexible Ceramic Pad Heaters provide an effective way to heat thick structures for doubler repair. The ceramic heaters provide 28 Watts/square inch of heating surface and can provide the projection heating approach shown in Figure B-5. It is crucial to properly locate the heaters such that the target temperatures for the doubler cure cycle can be achieved.

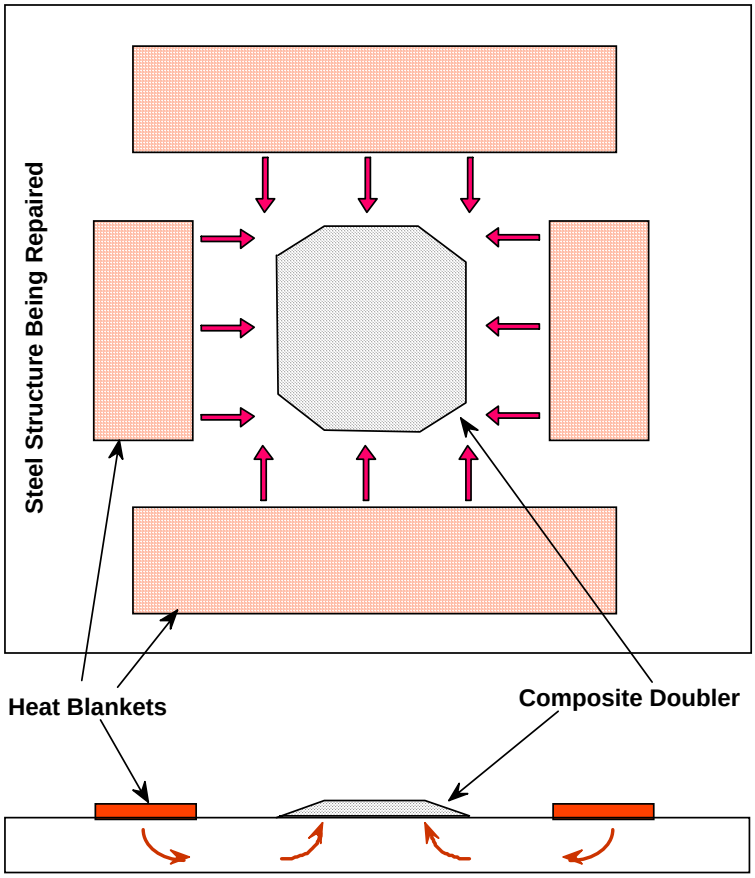


**Figure B-5 Basic Concept of Projection Heating**

### 3.1.3 Temperature Control

The temperature in and around the bond area shall be controlled in accordance with the appropriate cure cycle for bonded composite doubler repairs (see section. 10.0). During the heating process, the thermocouples should be monitored at least once per minute for the first 10 minutes, once every 5 minutes until the temperature has stabilized in the cure range, and once every 15 minutes thereafter until cure is complete.

The maximum temperature deviation between any two thermocouples in the curing area shall not exceed 40°F during the ramp-up phase and 25°F during the constant temperature cure phase. Record all readings or, alternately, monitor all readings at the stated intervals until the temperature is stabilized in the cure range. The temperature measuring system shall be capable of measuring temperatures up to 300°F with ±5 °F accuracy. Use 20-gage or finer thermocouple wire. Insulating materials and/or heat lamps may be used as required to improve temperature control or protect selected areas from heat.

## 3.2 Prohibited Materials

All oils, greases, and silicone compounds shall be prohibited from the immediate repair area during all bonding operations. Do not attempt to perform a bonded repair on any surface that is suspected of being contaminated by silicone compounds or other bond-inhibiting chemicals.

## 4.0 REPAIR MATERIALS AND SUPPLIES

See Table B-1 (Sheets 1 through 2) for repair materials and supplies needed for doubler repair.

| MATERIAL | SUPPLIER |
|---|---|
| Abrasive cloth (alum. oxide paper, 150 & 220-grit or finer) | Commercially available |
| Acetone | Fisher Scientific |
| Adhesive, Film (AF-163) | 3M Company<br>Springfield, MO |
| Adhesive, Film (FM73) | Heatcon Composite Systems<br>Seattle, WA |
| Air Filters, In-line, Balston models 2104N-1B1-BX and 2104N-1B1-DX | Parker Hannifin Corp, Filtration and Separation Div., Tewksbury, MA |
| Air Grinder, High Speed (rear exhaust) | Commercially Available |
| Auto Mixer w/magnetic stirrer (150-250rpm) | Fisher Scientific |
| Bleeder cloth (10 mil, 2.5 oz., bleeder fabric, 350°F use) | Airtech International Inc.<br>Huntington Beach, CA |
| Boron/epoxy Prepreg Tape, 5521F/4 | Specialty Materials Inc.<br>Lowell, MA |
| Breather cloth, 10 oz., 400°F cure | Airtech International Inc.<br>Huntington Beach, CA |
| Breather Cloth, 4 oz., 350°F cure | Airtech International Inc.<br>Huntington Beach, CA |
| Ceramic Heat Blankets | Cooperheat MQS Inc.<br>Houston, TX |
| Crown Spra - Tool Jar (#8212) | Fisher Scientific |
| Crown Spra - Tool Power Pac (#8211) | Fisher Scientific |
| Crown Spra - Tool spray head (#8213)) | Fisher Scientific |
| Distilled Water | Commercially Available |
| Fiberglass Cover Ply Material (style 120 glass pre-preg fabric) | Heatcon Composite Systems<br>Seattle, WA |
| Gloves, latex | Commercially available |
| Grit Blast System | Clemco Industries Corp.<br>Washington, MO |

**Table B-1: Composite Doubler Repair Materials and Supplies (sheet 1)**

| MATERIAL | SUPPLIER |
|---|---|
| Grit, Aluminum Oxide, 50 Micron | S.S. White Technologies |
| HeatCon HCS9200 Hot Bonder system (w/thermocouples and heat blankets) | Heatcon Composite Systems<br>Seattle, WA |
| Methyl Alcohol 99+% | Fisher Scientific |
| Paper Cutter | Commercially Available |
| Primer, BR6747-1; Type IA | Cytec Industries<br>West Paterson, NJ |
| Propanol | Commercially available |
| Release Fabric, Armalon (peel ply) | National Aerospace Supply<br>San Juan Capistrano, CA |
| Release Film, Non-perforated | Heatcon Composite Systems<br>Seattle, WA |
| Respirator with organic cartridge | Commercially available |
| Sanding Disks Grit (180-grit) | Abrasive Sales<br>Las Vegas, NV |
| Silane (3-Glycidoxypropyltrimethoxysilane, 98%) | Fischer Scientific<br>(Aldrich Chemical Co. Inc) |
| Tape, Flash Breaker, 1-inch and 2-inch | Airtech International Inc.<br>Huntington Beach, CA |
| Vacuum Bag Film (Nylon, Vac-Pac #8171) | Airtech International Inc.<br>Huntington Beach, CA |
| Vacuum device (Venturi positive air-to vacuum converter or equivalent) | Commercially available |
| Vacuum Sealant Tape | Heatcon Composite Systems<br>Seattle, WA |
| Wipes, lint-free (technicloth, cleanroom) | Fisher Scientific |

**Table B-1: Composite Doubler Repair Materials and Supplies (sheet 2)**

## 5.0 DAMAGE ASSESSMENT

A. This paragraph covers damage assessment methods.

B. Steps in assessing damage are as follows:

(1) Locate damage.

(2) Evaluate damaged area to determine type, depth, and size (see Table B-2).

(3) Re-assess after damage removal. If necessary, complete an Eddy Current Inspection at the end of any welding process to confirm that there is no cracking in or beyond the repaired area.

(4) Record size of repair for doubler sizing and future reference.

| Type of Defect | Inspection Method | | | |
|---|---|---|---|---|
| | Visual | Eddy Current | Ultrasonic | X-ray |
| External Damage | X | | | |
| Structural Cracks | | X | X | X |

**Table B-2. Typical Methods for Non-Destructive Inspection of Damage**

## 6.0 INITIAL SURFACE PREPARATION-REMOVAL OF ORGANIC SURFACE FINISH

### 6.1 Paint Removal

A. The following procedures are for removing paint and other finishes in the area of the repair.

B. Procedure for Removal of Organic Surface Finish

(1) Apply aluminum foil or polyester masking tape around repair area approximately 3 inches beyond the doubler footprint on all sides.

(2) Remove paint and primer:

(a) Use approved paint stripper and rinse with tap water.

(b) Use a plastic scraper or lightly apply fine grit sandpaper to complete removal of paint following the application of paint stripper.

**WARNING:** PAINT STRIPPER IS AN AGENT THAT IS AN IRRITANT. MAKE SURE ALL PERSONS OBEY ALL OF THE PRECAUTIONS WHEN PAINT STRIPPER IS USED.

- DO NOT USE IN AREAS WHERE THERE IS HIGH HEAT, SPARKS, OR FLAMES.
- USE IN AN AREA OPEN TO THE AIR.
- CLOSE THE CONTAINER WHEN NOT USED.

– DO NOT GET PAINT STRIPPER IN THE EYES, ON THE SKIN, OR ON YOUR CLOTHES.
– DO NOT BREATHE THE GAS.

**WARNING**: REFER TO THE APPLICABLE MANUFACTURER'S OR SUPPLIER'S MSDS FOR:
– MORE PRECAUTIONARY DATA
– APPROVED SAFETY EQUIPMENT
– EMERGENCY MEDICAL AID

TALK WITH THE LOCAL SAFETY DEPARTMENT OR AUTHORITIES FOR THE PROCEDURES TO DISCARD THIS HAZARDOUS AGENT.

## 6.2 Basic Surface Cleaning and Preparation

- **Note: Safety goggles, latex/rubber gloves, and proper ventilation (exhaust) system must be used when completing initial solvent wipe and degrease steps in this process. Safety goggles and leather gloves should be used when performing the abrade step. In most cases the volume, quantity, and duration of chemical use are low. Exposures are also intermittent because a given operation is seldom carried out continuously for more than 15-30 minutes at a time. See the appropriate MSDS for hazard information and any safety concerns for specific chemicals in use. Note: If an MSDS for a specific chemical is not available, that chemical should not be used.**

- Before starting degrease process ensure that the proper Personnel Protection Equipment (PPE) including latex/rubber gloves, goggles/safety glasses, and proper ventilation is available.

- Wipe off the masked area of the specimen with one of the following solvents: acetone, or isopropyl alcohol. With a lint-free cloth, wipe in one direction, frequently turning the cloth to a clean surface.

- Abrade the repair area using a 180-grit sanding disk with the air grinder set to the proper pressure (80-90 psi). Note: Depending on the hardness of the surface scale, it may be necessary to use a coarser sanding disk to start the paint/scale removal process. However, always finish with a 180-grit sanding disk. Visually check for any signs of corrosion, nicks, or scratches and carefully blend them out, removing the minimum metal possible.

Degrease using the following: methyl alcohol spray down (rinse) followed by acetone spray down (rinse) and wipe. **Note: Ensure proper PPE is being used for degrease and abrade processes. All excess rinse from this step must be captured and disposed of properly per all the applicable requirements.**

## 7.0 MECHANICAL SURFACE PREPARATION BY GRIT BLASTING

**NOTE: This operation has a 2-person requirement to set-up and perform grit blasting. The person doing the grit blasting may need to complete the appropriate (Respiratory Protection) training. The person doing the grit blasting will be required to wear a respirator helmet during blasting. Personnel participating in this task should have completed all the appropriate training required by company guidelines.**

- Review Safety and Health Hazards associated with Abrasive Blast Systems for safety issues and operating requirements. Inquire if personnel performing the operation have current training.

- Ensure all required PPE (steel-toe boots, blast suit, leather gloves, ear plugs, respirator helmet, face shields, dust mask, oxygen monitor, and goggles) is on-site. Inspect each item to make sure it is in good working condition (i.e., no tears or holes in blast suit) for each person participating in the operation.

- Set-up area where actual blasting will take place with proper containment for grit media (tarps, or other barriers). Establish barrier and appropriate signage such that no one enters area of grit blasting unless wearing proper protective gear.

- Set-up equipment for each specific operation by determining the placement of each structure to be repaired relative to the grit blast equipment. Special care should be given to the location of the air pump (away from any possible hazardous fumes and dust from blast area). Also, if using a compressor for the pressurized air source ensure its placement is downwind and to the side of the blast area.

- Test the operation of the air pump with respirator connected for proper air pressure (8-10psi) and flow followed by fit adjustments of respirator for user. To prevent excessive heat build-up in the respirator hose, stretch-out the hose and keep it in shaded areas when possible. (**Shut-off respirator air supply pump when not in use.)** The air pump inlet filter should be checked every 100hrs. of operation (per mfr. suggestion). Replace the outlet filter cartridge at least every 200hrs. of operation. Start and stop times of the air pump should be logged on a data card attached to the air pump.

- Oxygen Monitor Set-up - activate the monitor and let it warm-up and stabilize for 3-5 minutes in a known region of acceptable breathing air. Check the readout. It should be at 20.9%-21%. If in 2-3 minutes the monitor is not at the expected level, then adjust the monitor until it does register the appropriate reading.

- Place the oxygen monitor next to the respirator air pump and check at regular intervals (1-5 mins.) during the use of the respirator to insure an acceptable oxygen level. If the oxygen monitor is below the acceptable limit of 19.5%, alert the person using the respirator immediately and halt the blasting operation.

- Ground the grit blast machine if the operator of blast hose is getting static shocks from the operation of the grit blaster.

- Insert appropriate blast nozzle into blast hose and check for any unusual wear.

- Load abrasive into blast machine by pouring it into the concave head through the screen attachment. **The appropriate PPE for this step include latex gloves, goggles, and dust mask.**

- Direct air at ≤ 30psi from compressed air source through air hose to remove any existing moisture. Connect appropriate air filters (Balston BX & DX) in-line with the air source (to remove water and oil from the air supply). Connect a regulator downstream to insure proper air pressure control.

- See Figure B-6 for location of specific valves on grit blast system.

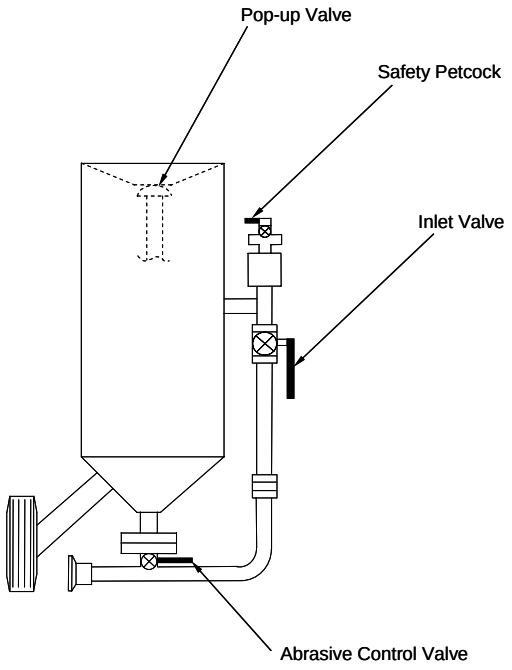


**Figure B-6 Grit Blast System with Basic Valve Controls**

- Before attaching air hose to blast machine open the safety petcock on the remote control valves, open the inlet valve (handle parallel with pipe) and ensure air pressure from compressor or house air is set to the proper setting and does not exceed the requirements of the blast system (125psi).

- **Always open safety petcock during work breaks and before filling the blast machine with blast media, to prevent unintentional blasting.**

- Ensure that all hoses are properly connected with no air leaks and that all safety cables are connected. (Recommendation: use safety cable when connecting air line to blast machine).

- Adjust air pressure (60-80 psi) at the regulator near the grit blast machine to the appropriate pressure for desired blast results.

- Before starting to blast, establish communication and stop signals between the safety observer and the blaster wearing the respirator helmet. Put on the appropriate protective gear (PPE). The blast operator must wear a blast suit, leather gloves, steel-toed shoes and respirator helmet. Make sure the air pump is on before putting on the respirator helmet. The observer (non-blast operator) also must have on a dust mask, goggles, and latex gloves.

- The start times of the air pump and blast machine should be recorded by the observer.

- Close the inlet valve, to allow the pop-up valve to seal off the filling port. If the pop-up valve does not seal on first attempt try re-opening and closing the inlet valve several times and raising the pressure ($\leq$ 100 psi) if necessary.

- When the pop-up valve seats properly, adjust the abrasive control valve for the proper air/abrasive blend. As a general rule, use as little abrasive as possible. The stream of abrasive coming out of the nozzle should barely discolor the air when seen against a light colored background.

- After the abrasive control valve is properly adjusted and the pressure regulator is set to the proper pressure (60-80 psi), the grit blast process is ready to begin. Note, blasting parameters should be explained to user for consistent surface results. This will include the proper operating pressure, distance nozzle should be from blasting surface (1.50-2.00 inches), setting of abrasive control valve, and proper speed in which to move the nozzle over the surface. The entire surface to be bonded should be scanned at least twice in two perpendicular directions. Once while moving back & forth in the horizontal rows and scan again while moving up & down in vertical rows. Select areas may need to be re-blasted if a visual inspection reveals that the surface finish does not look uniform.

- Note: A certain amount of abrasive surge is normal at start-up. Should the flow of abrasive continue to surge, quickly close and open the inlet valve to stabilize the flow.

- Once blasting is completed open the petcock to reduce the pressure in the system prior to disconnecting the air line. Disconnect the air line from the blast system. Record the stop time on the equipment usage log card attached to the blast machine.

- Collect the spent blast media. All equipment should be cleaned by wiping the excess media from its surfaces. This includes removal of media from any tarps or barriers used to contain the drift of blast media.

Clean-up involves: 1) wiping down adjacent areas covered with the spent blast media, 2) recovering all the spent media by sweeping, and 3) putting spent media into appropriate containers for disposal. Personnel participating in media clean-up must put on appropriate PPE (goggles, latex gloves, and dust mask). If winds cause the spent media to become air borne during cleanup, this work should be completed by personnel wearing the respirator helmet.

- When finished with the respirator system, the safety observer should shut Oxygen Monitor unit off and record the time at the end of the monitoring session.

- Attach the oil and water filters to a compressed air line and use a dusting nozzle to blow any media remaining on the area to be bonded.

## 8.0 CHEMICAL SURFACE PREPARATION: SILANE TREATMENT METHOD FOR ADHESIVE BONDING

The final surface preparation method is a Silane treatment followed by the primer application.

### 8.1 Silane Preparation Process

#### 8.1.1 Silane Mixing

- **Note: Safety goggles, latex/rubber gloves, and ventilation (exhaust) system must be used when completing silane mixing. In most cases the amount of silane used and the duration of use are low. Exposure times last on average from 1-2 hours during the mixing/application process. See the appropriate MSDS for hazard information and any safety concerns when using silane. Note: If the current MSDS is not available, then the silane process should not be started.**

- Mix Silane in a clean glass or polyethylene beaker using a solution of 99 parts (weight or volume) of distilled water and 1 part (+1/-0) of Dow Corning Z6040 Silane (Glycidoxypropyltrimethoxysilane). A 100ml (3.4 oz.) of solution is sufficient to treat a 60 square inch (0.42sq. ft.) area. Approximately 31oz. of Silane mix would be needed to cover a 4 sq. ft. area.

- Place a clean mixing magnet in the beaker. Cover the beaker to avoid contamination and agitate on a magnetic mixer for a minimum of 1-hour prior to use. Continue agitating until the solution is used. Max. solution life is 4 hours after the 1 hour mix.

### 8.1.2 Silane Application

- When the application area is prepped for Silane treatment, clean a bristle brush with acetone and rinse with distilled water. Use the brush to apply the Silane solution to the repair area for a minimum of 10 minutes after the entire area is wet. **(Note: All excess Silane solution must be captured for proper disposal per all applicable requirements.)**

- While applying the liquid solution, inspect the treated area for water breaks. If a water-break-free surface is not achieved, the process must be restarted at the mechanical surface prep step (grit blast).

- Apply Silane solution to the repair area continuously to maintain a film of solution on the surface throughout the 10-minute time period. Do not allow the surface to dry. **Ensure that the brush does not touch the surrounding uncleaned structure.**

  **Note: Complete the following step only if the repair surface does not drain sufficiently on its on accord.**

- Connect an air nozzle to approved highly filtered air, and remove the Silane solution from the repair area by starting at the center of the repair area and working outward in all directions. **Do not allow anything to be blown onto the treated area from the surrounding areas and make sure the air pressure is set at ≤ 20 psi before starting.**

### 8.1.3 Silane Pre-Cure Process

- Place 1-4 thermocouples around the perimeter of the treated area without touching the area to be repaired. The thermocouple ends must be in contact with the surface and taped with high temperature tape. Plug the thermocouples into either a hot bonder or thermocouple reading device.

- Insulate around the repair area (if necessary) to achieve good thermal distribution. Insulation materials must be temperature resistant to at least one and a half times the curing temperature.

- Center infrared lamp(s) or other heating device over the repair area without allowing anything to touch the repair surface. Apply heat to the repair area until all thermocouples are in a range of 120° F to 160° F. Maintain heat for 60 minutes plus 5 minutes, minus 0 minutes, monitoring the thermocouples and adjusting the heat source as necessary. Record temperatures throughout the cure cycle. Prevent cross ventilation to the repair area as much as possible.

It may be necessary to build a temporary screen or curtain from bagging material to prevent wind from crossing the repair site and causing contamination or thermal cooling problems. **If Silane cure temperature exceeds 215°F, the silane cure process must be started over.**

- The recommended time allowed between Silane drying and application of heat is 30 minutes. This time must not exceed 60 minutes.

- After the 1-hour Silane cure, remove the infrared lamp(s) or other heating devices. Allow the repair area to cool to 100°F or ambient whichever is higher.

- The surface is now ready for primer application.

### 8.2 Application of Bond Primer (Post Silane)

**The application of the primer requires the following safety precautions. The proper PPE must be used when spraying the primer. This includes; latex/rubber gloves, lab coat, a full-face air-purifying respirator (combo cartridge for both vapors & particulate) and, if operating indoors, local exhaust ventilation (e.g., laboratory hood, canopy hood) must be located in the area of the application and operated when applying this primer (Cytec-Fiberite BR6747-1). The user of the respirator must complete the proper training prior to this operation and be approved to use the respirator. The lab room or spray area (20 ft. radius) must be vacated with the exception of the personnel wearing the respirators. See the appropriate MSDS for additional hazard information and any safety concerns when using this primer.**
**Note: If MSDS is not available, then the primer process should not be started.**

Apply Cytec-Fiberite BR 6747-1 adhesive primer onto the bond surface to obtain a cured film thickness of 0.0001 to 0.0004 inch (0.1 to 0.4 mil). Method of application should be with an atomizing sprayer.

#### 8.2.1 Removal of Moisture from Primer

A. Use infrared lamps to drive off water. Apply heat @ 120° - 150° F for 15-20 minutes. Allow structure to cool to less than 100° F.

## 9.0 FABRICATE WITNESS COUPONS (Peel-Proof Strips)

Witness Coupons for Wedge Tests –For this quality assurance test, two steel strips are bonded to the parent structure immediately adjacent to the doubler. Preparation of the steel strips takes several hours and must be completed before the installation of the doubler is to take place.

As part of the preparation for this process, remove the appropriate primer (BR6747-1) from the refrigerator a half hour prior to the application and mix it well ensuring there is no sediment left in bottom of container. After installation, a plastic or phenolic wedge is used to pry the strips off the structure as shown in Figure B-7. If adhesive is found on both the steel strip and the steel structure, this indicates that the adhesive fractured (cohesive failure) rather than disbonded (adhesive failure). Thus, the surface preparation is good and the full adhesive strength has been achieved. Figure B-8 depicts this surface preparation QA test and the two potential failure modes.

A. Prepare the surface of a 0.060" to 0.070" thick steel sheet with the same surface prep being used on the steel structure. Starting by making a water-break-free surface on the sheet. Next, complete the Silane surface preparation per section 8.0. This includes the application of the appropriate primer.

B. Once completed with surface prep and treatment (Silane), the sheet is ready to be primed using the appropriate primer.

C. Cut the steel sheet into 1" x 4" strips taking precautions to not contaminate the prepped surface. A minimum of two witness coupons are needed for each repair area.

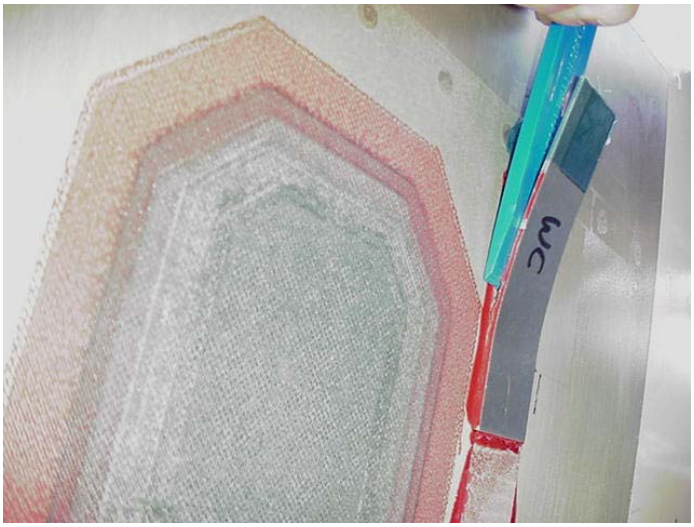

**Figure B-7. Plastic Wedge being used to Pry Off Witness Coupon**

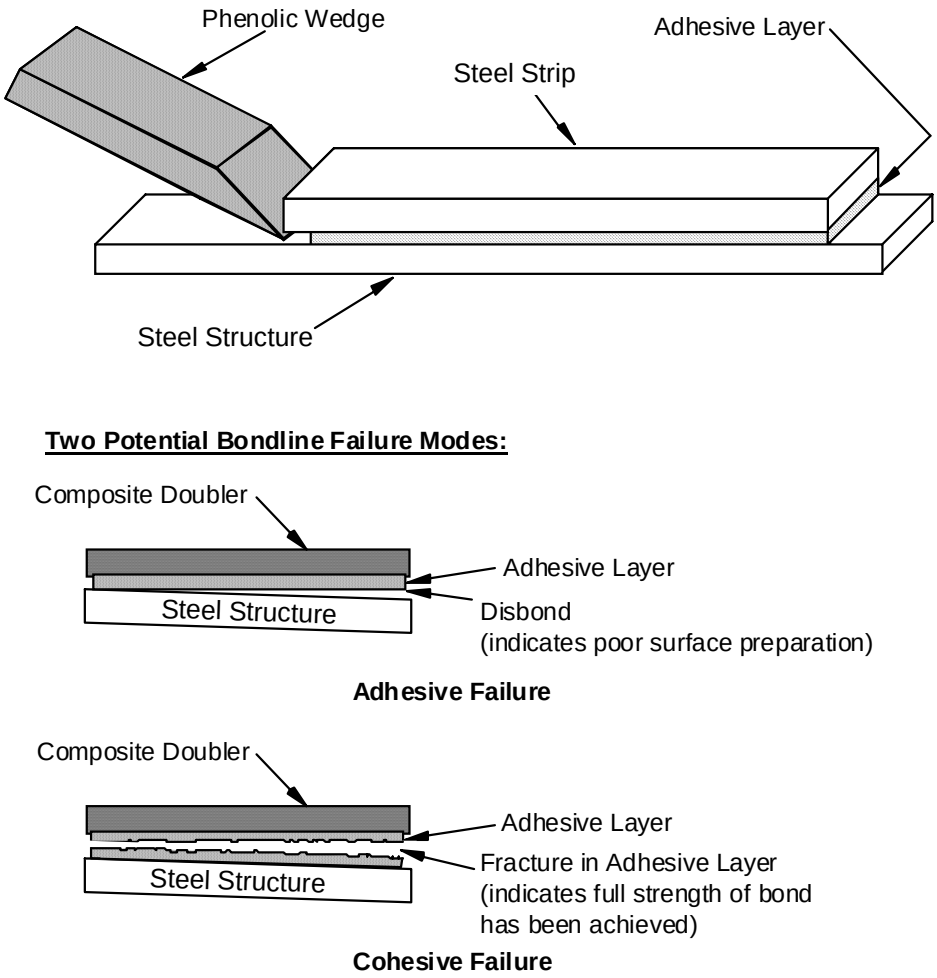


**Figure B-8 Use of Witness Coupons in Quality Assurance Wedge Test for Surface Preparation**

D. Take witness coupons and wrap a 1” wide piece of flash breaker tape around one end of the coupon ensuring that tape is flush with the end. A 1” x 1” area is now covered with tape as shown in Figure B-9.

E. With the adhesive removed from the freezer cut 1” x 3” strips of the adhesive and apply them to the end of the coupons without the tape as shown in Figure B-9. Once this step is completed and adhesive is stuck to each witness coupon, place them into a clean protective bag and put into the freezer until needed during doubler application.

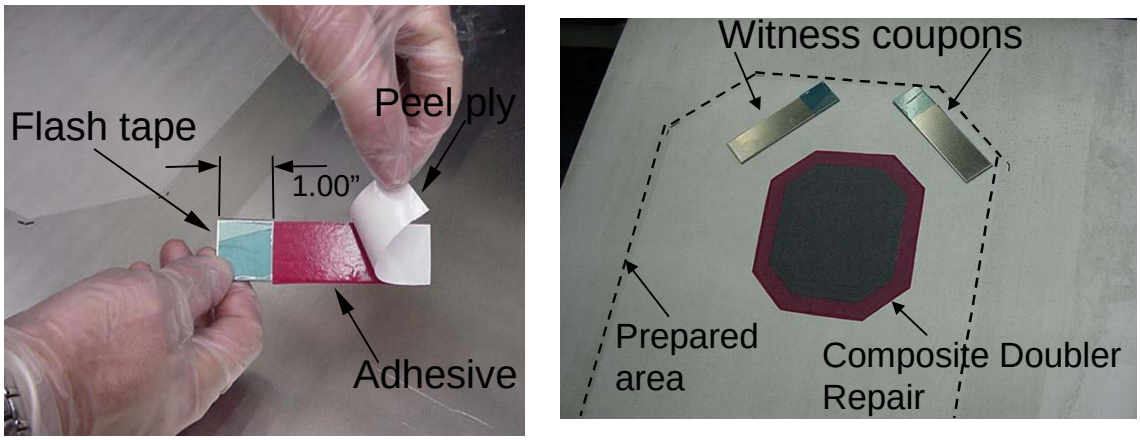


**Figure B-9 Application of Adhesive Strips to Witness Coupons and Placement of Coupons Next to Doubler During Cure Process**

## 10.0 BORON/EPOXY DOUBLER REPAIR

### 10.1 Preparation of Boron/epoxy Doublers

To make optimum use of time, doublers may be assembled prior to or in parallel with the surface preparation operations.

A. Remove the pre-impregnated Boron/epoxy tape from the freezer. Allow the prepreg to thaw at room temperature, not to exceed 100°F, until all condensation has evaporated from the exterior of the bag.

**CAUTION:** Do not unseal the bag until condensation has completely evaporated.

B. Freezer out-times shall be recorded for all time-and-temperature sensitive material and noted on the roll condition log.

**Note:** Boron/epoxy manufacturer guarantees 10.5 days out-time at 70°F. Material out time is reduced above 80°F.

C. Boron/epoxy tape shall be cut in an area free from contaminates. Clean, non-contaminating gloves shall be worn during all cutting and handling operations. Uncured tape shall be protected from contamination prior to cure.

D. Boron fibers will dull cutting blades quickly. Ensure that fresh sharp blades are used for all cuts on Boron/epoxy tape. A shearing (paper) cutter, rolling knife blade, or scissors will provide longer cutter life.

E. Boron/epoxy plies shall be cut to the dimensions and fiber orientations of the applicable doubler drawing. Mylar templates can be used to aid the cutting & fiber orientation process.

F. Cut plies shall be layed-up in the drawing stacking order. When possible, layup the doubler in a controlled contamination area then transport the doubler to the repair area.

G. Manually sweep each ply down using a non-contaminating polyethylene sweep or hand roller (see Fig. B-10). Vacuum debulk the layup every 4-6 plies at a minimum (see Figure B-10).

H. Tape material that has gaps between tows greater than 0.03" shall not be used in the fabrication of doublers.

I. Plies shall be applied with the backing paper side facing up. The backing paper shall be carefully removed after the ply has been pressed in place. Note: the first ply is the only ply to be placed with the backing paper down. This backing paper should be left in place for the duration of the doubler lay-up process. Continue until all boron epoxy plies & the fiberglass cover ply have been placed and debulked. The fiberglass cover ply should be larger than the Boron/epoxy doubler footprint by 0.5 inches in all directions.

J. Place assembled doublers into clean protective sealed bags. Place sealed doublers in refrigerated storage unless they will be cured in the next 24 hours.

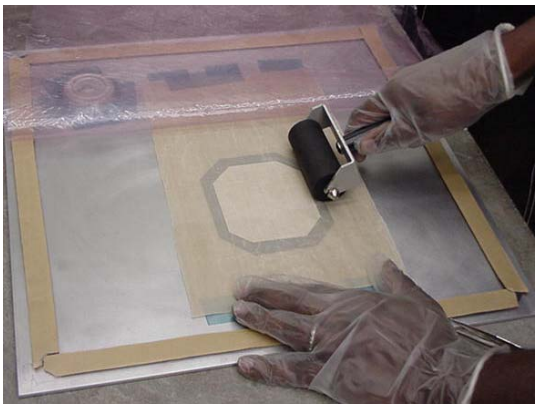

Sweeping down each ply of doubler during lay-up

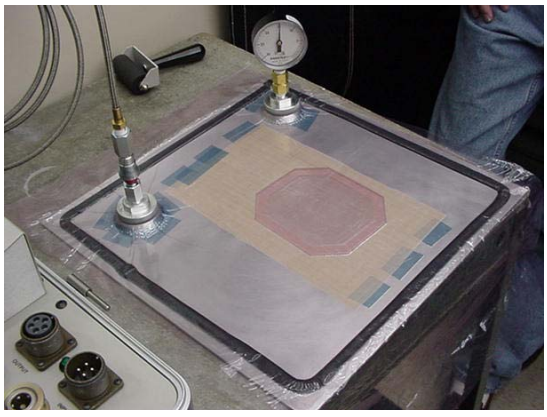

Vaccum debulk of doubler every 4 plies minimum

**Figure B-10. Manual Sweep of Each Ply and Vacuum Debulk of Doubler Lay-Up**

## 10.2 Preparation of Film Adhesive

A. Remove film adhesive from the freezer. Allow the adhesive to thaw at room temperature, not to exceed 100°F, until all condensation has evaporated from the exterior of the sealed bag.

**Note:** Do not unseal the bag until condensation has completely evaporated.

B. Freezer out-times shall be recorded for all time-and-temperature sensitive material and noted on the roll condition log.

**Note:** Film adhesives have 10 days out-time at 70°F. Material out-time is reduced above 90°F.

C. Film adhesive shall be cut in an area free from contaminates. Clean, non-contaminating gloves shall be worn during all cutting and handling operations. The film adhesive may be pre-kitted in sealed bags alone or with Boron/epoxy material. Return kits to cold storage prior to use and draw as necessary.

D. Cut film adhesive for each bond faying surface. The film adhesive should be placed on the bottom of the doubler and trimmed such that it is larger than the fiberglass cover ply by at least 0.125 inches in all directions. Do not fold or stretch the adhesive film. One or more additional plies of adhesive may be needed in areas with surface irregularities. Small sections of added adhesive should be used to fill local voids and undulations in the surface to provide an even surface for uniform doubler contact/bonding.

## 10.3 Doubler Installation

The operations of this section apply to the installation of patches to the repair area and the subsequent cure operations. Apply the adhesive and composite doubler to the silane treated and primed surface using the process described below. Avoid relative movement of the parts being bonded during assembly. Co-cure the adhesive, composite doubler, according to the temperature profiles described below.

### 10.3.1 Co-Cured Doublers

A. If not already available, remove the film adhesive and doublers from the freezer. Allow the adhesive and doublers to thaw at room temperature, not to exceed 100°F, until all condensation has evaporated from the exterior of the sealed bag.

B. Lightly mark the outline of the repair surface with a non-contaminating marker. Place doubler centerline indicators outside the perimeter of the surface prepped area.

These centerline marks, in both x and y directions, will be used to properly locate the doubler, heat blankets, and insulation materials.

C. Apply film adhesive to the bottom bond surface of the Boron/epoxy doubler. Remove any backing paper from the bottom of the doubler before applying adhesive.

D. Apply the Boron/epoxy doubler & adhesive film to the repair surface in the stack-up and orientation indicated on the engineering drawing. Assure that the film adhesive extends beyond the edge of the cover ply by .125 inches all-around.

### 10.3.2 Preparation for Cure

A. Apply flash breaker tape around the edge of external details to allow adhesive squeeze-out (flash) to run out onto the tape and aid in post-cure cleanup.

B. When specified by the responsible engineer, a witness coupon shall be fabricated and cured concurrent to the repair doubler as shown in Figure B-9. The witness coupon shall be an adhesive bonded steel lap shear panel per Figure B-9. The lap shear blank surfaces shall be prepared for bonding concurrently with the Silane treatment and priming operations.

C. Bag the doubler laminate in accordance with Figure B-11. Note that one ply of bleeder cloth should be used for each 3-4 plies of Boron/epoxy material in the doubler.

D. Apply vacuum pressure of 17” ± 2”Hg to the bag. Remove the vacuum source and verify that the bag vacuum pressure loss is less than 1”Hg over a 1 minute period. If the leak rate is greater than this find the vacuum leak and repeat this step. If it can be identified that the leak is outside the patch area and the leak path will not be across the patch then the leak is acceptable as long as the proper pressure can be maintained.

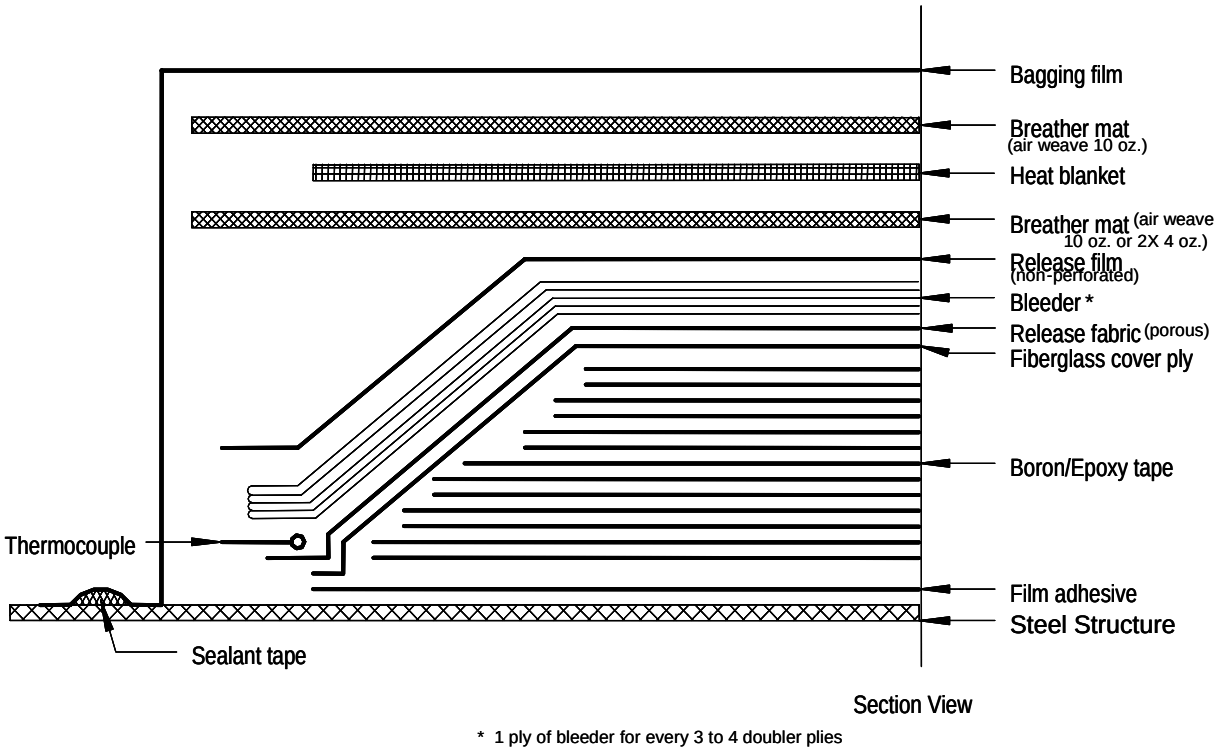


**Figure B-11. Vacuum Bagging for Cure of Doubler on Steel Structure**

### 10.3.3 Process for Doubler Cure to Steel Structure

A. Autoclave cure cycles shall be performed in accordance with Figure B-12.

B. When using portable heating equipment for cures, a temperature survey on the repair surface may be desirable. Additional insulation, controller programming changes, additional heaters, and/or other measures may be required to maintain adequate temperature control on some surfaces. At least four thermocouples should be used to monitor and control the temperature in the repair region.

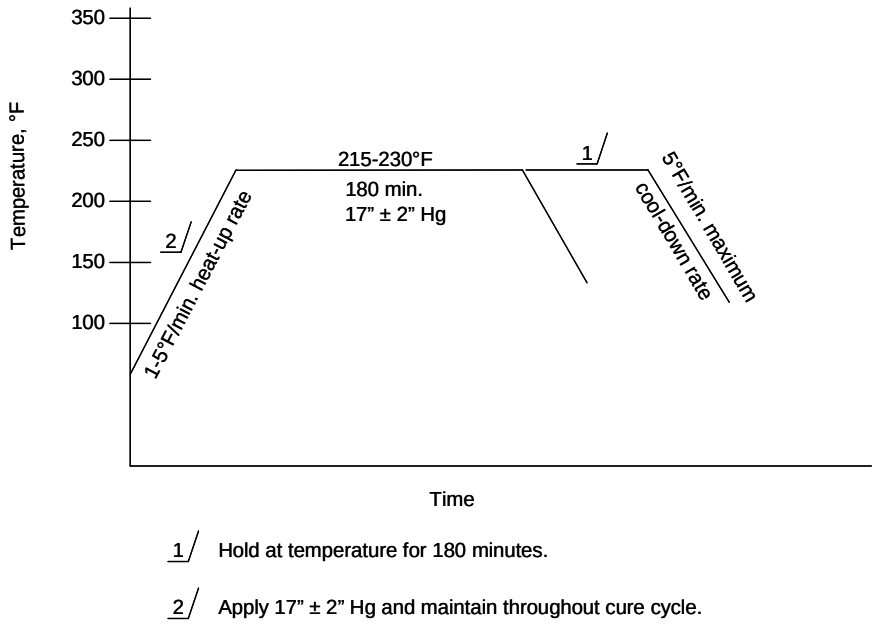


**Figure B-12. Cure Cycle for Doubler Installation on Steel Structure**

C. Cure cycles achieved with portable heating equipment shall use the following parameters:

(1) Apply 17" ±2"Hg vacuum pressure to the bag.

(2) Ramp from ambient to cure temperature at 1-5°F/minute heat-up rate.

(3) Hold at cure temperature per Table B-3.

| CURE TEMPERATURE (°F) | CURE TIME (Min.) |
|---|---|
| 240-255 | 90+30/-0 |
| 215-230 | 180+30/-0 |
| 190-205 | 360+30/-0 |

**Table B-3. Times at Cure Temperature for Doubler Installation on Steel Structure**

(4) Ramp down at 5°F/minute maximum from cure temperature to less than 140°F under full pressure.

D. Remove bagging material from doublers (see finished product shown in Figures B-13 & B-14).

E. Fillet seal periphery of doubler using MIL-S-81733 or equivalent sealant for environmental protection.

F. Prime the steel repair surface, then paint the repair area and the Boron/epoxy doubler using approved paint material.

G. Stencil the following note, in a contrasting color, and locate the note on the Boron/epoxy doubler: "Bonded Repair, Do Not Apply Paint Strippers in This Area".

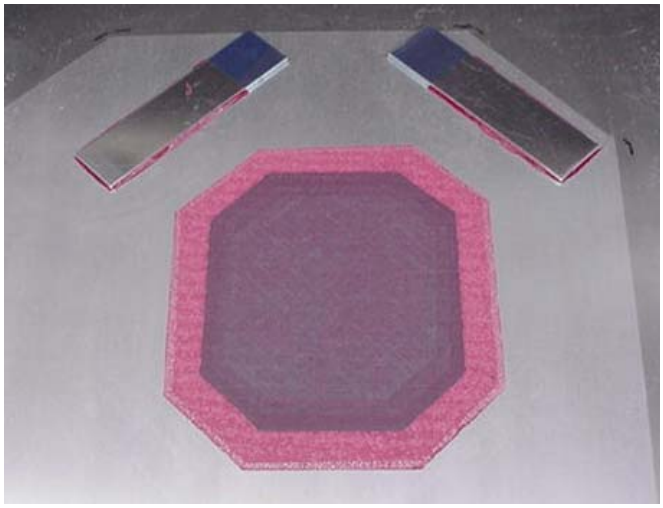

**Figure B-13 Sample Composite Doubler Repair with Witness Coupons**

**Figure B-14 Finished Product – Composite Doubler Repair Installed on Metal Aircraft Structure**

## 11.0 POST-REPAIR INSPECTION

A. Remove witness coupons using a wedge as shown in Figure B-6. If adhesive can be seen on the steel structure and the coupon surface then a cohesive fracture has occurred. This indicates a good surface preparation where the full strength of the adhesive can be achieved.

B. Visually inspect periphery of doubler to ensure that a bead of cured adhesive is evident. An area lacking the bead may indicate a void area. Conduct this inspection before item E in section 10.3.3.

C. Inspect installation using the ultrasonic inspection technique for composite doublers.

D. Disbonds and delaminations in the taper region shall not exceed 0.5 inches in diameter. A maximum of 5% of the central area of the doubler may have delaminations or voids. The central area is defined as the region of the Boron/epoxy doubler that is full thickness. The total number of disbonds and delaminations shall not exceed 2 in any doubler and shall be separated by 3 inches minimum.

E. Flaws found should be reported to engineering for disposition. If repair is defective, remove and repeat repair process.

F. Inspect Boron/epoxy doubler repair at the 6-month and 1-year intervals and thereafter during routine maintenance/inspections of the structure being repaired.

**This Page Intentionally Left Blank**

# APPENDIX C

## Design and Analysis Guidelines for Composite Doubler Repairs

# Design and Analysis Guidelines for Composite Doubler Repairs

The guidelines contained in Appendix C are applicable to repairs applied to one side of a defective structural member. The guidelines apply to repair of: 1) Cracks in metallic structure, and 2) metallic structure in which damage has been removed. The nomenclature used here is defined at the end of the Appendix.

The steps required for repair design are:

- Calculate the required patch thickness.
- Assess the component criticality and significance of the repair.
- Determine the structural loads appropriate for the design.
- Evaluate the design condition of the repair on the basis of the load capacity of the bond.
- Check the structural integrity of the repaired structure.
- Check the repair and structure for fatigue susceptibility.
- Calculate the required patch dimensions.
- Determine inspection requirements.

## CALCULATE THE REQUIRED PATCH THICKNESS

Patch thickness shall restore the original stiffness over the defect. Although a thickness is preferred which provided a stiffness match with the parent structure, a higher stiffness up to 20% above the parent structure stiffness is acceptable. The patch thickness required for a repair is therefore determined from:

$$\frac{E_i t_i}{E_o} \le t_o \le \frac{1.2 E_i t_i}{E_o} \qquad \text{(C-1)}$$

The variables are as shown in Fig. C-1.

## DETERMINE THE STRUCTURAL LOADS

The applied load is used to determine the Design Condition for the repair and to verify structural integrity and fatigue resistance. The remote load away from the defect is taken as DUL as determined from:

a. If Design Ultimate Load (DUL) is known, that load shall be used.
b. If Design Limit Load (DLL) is known, the load is taken as 1.5 times the load associated with DLL.
c. Where DUL and/or DLL are not known, design shall be based on the lower value of the load based on a reasoned engineering assessment taking into account issues such as

changes in section in the load path, stress concentrations, net section stresses, fastener bearing strength or buckling load limitations.

## EVALUATE THE DESIGN CONDITION OF THE BOND

The level of rigour required to develop repair designs is based on a comparison of the load capacity of the repair adhesive with the design loads, and the significance of the structure being repaired.

### Calculate the Potential Load Capacity of a Single Overlap Joint Allowing for Thermal Stresses

The load capacity is given by the lesser value of:

$$P = E_i t_i \left[ \left( \alpha_o - \alpha_{i_{eff}} \right) \left( RT - T_{cure} \right) + \left( \alpha_o - \alpha_i \right) \left( T_{oper} - RT \right) \right] + \sqrt{2\eta\tau_p \left( \frac{1}{2}\gamma_e + \gamma_p \right) E_i t_i \left( 1 + \frac{E_i t_i}{E_o t_o} \right)} \quad \text{(C-2)}$$

and,

$$P = 2E_o t_o \left[ \left( \alpha_{i\,eff} - \alpha_o \right) \left( RT - T_{cure} \right) + \left( \alpha_i - \alpha_o \right) \left( T_{oper} - RT \right) \right] + \sqrt{2\eta\tau_p \left( \frac{1}{2}\gamma_e + \gamma_p \right) E_o t_o \left( 1 + \frac{E_o t_o}{E_i t_i} \right)} \quad \text{(C-3)}$$

where

$$\alpha_{i_{eff}} = \frac{\alpha_i \left( 1 + \nu_i \right)}{2} \quad \text{(C-4)}$$

Note: adhesive data may be interpolated between known data points.

## EVALUATE STRUCTURAL INTEGRITY OF REPAIRED STRUCTURE

### A. Determine the Far-Field Stress Associated with DUL

The far-field stress for analysis of the repair is determined from DUL and the thickness of the structure at the defect:

$$\sigma^* = \frac{\mathbf{DUL}}{\mathbf{t_i}} \quad \text{(C-5)}$$

**B. Check the Structural Integrity of the Structure at the End of the Patch**

The maximum stress in the structure at the end of the patch is estimated from:

$$\sigma^{**} = \Omega_L \sigma^{*} + \left[E_i \left( \left( \alpha_o - \alpha_{i_{eff}} \right) \left( RT - T_{cure} \right) + \left( \alpha_o - \alpha_i \right) \left( T_{oper} - RT \right) \right) \right] \qquad \text{(C-6)}$$

where $\Omega_L$ is the load inclusion factor (see Table C-1) to allow for load attraction into the repair area due to the stiffness added by the patch. A Margin of Safety of 0.2 is recommended where:

$$MOS = \frac{\sigma_{ULT_i}}{\sigma^{**}} - 1 \qquad \text{(C-7)}$$

**C. Calculate the Stress Under the Repair**

Calculate the localized stress under the repair away from the defect:

$$\sigma_o = \frac{E_i t_i}{\left( E_o t_o + E_i t_i \right)} \sigma^{**} \qquad \text{(C-8)}$$

**D. Check the Adhesive Shear Strain**

The maximum shear strain in the adhesive (adjacent to the defect) is given by:

$$\gamma_o = \frac{\sigma_o t_i \lambda}{G} \qquad \text{(C-9)}$$

where

$$\lambda^2 = \frac{G}{\eta} \left( \frac{1}{E_i t_i} + \frac{1}{E_o t_o} \right) \qquad \text{(C-10)}$$

If the maximum strain value exceeds the elastic strain limit for the adhesive, the adhesive will be plastic near the defect, and the shear strain is given by:

$$\gamma_o = \frac{\tau_p}{2G} \left( 1 + \left( \frac{\sigma_o t_i \lambda}{\tau_p} \right)^2 \right) \qquad \text{(C-11)}$$

**E. Calculate the Stress Intensity in a Repaired Metallic Structure**

The following step is applicable to repair of cracks in metallic structures using single overlap repairs. The stress intensity for a repaired crack shall be calculated and compared with the fracture toughness of the material. The stress intensity of repaired cracks approaches an

asymptote, a value of stress intensity which the repaired crack never exceeds. The asymptotic stress intensity after repair is given by:

$$K_\infty = \sigma_o \sqrt{\frac{E_i t_i \lambda \eta}{G}} \tag{C-12}$$

for elastic behaviour in the adhesive, or

$$K_\infty = \sqrt{\frac{E_i \eta}{G}\left[\sigma_o \tau_p \left(1 + \left(\frac{\sigma_o \lambda t_i}{\tau_p}\right)^2\right) - \frac{\tau_p^2}{3\lambda t_i}\left(1 + 2\left(\frac{\sigma_o \lambda t_i}{\tau_p}\right)^3\right)\right]} \tag{C-13}$$

for plastic behaviour in the adhesive.

**F. Calculate the Peel Stresses**

Peel stresses in adhesive bonds are induced by load path eccentricity. Analytically, peel stresses are determined from vertical equilibrium of shear forces and moments due to load path eccentricity. The maximum peel stress in the adhesive (and the adherend) is given by:

$$\sigma_{c_{\max}} = \tau_p \left(\frac{3E_c' t_o \left(1-\nu^2\right)}{E_o \eta}\right)^{\frac{1}{4}} \tag{C-14}$$

where $\tau_p$ is the shear stress at the end of the adhesive. $E_c'$ is the effective transverse tensile modulus of the adhesive system. For adherends with the same interlaminar stiffness, the effective transverse stiffness shall be approximated by:

$$\frac{1}{E_c'} = \frac{1}{E_c} + \frac{6}{E_N} \tag{C-15}$$

where $E_N$ is the tensile elastic modulus of the adherend in the Normal direction and $E_c$ is the tensile elastic modulus of the adhesive. (The adhesive behavior is influenced by the tensile behaviour of the adherends perpendicular to the joint, and in-plane restraint of Poisson's contractions.)

Tapering of patch ends reduces the outer adherend thickness thereby reducing peel stresses. The reduction in peel stresses can be estimated from:

$$\frac{\left(\sigma_{c\max}\right)_{tapered}}{\left(\sigma_{c\max}\right)_{uniform}} = \sqrt{\frac{2}{1+\left(\frac{t_o}{t_e}\right)^3}} \tag{C-16}$$

where $\mathbf{t_e}$ is the thickness at the end of the taper.

To verify the peel resistance of a repair:

1. Compare the peel stresses with the tensile strength of the adhesive, and the through-thickness strength of the adherends. Currently, insufficient reliable data is available for peel strengths for most adhesives. Therefore, the following guidelines are to be applied:
    - For ductile adhesive systems (FM 73, AF 163, FM 300, and FM 300-2): Maximum allowable peel stress is 10,000 psi.
    - For brittle adhesive systems (AF130-1, AF 131): Maximum allowable peel stress is 6,000 psi.

2. In composite materials, peel stresses may result in delamination of the material. Currently, insufficient reliable data is available for through-thickness tensile strengths for most composite resin systems. Therefore, the following guidelines are to be applied:
    - If the **through-thickness tensile strength** is known, the recommended Margin of Safety is 0.2 above the known value.
    - If the **transverse tensile strength** is known, the recommended Margin of Safety is 0.2 above the known value. For all other repairs to composite materials, or for composite patches, the maximum allowable peel stress is 6,000 psi

**G. Check the Structural Integrity of the Patch**

The maximum stress in the patch is estimated from:

$$\sigma_p = \frac{t_i}{t_o}\sigma^{**} \qquad \text{(C-17)}$$

A Margin of Safety of 0.2 is recommended where:

$$MOS = \frac{\sigma_{ULT_o}}{\sigma_p} - 1 \qquad \text{(C-18)}$$

## CHECK THE REPAIR AND STRUCTURE FOR FATIGUE SUSCEPTIBILITY

This method does provides a simple method for elimination of fatigue critical repairs.

### A. Calculate the Fatigue Stress

For metallic structures, all repairs are to be designed such that the repair is fatigue resistant if subjected to a constant amplitude fatigue loading (with an assumed fatigue ratio $\mathbf{R} = 0$) with a maximum cyclic load equivalent to the lower value of 40% of $\boldsymbol{\sigma}^*$ used in the assessment of structural integrity.

$$\boldsymbol{\sigma}_\mathbf{f} = 0.4\boldsymbol{\sigma}^* \tag{C-19}$$

### B. Check the Fatigue Susceptibility of the Structure at the End of the Patch

The maximum stress in the structure at the end of the patch is estimated from:

$$\sigma^{\#\#} = \Omega_L \sigma_f + \left[\mathrm{E}_i \left(\left(\alpha_o - \alpha_{i_{eff}}\right)\left(RT - T_{cure}\right) + \left(\alpha_o - \alpha_i\right)\left(T_{oper} - RT\right)\right)\right] \tag{C-20}$$

From reference data for the structural material, determine if fatigue damage is anticipated at that stress level.

### C. Calculate the Fatigue Stress Under the Patch

Calculate the localized stress under the repair away from the defect:

$$\sigma^{\#} = \frac{E_i t_i}{\left(E_o t_o + E_i t_i\right)} \sigma^{\#\#} \tag{C-21}$$

### D. Calculate the Fatigue Shear Strain in the Adhesive at the Defect

Adhesives are fatigue resistant, and when properly designed and implemented, bonded repairs are not susceptible to fatigue. The maximum shear strain in the adhesive (adjacent to the defect) is given by:

$$\gamma_f = \frac{\sigma^{\#} t_i \lambda}{G} \tag{C-22}$$

where $\lambda^2 = \dfrac{\mathbf{G}}{\boldsymbol{\eta}}\left(\dfrac{1}{\mathbf{E_i t_i}} + \dfrac{1}{\mathbf{E_o t_o}}\right)$

If the maximum strain value exceeds the elastic strain limit for the adhesive, the adhesive will be plastic near the defect, and the shear strain is given by:

$$\gamma_f = \frac{\tau_p}{2G}\left(1+\left(\frac{\sigma^{\#} t_i \lambda}{\tau_p}\right)^2\right) \qquad \text{(C-23)}$$

The adhesive in the repair is considered fatigue resistant if the maximum shear strain is below twice the elastic shear strain limit.

$$\gamma_f < 2 \times \gamma_e \qquad \text{(C-24)}$$

**E. Calculate the Fatigue Stress Intensity in a Repaired Metallic Structure**

The stress intensity of repaired cracks approaches an asymptote, a value of stress intensity which the repaired crack never exceeds. The asymptotic stress intensity after repair is given by:

$$K_{\infty f} = \sigma^{\#}\sqrt{\frac{E_i t_i \lambda \eta}{G}} \qquad \text{(C-25)}$$

for elastic behaviour in the adhesive, or

$$K_{\infty f} = \sqrt{\frac{E_i \eta}{G}\left[\sigma^{\#}\tau_p\left(1+\left(\frac{\sigma^{\#}\lambda t_i}{\tau_p}\right)^2\right)-\frac{\tau_p^2}{3\lambda t_i}\left(1+2\left(\frac{\sigma^{\#}\lambda t_i}{\tau_p}\right)^3\right)\right]} \qquad \text{(C-26)}$$

for plastic behavior in the adhesive.

From reference data for da/dN variation with stress intensity range, the crack growth rate shall be predicted, from which the repair effectiveness may be determined. Alternatively, if fractographic analysis or recorded NDI result has determined growth rates with structure usage hours, an estimate of the stress intensity range reduction shall enable an estimate of inspection intervals from the past crack growth history.

**CALCULATE THE REQUIRED PATCH DIMENSIONS**

**A. Determine the Required Overlap Length**

The ***overlap*** length, ***L*** is the minimum distance from the edge of the repair patch to the crack or cut-out. The minimum overlap length is to be sufficient to ensure that the adhesive is never the critical element. To achieve this, the minimum overlap **L** is to be 1.5 times the plastic transfer length necessary to carry the stress:

$$L = \frac{1.5\sigma^* t_i}{\tau_p} \qquad \text{(C-27)}$$

for a single overlap repair.

## B. Determine the Overall Patch Length

The minimum overall patch length is twice the overlap length plus the size of the defect. The patch may be longer than this, but in all cases the overlap distance *L* from the edge of the patch to the defect should be observed.

## C. Determine the Patch Width

The patch width is usually determined by consideration of patch shape requirements and the required patch overlap length. For repairs to cracked metallic structure, the minimum patch width is such that the patch covers as much of the crack as possible, and the patch shall extend at least 1.0 in. ahead of the crack tip at both ends. The sides of the patch shall be aligned with the major load direction.

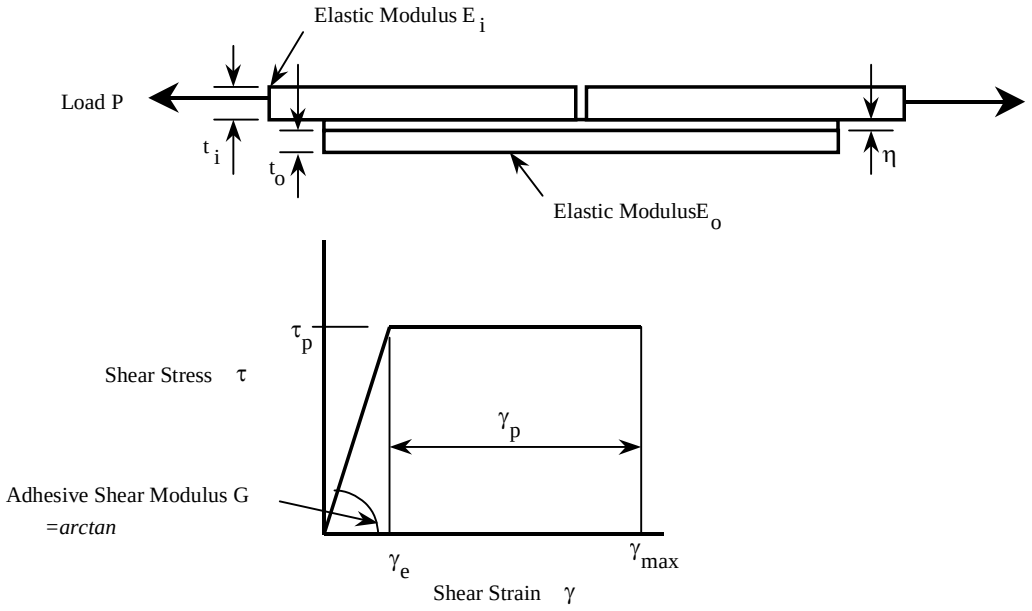


**Figure C-1: Single Supported Overlap Joint Geometric and Material Parameters**

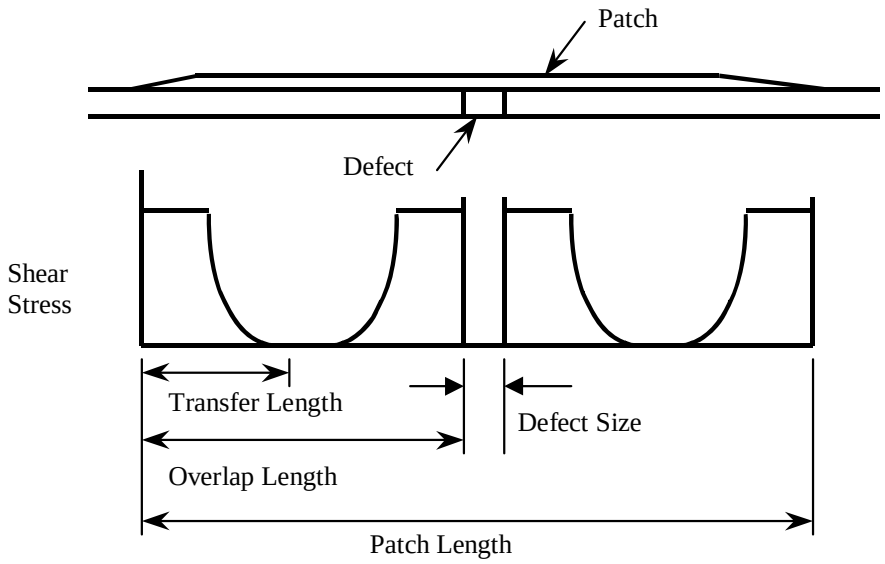


**Figure C-2: Relationship Between Transfer Length, Overlap Length and Patch Length**

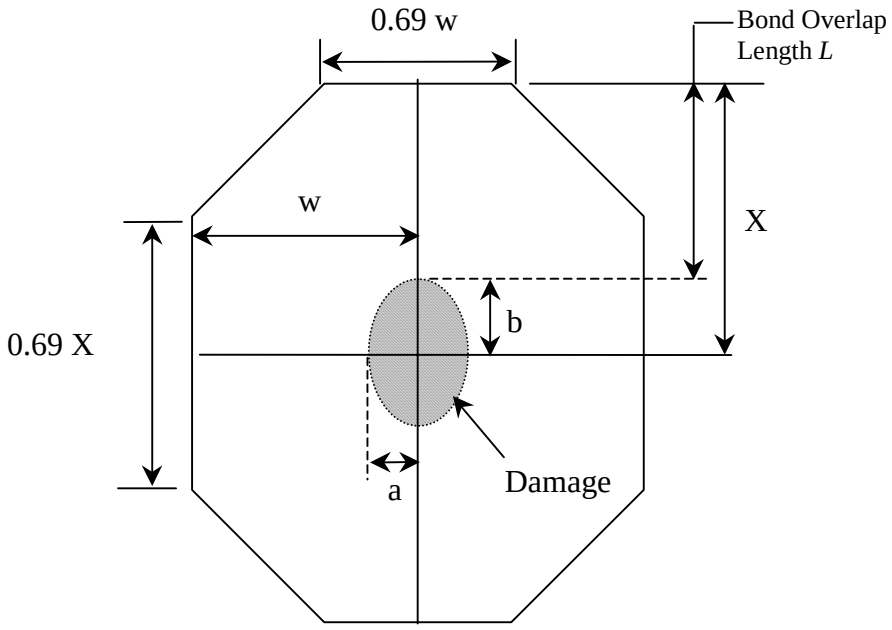


$w \geq a + 25mm$ for cracks OR

$w \geq L + a$ for other damage

$X = L + b$

$X/w \leq 1.0$

**Figure C-3: Dimensions of Patches for Optimal Reduction in Load Attraction**

| $L/w \rightarrow$ <br> $\frac{E_o t_o}{E_i t_i} \downarrow$ | 1 | 1.5 | 3 | 4 |
|---|---|---|---|---|
| **1** | **1.18** | **1.20** | **1.22** | **1.23** |
| **1.2** | **1.20** | **1.22** | **1.25** | **1.26** |
| **1.4** | **1.22** | **1.24** | **1.27** | **1.28** |
| **1.6** | **1.24** | **1.27** | **1.29** | **1.30** |

**Table C-1: Load Inclusion Factor $\Omega_L$ for Various Patch Aspect Ratios and Relative Stiffnesses**

| Material Property | Boron/Epoxy 5521/4 |
|---|---|
| Longitudinal Tension Strength $\mathbf{F_{1T}}$ <br> MPa (ksi) | 1520 <br> (220) |
| Longitudinal Modulus $\mathbf{E_1}$ <br> GPa (Msi) | 210 <br> (30) |
| Ultimate Longitudinal Strain[1] $\boldsymbol{\varepsilon_{1T}}$ | 0.00733 |
| Longitudinal Compression Strength $\mathbf{F_{1C}}$ <br> MPa (ksi) | 2930 <br> (425) |
| Transverse Tensile Strength $F_{2C}$ <br> Mpa - see Note 1 (ksi) | 48.3 <br> (7) |
| Transverse Modulus[1] $\mathbf{E_2}$ <br> GPa (Msi) | 19 <br> (2.7) |
| In-Plane Shear Strength $\mathbf{F}_{12}$ <br> MPa (ksi) | 103 <br> (15) |
| In-Plane Shear Modulus[1] **G** <br> GPa (Msi) | 6.89 <br> (1.0) |
| Major Poisson's Ratio[1] $\boldsymbol{\nu_{LT}}$ | 0.21 |
| Minor Poisson's Ratio[1] $\boldsymbol{\nu_{TL}}$ | 0.04 |
| Thickness per ply $\mathbf{t_{ply}}$, mm. (in.) | 0.13 <br> (0.0052) |
| Longitudinal Thermal Expansion Coefficient $\boldsymbol{\alpha_1}$ <br> x $10^{-6}°C^{-1}$ (x $10^{-6}°F^{-1}$) | 4.5 <br> (2.5) |
| Transverse Thermal Expansion Coefficient[1] $\boldsymbol{\alpha_2}$ <br> x $10^{-6}°C^{-1}$ (x $10^{-6}°F^{-1}$) | 29.5 <br> (16.38) |

**Table C-2: Design Data for Boron/Epoxy 5521/4 Pre-Preg Tape**

# APPENDIX C NOMENCLATURE

| SYMBOL | DESCRIPTION |
|---|---|
| $E_c$ | Elastic Modulus of Adhesive for the Purposes of Peel Stress Calculation |
| $E_c'$ | Effective Elastic Modulus of Adhesive for Peel Stress Calculation |
| $E_i$ | Elastic Modulus Inner Adherend (Structure) |
| $E_o$ | Elastic Modulus Outer Adherend (Patch) |
| $E_1$ | Longitudinal Modulus of a Composite Lamina |
| $E_2$ | Transverse Modulus of a Composite Lamina |
| $F_{1T}$ | Longitudinal Tensile Strength of a Composite Lamina |
| $F_{1C}$ | Longitudinal Compression Strength of a Composite Lamina |
| $F_{12}$ | In-Plane Shear Strength of a Composite Lamina |
| $F_{2T}$ | Transverse Tensile Strength of a Composite lamina |
| G | Shear Modulus |
| $\mathbf{K}_{\infty}$ | Stress Intensity Under a Repair for a Repaired Crack at Design Load Case |
| $\mathbf{K}_{\infty \mathbf{f}}$ | Stress Intensity Under a Repair for a Repaired Crack at Fatigue Load Case |
| ***DUL*** | Design Ultimate Load |
| ***DLL*** | Design Limit Load |
| ***ULT*** | Ultimate Strength of Inner Adherend (Structure) |
| $t_i$ | Thickness Inner Adherend (Structure) |
| $t_o$ | Thickness Outer Adherend (Patch) |
| $t_{ply}$ | Thickness of a Composite Lamina |
| $\alpha_i$ | Thermal expansion coefficient inner adherend (Structure) |
| $\alpha_o$ | Thermal expansion coefficient outer adherend (Patch) |

| SYMBOL | DESCRIPTION (continued) |
|---|---|
| $\alpha_{i_{eff}}$ | Effective Thermal expansion coefficient inner adherend (Structure) |
| $\varepsilon_{1T}$ | Ultimate Longitudinal Strain for a Composite Lamina |
| $\tau_p$ | Adhesive plastic shear stress |
| $G$ | Adhesive shear modulus |
| $\eta$ | Adhesive thickness |
| $\nu_{LT}$ | Major Poisson's Ratio for a Composite Lamina |
| $\nu_{TL}$ | Minor Poisson's Ratio for a Composite Lamina |
| $\nu$ | Poisson's Ratio |
| $\gamma_e$ | Adhesive elastic shear strain limit |
| $\gamma_p$ | Adhesive plastic shear strain limit |
| $\gamma_{\max}$ | Maximum shear strain in the adhesive at failure |
| $\gamma_f$ | Adhesive Shear Strain at Fatigue Load Case |
| $\sigma_0$ | Stress in Structure Under Patch Away from Defect at Design Load Case |
| $\sigma^*$ | Remote Stress at Design Load Case |
| $\sigma^{**}$ | Stress at the End of the Repair at Design Load Case |
| $\sigma_f$ | Remote Stress at Fatigue Load Case |
| $\sigma^{\#}$ | Stress in Structure Under Patch Away from Defect at Fatigue Load Case |
| $\sigma^{\#\#}$ | Stress at the End of the Repair at Fatigue Load Case |
| $\sigma_{c\max}$ | Peel Stress in the Adhesive at Design Load Case |
| $\sigma_p$ | Stress in the Patch at Design Load Case |
| $\sigma_p^{\#}$ | Stress in the Patch at Fatigue Load Case |

| SYMBOL | DESCRIPTION (continued) |
|---|---|
| $\Omega_L$ | Load Attraction Factor |
| $P$ | Load capacity of the adhesive in the joint |
| $P'$ | Load capacity of the adhesive in the joint after application of the Adhesive Variation Factor |
| $R$ | Load ratio for fatigue assessment, as determined by the ratio of minimum cycle load to the maximum cycle load |
| $\Delta T$ | Temperature range from cure temperature to design case temperature |
| $RT$ | Room Temperature |
| $\lambda$ | Elastic exponent |
| $l_e$ | Elastic load transfer length for the bond |
| $l_p$ | Plastic load transfer length for the bond |
| $L$ | Bond overlap length |
| $\phi_{\max}$ | Maximum tolerable defect size for adhesive |

**DISTRIBUTION**

**Syncrude Personnel**

Syncrude Research Site:
Syncrude Canada Ltd.
9421 17 Avenue
Edmonton, AB,
T6N 1H4

Syncrude Mining/Plant Site:
Syncrude Canada Ltd.
P.O. bag 4009, MD 0065
Fort McMurray, Alberta
T9H 3L1

Brent Campbell
Syncrude Canada Ltd.
P.O. bag 4009, MD A400
Fort McMurray, Alberta, Canada, T9H 3L1

Mal Carroll
Syncrude Canada Ltd.
P.O. bag 4009, MD A250
Fort McMurray, Alberta, Canada, T9H 3L1

Stefano Chiovelli
Syncrude Canada Ltd.,
9421 - 17th Ave.
Edmonton, Alberta, Canada, T6N 1H4

Victor del Valle
Syncrude Canada Ltd.
P.O. bag 4009, MD 0049
Fort McMurray, Alberta, Canada, T9H 3L1

Doug Emberley
Syncrude Canada Ltd.
P.O. bag 4009, MD 2050
Fort McMurray, Alberta, Canada, T9H 3L1

Brian Fricker
Syncrude Canada Ltd.
P.O. bag 4009, MD 2050
Fort McMurray, Alberta, Canada, T9H 3L1

David Fudge
Syncrude Canada Ltd.
P.O. bag 4009, MD 0039
Fort McMurray, Alberta, Canada, T9H 3L1

Silvia Gonzalez
Syncrude Canada Ltd.,
9421 - 17th Ave.
Edmonton, Alberta, Canada, T6N 1H4

Stewart Johnson
Syncrude Canada Ltd.,
9421 - 17th Ave.
Edmonton, Alberta, Canada, T6N 1H4

Ian Leblanc
Syncrude Canada Ltd.
P.O. bag 4009, MD A250
Fort McMurray, Alberta, Canada, T9H 3L1

Khaled Obaia
Syncrude Canada Ltd.,
9421 - 17th Ave.
Edmonton, Alberta, Canada, T6N 1H4

Damien Reid
Syncrude Canada Ltd.
P.O. bag 4009, MD 0039
Fort McMurray, Alberta, Canada, T9H 3L1

Jeremy Wong
Syncrude Canada Ltd.
P.O. bag 4009, MD 0011
Fort McMurray, Alberta, Canada, T9H 3L1

**University of Alberta**

Roger Cheng
Dept. of Civil & Environmental Engineering
220 Civil/Electrical Building
University of Alberta
Edmonton, Alberta, Canada, T6G 2G7

Alaa Elwi
Dept. of Civil & Environmental Engineering
220 Civil/Electrical Building
University of Alberta
Edmonton, Alberta, Canada, T6G 2G7

Gilbert Grondin
Dept. of Civil & Environmental Engineering
220 Civil/Electrical Building
University of Alberta
Edmonton, Alberta, Canada, T6G 2G7

**Sandia National Labs:**

MS-0724 Les Shephard, 6000
MS-0741 Margie Tatro, 6200
MS-0741 Rush Robinett, 6210
MS-1138 John Mitchiner, 6220
MS-0708 Paul Veers, 6214
MS-0753 Bruce Kelley, 6245
MS-0615 Dick Perry, 6252
MS-0615 Julia Archibeque-Guerra, 6252
MS-0615 Jeff Blanchette, 6252
MS-0615 Mike Bode, 6252
MS-0615 Tony Delong, 6252
MS-0615 Tonimarie Dudley, 6252
MS-0615 Joe Dimambro, 6252
MS-0615 Josephine Graham, 6252 (10)
MS-0615 Gerry Langwell, 6252
MS-0615 David Moore, 6252
MS-0615 Ciji Nelson, 6252
MS-0615 Kirk Rackow, 6252
MS-0615 Dennis Roach, 6252 (30)
MS-0615 Phil Walkington, 6252
MS-9019 Central Technical Files, 8945
MS-0899 Technical Library, 9615 (2)